Solid and Solution State Recognition of Anions and Ion-Pairs by Acyclic Receptors

A Dissertation Submitted in Partial Fulfillment for the Degree of

Doctor of Philosophy

Arghya Basu

(Roll No. 08612216)

Supervisor: Professor Gopal Das

Department of Chemistry

Indian Institute of Technology Guwahati

August – 2013

Dedicated to my Parents

INDIAN INSTITUTE OF TECHNOLOGY GUWAHATI

Department of Chemistry

STATEMENT

I do hereby declare that the matter embodied in this thesis is the result of investigations carried out by me in the Department of Chemistry, Indian Institute of Technology Guwahati, India, under the guidance of Prof. Gopal Das, Department of Chemistry, Indian Institute of Technology Guwahati, India.

In keeping with the general practice of reporting scientific observations, due acknowledgements have been made wherever this work is based on the findings of other investigators.

5th August, 2013 **Arghya Basu**

IIT Guwahati

INDIAN INSTITUTE OF TECHNOLOGY GUWAHATI

Department of Chemistry

CERTIFICATE

This is to certify that Mr. Arghya Basu has been working under my supervision since January, 2009 as a regular registered Ph. D. student. His thesis entitled **"Solid and Solution State Recognition of Anions and Ion-Pairs by Acyclic Receptors"** is an authentic record of the results obtained from the research work carried out under my supervision in the Department of Chemistry, Indian Institute of Technology Guwahati, Assam, India. I am forwarding his thesis to submit for the award of degree of Doctor of Philosophy, from this institute. I hereby certify that he has fulfilled all the requirements, according to the rules of this institute regarding the investigations embodied in his thesis and this work has not been submitted elsewhere for a degree.

Prof. Gopal Das
(Thesis Supervisor)
Professor
Department of Chemistry
IIT Guwahati
Assam - 781039, India

Acknowledgement

At this final stage of truly memorable journey towards my intellectual destination, it is really hard to list all the people who sincerely helped me and I would like to thank all of them who have made this thesis possible.

First of all I would like to express my sincere gratitude to my thesis supervisor Prof. Gopal Das for his kind support, insightful advice and encouragement. I earnestly thank him for his nice guidance, freedom to work, encouragement and inspiration which helped me to enrich myself. I would also like to give sincere gratitude to my doctoral committee members, Prof. Manabendra Ray, Dr. Sandip Paul and Dr. A. S. Achalkumar for their advices and suggestions.

I extend my gratitude to my beloved parents and family, whose endless love and inspiration has always been strength for me. Their eternal blessing and constant support has guided me this far and positively, this will take me far forward in future to achieve the success they dreamt of. Further, no words would be sufficient to express my feelings for my best friend Moumita, whose affection and care have so luxuriously continued to enrich every fraction of my life. She has always been there to support and encourage me even in frustrating and difficult times of my life, for which I wish to put forward my hearty gratitude to her.

I take this opportunity to thank my Lab members and friends, Ballav Da, Avijit Da, Bedo Da, Bimlesh Da, Sandeep Da, Jiban, Chirantan, Nazbul, Romen, Abhijit, Barun and Soham for their co-operation and inspiration in my research work, without which it would not been easy to complete the PhD thesis. It was great to work and spend times with these interesting human beings and I will always cherish the memories of their jokes, laughter and humor throughout my life. I wish them great success in every aspects of their life.

Finally, I would like to pay my sincere thanks to my school, college and university teachers, their motivation and help has guided me to reach this far. Some friends whom I don't want to keep out from the list are Chandan, Supriyo, Rohit, Soumya and Suvendu, whose friendship had enrich my life.

Arghya

The contents of this thesis entitled **"Solid and Solution State Recognition of Anions and Ion- Pairs by Acyclic Receptors"** have been divided into six chapters based on the results of experimental work performed during the research period.

Chapter 1: Introduction

This chapter provides a brief introduction on 'supramolecular host-guest chemistry' of ionic species with special reference to recognition of anions and ion-pairs. Cationic and anionic charged species are omnipresent and their importance in chemical, biological, medical, environmental, and industrial processes cannot be underestimated. Over the past several decades, a large number of acyclic and macrocyclic compounds have been synthesized for cations and recently for anions and ion-pairs. Therefore, our focus is on recent field of interest that is anion and ion-pair receptor chemistry.

Anions are ubiquitous in the natural world playing many vital roles in biological systems for the maintenance of life and they also have adverse effects on the environment in the form of anionic pollutants. Therefore, sensing and recognition of anionic guest species are very much important. The binding of anion guests within pre-organized macrocyclic systems are relatively straight forward to understand but the binding processes of acyclic receptors remain more elusive. Further, multi-armed acyclic receptors have often been found to coordinate with targeted ionic species *via* formation of capsular assemblies. Cavitands and capsules are fascinating associates of the receptor family, where the confined interior space or cavity formed by self-assembly of the monomeric unit through noncovalent interactions has been employed for various technological and biomedical applications. When two or more identical subunits are geometrically and functionally complementary with one another, they may self-assemble to form a super molecule. Structural features of the cavity or crystal void such as, shape, size or electronic properties, determine the usefulness of the super-structure. These capsular assemblies have shown a number of interesting properties e.g. encapsulation of anion–water clusters, capturing aerial carbon dioxide as carbonate, selective salt extraction from water and anion transportation. Despite, the intense investigations, metal assisted assemblies are well explored than the anion-assisted assemblies. However, recently we have observed an expansion of research activities in the area of anion-assisted assemblies.

On the other hand, recognition of ion-pair is a new field of research emerging from coordination chemistry of cations and anions. Definite types of heteroditopic receptor

designs for ion-pairs and the complexity of ion-pair binding are discussed to illustrate key concepts such as cooperativity. The importance of this area of research is reflected by the wide variety of potential applications of ion-pair receptors, including salt solubilization, extraction, membrane transport and sensors. However, in spite of their potential applications in various fields, the number of well characterized ion-pair receptors remains limited. This could reflect a combination of synthetic challenges (the systems reported to date have not been easy to prepare) and experimental complexities associated with tracking multiple ionic species as well as the high inherent lability of many ion-pairs.

Chapter 2: Experimental methods and characterization

In this chapter, a detailed report of the various reagents used in the detail synthesis of the receptors, their synthetic procedures, crystallization details, binding study and specifications of analytical instruments employed in the characterization of synthesized receptors and their various complexes.

Chapter 3: A Fluoride selective chromogenic receptor with a thiadiazole spacer

This chapter describes a newly synthesized neutral acyclic receptor $\mathbf{H_2L_1}$ with a thiadiazole spacer, which behaves as a selective chemosensor for F^- ion**.** The fluoride recognition chemistry is immediately detected in solution by a dramatic increase in solubility of the receptor in CH_3CN with a concomitant optical signalling upon addition of TBAF and confirmed by UV/Vis spectroscopy. The detail UV/Vis spectroscopic titration experiments with increasing equivalents of fluoride anion suggest formation of a H-bonded complex with subsequent stepwise deprotonation of two N−H groups, which can be visually monitored by a change in color from yellow to blue *via* pink. Further, the solid state crystal structure of halide complexes of the receptor is also reported. Crystal structure analysis of the halide complexes elucidate the fact that fluoride forms an unusual 1:1 hyrogen-bonded complex with monodeprotonated receptor, whereas in the case of other congeners, such as chloride and bromide, the receptor binds two halide anions along with formation of a halide bridged 1D polymeric chain network by participation of N−H···X^- and aromatic C−H···X^- hydrogen-bonding (where X = Cl and Br) interactions. The presence of a rigid thiadiazole spacer presumably opens up enough space for capturing two halide anions by a single receptor molecule, where the coordinated −NH protons are

pointed in the same direction with respect to the spacer and eventually favor formation of halide (Cl^- and Br^-) induced polymeric architecture, although no obvious chloride or bromide-directed polymeric assembly is found in solution.

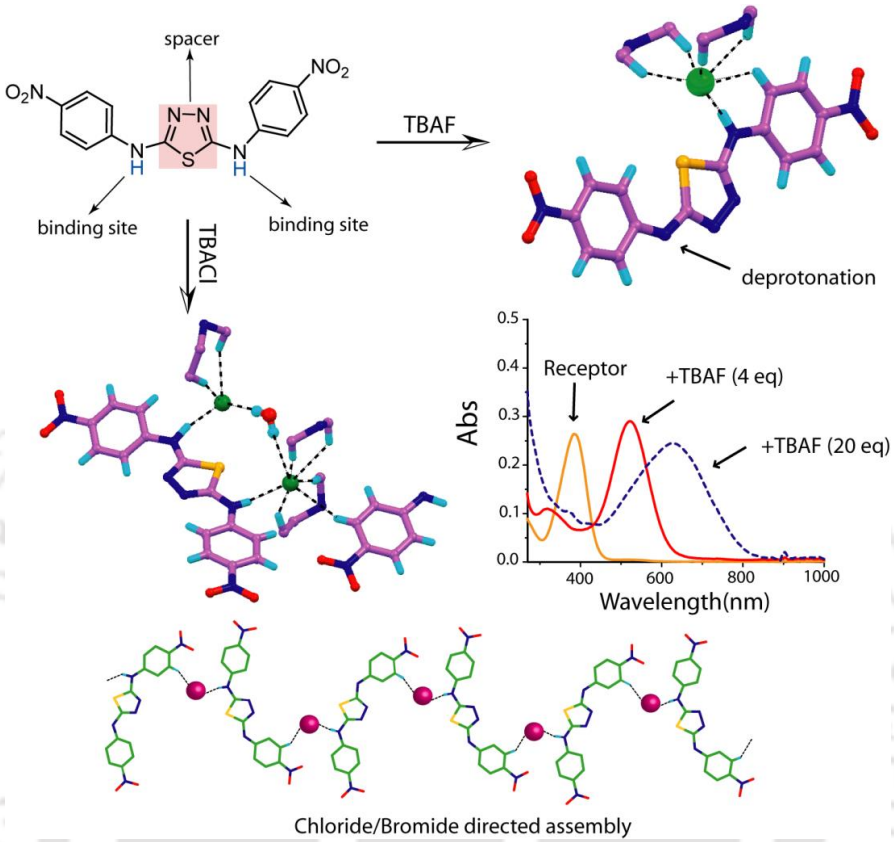

Scheme 1. A comprehensive representation of the research work included in this chapter

Chapter 4: Encapsulation of sulfate and thiosulfate within the dimeric capsular assembly of a tripodal thiourea receptor

In this Chapter a simple tris(2-aminoethyl)amine based meta-chloro substituted tripodal thiourea receptor **L_2** has been extensively studied with two divalent oxyanions of sulfur, such as sulfate and thiosulfate, with identical dimensionality. The solid state crystal structure of the anion complexes with **L_2** reveal that the anions are encapsulated within the dimeric rigid capsular assembly of the receptor *via* N–H···anion interactions. To the best of our knowledge this is the first report on the encapsulation of thiosulfate within dimeric capsular assembly of a neutral receptor. The tight capsular sizes for both anion complexes are quite comparable, whereas the coordination mode of the anions and the hydrogen bonding parameters are significantly varied. The three dimensional solid state structural orientations of the capsular complexes are mainly governed by the Cl···Cl (for thiosulfate

complex) and Cl···S (for sulfate complex) halogen bonding interactions. The solution-state binding and encapsulation of oxyanions by N–H···anion hydrogen bonding has also been confirmed by quantitative ^{1}H NMR titration and 2D NOESY NMR experiments. Both the experiments confirm that in contradiction of 2:1 solid state binding, in solution the studied anions are bound within the pseudocavity of the receptor with 1:1 binding stoichiometry. Moreover, the change in chemical shifts of thiourea –NH protons and the binding constant values suggest the receptor–sulfate interaction is more energetically favorable compared to the receptor thiosulfate interaction.

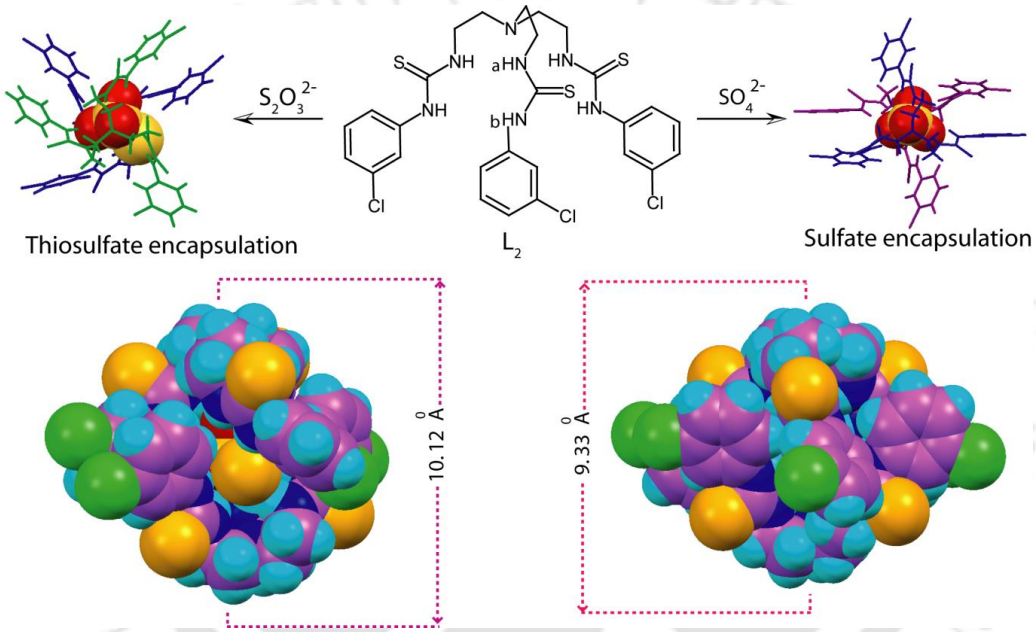

Scheme 2. A comprehensive representation of the research work included in this chapter.

Chapter 5: Recognition of anion/anion-water cluster by a tripodal amide receptor

The highlight of this chapter is encapsulation tetrameric halide water cluster $[X_2(H_2O)_2]^{2-}$(X = Cl^-/Br^-) within dimeric capsular assembly of a newly synthesized conformationally flexible C_{3v} symmetric N-bridged tripodal amide receptor **L_3**. The cluster is formed *via* strong chloride/bromide–water interactions and possesses a planar cyclic tetrameric arrangement where each chloride/bromide anion is hydrogen bonded with the two water molecules. Close inspections of the distance and angle measurement values of the terameric water cluster confirmed it to be a perfect parallelogram. However, in the case of higher homologous iodide anions the receptor **L_3** prefers to adopt a non-capsular polymeric aggregation. Interestingly, crystallization of the receptor in presence of HF in

glass container gives SiF_6^{2-} complex, and depending on crystallizing solvent the receptor forms both capsular and non-capsular assemblies in presence of SiF_6^{2-} anion. The thermal stability of the halide–water cluster in complexes has also been studied by thermo-gravimetric analysis, which indicates the strong hydrogen bonding between the anion–water cluster and the host molecules present in the complexes. Furthermore, a detailed ^1H NMR titration and 2D-NOESY NMR experiments have been carried out to validate the binding and encapsulation of halide and halide water cluster within the receptor scaffold.

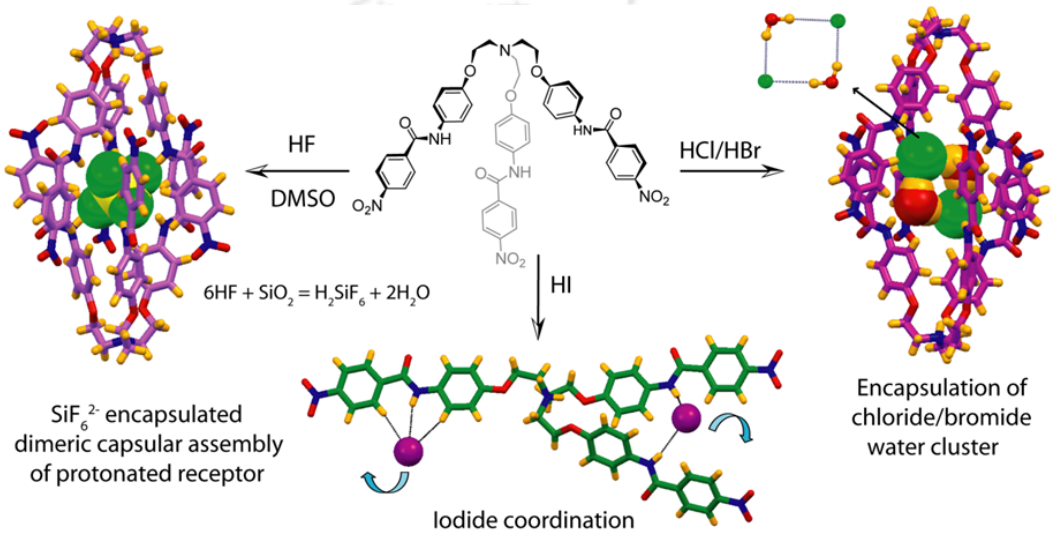

Scheme 3. A comprehensive representation of the research work included in this chapter.

Chapter 6: A heteroditopic tripodal urea receptor for recognition of ion-pairs

In this chapter a new C_{3v} symmetric N-bridged flexible urea based tripodal heteroditopic receptor L_4 was designed, synthesized, and characterized. Detail ^1H NMR spectroscopic investigations in solution and solid-state crystallographic analysis shows that the receptor can form complex with both anion and ion pair. In presence of Group I metal ions (Li^+, Na^+ and K^+, as their perchlorate salts in 98:2 DMSO-d_6:D_2O) the receptor **L_4** gave rise significant enhancement of binding property with hydrogensulfate(HSO_4^-) and di-hydrogenphosphate($H_2PO_4^-$) anions compared to metal free receptor. The enhancement in HSO_4^- and $H_2PO_4^-$ binding displays the ability of alkali metals to cooperatively affect -anion binding *via* preorgaziation of the receptor. The multiple ^1H NMR titrations and subsequent binding constant determinations reveal that the potassium cation coordinated

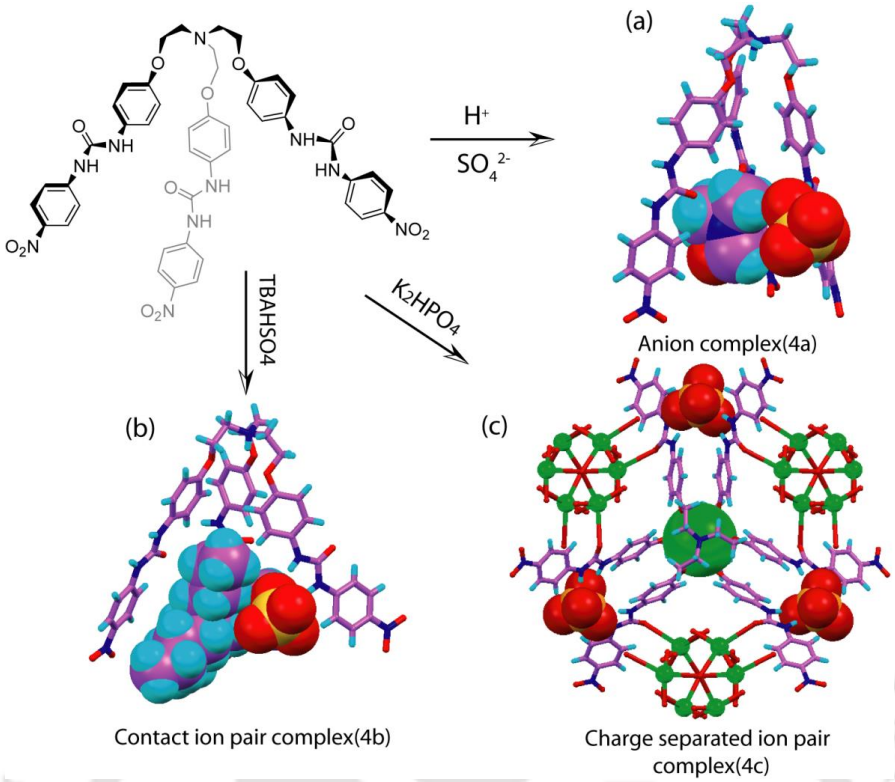

Scheme 4. A comprehensive representation of the research work included in this chapter.

receptor forms strongest association with HSO_4^- anion compared to metal free and Li^+/Na^+ coordinated receptor. The solid state crystal structure of anion and ion pair complexes of L_4 are also reported. The structural analysis of sulfate complex 4a shows encapsulation of single DMF solvent molecule in the tripodal cavity of the protonated receptor, and the SO_4^{2-} anion is located outside the tripodal cavity and stabilized by N−H···O hydrongen bonds from the urea functions of four receptor cations. Whilst, with $TBAHSO_4$ the receptor forms an unusual contact ion pair complex, where both the TBA cation and SO_4^{2-} anion are pseudo encapsulated in the distorted C_{3v} symmetric tripodal cavity of the protonated receptor. Further, the receptor also forms beautiful C_{3v} symmetric charge separated ion pair complex with potassium cation and hydrogenphosphate anion *via* formation of dimeric capsular assembly of the receptor, in which three nearby K^+ encapsulated dimeric capsular assemblies interdigitate to form a precise cavity that further encapsulate HPO_4^{2-} anion in its centre and subsequently generates 2D polymeric assembly of capsular complexes.

Conclusion

To conclude, this thesis provides some significant results in the domain of 'supramolecular chemistry of anions and ion pairs, where the anions and/or ion pairs binding capability of some newly synthesized acyclic receptors were explored in the solid-state and in solution as well. In general the present findings provide evidence of anion and ion pair induced formation of capsular, pseudo-capsular and polymeric assembly of the studied receptor molecules. Each receptor has shown an interesting property in presence of a specific anion or a set of ionic guests.

The receptor $\mathbf{H_2L_1}$ has been shown to selectively detect F^- ion *via* formation of H-bonded complex and subsequent stepwise deprotonation of two N−H groups, which can be visually monitored by a change in color from yellow to blue *via* pink. Additionally the receptor also forms halide (Cl^- and Br^-) induced polymeric architecture in crystalline solid state. Whereas, the multi armed tris-(thiourea) receptor $\mathbf{L_2}$ has been shown to encapsulate large sulfate and thiosulfate anions within the rigidified dimeric capsular assembly of L_2. The newly synthesized tripodal amide receptor $\mathbf{L_3}$ has been established as a competent hydrogen bonding scaffold for encapsulation of halide water cluster within rigidified molecular capsules, assembled by aromatic π-stacking interactions between the receptor side arms. In contrast, the urea receptor $\mathbf{L_4}$ has been shown to efficiently form complex with ion-pairs and also gave rise significant enhancement of binding property with hydrogensulfate (HSO_4^-) and di-hydrogenphosphate ($H_2PO_4^-$) in presence of Group I metal ions (Li^+, Na^+ and K^+) compared to free receptor.

Contents

Chapter 1 – Introduction

1.1 Supramolecular chemistry: An introduction 1

1.2 Hydrogen bond 2

1.3 Anion receptor chemistry 2

1.3.1 Chromogenic anion selective acyclic receptors 5

1.3.2 Anion coordination and anion directed assembly of multi-armed acyclic receptors 8

1.3.2a Tris(2-aminoethyl) amine based tripodal receptors 8

1.3.2b Arene based multiarmed acyclic receptors 16

1.4 Ion-pair receptor chemistry 19

1.4.1 Ion-pair recognition by acyclic receptors 20

1.4.1a Pridylureas and bipyridine-bis(urea) based ion-pair receptors 21

1.4.1b Tripodal and hexapodal ion-pair receptors 22

1.5 Concluding remarks 25

References 26

Chapter 2 – Experimental methods and characterization

2.1 Materials 29

2.2 Experimental methods 29

2.3 Single crystal X-ray crystallography 30

2.4 Synthesis and characterization of receptors, ($\mathbf{H_2L_1}$ and $\mathbf{L_2}$-$\mathbf{L_4}$)

2.4.1 N2,N5-bis(4-nitrophenyl)-1,3,4-thiadiazole-2,5-diamine, $\mathbf{H_2L_1}$ 31

2.4.2 Tripodal thiourea receptor, $\mathbf{L_2}$ 32

2.4.3 Tripodal amide receptor, $\mathbf{L_3}$ 32

2.4.4 Tripodal urea receptor, $\mathbf{L_4}$ 34

2.5 Synthesis and characterization of anion or/and ion-pair complexes of $\mathbf{H_2L_1}$ and $\mathbf{L_2}$-$\mathbf{L_4}$

2.5.1 Complexes of receptor $\mathbf{H_2L_1}$ 35

2.5.2 Complexes of receptor $\mathbf{L_2}$ 36

2.5.3 Complexes of receptor $\mathbf{L_3}$ 36

Contents

2.5.4 Complexes of receptor $\mathbf{L_4}$ 38

References 40

Chapter 3 – A Fluoride selective chromogenic receptor with a thiadiazole spacer

3.1 Background and focus of the chapter 41

3.2 Selective chromogenic sensing of fluoride anion 42

3.3 Halide binding study by ^{1}H NMR spectroscopy 45

3.4 Structural aspects of anion binding with $\mathbf{H_2L_1}$ 47

3.5 X-ray crystal structure analysis of receptor halide complexes

3.5.1 Structural description of fluoride complex, (**1a**) 48

3.5.2 Structural description of chloride complex, (**1b**) 50

3.5.3 Structural description of bromide complex, (**1c**) 51

3.8 Conclusion 53

References 59

Chapter 4 – Encapsulation of sulfate and thiosulfate within the dimeric capsular assembly of a tripodal thiourea receptor

4.1 Background and focus of the chapter 60

4.2 Structural description of $\mathbf{L_2}$ 61

4.3 Structural aspects of anion binding with $\mathbf{L_2}$

4.3.1 Structural description of SO_4^{2-} encapsulated molecular capsule, (**2a**) 63

4.3.2 Structural description of $S_2O_3^{2-}$ encapsulated molecular capsule, (**2b**) 65

4.4 Sulfate and thiosulfate binding studies by ^{1}H NMR spectroscopy 68

4.5 Conclusion 72

References 77

Chapter 5 – Recognition of anion/anion-water cluster by tripodal amide receptor

5.1 Background and focus of the chapter 78

5.2 Structural aspects of anion binding with $\mathbf{L_3}$ 79

Contents

5.2.1 Structural description of chloride complex, **(3a)** 79

5.2.2 Structural description of bromide complex, (**3b**) 81

5.2.3 Structural description of iodide complex, (**3c**) 83

5.2.4 Structural description of hexafluorosilicate complex, (**3d**) 84

5.2.5 Structural description of hexafluorosilicate complex, (**3e**) 86

5.5 Anion-binding studies by ^{1}H NMR spectroscopy 88

5.6 Conclusion 90

References 98

Chapter 6 – A heteroditopic tripodal urea receptor for recognition of ion-pairs

6.1 Background and focus of the chapter 99

6.2 6.2 Structural description of **L_4** 100

6.3 Structural aspects of anion and ion-pair binding with **L_4**

6.3.1 Structural description of complex **4a** 102

6.3.2 Structural description of complex **4b** 103

6.3.3 Structural description of complex **4c** 105

6.4 Solution-state ^{1}H NMR binding studies 108

6.5 Conclusion 112

References 120

Conclusion and Future perspective 121

List of publications 123

Annexures 1 – 5 Attached CD

Crystallographic files Attached CD

Chapter 1

Introduction

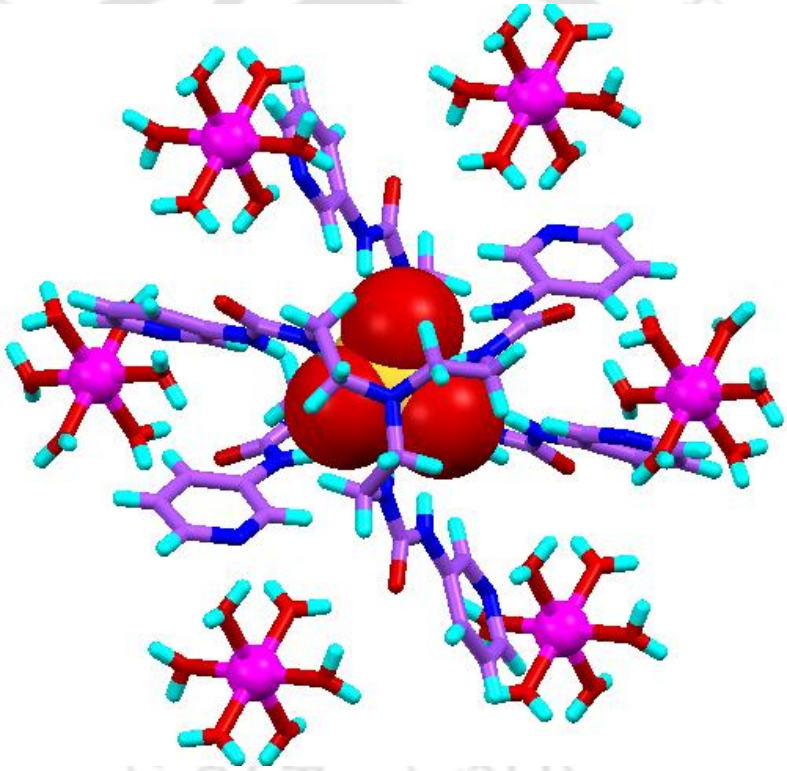

1.1 Supramolecular chemistry: An introduction

Supramolecular chemistry has been defined by one of its leading proponents, Jean-Marie Lehn, who won the Nobel Prize for his work in the area in 1987, as the 'chemistry of molecular assemblies and of the intermolecular interactions'. More colloquially this may be expressed as 'chemistry beyond the molecule'. Other definitions include phrases such as 'the chemistry of the non-covalent bond' and 'non-molecular chemistry'. Basically supramolecular chemistry refers to the domain of chemistry beyond that of molecules and focuses on the chemical systems made up of a discrete number of assembled molecular subunits or components. While traditional chemistry focuses on the covalent bond and coordinative bond formation, supramolecular chemistry examines the weaker and reversible noncovalent interactions between molecules such as hydrogen bonding, ion-ion and ion-dipole interactions, cation–π and anion–π interactions, π–π interactions, Van-der Waals forces, and hydrophobic effects.[1] Understanding these noncovalent interactions and exploiting them in new ways continues to define the essence of the field. Not surprisingly, the challenges and opportunities continuing to attract increasing number of ever more talented researcher into the area, while fueling its nearly exponential growth as venue for intellectual discovery and useful, real world relevant contribution. This is particularly true in the area of anion and ion-pair receptor chemistry.

In supramolecular host-guest chemistry, the host is commonly referred to a large molecule or aggregate such as an enzyme or synthetic cyclic and acyclic compounds possessing a sizeable central hole or cavity.[1] The guest may be an ionic species (cation/anion), a neutral molecule or a more sophisticated molecule such as a hormone, pheromone or neurotransmitter. The thermodynamic stability of a supramolecular host-guest complex may be enhanced by operation of a chelate effect or macrocyclic effect. The macrocyclic effect makes cyclic hosts such as corands (e.g. crown ethers) up to a factor of 10^4 times more stable than closely related acyclic podands with the same type of binding sites. Therefore, the binding of guests within pre-organized macrocyclic systems are relatively straight forward to understand but the binding processes of acyclic receptors remain more elusive. Furthermore, in order to bind, a host molecule must have binding sites that are of the correct electronic character (polarity, hydrogen bond donor/acceptor ability, hardness or softness etc.) to complement the guest. If a host molecule does not undergo a significant conformational change upon guest binding, it is said to be preorganized. Host preorganization is a key concept because it represents a major enhancement in the overall free energy of guest complexation.[2]

1.2 Hydrogen bond

A hydrogen bond may be regarded as a particular kind of dipole-dipole interaction in which a hydrogen atom attached to an electronegative atom (or electron withdrawing group) is attracted to a neighboring dipole on an adjacent molecule or functional group. Hydrogen bonds are commonly written D–H···A and usually involve a hydrogen atom attached to an electronegative atom such as O or N as the donor (D) and a similarly electronegative atom, often bearing a lone pair, as the acceptor (A). There are also significant hydrogen bonding interactions involving hydrogen atoms attached to carbon, rather than electronegative atoms such as N and O (electronegativities: C: 2.55, H: 2.20, N: 3.04, O: 3.44). Because of its relatively strong and highly directional nature, hydrogen bonding has been described as the 'masterkey interaction in supramolecular chemistry'.[1] Typical examples include, the formation of carboxylic acid dimer and base pairing in DNA by hydrogen bonding (Scheme 1.1). Hydrogen bonding is perhaps the most important discriminating cohesive force in directing the crystallization and self-assembly of organic molecules.[3] Self-assembly is the process by which molecules adopt a defined arrangement by virtue of rotations about single bonds (intramolecular torsions) and intermolecular hydrogen bonding. Self-assembly is highly precise, self-controlling and self-repairing since equilibrium-controlled processes are implicated.[4]

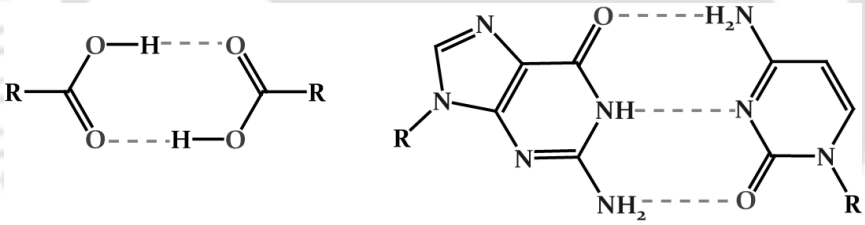

Scheme 1.1 A hydrogen bonded carboxylic acid dimer and base pairing in DNA (Guanine–Cytosine) by hydrogen bonding.

The objective of the thesis is to develop some new acyclic receptors for selective recognition of anions and ion-pairs both in solid and solution state, with special emphasis on the anion and ion-pair induce assembly process of the receptors.

1.3 Anion receptor chemistry

Anions are ubiquitous in biology. They are present in roughly 70% of all enzymatic sites, play essential structural roles in many proteins, and are critical for manipulation and storage of genetic information (DNA and RNA are polyanions). Anions are also in regulating osmotic pressure, activating signal transduction pathways, maintaining cell volume and in the production of electrical signal. Not surprisingly, the disruption of anion flux across the cell membranes is increasingly recognized as being the primary determinant of many diseases. In fact the transport of anions

through cell phospholipid bilayers is known to be mediated by a variety of channels and anion transport proteins with at least 14 mitochondrial anion transport system have been identified so far. These include (among others) systems responsible for the trafficking of ADP, ATP, phosphate, citrate maleate, oxaloacetate, sulphate, glutamate, fumarate and halide anions. Recently, several X-ray crystal structures have been solved that have allowed the direct visualization of enzyme–anionic substrate complexes that are stabilized via multiple hydrogen-bonding interactions (Figure 1.1).[5]

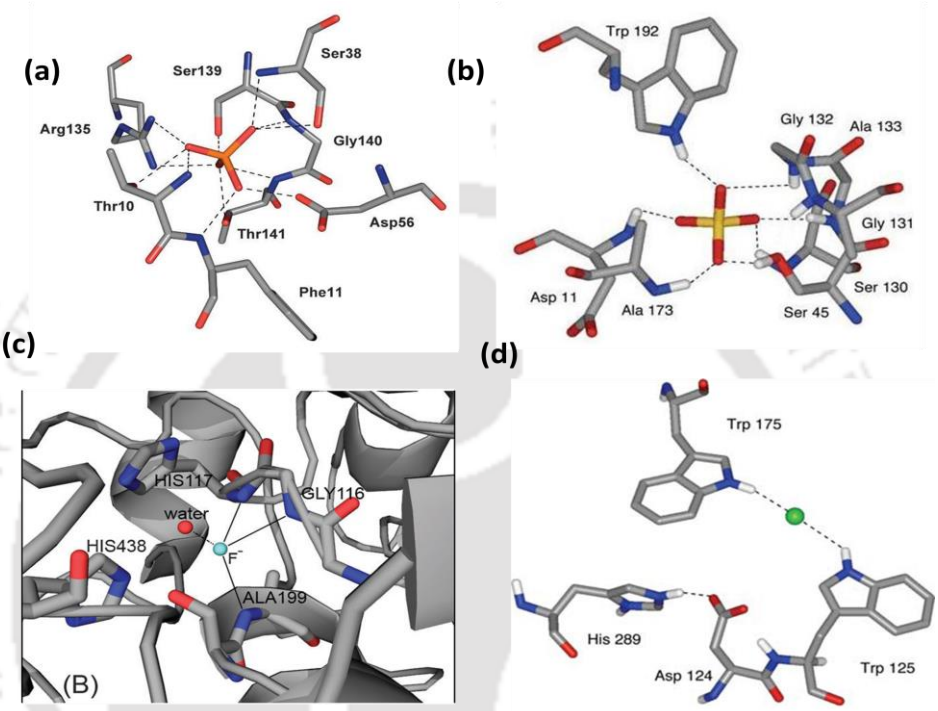

Figure 1.1 Anion binding in biology (a) Showing binding mode of phosphate anion in phosphate-binding protein; (b) X-ray crystal structure of Sulfate-binding protein. The sulfate anion is bound by seven hydrogen bonds from NH and OH bond donor group; (c) Showing bound mono hydrated fluoride anion in human butyrylcholinesterase complex (PDB code = 2XMC); (d) Enzymatic active site of haloalkane dehalogenase the presence of a bound chloride anion.

Apart from biological interest, the anion receptor chemistry has also attracted growing attention in supramolecular chemistry[6] due to the essential roles that anions play in catalysis, and environmental science.[5] Binding affinities between anions and their hosts are mostly attributed to hydrogen-bonding and/or electrostatic interactions, with the former being the more influential in promoting selective binding through topological complementarity. As Moyer and Bonnesen et al. has pointed out, it is important to understand the factors influencing anion recognition in the traditional analytical sense, where simple physical properties such as size, charge, basicity and hydrophilicity tend to govern selective exchange of one anion over another. They introduced the term *bias* for this type of phenomenon and deduce that truly selective anion receptors must involve some elements of strategic design, including appropriately positioned hydrogen bond coordination sites.[7] The

introduction of multiple hydrogen bonding sites along with the resulting topological considerations in anion receptors leads to the concept of double valence for anions as well as for transition-metal ions. For anions, however, the primary valence is the negative charge on the anion and the secondary valence is provided by hydrogen bonds to the anion.[8] Bowman-James et al. has categorized the binding of anions based on their coordination numbers which is helpful in defining the notions of complementarity for a given anion and can aid to the design of optimal anion-binding host structures.[9]

The most effective way to bind anions consist in taking advantage of their negative charge and accordingly, ammonium and quaternary ammonium receptors have been the principal receptor of choice since, they ensure an adequate electrostatic attraction reinforced by hydrogen bond contacts with the coordinated anions.[10] However, pyrrole, indole, amide and urea/thiourea functions have been the subject of intensive investigations for its performance in the construction of neutral anion receptors *via* favourable hydrogen bonding interactions.[11] However, if the -NH protons are acidic enough, in particular when an electron-withdrawing substituent is introduced into the receptor molecule, deprotonation may occur in the presence of a highly basic anion, such as fluoride and acetate.[12] Wide structural modifications on the hydrogen bonding scaffold have been attempted to increase the acidity of the -NH protons by introducing electron-withdrawing substituents, e.g., $-NO_2$ and $-CF_3$ *via* the mediation of a π-system and to form a preorganized binding cleft or cavity using a rigid (calixarene or polynorbornane) or flexible structural skeleton that leads to a binding environment with size and shape complementary for a given anion. Recently, Custelcean et al. has reviewed the structural role of anions in crystal engineering since anions play diverse roles in the formation of crystals.[13] Besides conventional N–H···A^- hydrogen bonding, theoretical calculations on electrostatic anion–π interactions have been complemented by mounting experimental evidences for their existence in the solid state and in solution.[14] However, true examples of anion–π interactions in crystals remain extremely rare because of the competition with C–H···A^- hydrogen

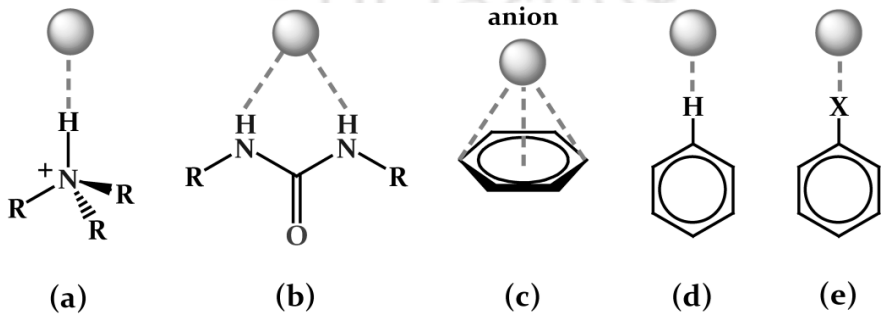

Scheme 1.2 Anion binding by different types of noncovalent interactions; (a) electrostatic N–H···A^- interaction by an ammonium cation; (b) complementary N–H···A^- interaction by a urea function; (c) anion–π interaction; (d) C–H···A^- interaction by an aryl function and (e) C–X···A^- halogen bonding by a halocarbon (X = F^-, Cl^-, Br^- and I^-).

bonds, which tend to prevail.[15] Another competitor is the weak σ interaction involving a small amount of charge transfer from the anion to an arene system, which is geometrically characterized by the anion being situated above the periphery rather than the centre of the arene. More recently, a new type of noncovalent interaction involving an electrophilic halogen atom (halocarbon) and a high electron density centre (like anion), has been established both experimentally and theoretically.[16] Halogen bonds are highly directional (∠D−X—A close to linear), in many respects behave like hydrogen bonds.

1.3.1 Chromogenic anion selective acyclic receptors

Colorimetric receptors have drawn special attention due to their ‘‘naked eye’’ detection of target species and also have the viability to offer both qualitative and quantitative insights of the receptor–guest interaction by using inexpensive spectrophotometric techniques. The design and study of colorimetric receptors for biologically relevant anions has become a very active area of research within the field of supramolecular chemistry.[5,6] Anions like fluoride, acetate and phosphate play imperative roles in a broad range of chemical and biological systems and sometimes they are of environmental concern.[17] Therefore, synthetic receptors proficient for sensing these biologically relevant anions are of utmost importance.

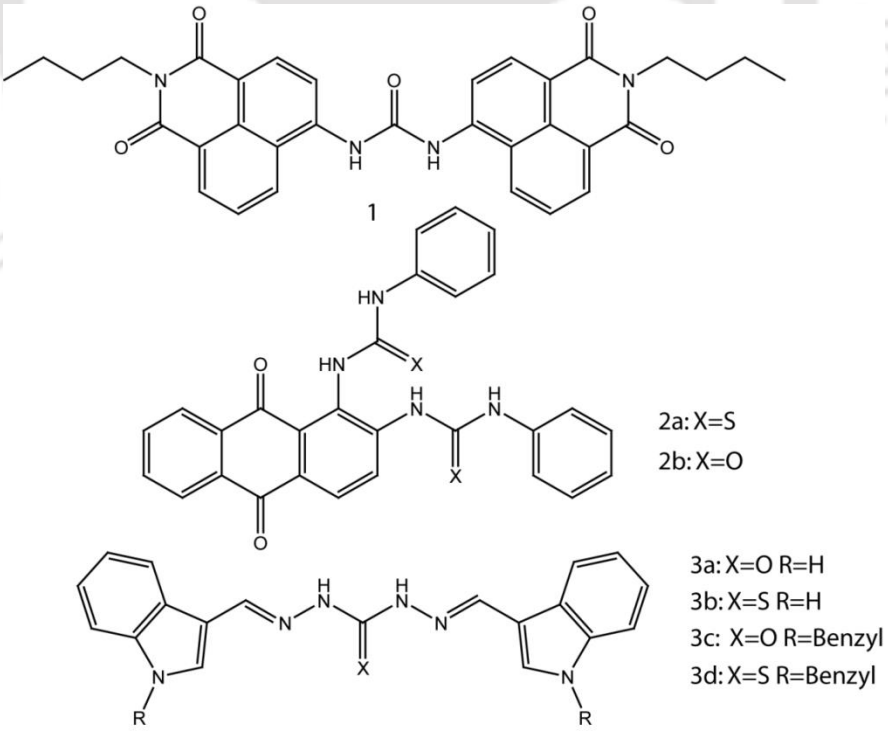

Scheme 1.3 Chemical formulae of the sensor molecules.

Fabbrizzi and coworker have reported urea-based receptor **1**, which had been symmetrically armed with a powerful chromogenic substituent, naphthalenimide, bringing a yellow color.[18] It was found

on addition of an excess of a few equivalents of $[Bu_4N^+]F^-$, the color of the DMSO solution of **1** turned from yellow to red. Then, on further addition of fluoride, up to ten equivalents, a blue color developed. Upon gradual addition of fluoride anion the charge transfer band of the naphthaleneimide chromophore undergoes a remarkable red shift (from 400 to 540 nm), is due to mono deprotonation of the receptor. The limiting absorbance is achieved on addition of 2 equiv of F^-. The occurrence of the N−H deprotonation is further confirmed by the upfield shift of all aromatic protons, as observed in a ^1H NMR titration experiment in DMSO-d_6. A similar behavior was observed on titration with $[Bu_4N^+]OH^-$, but in this case, the band at 540 nm reached its limiting absorbance on addition of 1 equiv of OH^-. Interestingly, further excess of $[Bu_4N^+]F^-$ (10 equiv and more), the color of the solution turned from red to blue (Annexure 1), while, in the visible spectrum (Figure1.2b), the band at 540 nm disappeared and a new band formed at 600 nm. Such a band reached its limiting intensity upon addition of ca. 30 equiv. It is suggested that the new band pertains to the doubly deprotonated receptor **1**. The double deprotonation phenomena is further confirmed by titrating the receptor with $[Bu_4N^+]OH^-$, but the limiting value of the band at 600 nm is achieved on addition of a smaller anion excess (5−6 equiv) than for fluoride. Acetate induces deprotonation of one N−H fragments, according to a 1:1 stoichiometry with log K= 4.97 (0.01), but no appearance of the band at 600 nm and development of the blue color are observed, even after the addition of a huge excess of $[Bu_4N^+]CH_3COO^-$.The less basic anion $H_2PO_4^-$ is able to remove one proton from **1** but only after large excess addition. No deprotonation at all is observed with less basic oxoanions such NO_2^-, NO_3^-, HSO_4^-, and remaining halides, Cl^- and Br^-.

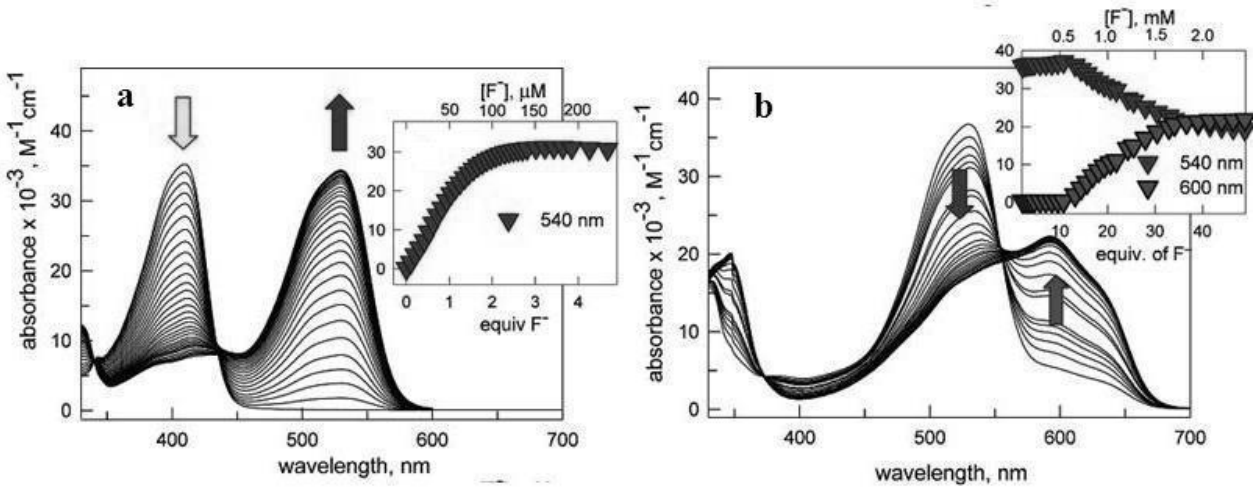

Figure 1.2 Family of UV/Vis spectra taken over the course of the titration of a DMSO solution 5.0 x 10^{-5} M in receptor **1**) with a standard solution of $[Bu_4N^+]F^-$ at 25 °C. (a) From 0 to 5 equiv of $[Bu_4N^+]F^-$ (the band that develops at 540 nm pertains to the monodeprotonated receptor); (b) From 5 to 50 equiv of $[Bu_4N^+]F^-$ (the band that develops at 600 nm pertains to the doubly deprotonated receptor). Figures are reproduced from reference **18**.

Similarly, Das, Ganguly and coworker reported selective naked eye sensing of fluoride anion by receptor **2a** and **2b** containing anthraquinone as chromogenic signaling subunit and thiourea (N,N´-(9,10-dihydro-9,10-dioxo-1,2-anthracenediyl)bis[N´-phenyl]) and urea(N,N´-(9,10-dihydro-9,10-dihydro-9,10-dioxo-1,2- antrhacenediyl)bis[N-phenyl]) binding sites respectively.[19] It was found that the receptor **2a** able to sense fluoride anion at RT, whereas receptor **2b** senses fluoride at 60°C. Both the receptors **2a** and **2b** have shown little or no affinity towards Cl^-, Br^-, and I^- ions. From quantum chemical calculations it was concluded that the comparative strong intramolecular hydrogen bonding between two urea functions of **2b** does not allow the fluoride ion to complex with the N−H donor atoms at RT.

Recently, Ghosh and coworker have shown visible and near-infrared sensing of fluoride by indole conjugated urea/thiourea ligands. It was found in the case of **3a** and **3b**, F^- shows selective color changes from colorless to pink even in the presence of other anions like Cl^-, Br^-, I^-, AcO^-, NO_3^-, $H_2PO_4^-$ (Figure 1.3).[20] It was found that fluoride deprotonates the indolic NHs in **3a–b** while other anions such as Cl^-, Br^-, I^-, AcO^-, NO_3^- and $H_2PO_4^-$ do not. The highly extended electronic conjugation of the planar deprotonated species results in absorption in the NIR region (λ_{max} equal to 904 nm and 936 nm for **3a** and **3b**, respectively). Test experiments with the bis-benzyl alkylated **3c–d** confirm the occurrence of the deprotonation at the indolic moiety as the event responsible for the NIR response. The arising of such an uncommon NIR band can have interesting applications whenever the presence of an endogenous chromophore in the UV/Vis region could interfere.

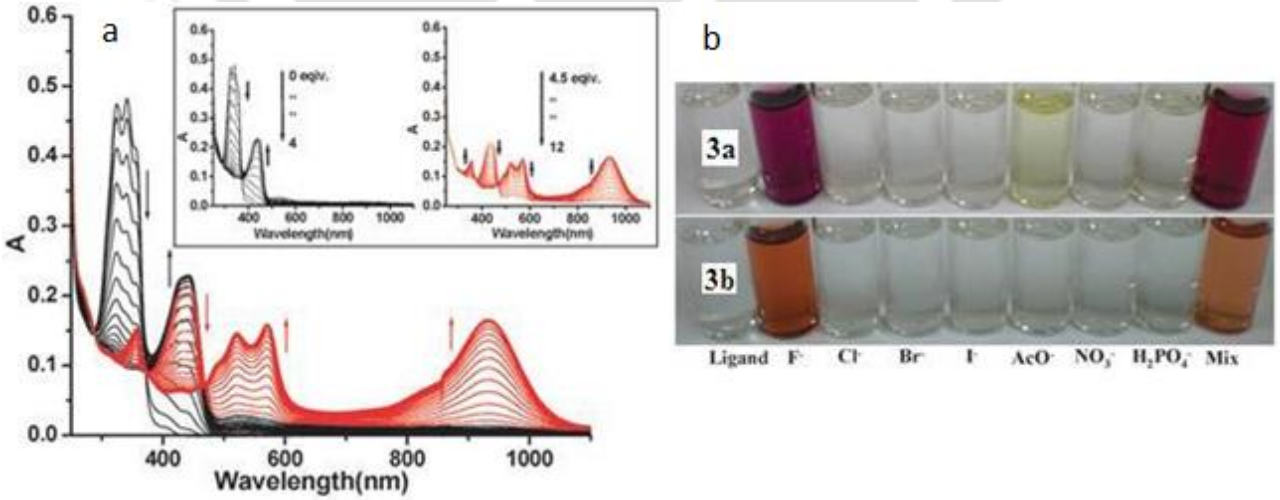

Figure 1.3 (a) UV/Vis absorption titration of **3a** (1.0×10^{-5} M) in MeCN–DMF (9.6 : 0.4 v/v) solution upon addition of fluoride ions. Inset showing separated spectra from the titration plot; (b) Color changes observed with the addition of anions to acetonitrile/dimethyl formamide 9.6:0.4 (v/v) solution of **3a** and **3b**. Figures are reproduced from reference **20**.

1.3.2 Anion coordination and anion directed assembly of multi-armed acyclic receptors

Although Nature exemplify how proteins can selectively and efficiently bind anions by weak intermolecular forces, the development of novel artificial receptors for the selective recognition of anions in solid state still remains a challenging task, with hydrogen bonds being fundamental in determining binding selectivity *via* topological complementarity. Anions generally have very high solvation energies that must be compensated by the host for effective anion recognition and complexation. Among the numerous design choices, multi-armed acyclic receptors have been especially of interest because of their potential ability to encapsulate the anions, such as nitrate, phosphate, and sulfate. The binding ability multi-armed acyclic receptors vary with the attached functionality unit, since functional groups modify the hydrogen bonding capability.

1.3.2a Tris(2-aminoethyl) amine based tripodal receptors

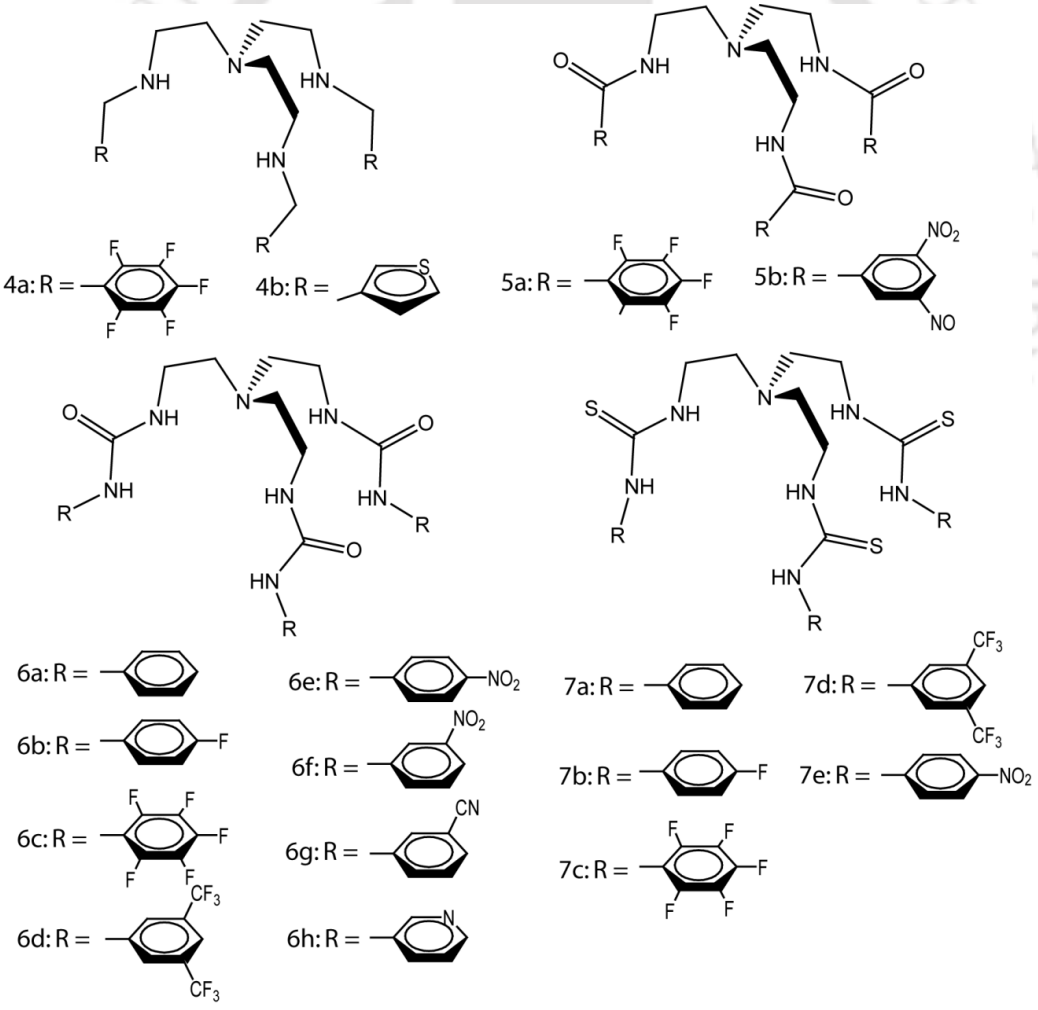

Scheme 1.4 Various *N*-bridged(tren based) tripodal anion receptors.

Tren-based tripodal amine receptors have been shown to coordinate with anions of different dimensionality in its triprotonated form. In this section, we take into account of two such tripodal

amine receptors, **4a** and **4b** (Scheme 1.4) bearing peripheral aromatic functions to discuss the structural aspects of anion binding in their protonated forms.

Ghosh and co-worker have shown a interesting example of anion binding by a tren based tripodal amine receptor by introducing a pentafluorophenyl unit as the aryl terminal to the tripodal scaffold (receptor **4a**).[21] Structural elucidation of the isostructural halide (F^-, Cl^- and Br^-) complexes, [(H_3**4a**)(X^-)$_3$] showed binding and encapsulation of a halide anion within the C_3v symmetric cavity of triprotonated **4b** *via* three N−H···X^- interactions (Figure 1.4a). In the case of complex [(H_3**4a**)(OTs^-)$_3$], tetrahedral *p*-toluenesulphonate anion is partially engulfed within the protonated

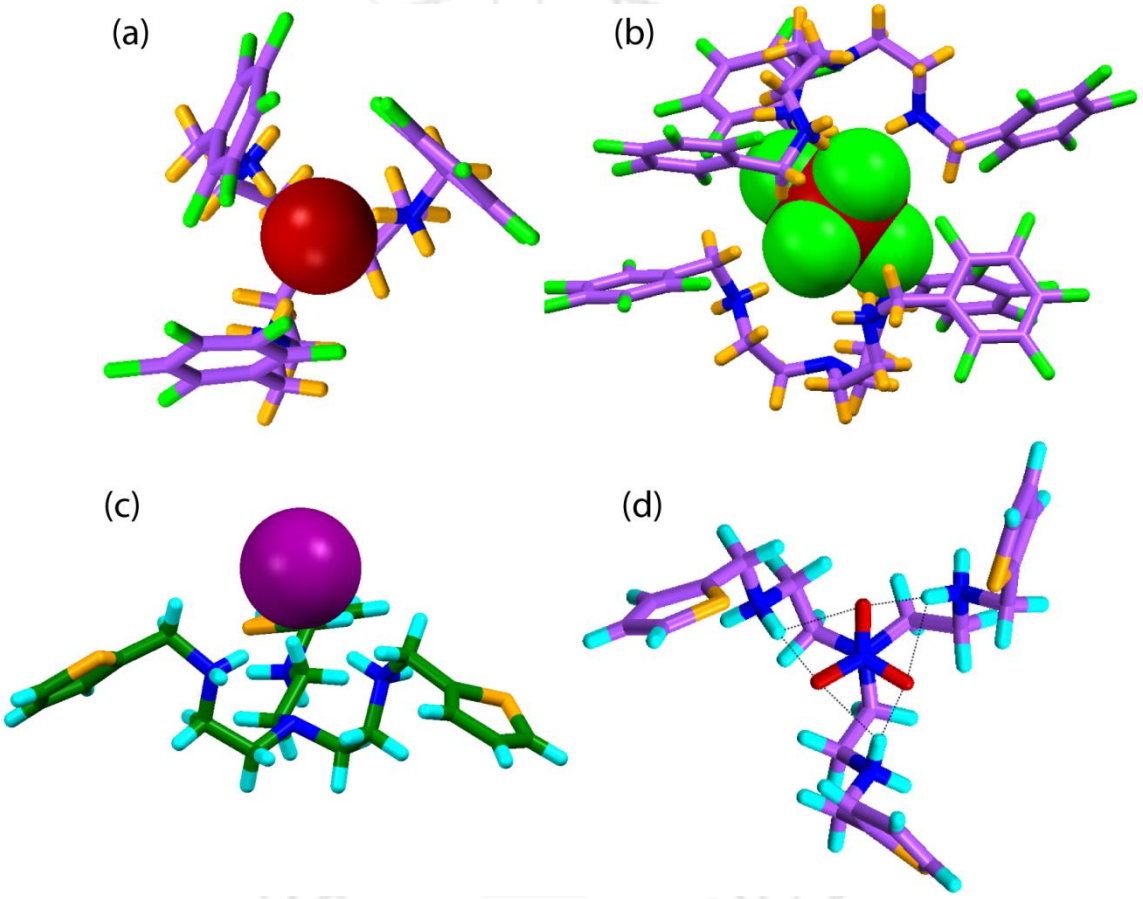

Figure 1.4 X-ray structures showing, (a) Binding and encapsulation of a Br^- anion by protonated **4a** in complex [(H_3**4a**)(Br^-)$_3$]; (b) Binding and pseudo-encapsulation of the SiF_6^- anion by two units of protonated **4a** in complex [(H_3**4a**)$_2$(SiF_6^{2-})(BF_4^-)$_4$]$CH_3OH{\cdot}H_2O$; (c) Binding of a I^- anion above the C_3 plane of protonated **4b** in complex [(H_3**4b**)(I^-)$_3$]; (d) Binding and encapsulation of a NO_3^- anion within the C_3 cavity of protonated **4b** in complex [(H_3**4b**)(NO_3^-)$_3$].

-receptor cavity *via* N−H···O interactions (Annexure 1). Interestingly, in the mixed anion complex [(H_3**4a**)$_2$(SiF_6^{2-})(BF_4^-)$_4$]$CH_3OH{\cdot}H_2O$, octahedral hexafluorosilicate anion is encapsulated within the dimeric capsular assembly of two inversion symmetric (H_3**4a**)$^{3+}$ units by a number of N−H···F hydrogen bonds (Figure 1.4b). The potentiometric titration experiments in a methanol/water (1:1

v/v) binary solvent system showed high affinity of the receptor toward more basic fluoride and acetate anions, with a lesser affinity for other inorganic anions.[21b]

Another interesting example of anion binding by a tripodal amine scaffold with a thiophene terminal **4b** has been demonstrated by Hossain et al. which shows encapsulation of a nitrate anion in a selective orientation, forming a C_3 symmetric complex, $[(H_3\mathbf{4b})(NO_3^-)_3]$.[22] The anion is coordinated to three protonated secondary amines with six N−H···O hydrogen bonds in a plane perpendicular to the principal rotation axis passing through the bridgehead nitrogen of the protonated receptor and the nitrogen of the encapsulated nitrate (Figure 1.4c). On the other hand, in the structure of the iodide complex $[(H_3\mathbf{4b})(I^-)_3]$, an iodide anion is bound above the quasi-planar tripod with the three arms pointing outward in a trigonal-planar-like arrangement (Figure 1.4d). ^{1}H NMR titration studies showed that the triprotonated receptor forms a 1:1 complex with nitrate yielding a binding constant of K = 315 M^{-1} in chloroform and showing a moderate selectivity over halides. Thus, the attached aryl terminals in the receptor designing could play an important role towards the formation of different microenvironment for selective anion binding and encapsulation.

However, the pentafluorophenyl-based tris(amide) receptor **5a** has been found to encapsulate a monohydrated F^- anion [TBA(**5a**·F^-H_2O)] and a naked Cl^- anion [TBA(**5a**·Cl^-)] within the receptor cavity when crystallized in presence of excess TBAF and TBACl from individual aqueous solutions of **5a** (Figure 1.5a and b).[23] In the crystal structure of complex [TBA(**5a**·F^-H_2O)], the F^- anion is bound in a distorted tetrahedral fashion *via* three amide N−H···F^- hydrogen bonds and a O−H···F^- hydrogen bond donated from the encapsulated water molecule (Figure 1.5a). Furthermore, the oxygen of the encapsulated water is in strong lp(lone pair)···π interaction with the pentafluorophenyl rings resulting in ditopic recognition of F^- and H_2O inside the small cavity of **5a** (Figure 1.5a). Whereas, monotopic recognition of Cl^- was observed in complex [TBA(**5a**·Cl^-)] where the Cl^- anion is in strong hydrogen bonding interaction with the three amide protons (Annexure 1). Recently, Das and co-worker have shown a π–acidic tris(amide) receptor, **5b** (Scheme 1.4) which behaves as a selective chemosensor for F^- ion by strong anion–π CT interaction and thereby, exhibits solvatochromism in different aprotic solvents.[24] Interestingly, the receptor showed a distinct behaviour towards complexation of F^- anion when tetrabutylammonium fluoride (TBAF)[24a] and potassium fluoride (KF) salts were individually employed for recognition of F^- with **5b**.[24b] Single crystal X-ray diffraction analyses showed that an F^- anion is bound within the receptor cavity by strong N−H···F^- and C−H···F^- hydrogen bonds irrespective of solvent of crystallization, when TBAF was employed as an F^- source. However, in presence of KF, the receptor is involved in side-cleft binding of a hydrated KF contact ion-pair governed by an amide N−H···F^-, an aryl C−H···F^- and a lp(F^-)···π interactions demonstrating a binding discrepancy of fluoride in quaternary

ammonium and alkali salts by **5b** in the solid-state. In case of other anions (Cl^-, Br^-, ClO_4^- and HSO_4^-) X-ray crystallography results showed that, anion binding with the protonated receptor is attributable entirely to N−H···A^- and C−H···A^- interactions in all the isolated complexes and in none of the cases anion encapsulation inside the receptor cavity was observed (Figure 1.5d).[24c]

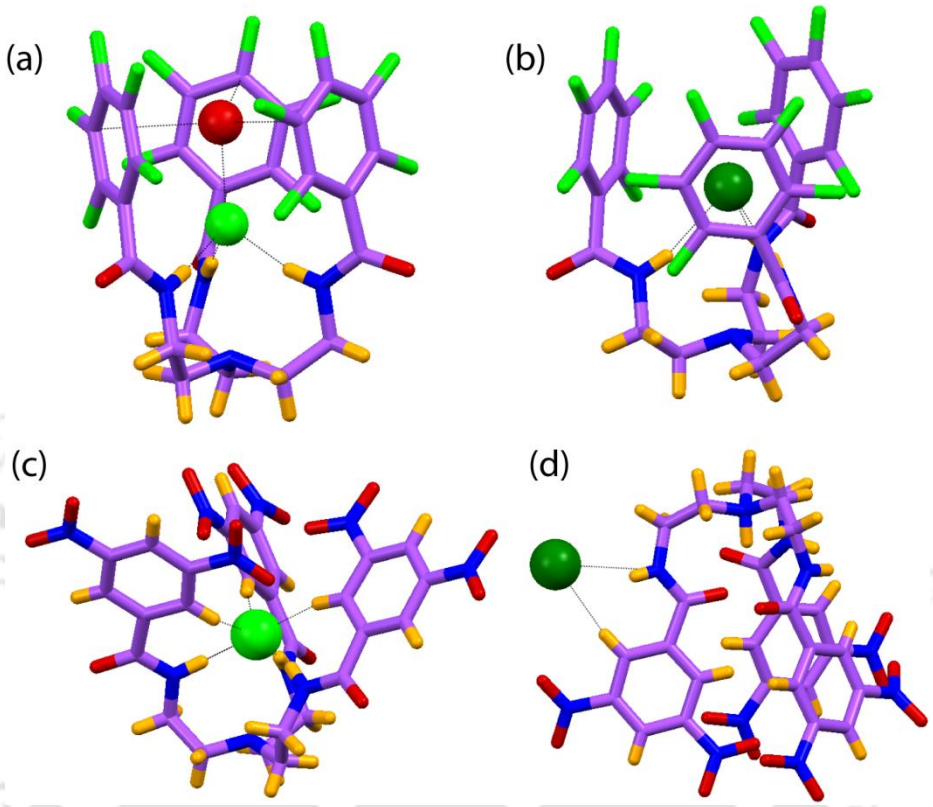

Figure 1.5 X-ray structures showing, (a) Encapsulation of a monohydrated F anion by receptor **5a**; (b) Chloride encapsulation within the receptor cavity of **5a**; (c) Encapsulation of naked F anion by receptor **5b**; (d) Outer capsular side cleft binding of chloride anion with protonated receptor **5b**.

Since the pioneering work of Wilcox[25] and Hamilton[26] that showed urea moieties can act as appropriate binding sites for anions, in particular oxoanions, a variety of acyclic receptors containing urea and thiourea subunits have been developed and applied for anion complexation and sensing over the past years. In particular, urea and thiourea functions can establish two directional hydrogen bonds with the planar anions (e.g., AcO^- and HCO_3^-) or chelate a spherical anion (e.g., halides). Thiourea is a much stronger acid than urea (pK_A = 21.1 and 26.9, respectively in DMSO), thus it is expected that thiourea containing receptors establish stronger hydrogen bond interactions and form more stable complexes with anions than their urea containing counterparts.[27] Furthermore, survey of tripodal anion receptors showed the dominant utility of urea and thiourea functionality over other classes of hydrogen bond donors.

Anion binding properties of tripodal urea and thiourea receptors **6a** and **7a** were studied using ^{1}H-NMR experiments.[28] In both the cases, a 1:1 complex stoichiometry was suggested upon binding of

a dihydrogen phosphate anion *via* six hydrogen bonds inside the tripodal cavity. However, based on the experimental results, Gale et al. has suggested that the thiourea receptor **7a** is capable of both chloride/nitrate antiport and more significantly of transporting the more hydrophilic bicarbonate anion *via* a chloride/bicarbonate antiport mechanism than its urea analogue **6a**.[29] The crystal structures of the carbonate complex of **6a** revealed that two receptor molecules are oriented in a face-to-face fashion and encapsulates a carbonate anion in the centre *via* twelve strong hydrogen bonding interaction.[29] With the continuation of previous work the same author has recently prepared a series of fluorinated tripodal anion receptors containing urea and thiourea groups including **6b-d** and **7b-d** (Scheme 1.4) and studied their anion complexation and transport properties.[30] ^{1}H NMR titration and subsequent binding constant determination showed that tripodal receptors **6b-d** and **7b-d** can bind anions in DMSO/water solutions according to the trend SO_4^{2-} > $H_2PO_4^-$ > Cl^- > HCO_3^- > NO_3^- with various deprotonation events occurring upon interaction with $H_2PO_4^-$ or HCO_3^-. They have also shown that, in competitive DMSO/water mixtures, the compounds with the most acidic NH protons have the lowest association constants—resulting in higher binding constants for the ureas compared to those of thioureas and for those of the unfluorinated compounds compared to those of the fluorinated compounds. Whereas, X-ray diffraction revealed the ability of the tripodal receptors to bind different anions with varying affinities in a 1:1 or 2:1 stoichiometry in solution and in the solid state.

Interestingly, Ghosh and coworker have shown efficient fixation of aerial carbon dioxide as carbonate by a tripodal urea receptor in presence of TBAOH is demonstrated **6c** by crystallizing the carbonate encapsulated molecular capsule in almost quantitative yield, followed by regeneration of free receptor from the capsule under mild conditions.[31] Structural elucidation of the complex revealed that a CO_3^{2-} anion is encapsulated within the dimeric cage structure of two **6c** molecules by as much as 16 hydrogen bonds from the six urea groups (Figure 1.6c). The ^{1}H NMR titration data gave the best fit for a 1:2 stoichiometry of guest to host with an overall association constant of log K = 4.04, which supported the solution state existence of capsular assembly as observed in the solid state structure. Latter, similar fixation of aerial carbon dioxide by the *meta* nitro substituted tripodal urea receptor **6f** in presence of both TBAOH and TBAF has shown by Das and coworker.[32]

Similar to carbonate encapsulation, Gosh and coworker have also shown that the receptor **6c** can able to encapsulate sulfate anion within its dimeric capsular assembly (Figure 1.6c), and the disordered sulfate anion is stabilized *via* 14 N−H···O hydrogen bonds with six urea functions.[33] An identical mode of sulfate binding (2:1 host-guest) within the cage of two inversion-symmetric molecules of receptor (**6b** and **6f**) has reported by Gale et al and Das et al individually.[30,32] Another interesting example of 1:1 hydrated sulfate encapsulation by the urea receptor **6e** has shown by Ganguly, Das and co-worker.[34] Structural analysis of the sulfate complex of **6e** showed that, all

three urea functions are involved in N−H···O hydrogen bonding with a sulfate anion which is further hydrogen bonded to three water molecules resulting in a nine coordination number for the encapsulated sulfate (Annexure 1). The concurrent interactions of three lattice water molecules with two encapsulated sulfate anions by O···H−O−H···O hydrogen bonds generates a rugby ball shaped sulfate–water–sulfate adduct held inside a pseudo dimeric assembly of receptor **6e**. The binding constant values calculated from the UV/Vis titration experiments revealed the preferential binding of SO_4^{2-} and $H_2PO_4^-$ over other oxyanions in an acetonitrile/water mixture (95/5, v/v) solution.

In contrast to the urea based receptor **6c**, the sulfate complex of the thiourea analogue **7c** showed a 1:1 stoichiometry as observed in solution. Six strong hydrogen bonds between the sulfate oxygen atoms and the thiourea –NH functions are responsible for the complex formation. Additionally, one of the TBA counter ions is held in close contact with the encapsulated sulfate anion *via* three C−H···O interactions donated from the CH_2 groups adjacent to the positively charged nitrogen in TBA cation (Figure 1.6e). An identical mode of cation sealed sulfate binding by tris-(thiourea) receptor **7e** (1:1 host-guest) has recently reported by Das et al (Figure 1.7d).[35]

Structural analysis of the crystals of the dihydrogen phosphate complexes of **6c** and **7c** showed that a $H_2PO_4^-$ anion is bound inside the tripodal cleft by seven hydrogen bonding interactions. Additionally, the encapsulated $H_2PO_4^-$ is hydrogen bonded with another $H_2PO_4^-$ to form a centrosymmetric dimer, with non-intercalated arms between the two tripodal receptor units (Figure 1.6e).[30,36] Interestingly, it was found that the addition of 2 equivalents TBAOH in to the DMSO solution of the dihydrogen phosphate complexes of **6c** results 2:1 receptor-HPO_4^{2-}complex.[36b] The charge dependent anion binding discrepancy of phosphates has been further demonstrated by simple acid/base treatment *via* solution state ^{31}P-NMR studies. On the other hand, the complexes formed by **7b** and **7d** with TBA(H_2PO_4) showed the deprotonation of bound $H_2PO_4^-$ anion as observed in solution during ^{1}H NMR titrations and crystallized as 2:1 receptor-HPO_4^{2-} complexes in the presence of excess TBA(H_2PO_4). In both the cases, a HPO_4^{2-} anion is bound inside the dimeric capsular assembly of the receptor by 14 hydrogen bonds to the six thiourea functions.[30] Interestingly, receptor **7e**, in the presence of excess $H_2PO_4^-$ has been found to encapsulate a trivalent phosphate ion within a π-stacked dimeric capsular assembly of the receptor with twelve strong H-bonds *via* deprotonation. The deprotonation process exemplified in solution by ^{1}H NMR titration with $H_2PO_4^-$ ions, where slow exchange of complexes were observed involving the change of the binding mode from a 1:2 to a 2:1 host–guest stoichiometry.[37]

The tetrabutylammonium chloride complexes of receptors **6b**, **6b**, and **6c** crystallized as 1:1 complexes, reflecting the stoichiometry observed in solution. In all three complexes, a chloride anion is bound within the tripodal cavity by six N−H···Cl^- hydrogen bonds, one from each NH group.[30,33] Similarly, binding of fluoride within the tripodal cavity is also governed by six N−H···F^-

hydrogen bonds (Figure 1.6a), as observed in the crystal structure of fluoride complex of **6c**. The solution state binding of F^- with **6c** was also clearly shown by the ^{19}F-NMR spectrum in DMSO-d_6.[33] Interestingly, hydroxide encapsulated pseudocapsular, complex of **6c** was formed when the receptor (**6c**) is treated with $Bu_4N^+CN^-$ (Figure 1.6b).[36b] The in situ generated OH^- inside the cavity of **6c** and atmospheric moisture are playing the role behind the encapsulation of hydroxide in presence of TBACN.[36b]

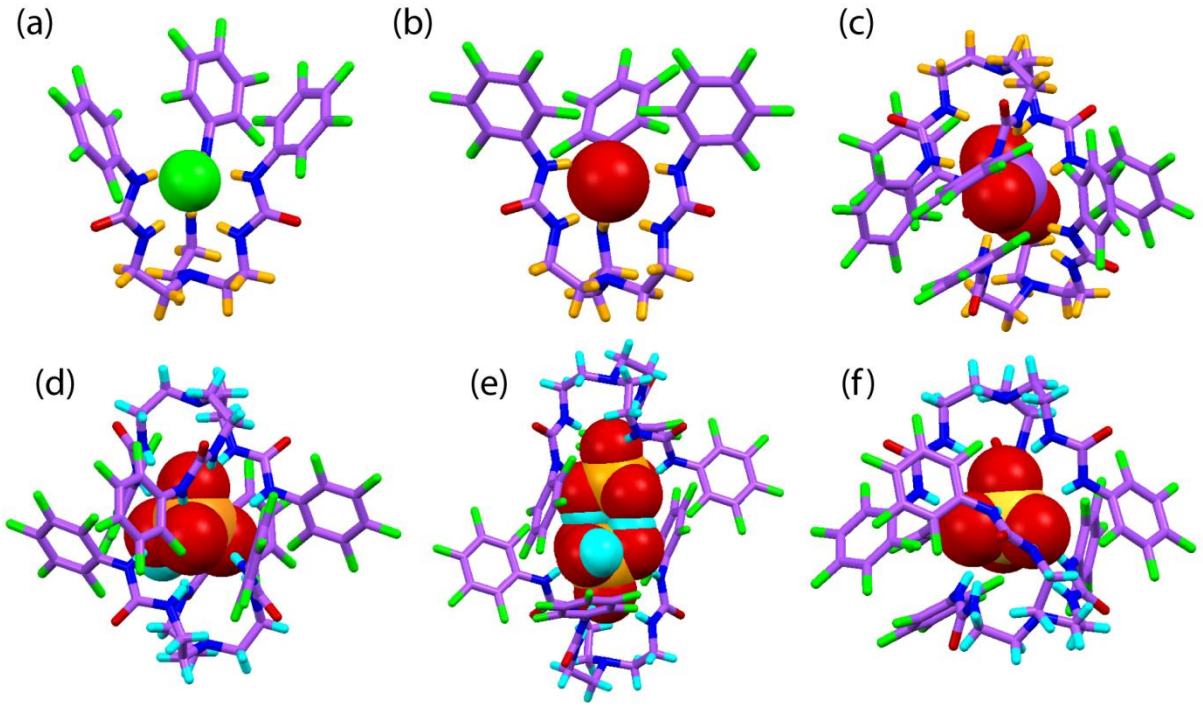

Figure 1.6 X-ray structures showing, (a) Fluoride encapsulation within the receptor cavity of **6c**; (b) Fluoride encapsulation within the receptor cavity of **6c** (obtained in presence of CN^-); (c) CO_3^{2-}–encapsulated dimeric capsule of **6c** (obtained in presence of OH^-); (d) HPO_4^{2-}–encapsulated dimeric capsular assembly of **6c**; (e) Encapsulation of hydrogen bonded $H_2PO_4^-$ dimer within a pseudo-dimeric capsular assembly of receptor **6c**; (f) SO_4^{2-}–encapsulated dimeric capsular assembly of **6c**.

It is however, interesting to note that functionalization of **6a** with metal-coordinating *m*–CN groups afforded the receptor **6g** that has been utilized by Custelcean et al. for the selective separation of SO_4^{2-} over other anions *via* the formation of a selective MOF (Metal–Organic Framework).[38] Complexation of **6g** with 0.5 equivalents of Ag_2SO_4 in water/acetone yielded a coordination polymer with the composition $[Ag_2(\mathbf{6g})_2(SO_4)](acetone)1.5(H_2O)_{3.7}$, as indicated by elemental analysis and single-crystal X-ray diffraction. Both molecular modelling (MMFF94) and crystal structure analyses showed that SO_4^{2-} is coordinated to two molecules of **6g** with twelve hydrogen bonds from the six urea groups. Additionally, two receptor molecules that encapsulate a SO_4^{2-} anion are held together by CN–Ag and C=O–Ag coordinative bonds to form a molecular cage (Figure 1.8a). Attempts to crystallize **6g** with other soluble silver salts having anions of different

geometry and basicity such as $AgBF_4$, $AgNO_3$, $AgMeSO_3$ and $AgMeCO_2$ failed to produce coordination polymers and yielded crystals of the free ligand only. Similarly, crystallization of **6f** in presence of $(Me_4N)_2SO_4$ was also unsuccessful which indicated that silver coordination and MOF formation are critical in stabilizing the sulfate encapsulated dimeric capsule.

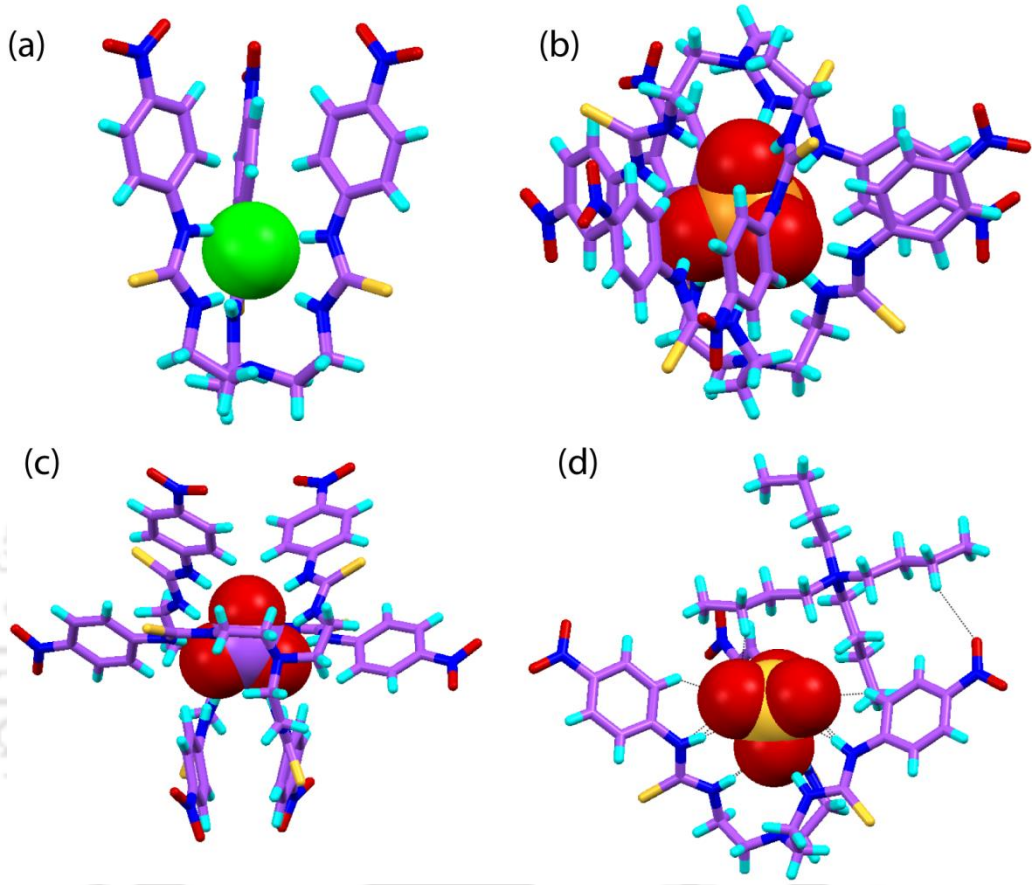

Figure 1.7 X-ray structures showing, (a) Fluoride encapsulation within the receptor cavity of **7e**; (b) encapsulation of a trivalent phosphate (PO_4^{3-}) within a dimeric capsular assembly of receptor **7e**; (c) Carbonate encapsulated dimeric capsular assembly of cavity of **7e**; (d) Showing the formation of the TBA cation sealed SO_4^{2-} encapsulated unimolecular capsule **7e**.

Based on similar ideas, Custelcean et al. and Wu et al. have independently prepared the urea receptor **6h**, for the effective binding of oxyanions by the formation of crystalline capsules.[39] It was found that the external countercations can drastically influence the size of the capsules by controlling their close packing in the crystalline state. This structural trend can be most conveniently followed in series of structures with similar packing modes. The ligand **6h** was found to persistently crystallize with various oxoanion salts M_nX (M = Na, K, Mg, Ca, Cd; X = SO_4^{2-}, SeO_4^{2-}, CrO_4^{2-}, SO_3^{2-}) into isomorphous series of frameworks with three different compositions: $MX(\mathbf{6h})_2(H_2O)_6$ (M = Mg, Ca, Cd) (I), $Na_2X(\mathbf{6h})_2(H_2O)_4$ (II), and $K_2X(\mathbf{6h})_2(H_2O)_2$ (III).[40] All three series of crystal structures (I–III) displayed similar NaCl-type packing consisting of alternating

$X(\mathbf{6h})_2^{2-}$ anionic capsules and $M(H_2O)_6^{2+}$, $Na_2(H_2O)_4^{2+}$, or $K_2(H_2O)_2^{2+}$ cations (Figure 1.8 and Annexure 1). In all of these crystals, the anionic capsules are in close contact to each other as they pack octahedrally around the countercations and optimize their Van der Waals interactions. Consequently, as the cations decrease in size in the order $M(H_2O)_6^{2+}$ (Ca > Cd > Mg) > $Na_2(H_2O)_4^{2+}$ > $K_2(H_2O)_2^{2+}$, so does the size of the anionic capsules as they pack more closely together to compensate for the difference in the cations' volume. The most prominent change is observed in the heights of the capsules, as measured between the two tertiary bridgehead N atoms belonging to the two opposite ligands, which were found to vary between 9.20 and 9.83 Å. In fact, there is a good linear correlation between the height of the capsules and either the volume or the surface area of the countercations (Annexure 1).[40] Further, the competition experiments of **6h** with these anions established the following anion selectivity order: SO_4^{2-} > SeO_4^{2-} > CO_3^{2-} > SO_3^{2-} which is different from both the Hofmeister bias and anion basicity scale whereas the trend was in agreement with the lattice energy calculations on the crystal structures. Custelcean et al. has further investigated the fundamental factors controlling the anion selectivity of **6h** by solution and solid state thermodynamic measurements and anion competition experiments in water.[41]

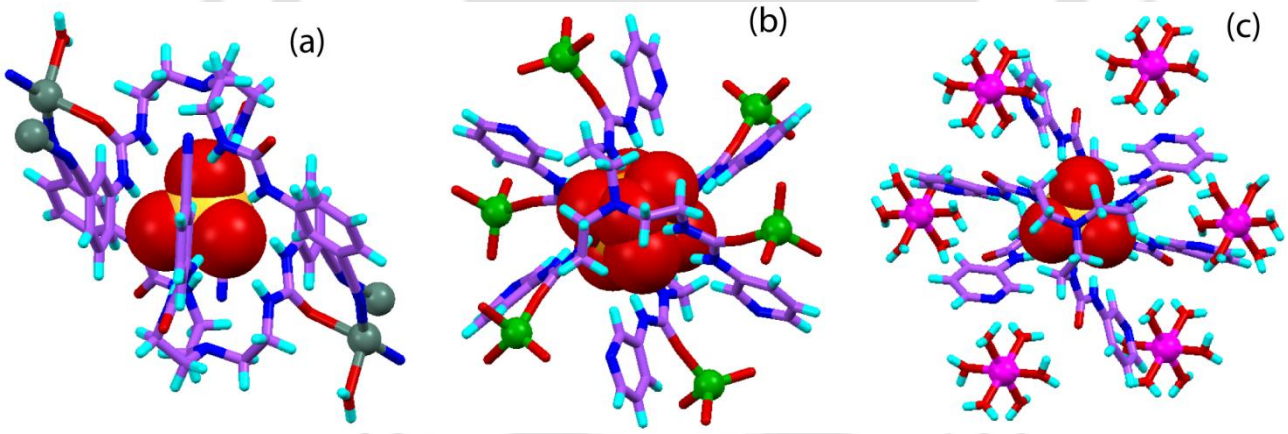

Figure 1.8 X-ray structures showing, (a) SO_4^{2-} encapsulated rigid dimeric cage in complex $[Ag_2(\mathbf{6h})_2(SO_4)](acetone)1.5(H_2O)_{3.7}$ stabilized by Ag^+ coordination; (b) SO_4^{2-}–encapsulated rigid dimeric cage in complex $[LiSO_4(\mathbf{6h})_2(H_2O)_2]$, stabilized by multiple hydrogen bonded water bridges, and (c) SO_4^{2-}–encapsulated rigid dimeric cage in complex $[ZnSO_4(\mathbf{6h})_2(H_2O)_6]$, stabilized by Zn^{2+} coordination and hydrogen bonded water bridges.

1.3.2b Arene based multiarmed acyclic receptors

Similar to the *N*-bridged (tren based) receptors, arene-based multiarmed acyclic receptors have also been found to encapsulate anion/anion water clusters.

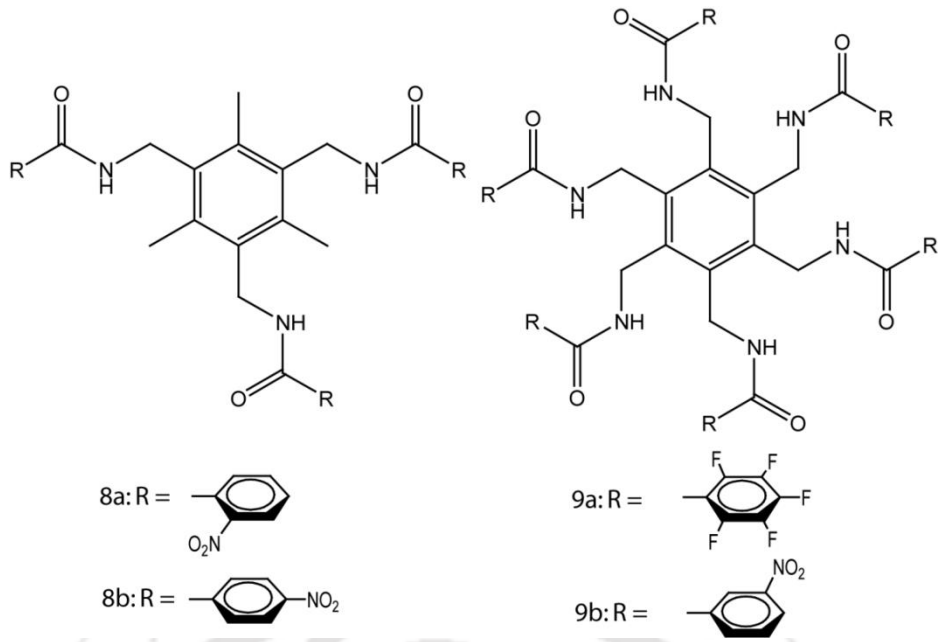

Scheme 1.5 Various arene based tripodal and hexapodal anion receptors.

Ghosh et. al structurally demonstrated the selective formation of a hydrated fluoride anion, $[F_2(H_2O)_6]^{2-}$, cluster induced dimeric capsule from an arene based tripodal amide receptor with a ortho-nitrophenyl terminal, **8a** (Scheme 1.4).[42] The amidic NH sites of the receptor are too widely separated to offer a suitable binding pocket for a single fluoride anion. This results the formation of an interesting aggregate (Figure 1.9a). The anion–water cluster is formed *via* hydrogen bonding interactions such as O–H···O and O–H···F and the hydrated fluoride guest is hydrogen bonded with the receptor *via* N–H···O and N–H···F interactions. It was found the receptor **8a** did not form a capsular assembly upon complexation with other anions like nitrate, acetate and chloride. These anions showed simple recognition inside the receptor cavity (Figure 1.9c and e). Similar tripodal triamide receptor with $–NO_2$ substituents at the para position, **8b** was found to form complex with NO_3^-, AcO^-, F^- and Cl^-. All these anions assisted the formation of the dimeric capsular assembly by encapsulating two nitrates, $[AcO(H_2O)_4]_2^-$, $[F_2(H_2O)_6]_2^-$ and $[Cl_2(H_2O)_4]^{2-}$, as an anionic species inside the capsular cavity (Figure 1.9b, d and f).[42b] Therefore, simple variation in the position of the electron withdrawing substituents in the aryl terminals of the tripodal receptor shows subtle change in the pattern of anion induced assembly.

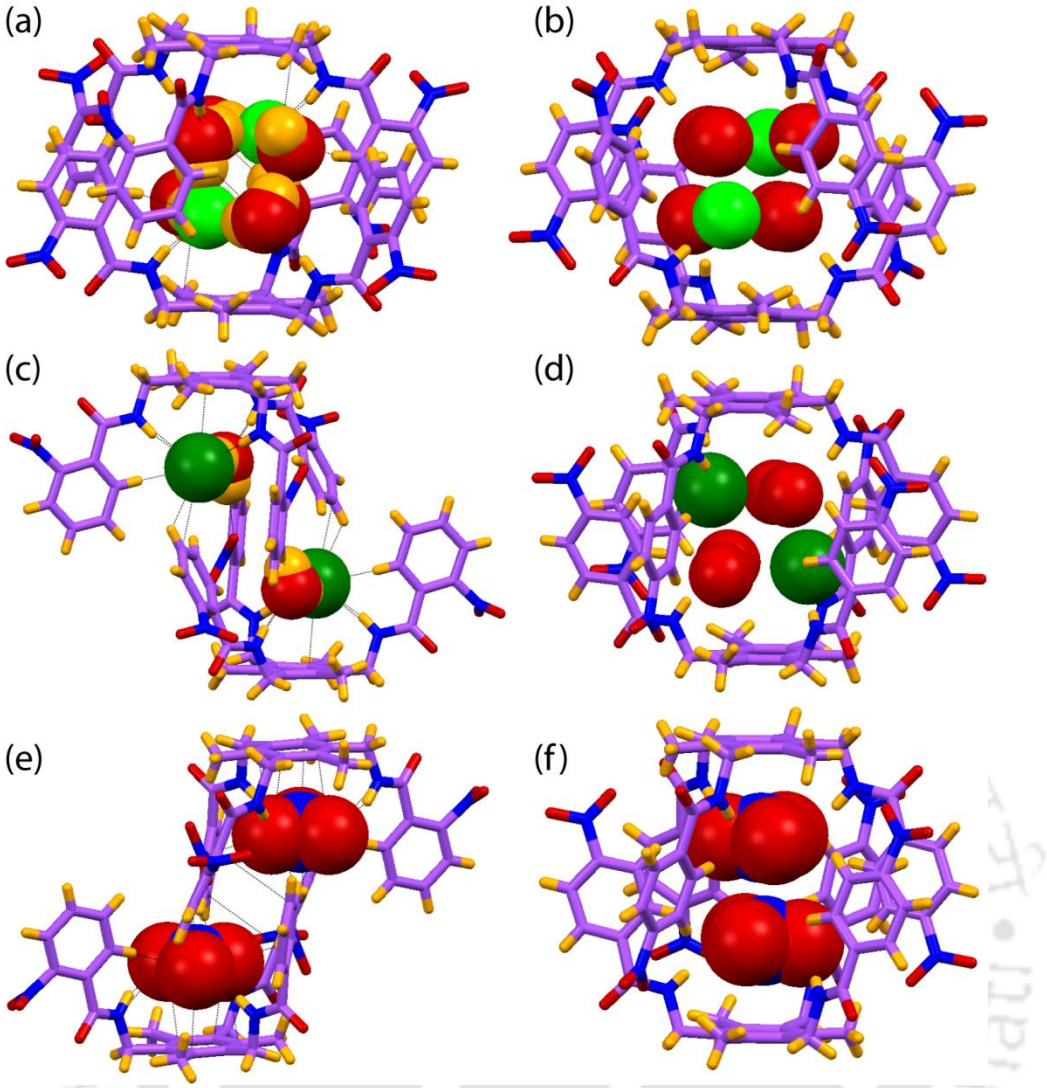

Figure 1.9 X-ray structures showing, (a) Encapsulation of $[(F^-)_2(H_2O)_6]$ adduct within the dimeric assembly of **8a**; (b) Encapsulation of $[(F^-)_2(H_2O)_6]$ adduct within the dimeric assembly of **8b**; (c) Non-capsular aggregation of **8a** upon chloride anion binding; (d) Encapsulation of $[(Cl^-)_2(H_2O)_4]$ adduct within the dimeric assembly of **8b**; (e) Non-capsular aggregation of **8a** upon nitrate anion binding; (f) Showing the encapsulated nitrate inside the dimeric capsule of **8b**.

With the continuation of previous work the same group has expanded the dimension of the anion receptors from tripodals to hexapodals. A hexasubstituted benzene platform was decorated with amide functionality as an appropriate anion binding element around the benzene platform. the hexa armed amide receptor **9a** with pentafluorophenyl terminals was found to bind with multiple anions in its bistripodand fashion.[43] The nitrate complex of **9a** showed the recognition of four nitrate anions and two water molecules as a cascade complex in its more stable bistripodand conformation (Figure 1.10a). Interestingly, in an acetate complex, the receptor moiety of **9a** in the acetate bound state showed the formation of a pseudo cage from two half-units of the receptor, composed of six arms that hold two acetate anions inside each cage of an infinite capsular network as shown in (Figure 1.10b and Annexure 1). The same group further demonstrated the usefulness of hexapodal

receptors by showing the structural evidence of $[F_4(H_2O)_{10}]^{4-}$ assisted dimeric assembly of hexaamide **9b** with m-NO_2-C_6H_4 terminals (Figure 1.10c).[44] The Job's plot for **9b** with F^- showed a host–guest stoichiometry of 1:2. The solid state structure of the fluoride complex of **9b** revealed that all arms of **9b** are projected unidirectionally to engulf the fluoride–water cluster, $[F_4(H_2O)_{10}]^{4-}$, in the cavity of the capsular assembly (Figure 1.10c).

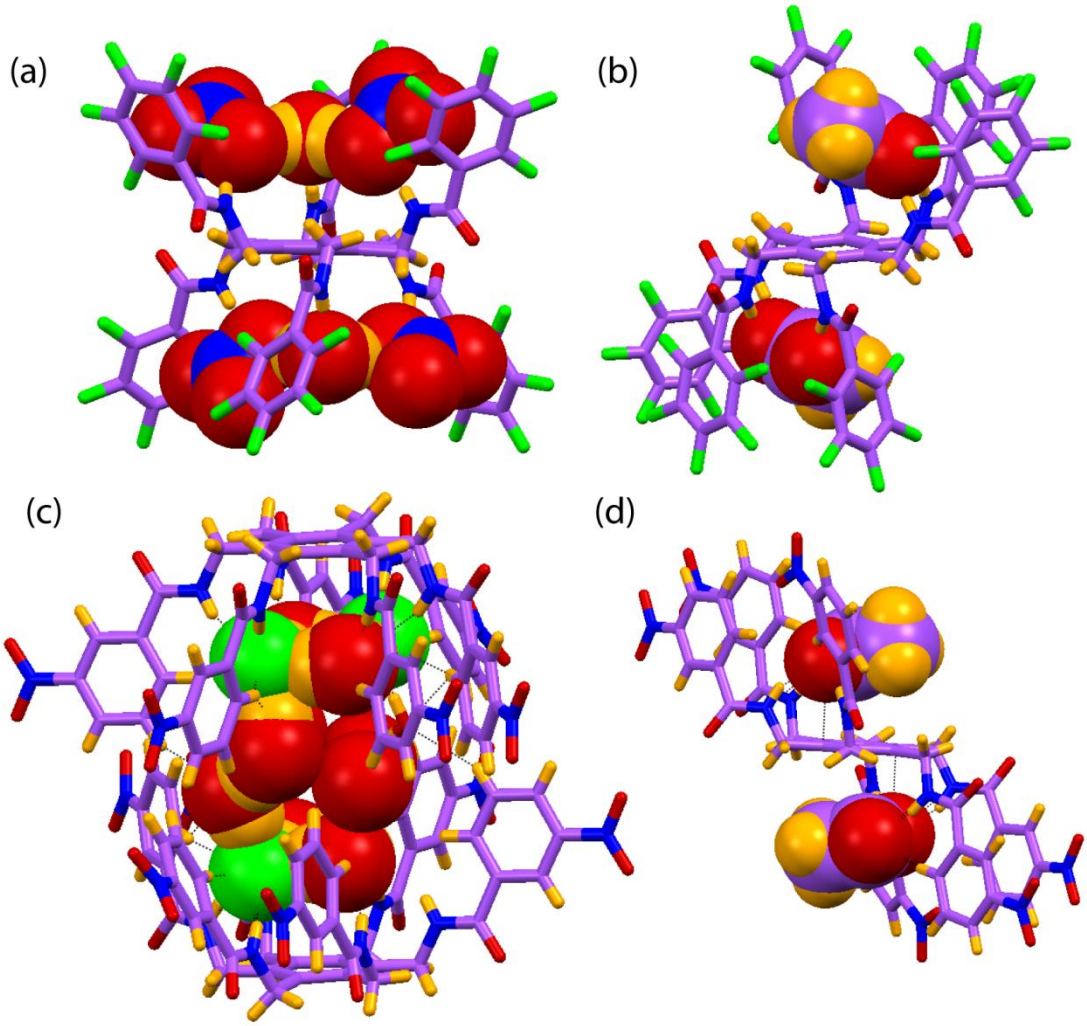

Figure 1.10 X-ray structures showing, (a) Space filling view of the encapsulated nitrates and water molecules inside the double-decker host of **9a**; (b) Showing the encapsulated acetate ion molecule above and below the benzene scaffold of **9a**; (c) Encapsulation of $[F_4(H_2O)_{10}]^{4-}$ cluster inside the dimeric capsule-like assembly of **9b**; (d) Showing the encapsulated acetate ion molecule above and below the benzene scaffold of **9b**.

1.4 Ion-pair receptor chemistry

For many decades there has been considerable interest in the design of synthetic host systems for cations, and more recently for anions. However, these monotopic receptors are designed to bind a cation or anion only. As a consequence, there is an energetic cost that has to be overcome to separate the individual cation or anion from its counter ion for binding to take place. The design of

heteroditopic receptors containing recognition sites for both the cation and anion, that is, ion-pair recognition, is an emerging field of research.[45,46] Ion-pair recognition has important applications in the development of membrane transport, salt extraction, and salt solubilization agents and sensors.[47,48]

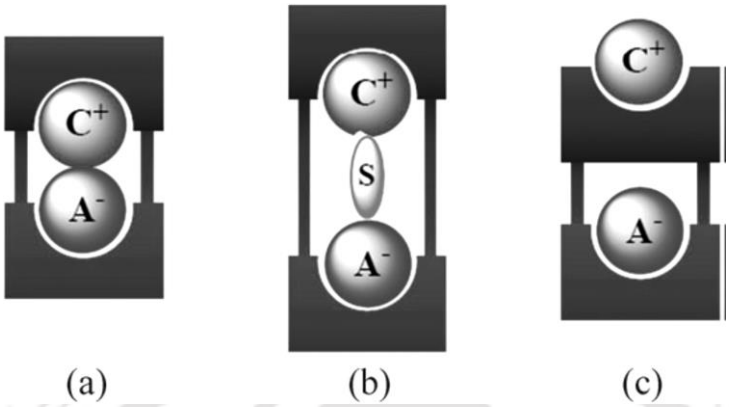

Scheme 1.6 Limiting ion-pair interactions relevant to receptor-mediated ion-pair recognition: (a) Contact; (b) Solvent-bridged, and (c) Host separated. In this schematic, the anion is shown as ''A^{-}'', the cation as ''C^{+}'', and the solvent is represented as ''S''. This scheme is reproduced from reference **50**.

The classification of ion-pair receptors depends on how they bind the cations and the anions of targeted ion-pairs. Here, three different binding modes can be defined. These limiting modes are depicted in Scheme 1.6 and differ in how the ion-pair is held within a host molecule. The first involves a contact ion-pair, wherein the anion and the cation are in a direct contact (Scheme 1.6a); the second, termed a solvent-bridged ion-pair, is where one or more solvent molecules bridges the gap between the anion and the co-bound cation (Scheme 1.6b), while the third consists of a host-separated ion-pair, wherein the anion and the cation are bound relatively far from one another, usually by the receptor framework (Scheme 1.6c).[49,51] Depending on the identities of co-bound ions, the separation distance between ion-pairs, the nature of the constituent recognition sites, and the nature of the solvents, a given receptor can bind a given ion-pair in one or more of these limiting modes.

1.4.1 Ion-pair recognition by acyclic receptors

Since the pioneering of the field Smith,[46] Beer[50] and Sessler[51] have shown various macrocyclic or crown ether based receptors for recognition of ion-pairs. But it is important to mention that the binding of any guests within pre-organized macro cyclic systems are relatively straight forward to understand but the binding processes of acyclic receptors always remain more elusive and the examples of acyclic receptors in literature are very less compare to cyclic or macrocyclic ion-pair

receptors.[50,51] Therefore, in this section we have focused the examples of heteroditopic acyclic receptors that can bind both cation and anion simultaneously.

1.4.1a Pridylureas and bipyridine-bis(urea) based ion-pair receptors

Steed and co-worker have reported the solid and solution state binding properties of pridylureas **10a** and **10b** in the presence of silver nitrate, sulfate and triflate salts (Scheme 1.7).[52] These researchers found that when the counter anion was nitrate a 1:1 receptor-salt complex was formed, while the sulfate and triflate salts serve to stable extended structures in the solid state with pyridal ligands (Figure 1.11a and Annexure 1). On the basis of ^{1}H NMR spectroscopic studies, the authors concluded that the simple silver nitrate complex also forms in solution. These same researchers subsequently put forward other examples of this paradigm.[53]

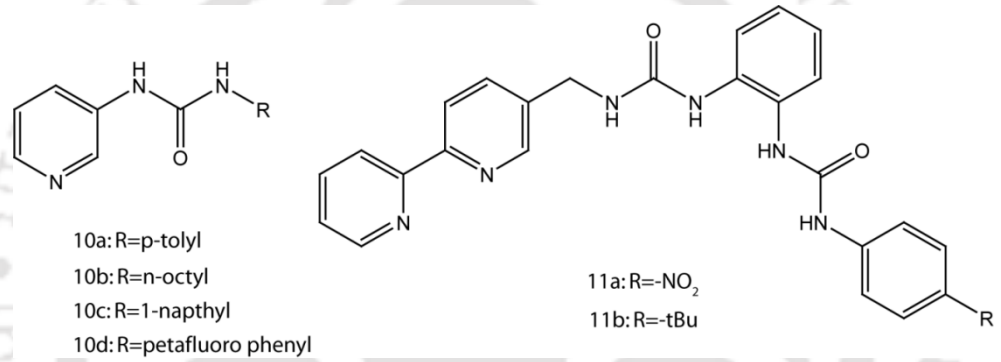

Scheme 1.7 Various pyridine and bipyride based acyclic ion-pair receptors having anion binding urea functions.

Based on similar ideas, Wu et al. and Ghosh et al. have independently prepared the urea receptor **10c** and **10d** respectively, for the effective binding of sulfate anion in presence of Cu^{2+} counter ion. The receptor **10c** forms ion-pair complex with $CuSO_4$, the crystal structure of ion-pair complex shows that the Cu^{2+} ion is coordinated by six **10c** molecules in an octahedral (O_h symmetry) arrangement, thus forming two oppositely located, inversion-related C_3-symmetric clefts.[54] Two complex molecules are aligned along the C_3-axis to create a cavity that encapsulates a sulfate ion in its center (Figure 1.11b). The capsules further extend into an infinite 1D chain (Annexure 1). All the six urea arms within a capsule participate in hydrogen bonding with the encapsulated sulfate ion.

The $CuSO_4$ complex of **10d** shows that the Cu^{2+} is coordinated by four **10d** and two DMF molecules trans to each other in a distorted octahedral arrangement, thus forming two oppositely located inversion-related C_2-symmetric clefts. Two molecules of the Cu^{2+} complex are aligned along the C_2-axis to create a cavity that encapsulates a SO_4^{2-} ion in its centre (Figure 1.11c). All the four urea arms within a capsule participate in hydrogen bonding interactions with the encapsulated SO_4^{2-}.[55]

Recently Custelcean and coworker developed ditopic 2,20-bipyridine-bis(urea) receptors **11a** and **11b**. The receptors forms ion-pair triple helicates and mesocates with $NiSO_4$ or $FeSO_4$ *via* self-assembly process. In these ion-pair complexes the metal ion (Ni^{2+}/ Fe^{2+}) is stabilized *via* octahedral coordination of three bipyridine units, and the sulfate anion is encapsulated by three bis-urea functions *via* formation of 12 N−H···O hydrogen bonds (Figure 1.11e).[56]

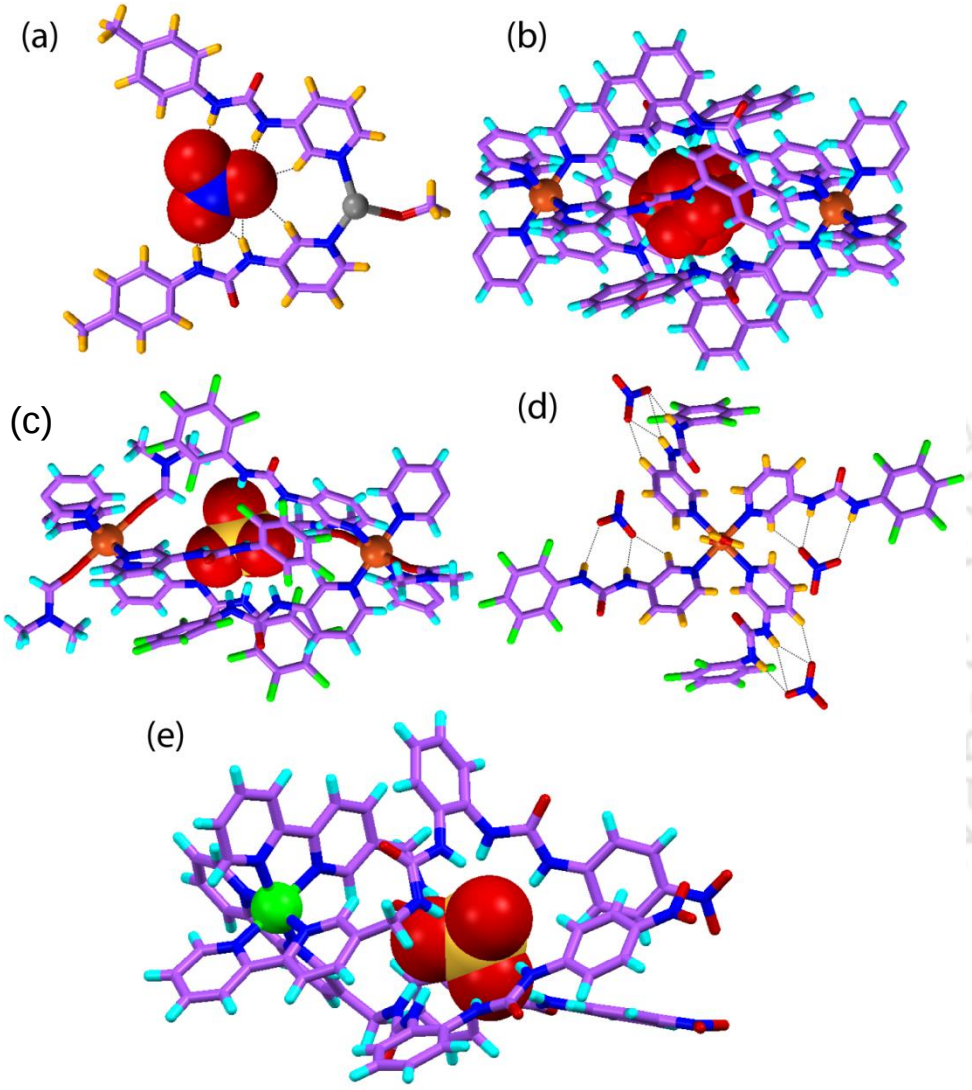

Figure 1.11 X-ray structures showing: (a) Formation of the discrete [Ag(**10a**)$_2$]NO_3 MeOH complex; (b) $CuSO_4$ complex of **10c**; (c) Second sphere recognition of SO_4^{2-} in $CuSO_4$ complex of **10d**; (d) $CuNO_3$ complex of **10d**; (e) Charge separated ion-pair complex of **11a** with $NiSO_4$.

1.4.1b Tripodal and hexapodal ion-pair receptors

Similar to the anion coordination chemistry the *N*-bridged and arene-based multiarmed acyclic receptors (Scheme 1.8) have also been found to form stable ion-pair complexes.

In 2005, Resnati and coworkers reported the tripodal ion-pair receptor **12a** that relies on halogen bonding (XB) for the recognition of anions, such as halides (Figure 1.12a).[57] The four strong electron-withdrawing fluorine atoms on the aromatic ring of receptor **12a** make the iodine atom an

effective XB donor. An X-ray crystal structure of the NaI complex revealed that in the solid state, receptor **12a** binds both the Na^+ cation and the I^- anion concurrently. However, as can be inferred from an inspection of Figure 1.12a, these latter species are spatially separated by the receptor at a distance of ca. 5.59 Å. This structure also revealed that the Na^+ cation is completely encompassed by the arms of the receptor and that the I^- anion is bound to the iodine atom of the tetrafluoroaromatic ring *via* an XB interaction. Compared to that of control compound **12b**, which lacks an XB donor (K_a = 1.3 x 10^4 M^{-1}), the binding constant of receptor **12a** was found to be 20 times larger (K_a = 2.6 x 10^5 M^{-1}). On this basis, it was concluded that the I···I^- XB interaction has a positive effect on the Na^+ binding in the case of receptor **12a**.

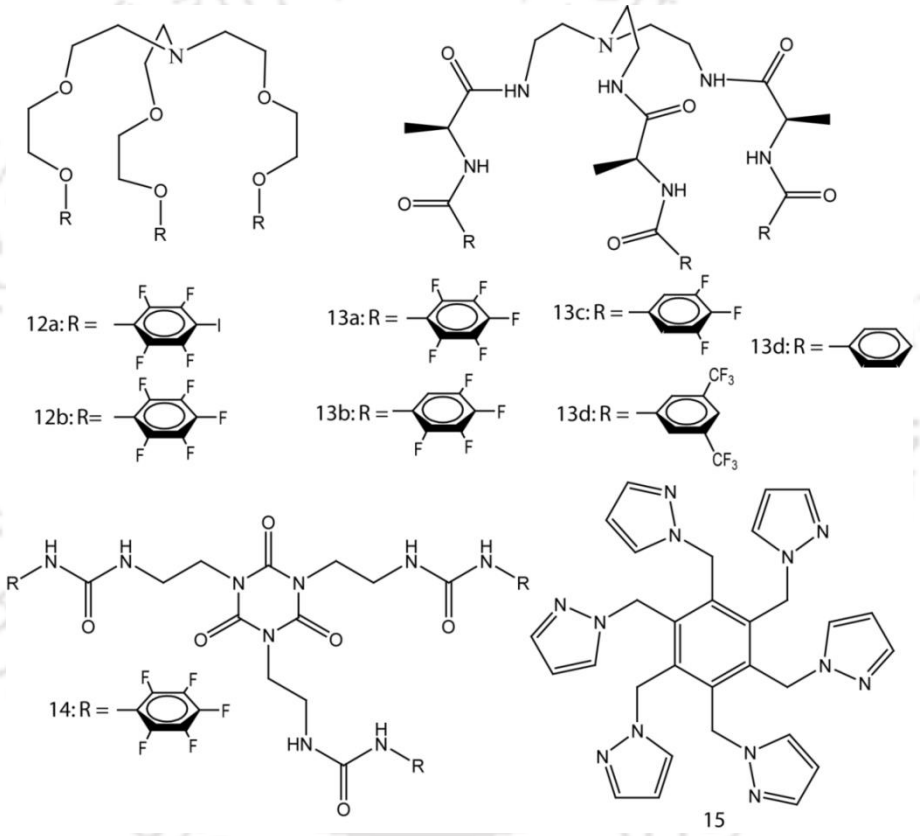

Scheme 1.8 Various *N*-bridged and arene-based tripodal and hexapodal ion-pair receptors.

Ghosh and coworker have shown a series of tris(2-aminoethyl) amine (tren)-based l-alanine amino acid backboned tripodal hexaamide receptors **13a-d** that can form ion-pair complexes with tetraalkylammonium (Me_4N^+, Et_4N^+ and Bu_4N^+) salts of Cl^-.[58] Single-crystal X-ray diffraction clearly showed that the pentafluorophenyl-functionalized amide receptor **13a** encapsulated Cl^- in its cavity by hydrogen bonds from amides, and the cavity of **13a** was capped with a TBA cation through hydrogen bonding and ion-pair interactions to form a capped-cleft orientation. The TBA counter cation is stabilized *via* hydrogen bonds and cation···π interactions with pentafluoro phenyl

rings of **13a** (Figure 1.12b). The detailed Cl^- binding studies with three different tetraalkylammonium (Me_4N^+, Et_4N^+, and Bu_4N^+) salts of Cl^- confirmed the role of cationic counterpart in solution-state Cl^- binding processes with this series of receptors**13a-d**. It was found these receptors with different tetralkylammonium salts of Cl^- gave binding constants with the TBA cation in the following order: butyl>ethyl>methyl. On the basis this study, it was concluded that the TBA counteraction has prominent role in ion-pair recognition by this series of receptors.

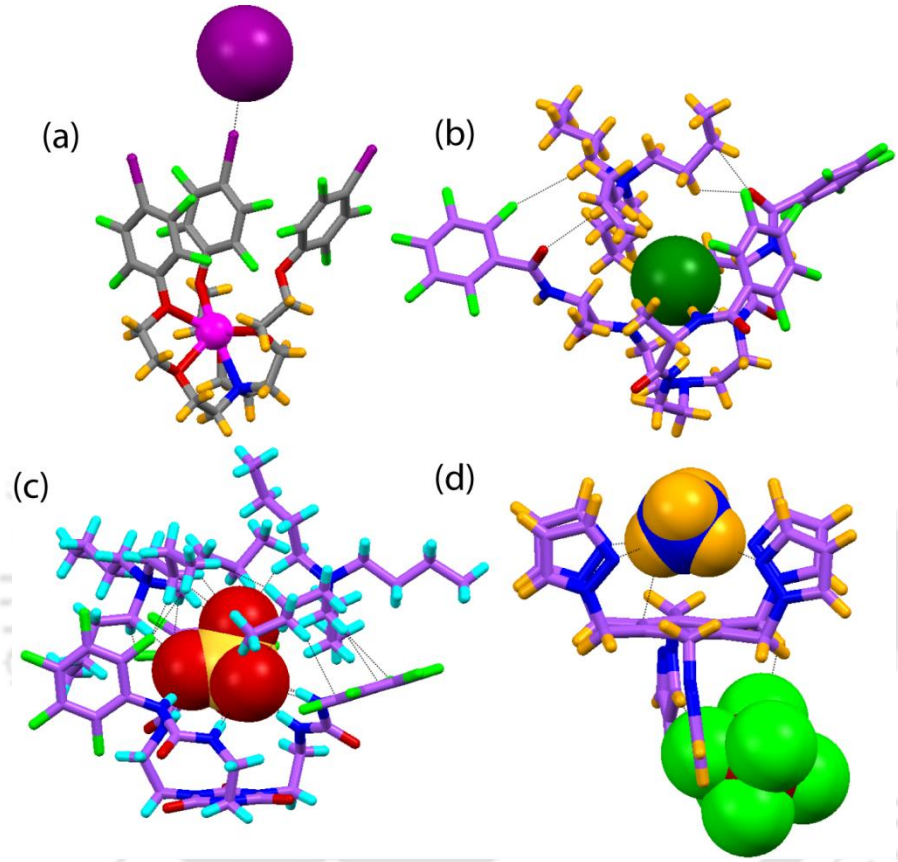

Figure 1.12 X-ray structures showing: (a) Crystal structure of NaI complex of **12a**. Iodide anion is stabilized *via* halogen bonding interactions; (b) Recognition of TBACl as contact ion-pair by an amino acid functionalized tripodal hexaamide anion receptor **13a**; (c) Contact ion-pair recognition of $(n\text{-}Bu_4N)^+{}_2SO_4^-$ by a cyanuric acid based receptor **14**; (d) The compartmental binding and ditopic recognition of NH_4^+ and PF_6^- in **15**.

The same group has shown another example of contact ion-pair ($(n\text{-}Bu_4N)^+{}_2SO_4^-$) recognition by a tripodal urea receptor **14** functionalized with pentafluorophenyl side arms on a rigid cyanuric acid platform.[59] The crystal structure of the ion-pair complex revealed that that SO_4^{2-} was completely encapsulated inside the shallow tripodal cavity *via* N–H···O hydrogen bonding interactions with all six urea –NH protons of **14** where both the TBA^+ counter cations are in close contact with the encapsulated SO_4^{2-} *via* C–H···O interactions. Apart from contact ion-pair interaction with anion the TBA counter cations are further stabilized *via* hydrogen bonding and cation···π interactions with the pentafluoro phenyl rings (Figure 1.12c). The gas-phase existence of a contact ion-pair was also

observed from the ESI mass analysis. The solution-state contact ion-pair recognition was also evident from the same diffusion coefficients value observed for the receptor and TBA^+ from the ^1H-DOSY NMR spectral data. The hydrodynamic radii calculated from the diffusion measurements were also in good agreement with that of the average of the dimension calculated from the single crystal X-ray crystallographic structure. The variable temperature ^1H-DOSY experiments showed that with the increase in temperature the development of two different sets of signals is observed for the anion bound receptor and TBA^+ cation. When the temperature of the solution was cooled down to 298 K, the DOSY spectrum exactly matched with the spectrum of the associated ion-pair complex. Thus, at ambient temperature the receptor **14** forms a TBA^+ capped unimolecular capsule with SO_4^{2-} encapsulated in the tripodal cavity in solution, solid and gas phases.

The hexapodal receptor **15** was found to form charge separated 1:1 ion-pair complex with $NH_4^+PF_6^-$.[60] The crystal structure of the ion-pair complex showed that four of the pyrazoles of the receptor are on the same side of the center benzene ring (upper cleft), and among them two pyrazole units are hydrogen bonded to NH_4^+ *via* N−H···N interactions and the counteranion PF_6^- is located at the lower cleft which is formed by the rest of the two arms of **15**, below the plane of the benzene ring *via* three C−H···F interactions (Figure 1.12d). ^1H NMR titration studies showed that the receptor forms a 1:1 complex with $NH_4^+PF_6^-$ yielding a binding constant of log K = 2.67.

1.5 Concluding remarks

In general, acyclic receptors with appropriately positioned binding sites can recognize anions and ion-pairs both in solid and solutions and also assist the self-assembly process. In anion receptor chemistry, tris(2-aminoethyl)amine based tripodal receptors have shown their high potential towards anion assisted capsule and pseudo-capsule formation. It was found that the attached aryl terminals and the anion binding functions in the receptors play an important role towards the formation of different microenvironment for selective anion binding and encapsulation. Usually higher coordination number of oxyanions like sulfate, phosphates and carbonate assist in dimeric capsular assembly formation, while halides tend to form unimolecular capsules. On the other hand tripodal and hexapodal amide receptors on a benzene platform have shown their potential for recognition of large anionic guests, especially hydrated anions, *via* capsular assembly formation or *via* compartmental recognition. In case of ion-pair recognition, the pridylureas and bipyridine-bis(urea) based receptors were found to form charge separated ion-pair complex through assembly process. While, the tripodal and hexapodal ion-pair receptors formed both charge separated and contact ion-pair complexes, and in contrast to the anion receptor chemistry the tripodal and hexapodal heteroditopic receptors were not found to form any dimeric capsular assembly upon ion-pair coordination. The recognition and binding of anions and ion-pairs, and anions and their role

towards formation of molecular assembly is definitely a field which can expand considerably and bring immense advances in specialised applications such as: (a) removal and extraction toxic anions and salts from water, (b) drug delivery applications, (c) trapping reactive intermediates inside the molecular cavity, (d) membrane transport and (e) solubilize insoluble anions/salts.

References

1. J. W. Steed and J. L. Atwood, *Supramolecular chemistry*, John Wiley and Sons, Ltd; 1997.
2. D. J. Cram, *Angew. Chem., Int. Ed*., 1986, **25**, 1039−1057.
3. T. Steiner, Hydrogen Bond in the Solid State. *Angew. Chem., Int. Ed*., 2002, **41**, 48−76.
4. (*a*) D. S. Lawrence, T. Jiang and M. Levett, *Chem. Rev*., 1995, **95**, 2229; (*b*) L. M. Greig and D. Philp, *Chem. Soc. Rev*., 2001, **30**, 287−302.
5. J. L. Sessler, P. A. Gale and W. S. Cho, *Anion Receptor Chemistry*, The Royal Society of Chemistry, Cambridge, UK, 2006.
6. A. Bianchi, K. Bowman-James and E. Garcia-Espana, *Supramolecular Chemistry of Anions*, Wiley-VCH, New York, 1997.
7. B. A. Moyer and P. V. Bonnesen, *Physical factors in anion separations, In Supramolecular Chemistry of Anions*; Wiley-VCH: New York, 1997; chapter 1.
8. D. J. Mercer and S. J. Loeb, *Chem. Soc. Rev*., 2010, **39**, 3612−3620.
9. K. Bowman-James, *Acc. Chem. Res*., 2005, **38**, 671−678.
10. (*a*) H. -J. Schneider and A. K. Yatsimirsky, *Chem. Soc. Rev*., 2008, **37**, 263−277; (*b*) E. Garcia-Espana, P. Diaz, J. M. Llinares and A. Bianchi, *Coord. Chem. Rev*., 2006, **250**, 2952−2986; (*c*) S. O. Kang, M. A. Hossain and K. Bowman-James, *Coord. Chem. Rev*., 2006, **250**, 3038−3052.
11. (*a*) P. A. Gale, *Chem. Commun*., 2008, 4525; (*b*) C. Caltagirone and P. A. Gale, *Chem. Soc. Rev*., 2009, **38**, 520−563; (*c*) P. A. Gale, *Acc. Chem. Res*., 2006**, 39**, 465; (d) A-F. Li, J-H. Wang, F. Wang and Y-B. Jiang, *Chem. Soc. Rev*., 2010, **39**, 3729−3745.
12. (*a*) T. Gunnlaugsson, P. E. Kruger, P. Jensen, F. M. Pfeffer and G. M. Hussey, *Tetrahedron Lett*., 2003, **44**, 8909−8913; (*b*) S. Camiolo, P. A. Gale, M. B. Hursthouse and M. E. Light, *Org. Biomol. Chem*., 2003, **1**, 741−744; (*c*) V. Amendola, D. Esteban-Gomez, L. Fabbrizzi and M. Licchelli, *Acc. Chem. Res*., 2006, **39**, 343−353.
13. R. Custelcean, *Chem. Soc. Rev*., 2010, **39**, 3675−3685.
14. (*a*) B. L. Schottel, H. T. Chifotides and K. R. Dunbar, *Chem. Soc. Rev*., 2008, **37**, 68−83; (*b*) H. T. Chifotides, B. L. Schottel and K. R. Dunbar, *Angew. Chem., Int. Ed*., 2010, **49**, 7202−7207.
15. (*a*) B. P. Hay and V. S. Bryantsev, *Chem. Commun*., 2008, 2417−2428; (*b*) B. P. Hay and R. Custelcean, *Cryst. Growth Des*., 2009, **9**, 2539−2545.
16. G. Cavallo, P. Metrangolo, T. Pilati, G. Resnati, M. Sansoteraa and G. Terraneo, *Chem. Soc. Rev*., 2010, **39**, 3772−3783.
17. (*a*) K. L. Kirk, *Biochemistry of the Halogens and Inorganic Halides*, Plenum Press, New York, 1991, p 58; (*b*) M. Cametti and K. Rissanen, *Chem. Commun*., 2009, 2809−2829; (*c*) P. A. Gale, S. E. García-Garrido and J. Garric, *Chem. Soc. Rev*., 2008, **37**, 151–190.
18. D. Esteban-Gomez, L. Fabbrizzi and M. Licchelli, *J. Org. Chem*., 2005, **70**, 5717−5720.
19. D. A. Jose, D. K. Kumar, B. Ganguly and A. Das, *Org. Lett*., 2004, **6**, 3445−3448.
20. P. Bose and P. Ghosh, *Chem.Commun*., 2010, **46**, 2962–2964.
21. (*a*) P. S. Lakshminarayanan, I. Ravikumar, E. Suresh and P. Ghosh, *Inorg. Chem*., 2007, **46**, 4769–4771; (*b*) P. Bose, I. Ravikumar, and P. Ghosh, *Inorg. Chem*., 2011, **50**, 10693−10702.
22. M. Isiklan, M. A. Saeed, A. Pramanik, B. M. Wong, F. R. Fronczek, and M. A. Hossain, *Cryst. Growth Des*., 2011, **11**, 959−963.
23. I. Ravikumar, Subrata Saha and Pradyut Ghosh, *Chem. Commun*., 2011, **47**, 4721–4723.

24. (*a*) S. K. Dey and G. Das, *Chem. Commun.*, 2011, **47**, 4983−4985; (*b*) S. K. Dey and G. Das, *Cryst. Eng. Comm.*, 2012, **14**, 5305−5314; (*c*) S. K. Dey and G. Das, *Cryst. Growth Des*., 2011, **11**, 4463−4473.
25. P. J. Smith, M. V. Reddington and C. S. Wilcox, *Tetrahedron Lett*., 1992, **33**, 6085−6088.
26. E. Fan, S. A. Van Arman, S. Kincaid and A. D. Hamilton, *J. Am. Chem. Soc*., 1993, **115**, 369−370.
27. F. G. Bordwell, *Acc. Chem. Res*., 1988, 21, 456−463.
28. C. Raposo, M. Almaraz, M. Martin, V. Weinrich, M. L. Mussons, V. Alcazar, M. C. Caballero and J. R. Moran, *Chem. Lett*., 1995, 759.
29. N. Busschaert, P. A. Gale, C. J. E. Haynes, M. E. Light, S. J. Moore, C. C. Tong, J. T. Davis and W. A. Harrell, Jr., *Chem. Commun*., 2010, **46**, 6252−6254.
30. N. Busschaert, M. Wenzel, M. E. Light, P. Iglesias-Hernandez, R. Perez-Tomas and P. A. Gale, *J. Am. Chem. Soc*., 2011, **133**, 14136−14148.
31. I. Ravikumar and P. Ghosh, *Chem. Commun*., 2010, **46**, 1082−1084.
32. S. K. Dey, R. Chutia and G. Das, *Inorg. Chem*., 2012, **51**, 1727–1738.
33. I. Ravikumar, P. S. Lakshminarayanan, M. Arunachalam, E. Suresh and P. Ghosh, *Dalton Trans*., 2009, 4160–4168.
34. D. A. Jose, D. K. Kumar, B. Ganguly and A. Das, *Inorg. Chem*., 2007, **46**, 5817–5819.
35. S. K. Dey and G. Das, *Dalton Trans*., 2012, **41**, 8960–8972.
36. (*a*) P. S. Lakshminarayanan, I. Ravikumar, E. Suresh and P. Ghosh, *Chem. Commun*., 2007, 5214–5216; (*b*) B. Akhuli, I. Ravikumar, and P. Ghosh, *Chem. Sci*., 2012, **3**, 1522−1530.
37. S. K. Dey and G. Das, *Dalton Trans*., 2011, **40**, 12048–12051.
38. R. Custelcean, B. A. Moyer and B. P. Hay, *Chem. Commun*., 2005, 5971−5973.
39. (*a*) R. Custelcean, P. Remy, P. V. Bonnesen, D.-e. Jiang and B. A. Moyer, *Angew. Chem., Int. Ed*., 2008, **47**, 1866−1870; (*b*) B. Wu, J. Liang, J. Yang, C. Jia, X.-J. Yang, H. Zhang, N. Tang and C. Janiak, *Chem. Commun*., 2008, 1762−1764. (*c*) R. Custelcean, *Chem. Commun*., 2013, **49**, 2173−2182.
40. A. Rajbanshi and R. Custelcean, *Supramol. Chem*., 2012, **24**, 65.
41. R. Custelcean, A. Bock and B. A. Moyer, *J. Am. Chem. Soc*., 2010, **132**, 7177−7185.
42. (*a*) M. Arunachalam and P. Ghosh, *Chem. Commun*., 2009, 5389–5391; (*b*) M. Arunachalam and P. Ghosh, *Inorg. Chem*., 2010, **49**, 943–951.
43. M. Arunachalam and P. Ghosh *Org. Lett*., 2010, **12**, 328−331.
44. M. Arunachalam and P. Ghosh, *Chem. Commun*., 2011, **47**, 6269–6271.
45. J. M. Mahoney, A. M. Beatty and B. D. Smith, *Inorg. Chem*., 2004, **43**, 7617–7621.
46. B. D. Smith, *Macrocyclic Chemistry: Current Trends and Future Perspectives, Springer*, Dordrecht, 2005.
47. (*a*) D. M. Rudkevich, J. D. Mercer-Chalmers, W. Verboom, R. Ungaro, F. de Jong, D. N. Reinhoudt, *J. Am. Chem. Soc*., 1995, 117, 6124–6125; (*b*) N. Pelizzi, A. Casnati, A. Friggeri, R. Ungaro, *J. Chem. Soc. Perkin Trans. 2*, 1998, 1307–1311.
48. D. J.White, N. Laing, H. Miller, S. Parsons, P. A. Tasker, S. Coles, *Chem. Commun*., 1999, 2077–2078.
49. G. J. Kirkovits, J. A. Shriver, P. A. Gale and J. L. Sessler, *J. Inclusion Phenom. Macrocyclic Chem*., 2001, **41**, 69–75.
50. S. K. Kim and J. L. Sessler, *Chem. Soc., Rev*. 2010, **39**, 3784–3809.
51. A. J. McConnell and P. D. Beer, *Angew. Chem. Int. Ed*., 2012, **51**, 5052–5061.
52. David R. Turner, E. C. Spencer, J. A. K. Howard, D. A. Tocher and J. W. Steed, *Chem. Commun*., 2004, 1352−1353;
53. (*a*) D. R. Turner, M. B. Hursthouse, M. E. Light and J. W. Steed, *Chem. Commun*., 2004, 1354−1355; (*b*) L. Applegarth, A. E. Goeta and J. W. Steed, 2005, 2405−2406; (*c*) D. R. Turner, B. Smith, E. C. Spencer, A. E. Goeta, I. R. Evans, D. A. Tocher, J. A. K. Howard and J. W. Steed, *New J. Chem*., 2005,**29**, 90−98; (*d*) N. L. S. Yue , D. J. Eisler , M. C. Jennings , and R. J. Puddephatt, *Inorg. Chem*., 2004, **43**, 7671–7681.
54. Z. Yang, B. Wu, X. Huang, Y. Liu, S. Li, Y. Xia, C. Jiaac and X-J. Yanga *Chem. Commun*., 2011, **47**, 2880–2882.

55. B. Akhuli and P. Ghosh, *Dalton Trans.*, 2013, **42**, 5818−5825.
56. R. Custelcean, P. V. Bonnesen, B. D. Roach and N. C. Duncan, *Chem. Commun.*, 2012, **48**, 7438−7440.
57. A. Mele, P. Metrangolo, H. Neukirch, T. Pilati and G. Resnati, *J. Am. Chem. Soc*., 2005, **127**, 14972–14973.
58. P. Bose, I. Ravikumar, B. Akhuli, and P. Ghosh, *Chem. Asian J*., 2012, **7**, 2373−2380.
59. I. Ravikumar and P. Ghosh, *Chem. Commun.*, 2010, **46**, 6741–6743.
60. M. Arunachalam, B. N. Ahamed and P. Ghosh, *Org. Lett*., 2010, **12**, 2742–2745.

Chapter 2

Experimental Methods and Characterization

In this chapter, a detailed report of the various reagents used in the synthesis of acyclic receptors, **H_2L_1** and **L_2-L_4** (Scheme 2.1), their synthetic procedures, crystallization details and specifications of instruments/equipments employed in the characterization of synthesized receptors and their various complexes with anions are presented.

2.1 Materials

All reagents and solvents were obtained from commercial sources and used as received without further purification. Tris(2-aminoethyl)amine (tren), 4-nitrobenzoyl chloride, 3-nitrophenylisocyanate, 4-nitrophenylisothiocyanate and Pd/C were purchased from Sigma-Aldrich (U.S.A) whereas, 4-nitrophenol, hydrazine hydrate, triethanolamine and thionyl chloride were purchased from Merck chemicals (India). All quaternary ammonium salts were purchased from Sigma-Aldrich (U.S.A) whereas, inorganic such as, HCl, HBr, HI, HF, HNO_3, $HClO_4$, H_2SO_4 and H_3PO_4 were obtained either from Merck or LOBA chemicals (India). All Sodium potassium and lithium salts and deuterated solvent DMSO-d_6 were purchased from Merck chemicals (India) and used as received. Solvents for synthesis and crystallization experiments were purchased either from Merck or LOBA chemicals (India) and dried using standard procedures, wherever mentioned in the synthetic procedures.

2.2 Experimental methods

^{1}H NMR and 2D NOESY NMR spectra were recorded on a Varian FT-400 MHz instrument and chemical shifts were recorded in parts per million (ppm) on the scale using tetramethylsilane (TMS) or residual solvent peak as a reference and ^{13}C spectra were obtained at 100 MHz at 298 K. FT-IR spectra were recorded on a Perkin-Elmer-Spectrum One FT-IR spectrometer with KBr disks in the range 4000-450 cm^{-1}. Powder X-ray diffraction patterns of dried crystalline powder were recorded using a Bruker-D8 Advance X-ray diffractometer with Cu-$K\alpha$ radiation at λ = 0.15418 nm. Thermal analysis (TGA and DSC) of dried samples was performed using an SDTA 851-E TGA thermal analyser (*Mettler Toledo*) with a heating rate of 5-10^{o}C/min in a N_2 atmosphere. The absorption spectra were recorded on a Perkin-Elmer Lambda-25/35 UV-Visible spectrophotometer with a quartz cuvette.

Association constants (log *K* or *K*) of anions with receptors (**H_2L_1** and **L_2-L_4**) were obtained by ^{1}H NMR titrations of the receptor with tetraethyl ammonium (TEA) or tetrabutyl ammonium (TBA) salts of anions in DMSO-d_6 at 298 K. The initial concentration of the receptor solution was 5 mM/10 mM. Aliquots of anions were added from the stock solutions up to 1:10 host-guest stoichiometry. The residual solvent peak in DMSO-d_6 (2.50 ppm) was

used as an internal reference, and each titration was performed with at least 10-15 measurements.

Following equation was used to determine the association constant (K) values.

$$\Delta\delta = \{([A]_0 + [\mathbf{L}]_0 + 1/K) +/- (([A]_0 + [\mathbf{L}]_0 + 1/K)^2 - 4[\mathbf{L}]_0[A]_0)^{1/2}\}\Delta\delta_{max}/2[\mathbf{L}]_0$$

Where, **L** = receptor and A = anion. An error limit in log *K* was less that 15%.

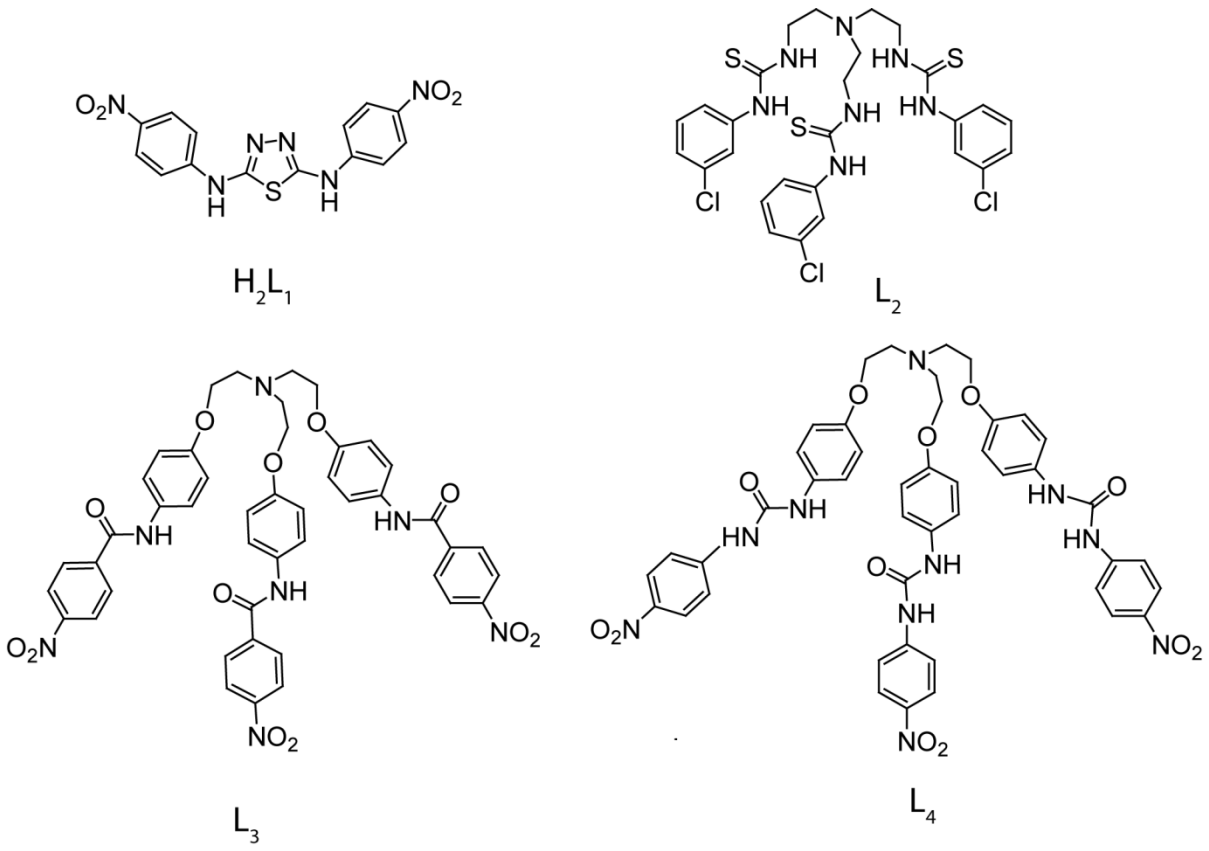

Scheme 2.1 Molecular structures of acyclic receptors (**H_2L_1** and **L_2-L_4**).

2.3 Single crystal X-ray crystallography

In each case, a crystal of suitable size was selected from the mother liquor and immersed in silicone oil, and it was mounted on the tip of a glass fiber and cemented using epoxy resin. The intensity data were collected using a Bruker SMART APEX-II CCD diffractometer, equipped with a fine focus 1.75 kW sealed tube Mo-K_α radiation (λ = 0.71073 Å) at 298(3) K, with increasing ω (width of 0.3° per frame) at a scan speed of 5 s/ frame. The SMART software was used for data acquisition. Data integration and reduction were undertaken with SAINT and XPREP software.[1] Multi-scan empirical absorption corrections were applied to the data using the program SADABS.[2] Structures were solved by direct methods using SHELXS-97[3] and refined with full-matrix least-squares on F^2 using SHELXL-97.[4] All non-

hydrogen atoms were refined anisotropically and hydrogen atoms attached to all carbon atoms were geometrically fixed and the positional and temperature factors are refined isotropically. However, in some cases the tetraalkylammonium cation(s) and/or solvent molecules were treated isotropically due to heavy disorder. Hydrogen atoms attached with the amide, urea and thiourea nitrogen atoms were located from electron Fourier map and refined isotropically. Usually, temperature factors of hydrogen atoms attached to carbon atoms are refined by restraints -1.2 or -1.5 U_{iso} (C), although the isotropic free refinement is also acceptable. PLATON/SQUEEZE[5] was also applied some cases to exclude disordered solvent electron densities. Structural illustrations have been drawn with MERCURY-3.0.[6] for Windows. Parameters for data collection and crystallographic refinement details of the receptors (**H_2L_1** and **L_2-L_4**) and their various anion and/or ion-pair complexes are summarized in the respective chapters.

2.4 Synthesis and characterization of receptors, (H_2L_1 and L_2-L_4)

2.4.1 N2,N5-bis(4-nitrophenyl)-1,3,4-thiadiazole-2,5-diamine, H_2L_1

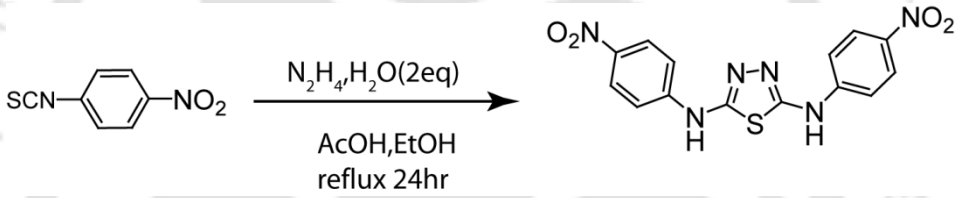

Scheme 2.2 Synthesis of the receptor **H_2L_1**.

The receptor **H_2L_1** was synthesized by refluxing the 1:2 mixture of 4-nitrophenylisothiocyanate and hydrazine hydrate in the presence of acetic acid (catalytic amount) in EtOH for 24 h. A total of 1.8 g (10 mmol) of 4-nitrophenyl isothiocyanate was dissolved in 30 mL of ethanol (EtOH) in a 100 mL round-bottomed flask. Then hydrazine hydrate (0.640mL 20mmol) was added drop wise to the solution. After that acetic acid (0.05ml) was added at once to this mixture and the mixture was refluxed for 24 h. The orange color precipitate was filtered and washed with 15 mL of ethanol five times to remove unreacted starting materials and impurities. An orange solid was obtained after drying the precipitate in a vacuum by using rotary evaporator and characterized by NMR, FT-IR, and ESI-MS spectroscopy (yield 62%).

Melting point: >300°C ^{1}H NMR (400 MHz, DMSO-d_6) δ (ppm): 10.852 (s, 2H−N), 8.216 (d, J = 8 Hz, 4H) and 7.760 (d, J = 8Hz, 4H). ^{13}C NMR (100 MHz, DMSO-d_6) δ (ppm): 116.63, 125.604, 140.544, 146.668, and 156.064. FT-IR (ν, cm^{-1}): 1263 (C−N), 1326 (NO_2),

1590 (C=C) and 3290 (N−H). ESI mass spectrometry: calcd for 359.06. [M + H^+], found 359.06 [M+ H^+].

2.4.2 Tripodal thiourea receptor, L_2

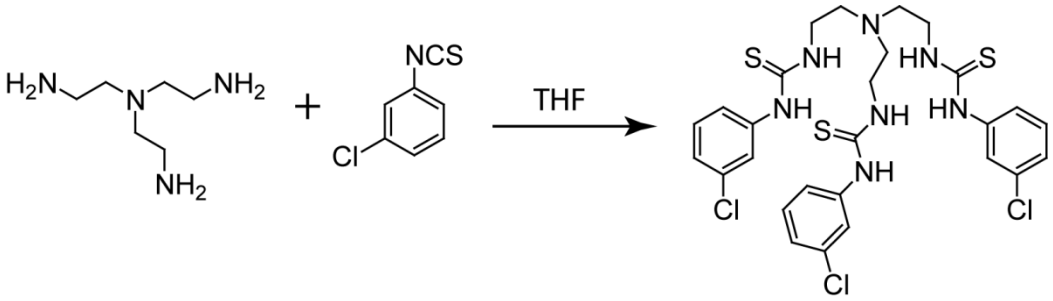

Scheme 2.3 Synthesis of the receptor $\mathbf{L_2}$.

Reaction of tris(2-aminoethyl)amine, (tren) with 3-chlorophenyl isothiocyanate in a 1:3 molar ratio at room temperature yielded the tris (thiourea) receptor, $\mathbf{L_2}$ in quantitative yield. A total of 507 mg (3 mmol) of 3-chlorophenyl isothiocyanate was dissolved in 30 mL of dry tetrahydrofuran (THF) in a 100 mL round-bottomed flask and 0.146 mL (1 mmol) of tren dissolved in 10 mL of dry THF were added drop wise over a period of 15 min with constant stirring at room temperature. The resulting solution mixture was stirred 12 hours at room temperature. Then, the volume of the solvent (THF) was reduced in vacuo by using rotary evaporator, and the obtained solid product was filtered off and washed with 10 mL of dichloromethane (DCM) a couple of times to remove the unreacted starting materials and impurities. The colorless precipitate was collected and dried in air and characterized by NMR, FT-IR, ESI-MS and single crystal X-ray diffraction analyses. Yield 88%.

Melting point: 183°C. ^{1}H NMR (400 MHz, DMSO-d_6) δ (ppm): 9.73 (s, H–N), 7.81 (s, H–N), 7.66 (s, 3H), 7.31 (m, 6H), 7.128 (t, J = 7.6 Hz, 3H), 3.50 (s (br), 6H) and 2.74 (s (br), 6H). ^{13}C NMR (100 MHz, DMSO-d_6) δ (ppm): 41.91, 52.00, 121.11, 122.23, 123.65, 130.18, 132.77 140.95 and 180.30. FT-IR (ν, cm^{-1}): 766 (C=S, asym), 1556 (C=S sym), 1589 (C=C), 3227 (N–H) and 3326 (N–H). ESI(+ve) mass spectrometry: calcd for 656.08. [M + H^+], found 656.28 [M+ H^+].

2.4.3 Tripodal amide receptor, L_3

To a solution of 4-nitrophenol (15.3 g, 0.11 mol) in EtOH (80 mL) was added NaOH (5.98 g, 0.15 mol), and the solution was stirred at rt for 1 hour.[7] To the resulting solution, tris (2-chloroethyl) amine hydrochloride (A) (8.0 g, 33.2 mmol) was added at once, and the mixture was refluxed for 10 h followed by removal of the solvents under reduced pressure and

addition of 20 mL of cold water. The expected product was extracted from this mixture, with 3 x 30 mL of dichloromethane (DCM). The organic layer was washed three times with 10% K_2CO_3 solution and then two times with cold water and dried over anhydrous Na_2SO_4, and solvents were removed under reduced pressure. The crude product was purified by column chromatography with 75% ethyl acetate (in petroleum ether) as the eluent. The desired compound (B) was a pale yellow solid. Yield 65%.

Compound B (1 g, 1.95 mmol) was suspended in ethanol (100 mL) in a 250 mL round-bottomed flask. Then 5% Pd/C (50 mg, 5wt. %) was added to the suspension. Hydrazine hydrate (1 ml, 16 equiv.) was added drop wise to this mixture. The mixture was refluxed for 10 h followed by removal of the solvents under reduced pressure give colorless solid of triamine (C).[8] Yield 85%.

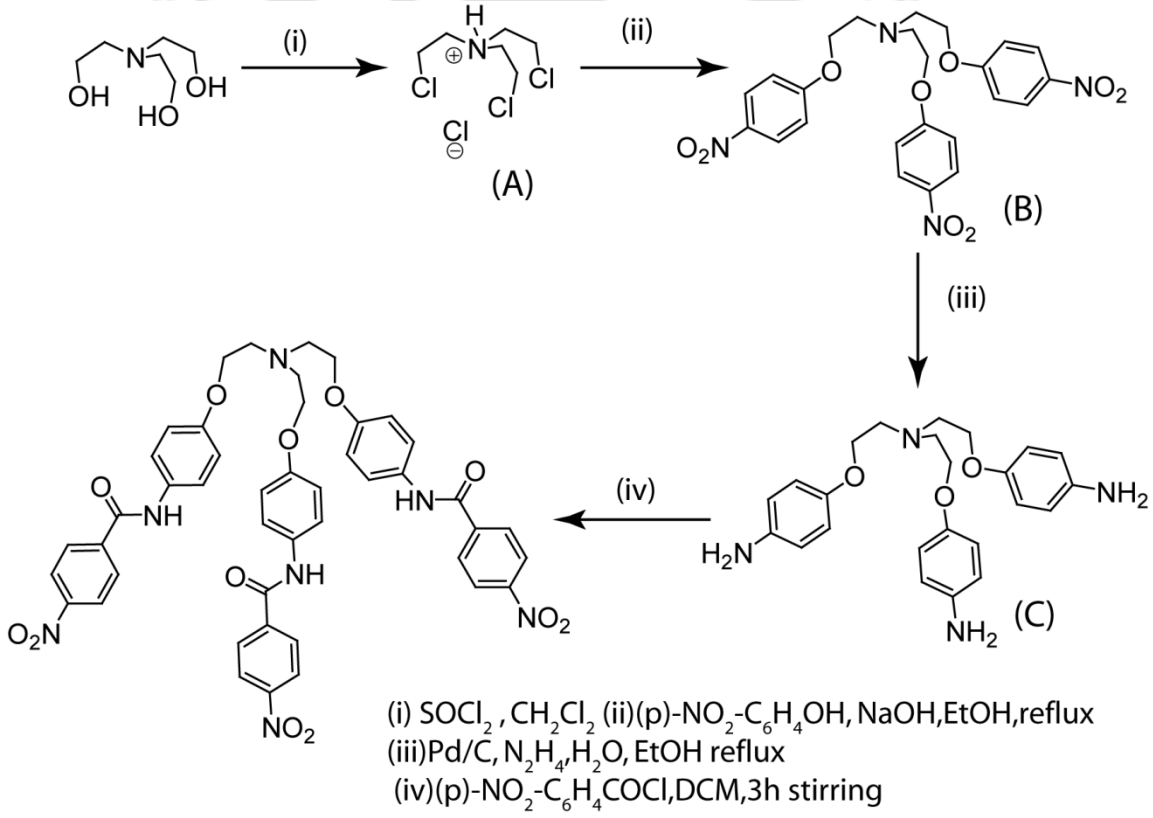

Scheme 2.3 Synthesis of the receptor $\mathbf{L_3}$.

Reaction of triamine (C) with 4-nitrobenzoyl chloride in a 1:3 molar ratio at room temperature yielded the tripodal amide receptor, $\mathbf{L_3}$ in quantitative yield. 0.422 g 1 mmol of triamine (C) was dissolved in 30 mL of dry DCM in a 100 mL round bottomed flask and 0.406 g (4.0 mmol) of dry triethylamine (Et_3N) was added to the reaction mixture. Then, 0.556 g of 4-nitrobenzoyl chloride (3 mmol) was added in portions to the reaction mixture over a period of 1 hour with constant stirring at room temperature. After the addition was

complete, a yellow precipitate formed and the reaction mixture was allowed to stir overnight at room temperature. The precipitate thus obtained was filtered and washed several times with (3 x 30 mL) water, a couple of times with (2 x 10) mL of methanol and finally with diethyl ether to get the desired product. The yellow product thus collected was dried in air and characterized by NMR, FT-IR, and ESI-MS. Yield 83%.

Melting point: 203-205°C. ^{1}H NMR (400 MHz, DMSO-d_6) δ (ppm): 10.44 (s, 3N–H), 8.32 (d, *J* = 8 Hz, 6H), 8.15 (d, *J* = 7.2 Hz, 6H), 7.65 (d, *J* = 7.6 Hz, 6H), 6.93 (d, *J* = 7.6 Hz, 6H), 4.07 (s (br), 6H) and 3.06 (s (br), 6H). ^{13}C NMR (100 MHz, DMSO-d_6) δ (ppm): 163.64, 155.43, 149.27, 140.94, 132.04, 129.35, 123.74, 122.38, 114.78, 67.03 and 53.99. FT-IR (ν, cm^{-1}): 1345 (NO_2), 1647 (C=O) and 3326 (N–H). ESI (+ve) mass spectrometry: calcd for 870.27 [M + H^+], found 870.13 [M + H^+].

2.4.4 Tripodal urea receptor, L_4

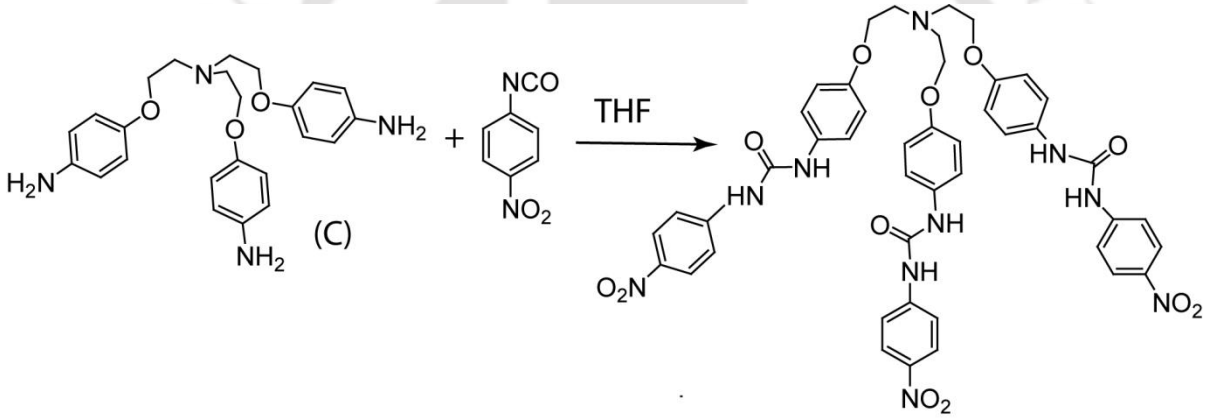

Scheme 2.4 Synthesis of the receptor **L_4**.

Reaction of triamine (C) with 4-nitrophenyl isocyanate in a 1:3 molar ratio at room temperature yielded the tripodal urea receptor, **L_4** in quantitative yield. A total of 492 mg (3 mmol) of 4-nitrophenyl isocyanate was dissolved in 30 ml of dry tetrahydrofuran (THF) in a 100 mL round-bottomed flask and (422 mg 1 mmol) of triamine (C) dissolved in 10 mL of dry THF were added drop wise (using a dropping funnel) over a period of 1 h with constant stirring at room temperature. The resulting solution mixture was stirred overnight at room temperature. Then, the volume of the solvent (THF) was reduced in vacuo by using rotary evaporator, and the obtained solid product was filtered off and washed with 10 mL of dichloromethane a couple of times to remove the unreacted starting materials and impurities. The yellow precipitate was collected and dried in desiccator and characterized by NMR, FT-IR, ESI-MS and single crystal X-ray diffraction analyses. Yield 82%.

Melting point: 194°C. ^{1}H NMR (400 MHz, DMSO-d_6) δ (ppm): 9.33 (s, 3H–N), 8.70 (s, 3H–N), 8.14 (d, *J* = 8.4 Hz, 6H), 7.65 (d, *J* = 8.4 Hz, 6H), 7.35 (d, *J* = 8 Hz, 6H), 6.88 (d, *J* = 8.4 Hz, 6H), 4.02 (s (br), 6H) and 3.03 (s (br), 6H). ^{13}C NMR (100 MHz, DMSO-d_6) δ (ppm): 58.90, 71.92, 120.01, 122.48, 125.75, 130.36, 137.17 146.05, 151.79, 157.34 and 159.41. FTIR (ν, cm^{-1}): 1230 (C−N), 1333 (NO_2 sym), 1555 (NO_2 asym), 1607 (C=C), 1656 (C=O) and 3356 (N−H). ESI (+ve) mass spectrometry: calcd for 915.31. [M + H^+], found 915.33 [M+ H^+].

2.5 Synthesis and characterization of anion and ion-pair complexes of the receptors (H_2L_1 and L_2-L_4)

2.5.1 Complexes of receptor H_2L_1

Fluoride complex $(TBA)^+_2[\mathbf{HL_1}(F^-)]$ (**1a**). Fluoride complex of $\mathbf{H_2L_1}$ was obtained as dark violet colour single crystals suitable for X-ray diffraction analysis by slow evaporation of a solution mixture of $\mathbf{H_2L_1}$ charged with an excess TBAF (20 equiv.) in acetonitrile (CH_3CN). Yield: 55%.

^{1}H NMR (400 MHz, DMSO-d_6) δ (ppm): 8.13 (d, *J* = 9.2 Hz, 4H), 7.65 (d, *J* = 7.8 Hz, 4H), 3.13 (t, *J* = 5.6 Hz, 16H), 1.54 (s (br), 16H), 1.28 (d, *J* = 6.4 Hz, 16H) and 0.93 (t, J = 6 Hz, 24H). FTIR (ν, cm^{-1}): 1254 (C−N), 1380 (NO_2) and 1598 (C=C).

Chloride complex $(TBA)^+_2[\mathbf{H_2L_1}(Cl^-)_2]\cdot H_2O$ (**1b**). Chloride complex of $\mathbf{H_2L_1}$ was obtained as yellow colour single crystals suitable for X-ray diffraction analysis by slow evaporation of a solution mixture of $\mathbf{H_2L_1}$ charged with an excess TBACl (20 equiv.) in acetonitrile. Yield: 42%.

^{1}H NMR (400 MHz, DMSO-d_6) δ (ppm): 11.42 (s, 2H–N), 8.22 (d, *J* = 9.2 Hz, 4H), 7.85 (d, *J* = 9.6 Hz, 4H), 3.17 (t, *J* = 5.6 Hz, 16H), 1.55 (s (br), 16H), 1.31 (d, *J* = 6.4 Hz, 16H) and 0.93 (t, *J* = 6 Hz, 24H). FTIR (ν, cm^{-1}): 1260 (C−N), 1393 (NO_2) and 1598 (C=C).

Bromide complex $(TBA)^+_2$ $[\mathbf{H_2L_1}(Br^-)_2]\cdot H_2O$ (**1c**). Bromide complex of $\mathbf{H_2L_1}$ was obtained as yellow colour single crystals suitable for X-ray diffraction analysis by slow evaporation of a solution mixture of $\mathbf{H_2L_1}$ charged with an excess TBABr (20 equiv.) in acetonitrile. Yield: 45%.

^{1}H NMR (400 MHz, DMSO-d_6) δ (ppm): 11.00 (s, 2H–N), 8.23 (d, *J* = 7.6 Hz, 4H), 7.81 (d, *J* = 7.2 Hz, 4H), 3.18 (t, *J* = 5.5 Hz, 16H), 1.57 (s (br), 16H), 1.31 (d, *J* = 6.4 Hz, 16H) and 0.93 (t, *J* = 6 Hz , 24H). FTIR (ν, cm^{-1}): 1266 (C−N), 1395 (NO_2) and 1598 (C=C).

2.5.2 Complexes of receptor L_2

Sulfate complex, $2TBA^{+}[2\mathbf{L_2}(SO_4^{2-})]$, (**2a**). Sulfate-encapsulated complex **2a** was obtained by mixing $\mathbf{L_2}$ and $(n\text{-}TBA)_2SO_4$/$(n\text{-}TBA)HSO_4$. In both the cases, 50 mg of $\mathbf{L_2}$ was dissolved in 5 mL of DMSO in a 25 mL round-bottomed flask. In the case of the $(n\text{-}TBA)_2SO_4$ salt, 3 mL of $(n\text{-}TBA)_2SO_4$ (50 wt.% in water) was added at once to the 5 mL of $\mathbf{L_2}$ solution whereas, in other case 25 mg of $n\text{-}TBAHSO_4$ was added at a time to the 5 mL of $\mathbf{L_2}$. Then in both cases, the mixtures were stirred for 1 h at room temperature and allowed to crystallize at room temperature in open test tubes. From both the solutions, colorless crystals of the sulfate complex of $\mathbf{L_2}$ suitable for X-ray diffraction were obtained after seven–ten days. Yield 88%.
Melting point: 184 °C. ^{1}H NMR (400 MHz, DMSO-d_6) δ (ppm): 10.36 (s, 3H–N), 8.69 (s, 3H–N), 7.82 (s (br), 3H), 7.38 (s (br), 3H), 7.17 (s (br), 3H), 7.026 (s (br), 3H), 3.50 (s (br), 6H), 3.13 (s (br) 8H), 2.59 (s (br), 6H), 1.53 (s (br), 8H), 1.28 (s (br), 8H) and 0.90 (s (br), 12H). ^{13}C NMR (100 MHz, DMSO-d_6) δ (ppm): 13.49, 19.22, 23.08, 41.91, 53.29, 57.598, 120.90, 122.07, 122.91, 129.37, 132.21 141.69 and 180.24. FT-IR (ν, cm^{-1}): 784 (C=S, asym), 1085 (SO_4^{2-}), 1604 (C=C), 1538 (C=S, sym) and 3277 (N–H, br).

Thiosulfate complex $2TEA^{+}[2\mathbf{L_2}(S_2O_3^{2-})]$, (**2b**). Thiosulfate-encapsulated complex **2b** was obtained by charging previously prepared 5 ml aqueous solution containing equimolar mixture of (n-TEA)Cl and $Na_2S_2O_3$ (10 equivalent each) into a 8 mL DMSO solution of $\mathbf{L_2}$ (50 mg). Then the mixture was stirred for 15 min at room temperature and warmed at 60 °C for 5 min. After cooling to room temperature, the resulting solution was filtered using a filter paper. Filtrate was collected in 20 mL test tube and allowed to crystallize at room temperature. Colorless crystals suitable for single-crystal X-ray crystallographic analysis of thiosulfate complex are obtained after ten days. Yield 65%.
Melting point: 134°C. ^{1}H NMR (400 MHz, DMSO-d_6) δ (ppm): 10.30 (s, 3H–N), 8.53 (s, 3H–N), 7.83 (s, 3H), 7.45 (d, J = 7.6 Hz, 3H), 7.22 (t, J = 8.0 Hz, 3H), 7.05 (d, J = 8.0 Hz 3H), 3.53 (s, 6H), 3.16 (q, J = 7.2 Hz, 8H), 2.64 (d, 6H) and 1.18 (t, J = 4.8 Hz, 12H). ^{13}C NMR (100 MHz, DMSO-d_6) δ (ppm): 7.10, 42.05, 51.47, 53.35, 121.12, 122.12, 123.04, 129.61, 132.30, 141.65 and 180.15. FT-IR (ν, cm^{-1}): 1095 ($S_2O_3^{2-}$), 1590 (C=C), 1531 (C=S, sym), 778 (C=S, asym) and 3277 (N–H, br).

2.5.3 Complexes of receptor L_3

Chloride complex, $[(\mathbf{L_3H})^{+}.Cl^{-}].H_2O$ (**3a**). Chloride complex of the receptor was obtained by adding 0.5 mL of 37% hydrochloric acid (HCl) to a 5 mL dimethylformamide (DMF) solution of $\mathbf{L_3}$ (100 mg, 0.12 mmol). After the addition of HCl, the solution was stirred for

about 1 hr and was allowed to slowly evaporate at room temperature, which yielded yellow block shaped crystals suitable for XRD analysis within a week. Yield 65%.

Melting point: 186-188°C. Calc.for $C_{45}H_{42}ClN_7O_{13}$: C, 58.47; H, 4.58; N, 10.61; Found: C: 58.83, H: 4.74 N: 10.27. ^{1}H NMR (400 MHz, DMSO-d_6) δ (ppm): 10.54 (s, 3N–H), 8.33 (d, *J* = 7.2 Hz, 6H), 8.17 (d, *J* = 7.2 Hz, 6H), 7.71 (d, *J* = 8 Hz, 6H), 7.00 (d, *J* = 8 Hz, 6H), 4.47 (s (br), 6H) and 3.80 (s (br), 6H). FT-IR (ν, cm^{-1}): 1345 (NO_2), 1670 (C=O), 3274 (O–H) and 3383 (N–H).

Bromide complex, $[(\mathbf{L_3H})^+.Br^-].H_2O$ (**3b**)

Bromide complex of the receptor was obtained by adding 0.5 mL of 37% hydrobromic acid (HBr) to a 5 mL dimethylformamide (DMF) solution of $\mathbf{L_3}$ (100 mg, 0.12 mmol). After the addition of HBr, the solution was stirred for about 1 hr. and was allowed to slowly evaporate at room temperature, which yielded yellow block shaped crystals suitable for XRD analysis within a week. Yield 58%.

Melting point: 136-138°C. Calc.for$C_{45}H_{42}BrN_7O_{13}$: C, 55.79; H, 4.37; N, 10.12; Found: C: 55.95, H: 4.82 N: 9.94. ^{1}H NMR (400 MHz, DMSO-d_6) δ (ppm): 10.50 (s, 3N–H), 8.34 (d, *J* = 8.4 Hz, 6H), 8.16 (d, *J* = 8 Hz 6H), 7.72 (d, *J* = 8.4 Hz, 6H), 7.01 (d, *J* = 8.8 Hz, 6H), 4.45 (s (br), 6H) and 3.82(s (br), 6H). FT-IR (ν, cm^{-1}): 1347 (NO_2), 1670 (C=O), 3277 (O–H) and 3386 (N–H).

Iodide complex, $[(\mathbf{L_3H})^+.I^-]$ (**3c**). Iodide complex of the receptor was obtained by adding 0.5 mL of 57% hydroiodic acid (HI) to a 5 mL dimethylsulfoxide (DMSO) solution of $\mathbf{L_3}$ (100 mg, 0.12 mmol). After the addition of HI, the solution was stirred for about 1 h and was allowed to slowly evaporate at room temperature, which yielded red needle shaped crystals suitable for XRD analysis within a week. Yield 56%.

Melting point: 165-166°C. ^{1}H NMR (400 MHz, DMSO-d_6) δ (ppm): 10.48 (s, 3N–H), 8.34 (d, *J* = 7.6 Hz, 6H), 8.15 (d, *J* = 7.6 Hz, 6H), 7.70 (d, *J* = 7.2 Hz, 6H), 7.00 (d, *J* = 7.6 Hz, 6H), 4.43 (s (br), 6H), 3.81 (s (br), 6H) and 2.54 (DMSO solvent). FT-IR (ν, cm^{-1}): 1345 (NO_2), 1670 (C=O), 3290 (O–H) and 3435 (N–H).

Hexafluorosilicate complex $[(\mathbf{L_3H})_2^+.SiF_6^{2-}]$ (**3d**) Hexafluorosilicate encapsulated complex of the receptor was obtained by adding 0.5 mL of 40% hydrofluoric acid (HF) to a 5 mL dimethylsulfoxide (DMSO) solution of $\mathbf{L_3}$ (100 mg, 0.12 mmol). After the addition of HF, the solution was stirred for about 1 h and was allowed to slowly evaporate at room

temperature, which yielded dark yellow block shaped crystals suitable for XRD analysis within a week. Yield 66%.

Melting point: 155-156°C. ^{1}H NMR (400 MHz, DMSO-d_6) δ (ppm): 10.46 (s, 3N–H), 8.33 (d, *J* = 7.2 Hz, 6H), 8.14 (d, *J* = 7.6 Hz, 6H), 7.65 (d, *J* = 7.2 Hz 6H), 6.96 (d, *J* = 7.2 Hz, 6H) and 4.23 (s (br), 12H). FT-IR (ν, cm^{-1}): 1345 (NO_2), 1671 (C=O) and 3286 (N–H).

Hexafluorosilicate complex, [(**L$_3$H**)$_2^+$.SiF_6^-]·2DMF,4H_2O (**3e**). Another hexafluorosilicate complex of the receptor was obtained by adding 0.5 mL of 40% hydrofluoric acid (HF) to a 5 mL dimethylformamide (DMF) solution of **L$_3$** (100 mg, 0.12 mmol). After the addition of HF, the solution was stirred for about 1 h and was allowed to slowly evaporate at room temperature, which yielded dark yellow block shaped crystals suitable for XRD analysis within a week. Yield 69%.

Melting point: 162-163°C. ^{1}H NMR (400 MHz, DMSO-d_6) δ (ppm): 10.44 (s, 3N–H), 8.33 (d, *J* = 8.4 Hz, 6H), 8.15 (d, *J* = 8.8 Hz, 6H), 7.94 (s, 1H, DMF solvent), 7.65 (d, *J* = 7.6 Hz, 6H), 6.96 (d, *J* = 7.4 Hz, 6H) and 4.18 (s (br), 12H). FT-IR (ν, cm^{-1}): 1339 (NO_2) and 1653 (C=O).

Perchlorate complex, [(**L$_3$H**)$^+$.(ClO_4)$^-$] (**3f**): Perchlorate complex was obtained by adding 0.5 mL of 49% perchloric acid ($HClO_4$) to a 15 mL MeOH suspension of **L$_3$** (150 mg,). After the addition of acid, the suspension was stirred for about 3 hours at room temperature. The resulting solution was filtered and the residue was collected and dried in vacuum. Yield 88%.

Melting point: 148-150°C. ^{1}H NMR (400 MHz, DMSO-d_6) δ (ppm): 10.49(s, 3N–H), 8.35(d, *J* = 8 Hz, 6H), 8.15 (d, *J* = 7.6 Hz, 6H), 7.70 (d, *J* = 8 Hz, 6H), 7.00 (d, *J* = 8 Hz, 6H), 4.44 (s (br), 6H) and 3.82 (s (br), 6H). FT-IR (ν, cm^{-1}): 1100 (ClO_4), 1345 (NO_2), 1671 (C=O) and 3387 (N–H).

2.5.4 Complexes of receptor L$_4$

Sulfate complex, [(**L$_4$H**)$_2^+$.(SO_4)$^{2-}$]·4DMF,2H_2O (**4a**). Complex **4a** was obtained by adding 3 ml aqueous solution of Na_2SO_4 (14mg 1mmol) to a 8 mL DMF solution of previously prepared perchlorate salt of receptor **L$_4$** (100 mg, 0.1 mmol). After the addition of aqueous Na_2SO_4, the mixture was stirred for about an hour at room temperature. The resulting mixture was filtered in a 20 ml conical flask and allowed to slowly evaporate at room temperature, which yielded block shape pale yellow crystals suitable for X-ray crystallography analysis within 8–10 days.

Melting point: 146°C. ^{1}H NMR (400 MHz, DMSO-d_6) δ (ppm): 9.57(s, 3H–N), 8.96(s, 3H–N), 8.10 (d, *J* = 9.2 Hz, 6H), 7.93(s, 2H, DMF solvent), 7.67 (d, *J* = 9.2 Hz, 6H), 7.39 (d, *J* = 8.8Hz 6H), 6.88 (d, *J* = 9.2 Hz, 2H), 4.25 (s (br), 6H), 3.51 (s (br), 6H), 2.874(s, 6H, DMF solvent) and 2.718 (s, 6H, DMF solvent). FT-IR (ν, cm^{-1}): 1214 (C−N), 1321 (NO_2 sym), 1561 (NO_2 asym), 1597 (C=C), 1717 (C=O) and 3307 (N−H).

TBAHSO$_4$ complex, $TBA^+[(\mathbf{L_4H})^+(SO_4^{2-})]\cdot 3H_2O$ (**4b**). Complex **4b** was obtained as single crystals suitable for X-ray diffraction (XRD) analysis by charging an excess $TBAHSO_4$ (10eq) to a 15 mL acetone suspension of receptor **L$_4$**. After the addition of $TBAHSO_4$, the suspension was stirred for about an hour at room temperature when a clear solution was formed. The resulting solution was filtered in a test tube and allowed to slowly evaporate at room temperature, which yielded pale yellow crystals suitable for X-ray crystallography analysis within 20 days.

Melting point: 158°C. ^{1}H NMR (400 MHz, DMSO-d_6) δ (ppm): 9.60 (s, 3H–N), 8.95 (s, 3H–N), 8.12 (d, *J* = 9.2 Hz, 2H), 7.67 (d, *J* = 9.2 Hz, 6H), 7.36 (d, *J* = 8.8 Hz, 6H,), 6.83 (d, *J* = 8.8 Hz, 6H), 4.06 (s (br), 6H), 3.15 (m (br), 18H), 1.55 (s (br), 8H), 1.26 (q, *J* = 7.2 Hz, 8H) and 0.92 (t, *J* = 7.2 Hz, 12H). FT-IR (ν, cm^{-1}): 1201 (C−N), 1335 (NO_2 sym), 1556 (NO_2 asym), 1601 (C=C) and 1714 (C=O).

K$_2$HPO$_4$ complex, $K^+[K^+(\mathbf{L_4})_2(HPO_4)^{2-}]\cdot 23H_2O$ (**4c**). Complex **4c** was obtained by adding previously prepared 3 ml aqueous solution of K_2HPO_4 (36mg 0.2mmol) to a 8 mL DMSO solution of **L$_4$** (185 mg, 0.2 mmol). After the addition of aqueous K_2HPO_4, the mixture was stirred for about an hour at room temperature. The resulting mixture was filtered in a 20 ml conical flask and allowed to slowly evaporate for crystallization at room temperature, which yielded tiny pale yellow crystals suitable for X-ray crystallography analysis within 15 days.

Melting point: 198°C. ^{1}H NMR (400 MHz, DMSO-d_6) δ (ppm): 9.69 (s, 3H–N), 9.02 (s, 3H–N) 8.11 (d, *J* = 9.2 Hz, 6H) 7.66 (d, *J* = 9.2 Hz, 6H), 7.36 (d, *J* = 8.8, Hz, 6H), 6.83 (d, *J* = 8.4 Hz 6H), 4.01 (t, *J* = 5.6 Hz, 6H) 3.00 (t, *J* = 5.2 Hz, 6H). FT-IR (ν, cm^{-1}): 1213 (C−N), 1333 (NO_2 sym), 1571 (NO_2 asym), 1604 (C=C), 1706 (C=O) and 3402 (N−H).

References

1. *SMART, SAINT and XPREP*; *Siemens Analytical X-ray Instruments Inc*.: Madison, WI, 1995.
2. G. M. Sheldrick, SADABS: *Software for Empirical Absorption Correction*; University of Gottingen, Institute fur Anorganische Chemieder Universitat: Tammanstrasse 4, D-3400, Gottingen, Germany, 1999-2003.
3. G.M. Sheldrick, *SHELXS-97*; University of Gottingen: Germany, 1997.
4. G. M. Sheldrick, *SHELXL-97*: *Program for Crystal Structure Refinement*; University of Gottingen, Gottingen, Germany, 1997.
5. P. V. d. Sluis and A. L Spek, *ActaCrystallogr.*,1990, *A46*, 194.
6. Mercury 2.3, Supplied with Cambridge Structural Database; CCDC, Cambridge, U.K., 2007.
7. S. K. Dey and G. Das, *Cryst. Growth Des.*, 2009, **12**, 750–760.
8. B. K. Dutta, C. Kar, A. Basu and G. Das, *Tetrahedron Lett*., 2013, **54**, 771–774.

Chapter 3

A Fluoride Selective Chromogenic Receptor with a Thiadiazole Spacer

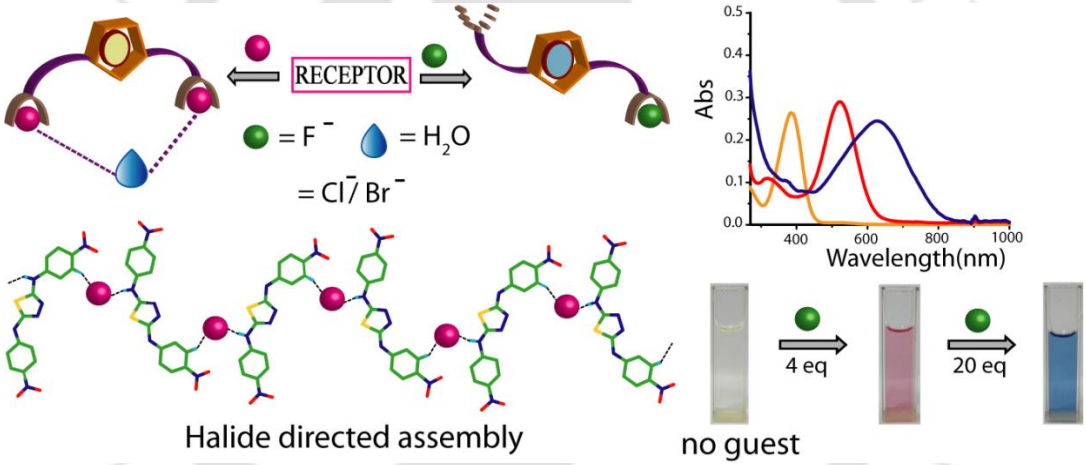

3.1 Background and focus of the chapter

The design and study of colorimetric sensors for biologically relevant anions has become a very active area of research within the field of supramolecular chemistry.[1] In particular, development of chemosensors for fluoride is more important due to their roles in the health, medical, and environmental sciences.[2] In the past few years, many synthetic receptors have been reported for sensing of fluoride ion along with the reports which show selective visible color changes in presence of this ion.[3] Colorimetric receptors have drawn special attention due to their ‘‘naked eye’’ detection of target species and also have the viability to offer both qualitative and quantitative insights of the receptor–guest interaction by using inexpensive spectrophotometric techniques.

On the other hand anion-directed assembly of coordination polymers has also attracted considerable attention motivated by their potential applications in recognition, separation, guest inclusion, and catalysis.[4] Indeed, several approaches have been fruitfully made to pursue anion-assisted variety of architectures by strengthening hydrogen bonding through electrostatic interaction with protonated ligands[5] or utilizing the metal−ligand interaction to assist formation of networks.[6] Moreover, anion-directed metal free self-assembled coordination polymer formation in a neutral system is rarely highlighted in the literature.[7] In this context, the structure of the receptor requires a tailored design to ensure that the anion-binding sites of the receptor should be well separated by a rigid spacer. The spacer favors formation of an anion-assisted self-assembled architecture by adapting suitable receptor−anion hydrogen-bonding interactions.

This chapter describes a newly synthesized neutral acyclic receptor $\mathbf{H_2L_1}$ with a thiadiazole spacer, which behaves as a selective chemosensor for fluoride ion. The fluoride recognition chemistry is immediately detected in solution by a dramatic increase in solubility of the receptor in CH_3CN with a concomitant optical signalling upon addition of TBAF and confirmed by UV/Vis spectroscopy. The detail UV/Vis spectroscopic titration experiments with increasing equivalents of fluoride anion suggest formation of a H-bonded complex with subsequent stepwise deprotonation of two N−H groups, which can be visually monitored by a change in color from yellow to blue *via* pink. Further, the solid state crystal structure of halide complexes of the receptor is also reported. Crystal structure analysis of the halide complexes elucidate the fact that fluoride forms an unusual 1:1 hydrogen-bonded complex with monodeprotonated receptor, whereas in the case of other congeners, such as chloride and bromide, the receptor binds two halide anions along with formation of a halide bridged 1D polymeric chain network by participation of N−H···X^- and aromatic C−H···X^- hydrogen-bonding (where X = Cl and Br) interactions. The presence of a rigid thiadiazole

spacer presumably opens up enough space for capturing two halide anions by a single receptor molecule, where the coordinated −NH protons are pointed in the same direction with respect to the spacer and eventually favor formation of halide (Cl^- and Br^-) induced polymeric architecture, although no obvious chloride or bromide-directed polymeric assembly is found in solution.

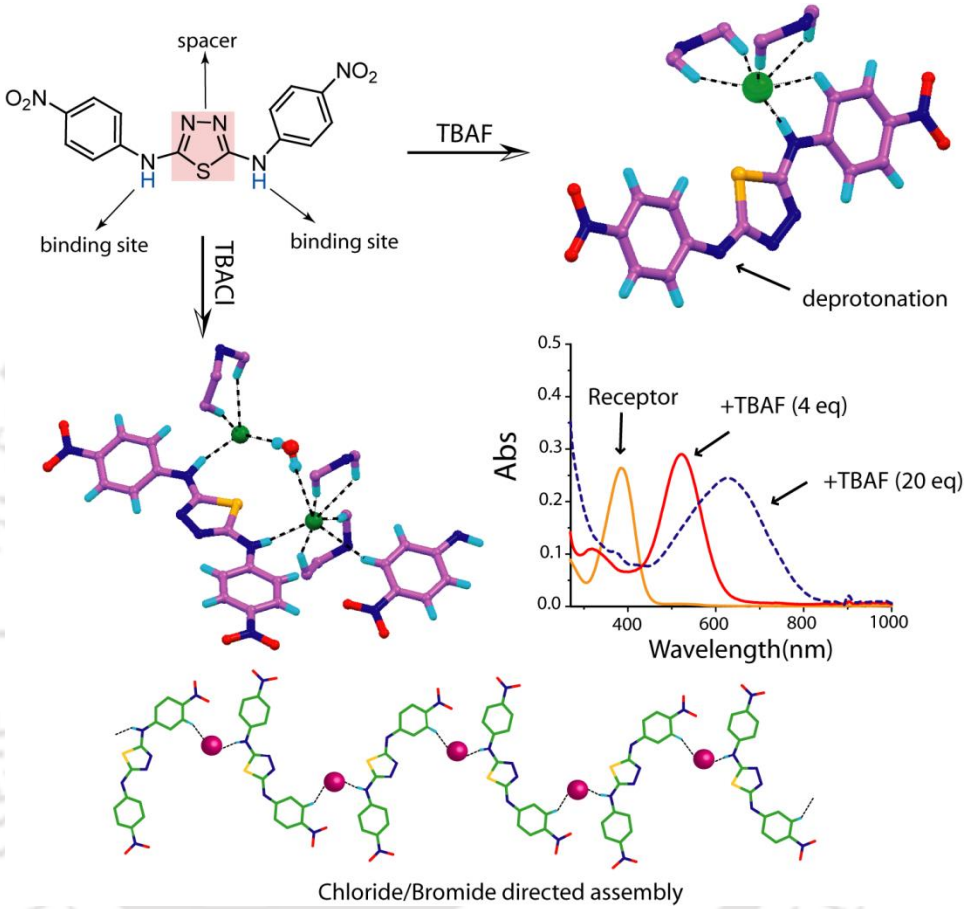

Scheme 3.1 Schematic representation depicting molecular structure of $\mathbf{H_2L_1}$, crystal structures of the halide complexes and fluoride selective step-wise UV/Vis spectral changes of the receptor.

3.2 Selective chromogenic sensing of fluoride anion

The fluoride recognition chemistry is immediately detected in solution by a dramatic increase in solubility of the receptor in acetonitrile (CH_3CN) with a concomitant optical signalling from colourless to blue upon addition of excess TBAF to the suspension of $\mathbf{H_2L_1}$. Whereas, addition of other halide anions such as, chloride, bromide and iodide do not induce any colorimetric response. The highly conjugated hydrogen bonding scaffold give rise to the colorimetric changes as the electron withdrawing, chromophoric nitrophenyl function being a part of the receptor, can possibly induce deprotonation and subsequent delocalization of the negative charge upon selective recognition of fluoride anion. The selective recognition of F^-

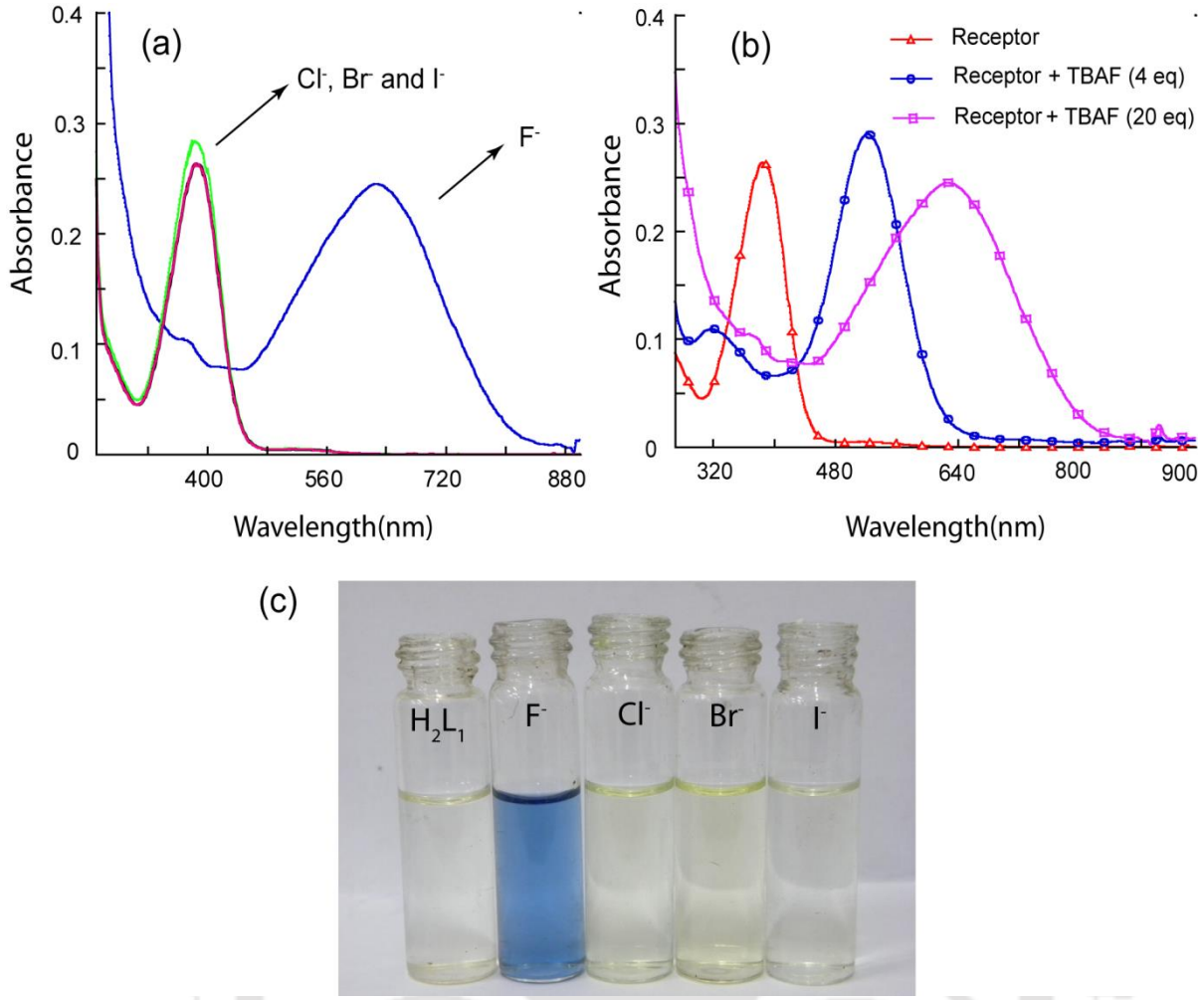

Figure 3.1 (a) Changes in the UV/Vis spectra of $\mathbf{H_2L_1}$ in CH_3CN upon addition of tetrabutylammonium salts of different halides (50 equiv); (b) Changes of UV/Vis spectra of $\mathbf{H_2L_1}$ (4.6×10^{-6} M) in CH_3CN upon addition of different equivalents of $[Bu_4N^+]F^-$ solution at 298 K ; (c) Color changes observed upon addition of different halides (50 equiv.) to CH_3CN solutions of $\mathbf{H_2L_1}$ ($\sim 10^{-5}$M).

by $\mathbf{H_2L_1}$ has been investigated in detail by UV/Vis spectroscopy. UV/Vis study suggests that $\mathbf{H_2L_1}$ can selectively detect fluoride ion in the visible region of the spectrum (Figure 3.1). Free receptor shows an absorption maximum at 385 nm in CH_3CN. However, addition of excess fluoride ion (50 equiv as TBA salt) shows the disappearance of the peak at 385 nm with concomitant emergence of a new peak at 628 nm (Figure 3.1a). A significant red shift of 243 nm is fairly comparable to the report by Zhao et al.,[3l] and Ghosh et al.[3m] To evaluate the fluoride binding, quantitative UV/Vis titration of $\mathbf{H_2L_1}$ is carried out with increasing equivalents of F^-. The titration experiment (Figures 3.2) reveals that a fluoride induced color change of the receptor occurs in a ratiometric fashion. Initially, at lower concentration of fluoride ions, the light yellow solution of $\mathbf{H_2L_1}$ turned pink at 4 equiv of F^- addition and then turned blue at higher F^- equivalents (~20 equiv) (Figure 3.2b). This significant change in

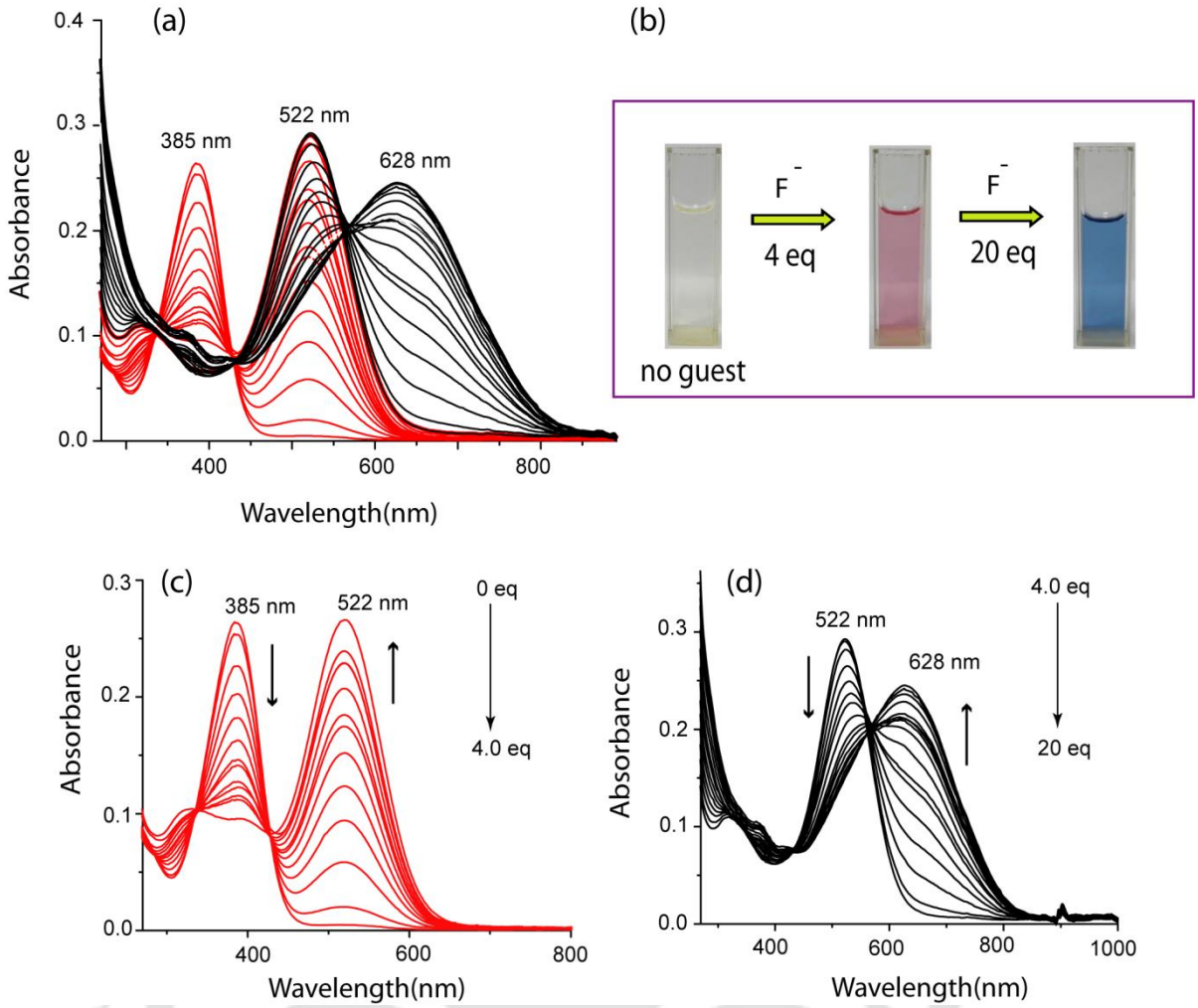

Figure 3.2 (a) UV/Vis absorption titration of $\mathbf{H_2L_1}$ (4.6 x 10^{-6} M) in CH_3CN solution upon addition of standard solution of fluoride ions; (b) Stepwise color change observed for the receptor $\mathbf{H_2L_1}$ ($\sim 10^{-5}$) upon addition of different equivalents of standard $[Bu_4N^+]F^-$ solution. Showing separated spectra from the titration plot (c) from 0 to 4 equiv of $[Bu_4N^+]F^-$; (d) from 4 to 20 equiv of $[Bu_4N^+]F^-$.

the UV/Vis spectrum of receptor $\mathbf{H_2L_1}$ upon quantitative addition of fluoride anion suggests that the interaction between the fluoride and $\mathbf{H_2L_1}$ takes place in three well-defined steps, similar to the sequence previously reported.[3d,m] In particular, upon gradual addition of standard fluoride solution (1 x 10^{-3} M) to the solution of $\mathbf{H_2L_1}$ (4.6 x 10^{-6} M) the UV/Vis absorption at 385 nm decreases and a new peak at 522 nm appears with two distinct isosbestic points at 426 and 335 nm up to 4 equiv of fluoride addition (Figure 3.2c). We assume this spectral change is due to the combination of both receptor−fluoride H-bonded complex formation and fluoride-induced monodeprotonation of the receptor.[3l] Moreover, further addition of fluoride decreases the intensity of the band centered at 522 nm with the emergence of a new band at 628 nm with a sharp isosbestic point at 562 nm (Figure 3.2d). This process is initiated when the fluoride concentration is more than 4 equiv and reaches its saturation after addition of 20 equiv of fluoride. Further generation of a new peak in the red-

shifted region (628 nm) indicates the fluoride-induced double deprotonation of the receptor in solution.[3d] The fluoride induced stepwise double deprotonation of the receptor **H_2L_1** was confirmed by titrating the receptor with standard $[Bu_4N^+]OH^-$ (Figure 3.3). The titration spectra display consecutive development of bands at 522 nm (associated to mono deprotonation) and 628 nm (associated to double deprotonation) after addition of 1 and 5 equiv of standard $[Bu_4N^+]OH^-$ solution respectively. [3d]

As the spectral changes due to formation of the H-bonded complex and the first deprotonation occur in the same concentration range of added F^-, the individual steps cannot be analyzed in solution. Therefore, the apparent binding constant of fluoride binding to **H_2L_1** is calculated on the basis of the change in absorbance at 522 nm and considering a 1:1 binding isotherm; a value of log K_{app} = 3.75 (error 10%) is determined.[3l] The apparent binding constant K_{app} is a combined binding constant for both the hydrogen-bonded complex and the first deprotonation steps. Moreover, the significantly high fluoride-induced red shift (243 nm) of the receptor is probably due to its planarity and conjugation, which help complete delocalization of the negative charge(s) of the deprotonated receptor.

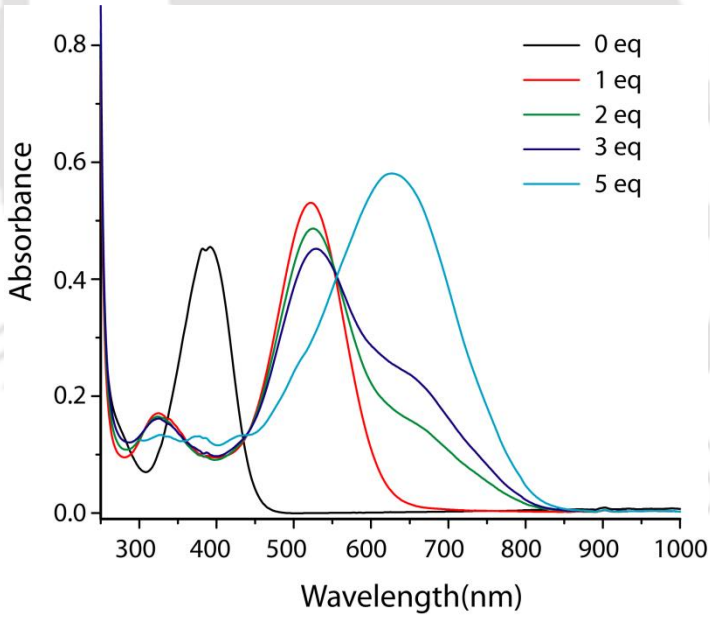

Figure 3.3 Family of spectra taken in the course of the titration of a CH_3CN solution 7.2 x 10^{-6} M in receptor **H_2L_1** with a standard solution of $[Bu_4N^+]OH^-$, at 25 °C.

3.3 Halide binding study by ^{1}H NMR spectroscopy

The binding properties of the receptor **H_2L_1** with halides in solution are investigated by ^{1}H NMR experiments in DMSO-d_6 in the presence of various halides as their $[Bu_4N^+]X^-$ salts (where X = F, Cl, Br, and I) at room temperature. Figure 3.4 shows the chemical shift changes found by addition of different halides to the receptor **H_2L_1** in DMSO-d_6. The most

substantial changes are observed for the −NH protons, indicating that the –NH protons of receptor **H_2L_1** provides suitable sites of interaction between the receptor and the halides (Figure 3.4). ^{1}H NMR titration of receptor **H_2L_1** with $[Bu_4N^+]F^-$ shows that upon gradual addition of standard F^- solution a small but important change in the chemical shift of the aryl −CH protons $\Delta\delta = 0.08$ is observed, indicating fluoride induced a change in the electronic environment (probably due to deprotonation) of the −CH protons (Figure 3.10). In addition, a significant disappearance of the −NH proton is observed. The disappearance of the −NH proton is noticed even after the first addition (0.25 equivalents) of fluoride ion (Figure 3.10). This is due to the binding induced broadening of the −NH signals rather than deprotonation, which is supported by the absence of a characteristic HF_2^- peak at ~16.0 ppm.[31] Moreover, after addition of 4 equiv of F^-, the appearance of broad HF_2^- signals at 16.1 ppm suggests deprotonation of the N−H protons of the receptor **H_2L_1** (Annexure 3). These results from ^{1}H NMR titration experiments preclude determination of a suitable binding constant with fluoride, whereas significant downfield shifts of the N−H proton $\Delta\delta = 0.84$ for Cl^- and $\Delta\delta = 0.15$ in the case of Br^- are observed. There is no notable change in the chemical shift of the NH protons with I^-, indicating the hydrogen-bonding interactions between receptor and the iodide anion are energetically unfavorable. Subsequently, ^{1}H NMR titrations were carried out with Cl^- and Br^- in DMSO-d_6 at 298 K. The ^{1}H NMR titration spectra of the receptor **H_2L_1** in the presence of increasing amounts of $[Bu_4N^+]Cl^-$ and $[Bu_4N^+]Br^-$ are shown in Figure 3.11 and Figure 3.13 respectively. The binding stoichiometry between the receptor **H_2L_1** and both anions is determined by Job plot experiments (Figure 3.12 and 3.14). The maximum changes in the chemical shift during the titrations are obtained when the mole fraction of both anions has reached about 0.67 which suggests a host−guest binding in a 1:2 stoichiometry. The cumulative binding constant for Cl^- ion ($\log \beta = 3.92$) is higher than that of Br^- ($\log \beta = 2.87$), indicating that the receptor preferentially binds chloride more than bromide. This is due to the higher basicity and smaller ionic radii of chloride compare to bromide anion. Detailed ^{1}H NMR titration experiments showed that the affinity order of different halides toward **H_2L_1** is $Cl^- > Br^- > I^-$. We kept the fluoride anion out of the halide binding affinity order of the receptor **H_2L_1** because the spectroscopic results demonstrate that apart from receptor−fluoride hydrogen-bonded complex formation the fluoride anion also deprotonates the receptor in the same concentration range (4 equiv). Therefore, it is difficult to get a real binding constant for fluoride from this experiment.

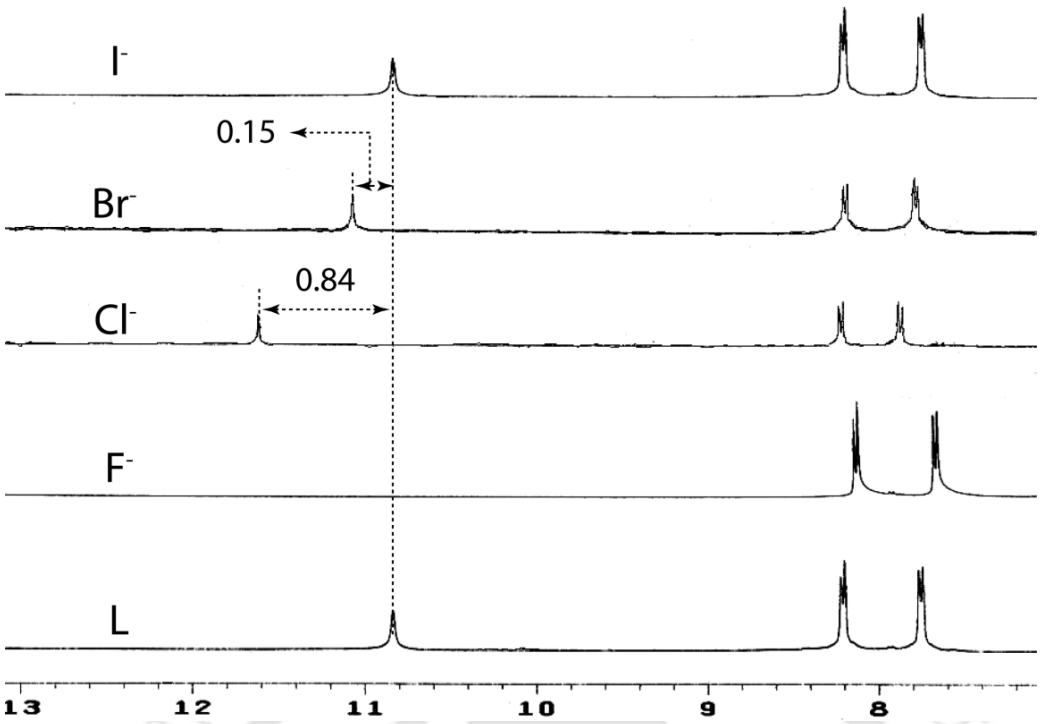

Figure 3.4 ^{1}H NMR spectra (400 MHz, DMSO-d_6, 298 K) of $\mathbf{H_2L_1}$ and change of −NH resonance upon addition of F^-, Cl^-, Br^-, and I^- as their tetrabutylammonium salts.

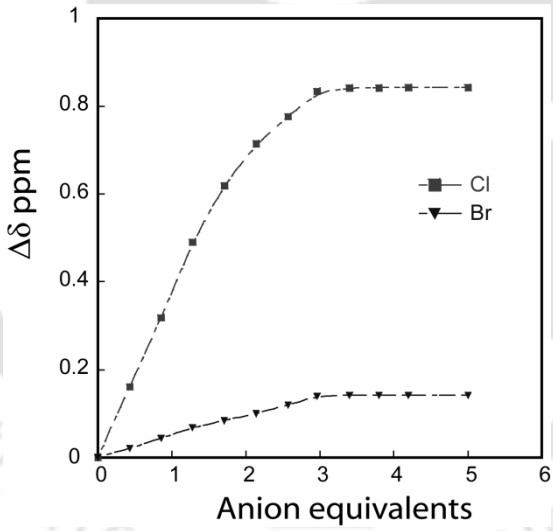

Figure 3.5 Plot of the change in the chemical shift of the −NH proton of $\mathbf{H_2L_1}$ with increasing amounts of $[Bu_4N^+]X^-$ in DMSO-d_6 at 298 K (where X = Cl and Br).

3.4 Structural aspects of anion binding with H_2L_1

Three anion complexes of the $\mathbf{H_2L_1}$ (**1a-1c**) were obtained as single-crystals suitable for X-ray diffraction analysis by slow evaporation of individual acetonitrile (CH_3CN) solutions of $\mathbf{H_2L_1}$ in presence of excess tetrabutylammonium salts of different halides (F^-, Cl^-, and Br^-). Structural information obtained from XRD analysis of the isolated crystals provide insight into the proper binding topology of halides (F^-, Cl^- and Br^-) with the receptor molecule, which are then related to the observed selectivity in solution.

3.5 X-ray crystal structure analysis of receptor halide complexes

3.5.1 Structural description of fluoride complex (1a)

The crystal structure of the fluoride complex revealed some interesting features of the complex. Dark violet block-shaped single crystals of the fluoride complex were grown from acetonitrile solution as [$\mathbf{HL_1}$(F)(n-$Bu_4N)_2$] with a satisfactory yield of about 55% upon iso-thermal slow evaporation of a mixture of $\mathbf{H_2L_1}$ and 5 equiv of [n-Bu_4N]F. The fluoride complex crystallizes in the orthorhombic system with a *Pnma* space group with

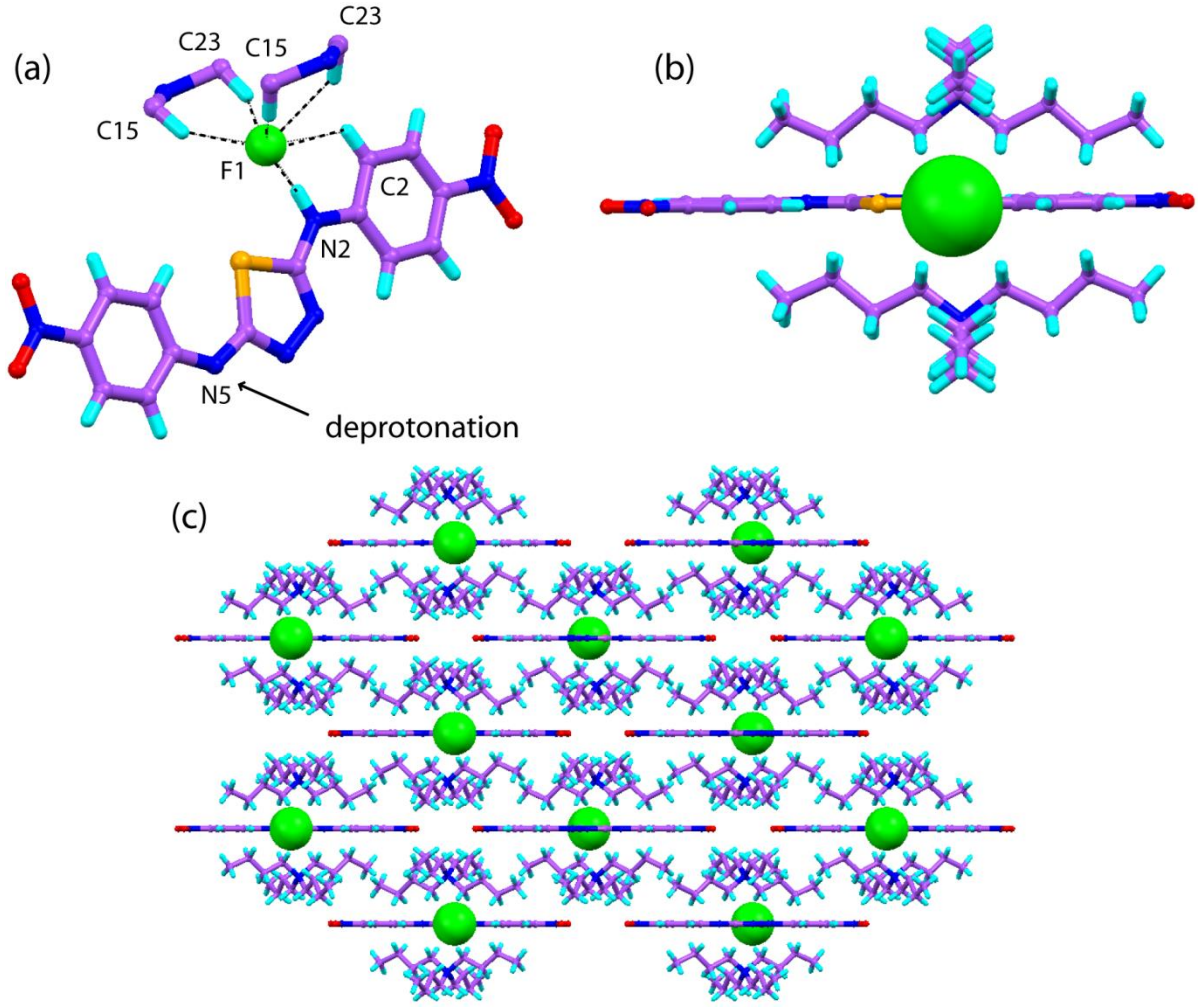

Figure 3.6 (a) Hydrogen-bonding interactions of fluoride anion with monodeprotonated receptor ($\mathbf{HL_1}^-$) and two tetrabutylammonium groups. Only the interacting parts of the tetrabutylammonium units have been shown for clarity. Dashed lines indicate the hydrogen bonding interactions; (b) Crystal structure of the fluoride complex showing the presence of F^- anion in the same molecular plane and the fluoride anion is exactly sandwiched between two tetrabutylammonium groups; (c) Crystal packing in complex **1a**, as viewed down the crystallographic c axis.

Z = 4 (Table 3.1). The structural analysis shows formation of an unusual 1:1 host−guest complex with monodeprotonated receptor and fluoride anion, and the fluoride anion is stabilized by six hydrogen bonds involving one −NH proton (N2H), one aryl –CH proton (C2H) of the monodeprotonated receptor, and four aliphatic−CH protons from the acidic

−CH_2 group, adjacent to the bridgehead nitrogen of two different tetrabutylammonium cations present in close proximity with fluoride anion. The presence of two tetrabutylammonium cations and a hydrogen-bonded fluoride in the crystal lattice of the fluoride complex supports the fact that the receptor present is in its monodeprotonated form, which is further confirmed by taking ^{1}H NMR spectra of the isolated pure crystals of the fluoride complex (Annexure 3). The significantly small N···F^- distance of 2.300(9) Å suggests that the deprotonated receptor forms strong hydrogen bond with fluoride. Notable, the unusual formation of a 1:1 fluoride complex with monodeprotonated receptor ($\mathbf{HL_1}^-$) in the solid state is well consistent with the fluoride-induced complex UV/Vis spectral behavior of the receptor $\mathbf{H_2L_1}$ in CH_3CN solution and the presence of the absorption band at 522 nm in the UV/Vis spectrum of isolated single crystals of the fluoride complex in CH_3CN solution supports our assumption (Annexure 3), that during UV/Vis titration the fluoride induced generation of new band at 522 nm is a combination of both receptor−fluoride H-bonded complex formation and fluoride induced monodeprotonation of the receptor ($\mathbf{H_2L_1}$). The mode of hydrogen-bonding interactions of the fluoride anion with monodeprotonated receptor and tetrabutylammonium groups is shown in Figure 3.6a, and the corresponding parameters are given in Tables 3.2 and 3.3. It is interesting to observe that in the fluoride complex (**1a**) the monodeprotonated receptor is present in its anti-conformation with respect to the thiadiazole spacer. This conformation is due to minimizing the repulsion between two negatively charged species (fluoride anion and N5 atom of monodeprotonated receptor). Furthermore, it is important to mention here that while interacting with the fluoride ion the monodeprotonated receptor ($\mathbf{HL_1}^-$) adopts an exactly planar geometry (Figure 3b) which is also well consistent with our prediction from UV/Vis titration experiment. The planarity of the receptor in complex **1a** eventually favors formation of an aromatic C−H···F^- interaction involving the aryl proton C2H of the adjacent nitro phenyl ring due to its directionality acquired because of the planarity. Close inspection of the crystal structure elucidates that the fluoride anion is getting sandwiched between two cationic tetrabutylammonium units by four aliphatic C−H···F^- interactions with an average donor to acceptor distance 3.15 Å (Figure 3.6b). Formation of a 1:1 complex between fluoride and monodepronated receptor could be justified due to the higher basicity of the fluoride ion. The approaches of more than two fluoride anions to the receptor $\mathbf{H_2L_1}$ initiate the deprotonation process, and thereby, we found in the fluoride complex the receptor present in its monodeprotonated form with a hydrogen-bonded fluoride anion.

3.5.2 Structural description of chloride complex (1b)

Light orange block-shaped crystals of chloride complex [$\mathbf{H_2L_1}(Cl)_2(n\text{-}Bu_4N)_2]\cdot H_2O$ suitable for single-crystal X-ray diffraction analysis were obtained after 20 days of slow evaporation of an acetonitrile (CH_3CN) solution of the receptor $\mathbf{H_2L_1}$ in the presence of excess [n-Bu_4N]Cl with an isolated yield of about 48%. The complex crystallized into the orthorhombic space group *Pna21* with Z = 4 (Table 3.1). Structural elucidation of the complex reveals that the receptor is involved in a 1:2 binding stoichiometry of host to guest where each chloride anion is bound to a single receptor molecule by a moderate N−H···Cl^- interaction (Figure 3.7a) together with the hydrogen-bonding participation from adjacent TBA countercations and the lattice water molecule. The hydrogen-bonding interactions of chloride anions with the receptor and adjacent tetrabutylammonium groups are shown in Figure 3.7b along with the atom numbering scheme. The crystallizing water molecule behaves as a hydrogen-bonded bridge between two coordinated anions forming a $[Cl_2H_2O]^{2-}$ triangle with a Cl^-−O−Cl^- angle of 114.9(1)° and Cl^-−Cl^- separation distance of 5.643(2) Å

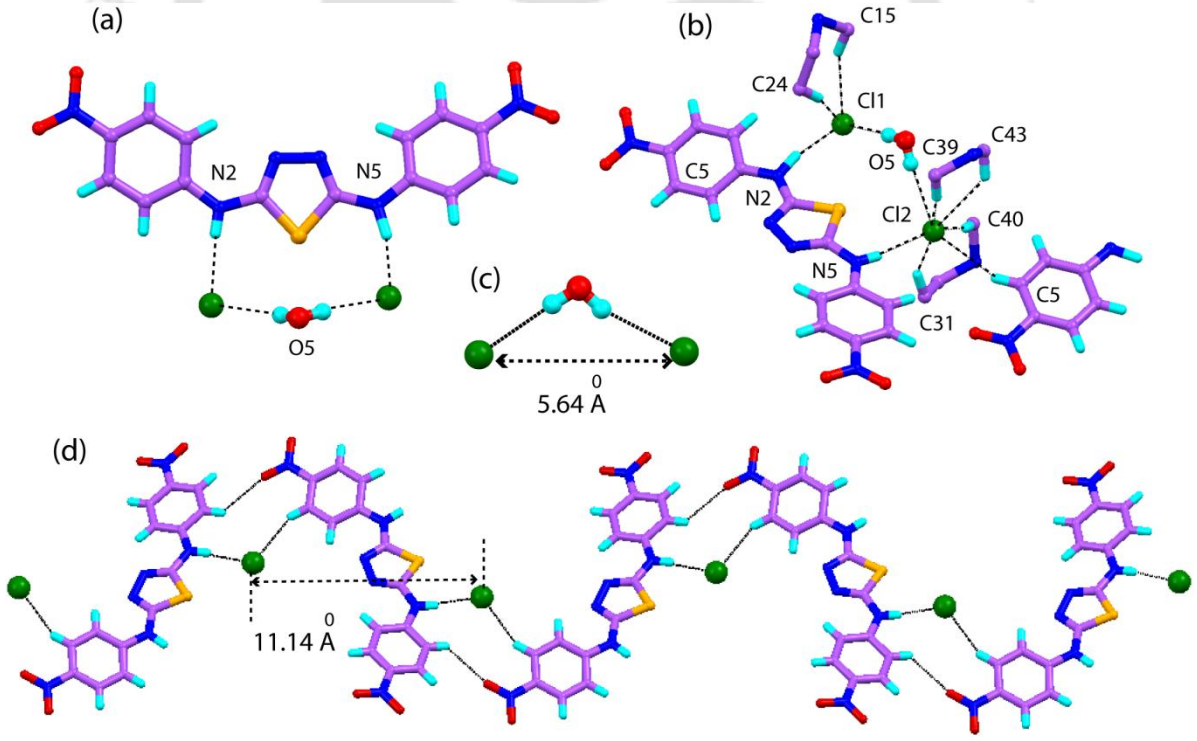

Figure 3.7 (a) Molecular structure of complex 1b. tetrabutylammonium cations are omitted for clarity; (b) Hydrogen-bonding interactions of chloride anions with receptor ($\mathbf{H_2L_1}$) and tetrabutylammonium groups in **1b**. Only the interacting parts of the tetrabutylammonium unit have been shown for clarity; (c) Magnified view of the water chloride hydrogen-bonding interactions. Dashed lines indicate the hydrogen-bonding interactions; (d) Formation of a chloride Cl^- (2) directed network obtained by self-assembly (view along the b axis). Countercations [n-Bu_4N^+] and solvent molecules and the other chloride anion (Cl^- (1)) are omitted for clarity. Hydrogen bonds have been drawn as dashed lines.

(Figure 3.7c).The presence of a rigid thiadiazole spacer between the two acidic NH protons of $\mathbf{H_2L_1}$ resists the convergent hydrogen bonding to a single chloride anion, whereas convergent hydrogen bonds to an acceptor species are quite common for urea/thioureabased anion receptors. In complex **1b** both the N−H protons of the receptor are directed in the same direction (syn) and participate in hydrogen bonding interactions with two different chloride anions. The donor−acceptor distances ($N\cdots Cl^-$) fall in the range 3.10−3.14 Å, which corresponds to formation of moderate hydrogen bonds, mainly electrostatic in nature, whereas, in case of fluoride complex the monodeprotonated receptor forms strong hydrogen bonds with fluoride anion.[8] Structural analysis of the complex (**1b**) reveals that Cl^- (1) is stabilized by four hydrogen bonds involving one −NH proton (N2H), one −OH proton (O5H, lattice water), and two aliphatic−CH protons (C15H and C24H) from a nearby tetrabutylammonium unit (Figure 3.7b and Tables 3.2 and 3.3). On the other hand, Cl^- (2) is stabilized by participation of seven hydrogen bonds involving one −NH proton (N5H), one aryl −CH proton (C5H), one −OH proton (O5H, lattice water), and four aliphatic −CH protons from two neighboring tetrabutylammonium units donating two $C-H\cdots Cl^-$ hydrogen bonds each (Figure 3.7b and Tables 3.2 and 3.3). One of the nitro phenyl rings is slightly twisted out of the plane relative to the central thiadiazole ring, where the angle between the planes of the two rings is 25.08°, indicating the receptor is not planer in complex **1b**. Additionally, one of the ortho aryl hydrogens (C5H) with respect to the nitro group of the twisted nitro phenyl ring forms a significant $C-H\cdots Cl^-$ hydrogen-bonding interaction with the neighboring Cl^- (2) anion. This $C-H\cdots Cl^-$ interaction leads to formation of an anion-bridged 1D polymeric chain network in association with the moderate $N-H\cdots Cl^-$ (2) H bond along with a weak intermolecular C−H···O (nitro) interaction (Figure 3.7d). The chloride Cl^-(2) anions in this polymeric chain extension are alternately arranged in a zigzag array with a distance of 11.49(2) Å and $Cl^-\cdots Cl^-\cdots Cl^-$ angle of 149.20(2)°. The other chloride anion Cl^- (1) is not involved in this polymeric array.

3.5.3 Structural description of bromide complex (1c)

Single crystals suitable for X-ray diffraction analysis of the bromide complex were obtained as $[\mathbf{H_2L_1}(Br)_2(n\text{-}Bu_4N)_2]\cdot H_2O$ with a fair yield (42%) by isothermal slow evaporation of an acetonitrile solution of the receptor $\mathbf{H_2L_1}$ in the presence of a large excess of $[Bu_4N^+]Br^-$. The complex crystallized into the orthorhombic space group *Pna21* with Z = 4 (Table 3.1). Interestingly, X-ray crystal structure analysis of the bromide complex reveals that the receptor $\mathbf{H_2L_1}$ interacts with bromide anions in exactly the same fashion as that of chloride anions (Figure 3.8). Hydrogen-bond distances of the bromide complex are slightly greater

than those of the chloride complex (Tables 3.2 and 3.3). This is due to the larger ionic radii and lower basicity of the bromide ion compared to chloride. Similar to the chloride complex, here also the bromide-bridged 1D chain polymeric network structure is observed. Notably this type of halide (Cl^-/Br^-) coordination induced formation of 1D polymeric chain network in a neutral system is not very common in literature.[7]

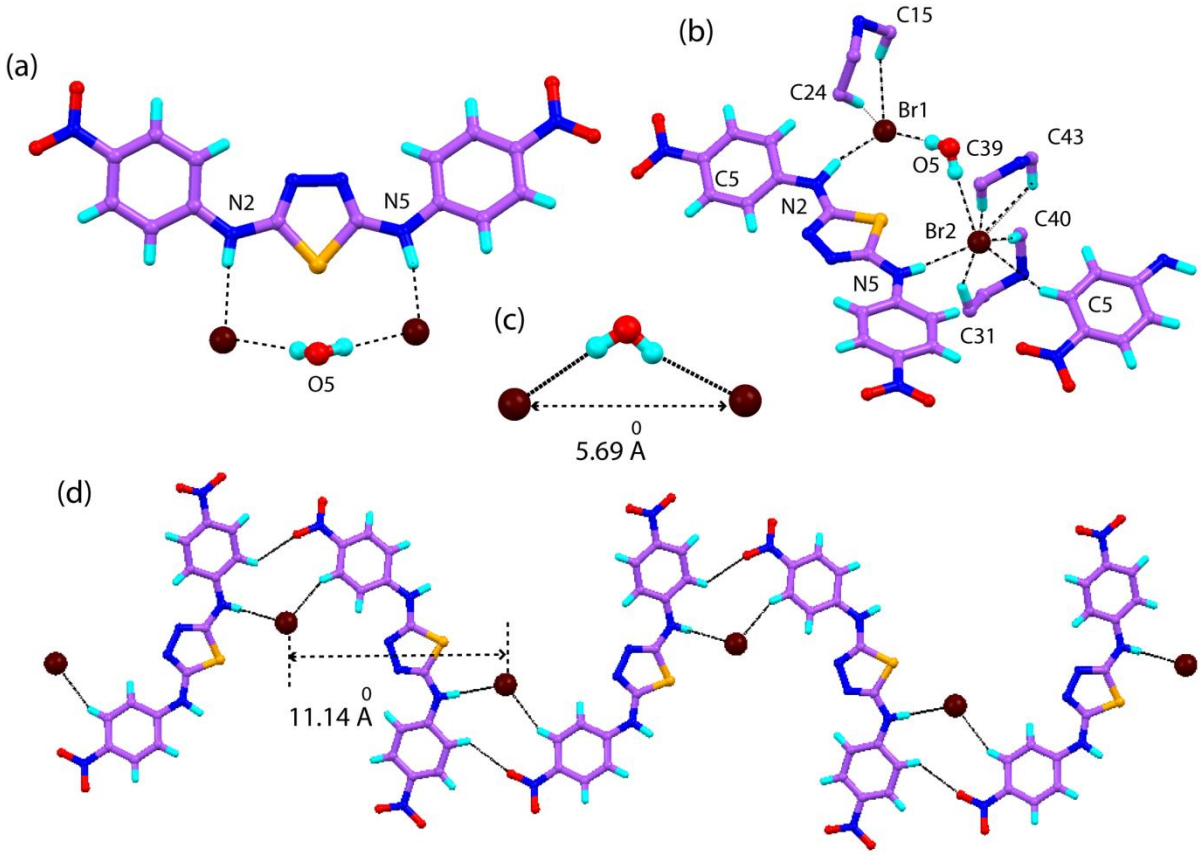

Figure 3.8 (a) Molecular structure of complex **1c**. tetrabutylammonium cations are omitted for clarity; (b) Hydrogen-bonding interactions of bromide anions with receptor (**H_2L_1**) and tetrabutylammonium groups in **1c**. Only the interacting parts of the tetrabutylammonium unit have been shown for clarity; (c) Magnified view of the water chloride hydrogen-bonding interactions. Dashed lines indicate the hydrogen-bonding interactions; (d) Formation of a chloride Br^- (2) directed network obtained by self-assembly (view along the b axis). Counter cations [n-Bu_4N^+] and solvent molecules and the other chloride anion (Br^- (1)) are omitted for clarity. Hydrogen bonds have been drawn as dashed lines.

The overall crystal structure analyses of the receptor−halide complexes reveal that 1:2 chloride and bromide complexes form a halide-bridged 1D polymeric chain network by participation of N−H···X^- and aromatic C−H···X^- hydrogenbonding (where X = Cl and Br) interactions. Most likely the rigid thiadiazole spacer opens up enough space to confine two halide anions by a single receptor molecule which eventually favors formation of halide (Cl^- and Br^-) induces 1D polymeric chain, whereas no such fluoride-induced polymeric architecture is observed in the fluoride complex. Presumably the fluoride induces formation

of a 1:1 complex between monodeprotonated receptor, and the fluoride anion prevents construction of any fluoride-induced polymeric assembly in the solid state. Significantly, in all three halide complexes the aliphatic CH protons of the tetrabutylammonium countercations actively participate in the hydrogen-bonding interactions with halides. This type of hydrogen-bonding interaction between anions and nonaromatic CH groups as hydrogen-bond donors is very rare in the literature and the C−H···anion interactions involving organic cations have also attracted considerable attention because of their biological and chemical importance.[9]

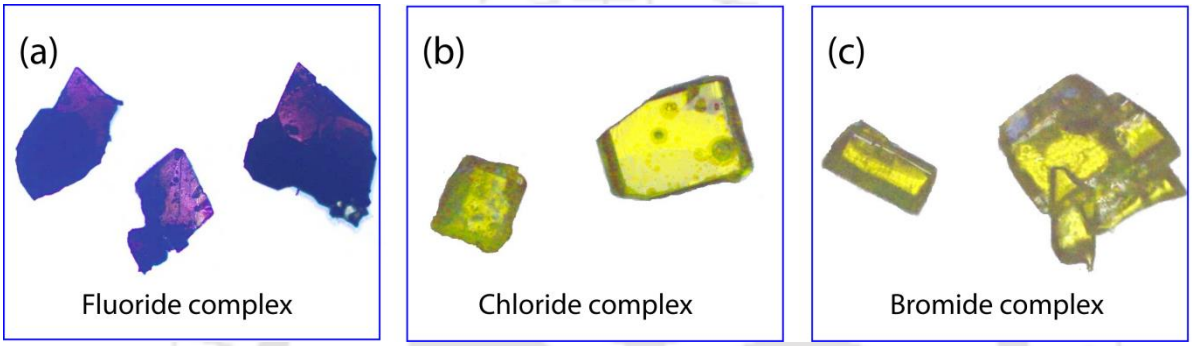

Figure 3.9 Optical micrograph images of crystals (a) Fluoride complex (**1a**); (b) Chloride complex (**1b**) and; (c) Bromide complex (**1c**).

3.6 Conclusion

We systematically investigated the halide binding of a newly synthesized anion receptor with a thiadiazole spacer $\mathbf{H_2L_1}$ both in solution and in the solid state. This receptor selectively recognizes fluoride among the other halides, which is manifested by a visual color change. A significant red shift of 243 nm in the absorption spectra of $\mathbf{H_2L_1}$ was solely observed in the presence of excess fluoride anion, which enables $\mathbf{H_2L_1}$ as an efficient colorimetric sensor for optical detection of fluoride anion (yellow to blue). Furthermore, spectroscopic titration experiments with increasing equivalents of fluoride anion suggest formation of a H-bonded complex with subsequent stepwise deprotonation of two N−H groups, which can be visually monitored by a change in color from yellow to blue *via* pink. Further the qualitative and quantitative ^{1}H NMR experiments corroborate that except iodide the receptor forms a hydrogenbonding complex with the other halides. Detailed crystal structure analysis of the halide complexes ascertains that the fluoride forms a 1:1 hydrogen-bonded complex with monodeprotonated receptor ($\mathbf{HL_1}^-$), while in the case of the other halides (Cl^- and Br^-) the receptor $\mathbf{H_2L_1}$ binds two halides along with formation of a halide-bridged 1D zigzag chain polymeric network structure by participation of N−H···X^- and aromatic C−H···X^- hydrogen-bonding interactions (where X = Cl and Br), although no chloride or bromide-

directed polymeric assembly are found in solution. Therefore, such structural features are worthwhile only in the solid state. Moreover, the presence of a thiadiazole spacer in the receptor significantly affects the hydrogen-bonding nature between the receptor and the halides, which in turn helps to form an anion-induced 1D polymeric structure.

Table 3.1 Crystallographic parameters and refinement details of halide complexes of the receptor **H_2L_1 (1a−1c)**.

Parameters	**1a**	**1b**	**1c**
Formula	$C_{46}H_{81}FN_8O_4S$	$C_{46}H_{84}Cl_2N_8O_5S$	$C_{46}H8_4Br_2N_8O_5S$
Fw	861.26	932.18	1021.08
Cry. system	Orthorhombic	Orthorhombic	Orthorhombic
Space group	*Pnma*	*Pna2(1)*	*Pna2(1)*
a/Å	40.264(7)	31.492(3)	31.372(7)
b/Å	12.8688(18)	8.0970(7)	8.1971(19)
c/Å	9.7766(16)	21.497(2)	21.581(5)
α/^{o}	90.00	90.00	90.00
β/^{o}	90.00	90.00	90.00
γ/^{o}	90.00	90.00	90.00
V/Å^3	5065.7(14)	5481.5(8)	5550.0(2)
Z	4	4	4
D_c/g cm^{-3}	1.131	1.130	1.222
μ (mm^{-1})	0.115	0.204	1.545
T/^{o}K	298(2)	298(2)	298(2)
Total reflns	56387	38664	24379
Ind. reflns	4598	4827	4604
Obs. reflns	4549	4780	4548
Parameters	314	583	585
R1; wR2 (I > 2σ(I))	0.0671, 0.0802	0.0533, 0.1677	0.0459, 0.1097
R(int)	0.1782	0.0633	0.0857
GOF (F^2)	1.099	0.893	0.992

Table 3.2 C−H···anion hydrogen-bonding interactions in receptor−halide complexes (**1a-1c**).

Complex	Donor group	D···A[Å]	H···A [Å]	D–H···A[°]	Acceptor atom
1a	C(2)–H(2)	3.255(1)	2.669(5)	121.5(7)	F1
	C(15)– H(15A)	3.063(5)	2.183(3)	150.3(3)	F1
	C(23)–H(23B)	3.255(5)	2.437(4)	141.8(3)	F1
1b	C(5)–H(5)	3.664(6)	2.810(1)	153.3(3)	Cl2
	C(39)–H(39A)	3.616(6)	2.717(1)	154.4(4)	Cl2
	C(43)–H(43A)	3.689(6)	2.917(1)	137.2(4)	Cl2
	C(31)–H(31A)	3.743(6)	2.787(1)	168.9(4)	Cl2
	C(40)–H(40B)	3.612(9)	2.771(1)	145.6(7)	Cl2
	C(15)–H(15A)	3.825(7)	2.913(1)	157.0(4)	Cl1
	C(24)–H(24B)	3.802(7)	2.905(1)	154.4(4)	Cl1
1c	C(5)–H(5)	3.673(8)	2.814(9)	154.0(4)	Br2
	C(39)–H(39A)	3.670(7)	2.774(9)	153.8(5)	Br2
	C(43)–H(43A)	3.800(8)	3.006(9)	140.0(5)	Br2
	C(31)–H(31A)	3.844(8)	2.878(8)	172.8(5)	Br2
	C(40)–H(40B)	3.640(1)	2.812(9)	144.1(9)	Br2
	C(15)–H(15A)	3.873(8)	2.963(8)	156.6(5)	Br1
	C(24)–H(24B)	3.899(9)	3.011(9)	152.8(6)	Br1

Table 3.3 N−H···anion and O−H···anion hydrogen-bonding interactions in receptor−halide complexes (**1a-1c**).

Complex	Donor group	D···A[Å]	H···A [Å]	D–H···A[°]	Acceptor atom
1a	N(2)–H(2N)	2.299(9)	1.440(5)	175.6(5)	F1
1b	N(2)–H(2N)	3.076(4)	2.216(4)	168.0(4)	Cl1
	N(2)–H(2N)	3.113(4)	2.258(6)	173.3(5)	Cl2
	O(5)–H(5O)	3.320(5)	2.465(6)	172.8(5)	Cl1
	O(5)–H(6O)	3.374(6)	2.537(7)	167.6(9)	Cl2
1c	N(2)–H(2N)	3.193(8)	2.300(8)	173.0(6)	Br1
	N(2)–H(2N)	3.255(7)	2.300(8)	166.6(4)	Br2
	O(5)–H(5O)	3.404(7)	2.568(7)	165.2(6)	Br1
	O(5)–H(6O)	3.464(6)	2.645(4)	162.0(5)	Br2

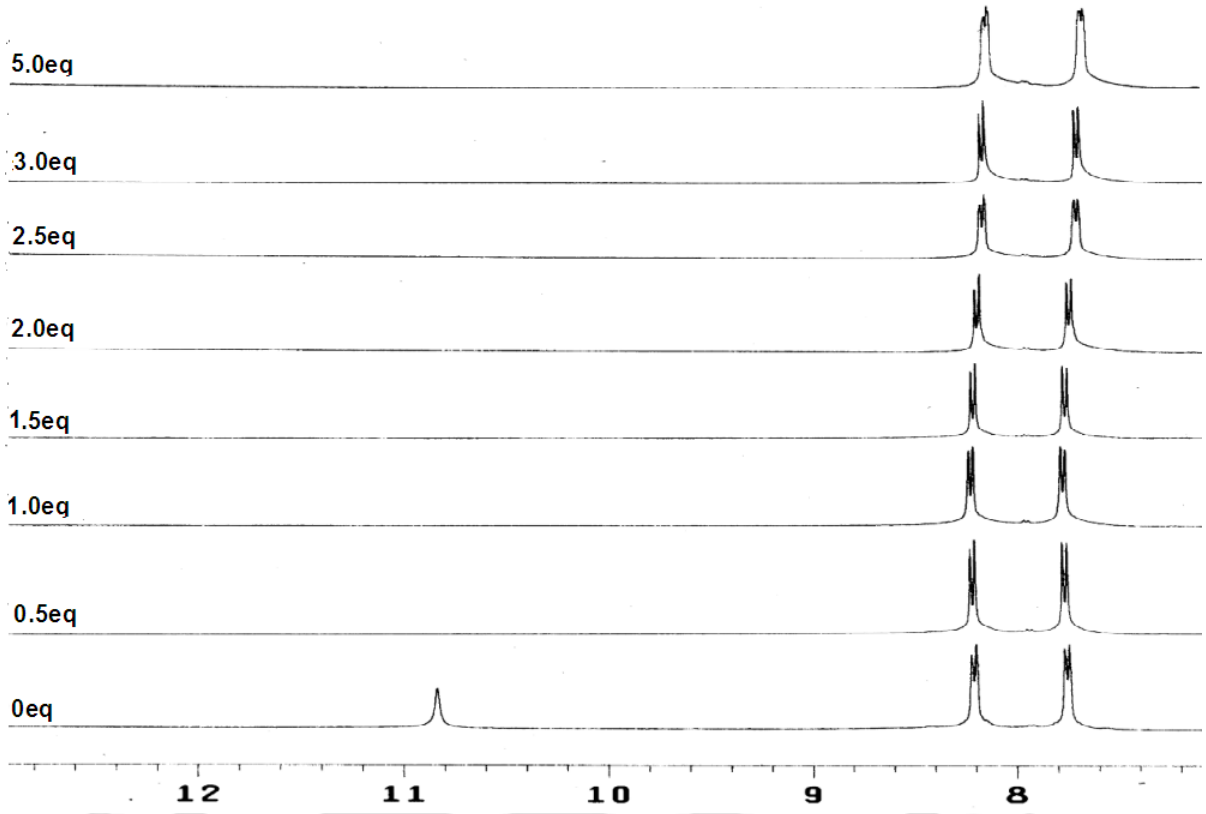

Figure 3.10 Stack plot of the ^{1}H NMR spectra of receptor $\mathbf{H_2L_1}$ in the presence of increasing amounts of $[Bu_4N^+]F^-$ recorded in DMSO-d_6.

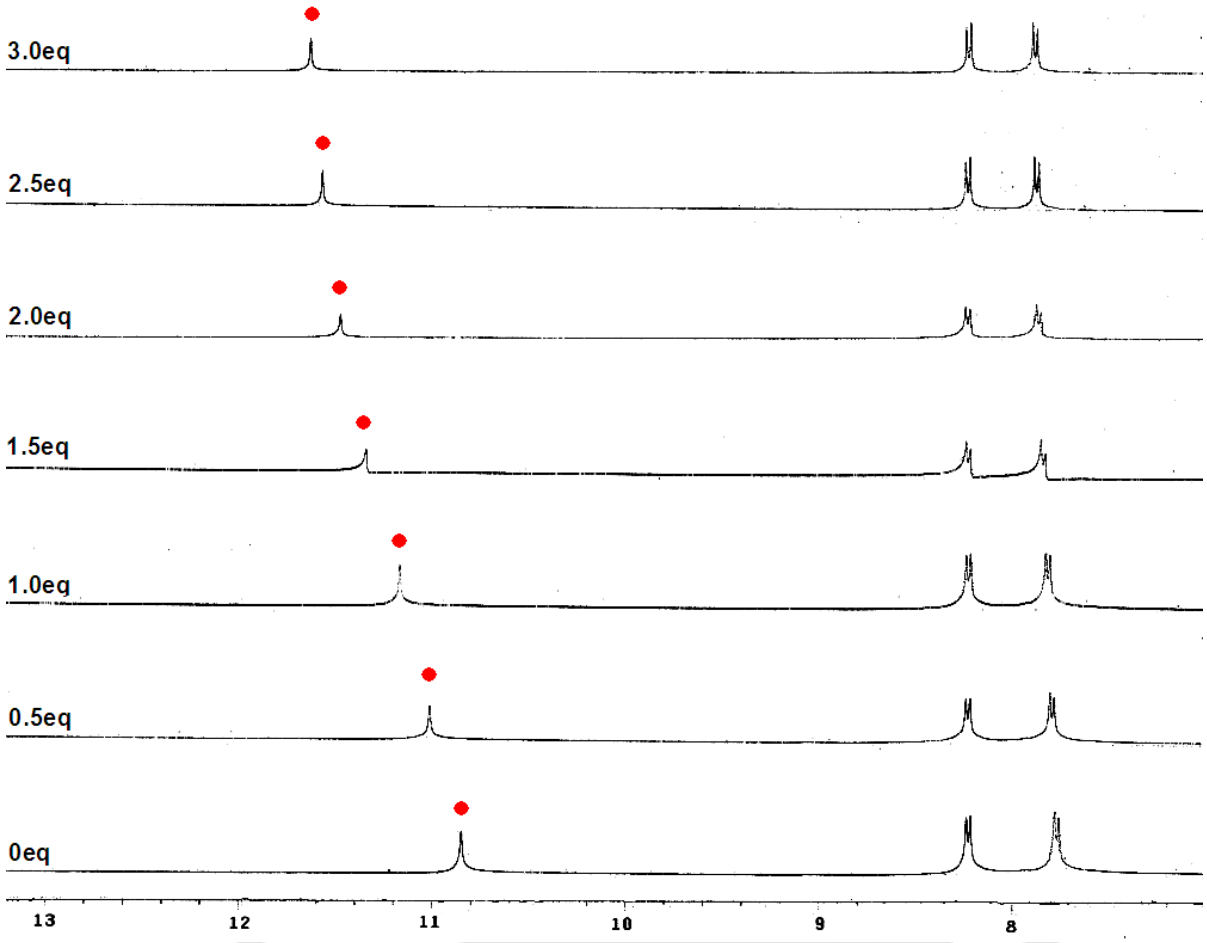

Figure 3.11 Stack plot of the ^{1}H NMR spectra of receptor $\mathbf{H_2L_1}$ in the presence of increasing amounts of $[Bu_4N^+]Cl^-$ recorded in DMSO-d_6.

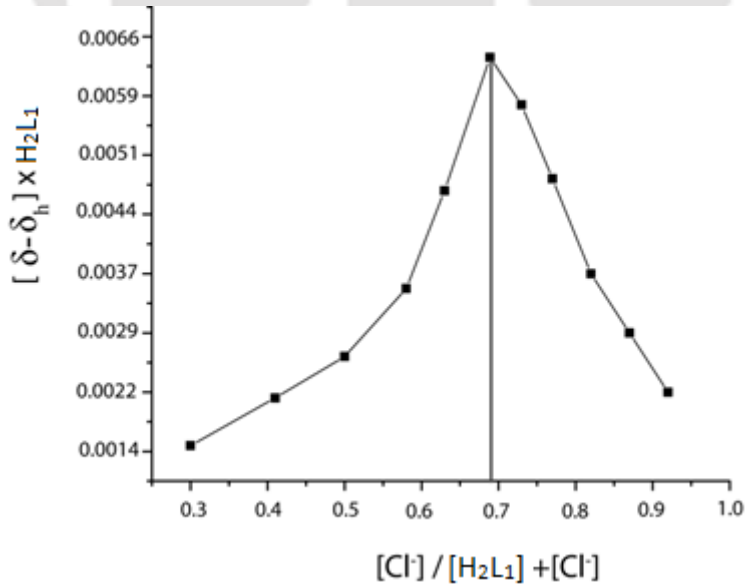

Figure 3.12 Job's plot for $\mathbf{H_2L_1}$ with $[Bu_4N^+]Cl^-$ in DMSO-d_6 at 298K.

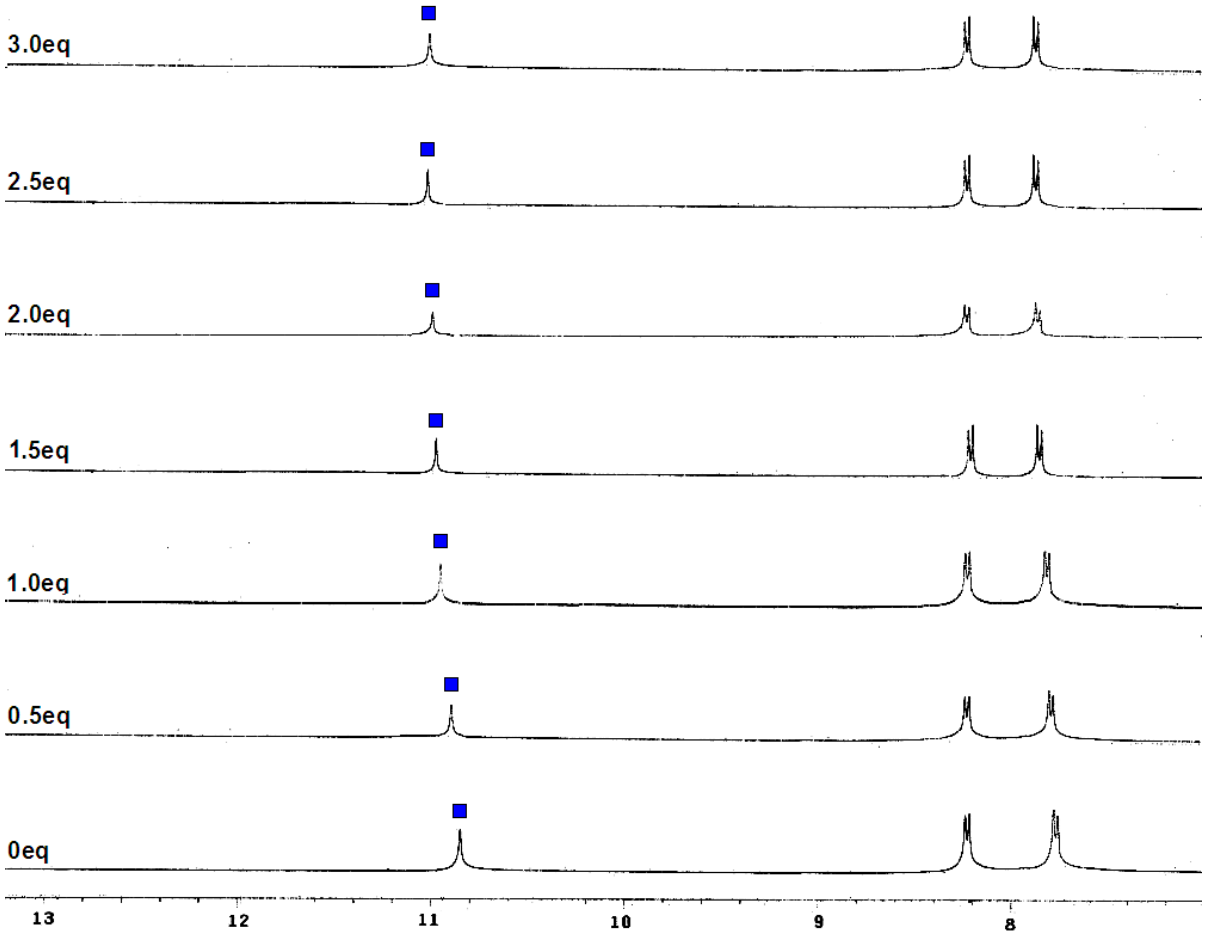

Figure 3.13 Stack plot of the ^{1}H NMR spectra of receptor $\mathbf{H_2L_1}$ in the presence of increasing amounts of $[Bu_4N^+]Br^-$ recorded in DMSO-d_6.

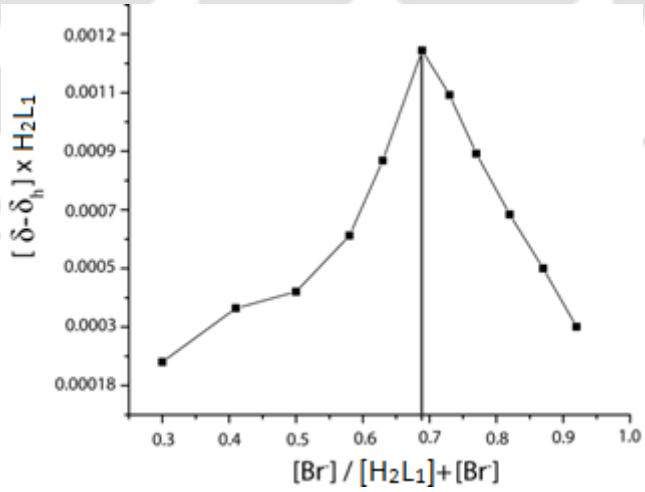

Figure. 3.14 Job's plot for $\mathbf{H_2L_1}$ with $[Bu_4N^+]Br^-$ in DMSO-d_6 at 298K.

References

1. (*a*) P. A. Gale and T. Gunnlaugsson, *Chem. Soc. Rev.*, 2010, **39**, 3595−3596; (*b*) P. A. Gale, *Chem. Soc. Rev.*, 2010, **39**, 3746−3771; (*c*) J. W. Steed, *Chem. Soc. Rev.*, 2010, **39**, 3686−3699; (*d*) B. P. Hay, *Chem. Soc. Rev.*, 2010, **39**, 3700−3708; (*e*) V. Amendola, L. Fabbrizzi and L. Mosca, *Chem. Soc. Rev.*, 2010, **39**, 3889−3915; (*f*) R. M. Duke, E. B. Veale, F. M. Pfeffer, P. E. Kruger and T. Gunnlaugsson, *Chem. Soc. Rev.*, 2010, **39**, 3936−3953; (*g*) M. Wenzel, J. R. Hiscock and P. A. Gale, *Chem. Soc. Rev.*, 2012, **41**, 480−520.

2.(*a*) K. L. Kirk, Biochemistry of the Halogens and Inorganic Halides, Plenum Press, New York, 1991, p 58; (*b*) Supramolecular Chemistry of Anions, A. Bianchi, K. Bowman-James and E. Garćia-Espãna, ed., Woley-VCH, New York, 1997; (*c*) P. D. Beer and P. A. Gale, *Angew. Chem., Int. Ed.*, 2001, **40**, 486−516; (*d*) J. L. Sessler, P. A. Gale and W.- S. Cho, Anion Receptor Chemistry, The Royal Society of Chemistry, Cambridge, UK, 2006; (*e*) M. Cametti and K. Rissanen, *Chem. Commun.*, 2009, 2809−2829; (*f*) P. A. Gale, S. E. García-Garrido and J. Garric, *Chem. Soc. Rev.*, 2008, **37**, 151−190; (*g*) T. Gunnlaugsson, A. P. Davis, J. E. O'Brien and M. Glynn, *Org. Lett.*, 2002, **4**, 2449−2452.

3. (*a*) D. A. Jose, D. K. Kumar, B. Ganguly and A. Das, *Org. Lett.*, 2004, **6**, 3445−3448; (*b*) M. Va´ zquez, L. Fabbrizzi, A. Taglietti, R. M. Pedrido, A. M. González-Noya and M. R. Bermejo, *Angew. Chem., Int. Ed.*, 2004, **43**, 1962−1965; (*c*) J. Y. Lee, E. J. Cho, S. Mukamel and K. C. Nam, *J. Org. Chem.*, 2004, **69**, 943−950; (*d*) D. Esteban-Gómez, L. Fabbrizzi and M. Licchelli, *J. Org. Chem.*, 2005, **70**, 5717−5720; (*e*) E. J. Cho, B. J. Ryu, Y. J. Lee and K. C. Nam, *Org. Lett.*, 2005, **7**, 2607−2609; (*f*) X. He, S. Hu, K. Liu, Y. Guo, J. Xu and S. Shao, *Org. Lett.*, 2006, **8**, 333−336; (*g*) L. S. Evans, P. A. Gale, M. E. Light and R. Quesada, *Chem. Commun.*, 2006, 965−967; (*h*) E. Quinlan, S. E. Matthews and T. Gunnlaugsson, *J. Org. Chem.*, 2007, **72**, 7497−7503; (*i*) M. H. Lee and F. P. Gabbaı¨, *Inorg. Chem.*, 2007, **46**, 8132−8138. (j) S. K. Dey and G. Das, *Chem. Commun.*, 2011, **47**, 4983–4985; (*k*) P. Bose, B. N. Ahamed and P. Ghosh, *Org. Biomol. Chem.*, 2011, **9**, 1972−1979; (*l*) P. Bose and P. Ghosh, *Chem.Commun.*, 2010, **46**, 2962−2964; (m) F. Han, Y. Bao, Z. Yang, T. M. Fyles, J. Zhao, X. Peng, J. Fan, Y. Wu and S. Sun, *Chem.−Eur. J*, 2007, **13**, 2880−2892.

4. (*a*) P. D. Beer and P. A. Gale, *Angew. Chem.*, 2001, **113**, 502−532; (*b*) J. L. Sessler, P. A. Gale and W. S. Cho, Anion Receptor Chemistry; RSC: Cambridge, 2006.

5. (*a*) R. Custelcean, D. E. Jiang, B. P. Hay, W. S. Luo and B. H. Gu, *Cryst. Growth Des.*, 2008, **8**, 1909−1915; (*b*) K. Uzarevic, I. Dilovic, D. Matkovic-Calogovic, D. Sisak and M. Cindric, *Angew. Chem.*, 2008, **120**, 7130−7133; (*c*) S. O. Kang, V. W. Day and K. Bowman-James, *Org. Lett.*, 2008, 10, 2677−2680; (*d*) P. Dechambenoit, S. Ferlay, N. Kyritsakas and M. W. Hosseini, *J. Am. Chem. Soc.*, 2008, **130**, 17106−17113; (*e*) M. W. Hosseini, *Acc. Chem. Res.*, 2005, **38**, 313−323; (*f*) A. Hossain, J. A. Liljegren, D. Powell and K. Bowman-James, *Inorg. Chem.*, 2004, **43**, 3751−3755; (*g*) M. W. Hosseini, *Coord. Chem. Rev.*, 2003, **240**, 157−166; (*h*) J. Keegan, P. E. Kruger, M. Nieuwenhuyzen, J. Obrien and N. Martin, *Chem. Commun.*, 2001, 2192−2193; (*i*) O. A. Gerasimchuk, S. Mason, J. M. Llinares, M. P. Song, N. W. Alcock, K. Bowman-James, *Inorg. Chem.* 2000, **39**, 1371−1375.

6. (*a*) R. Custelcean and P. Remy, *Cryst. Growth Des.*, 2009, **9**, 1985− 1989; (*b*) R. Custelcean, J. P. Bosano, V. Bonnesen, V. Kertesz and B. P. Hay, *Angew. Chem.*, 2009, **121**, 4085−4089; (*c*) R. Custelcean, P. Remy, P. V. Bonnesen, D. E. Jiang and B. A. Moyer, *Angew. Chem.*, 2008, **120**, 1892−1896; (*d*) R. Custelcean, *Chem. Commun.*, 2008, 295−307.

7. (*a*) T. Wang and X.-P. Yan, *Chem.−Eur. J.*, 2010, **16**, 4639−4649; (*b*) H. Maeda and Y. Kusunose, *Chem.−Eur. J.*, 2005, **11**, 5661−5666; (*c*) S. J. Brooks, P. A. Gale and M. E. Light, *CrystEngComm*, 2005, **7**, 586−591; (*d*) H. Juwarker and K.-S. Jeong, *Chem. Soc. Rev.*, 2010, **39**, 3664−3674.

8. Jeffrey, G. A. An Introduction to Hydrogen Bonding; Oxford Univerity Press: Oxford, 1997.

9. L. O. Abouderbala, W. J. Belcher, M. G. Boutelle, P. J. Cragg, J. W. Steed, D. R. Turner and K. J. Wallace, *Proc. Natl. Acad. Sci.*, U.S.A. 2002, **99**, 5001.

Chapter 4

Encapsulation of Sulfate and Thiosulfate within the Dimeric Capsular Assembly of a Tripodal Thiourea Receptor

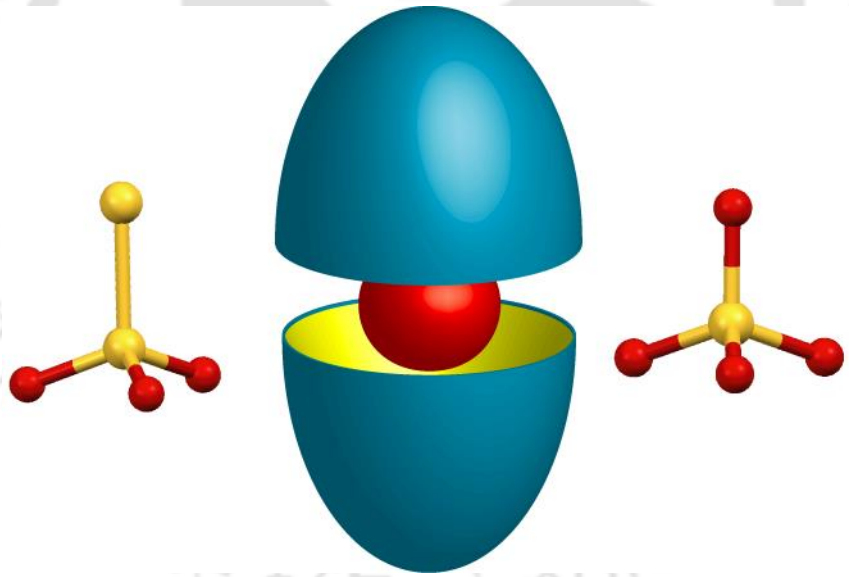

4.1 Background and focus of the chapter

Among the various oxyanions, the harmful effect of sulfate (tetrahedral oxyanion) has been recognized as a prominent species of concern in cleanup processes of nuclear waste and hard water; e.g., contamination of nuclear waste sites by this anion has been a matter of increased concern, hampering the vitrification process.[1] Because of its large standard Gibb's energy of hydration (−1080 kJ mol^{-1}), extraction of sulfate ions from an aqueous to an organic phase presents a particularly challenging task.[1b] To defeat this problem the receptor must have both exceptional affinity and selectivity for the sulfate ion. In this regard the most promising approach can be obtained from Nature's sulfate-binding protein, where sulfate isolation from the surrounding solvent is achieved by encapsulation of the anion inside hydrophobic cavities functionalized with suitable binding groups. The crystal structure of SBP reveals that an individual sulfate anion is completely encapsulated within the core of the protein (8 Å below the surface), between the two lobes of SBP through seven hydrogen bonds involving five from peptide –NH groups, one from serine –OH group, and the last from the tryptophan –NH group.[2] In recent years the tren-based tripodal trisurea/ thiourea backbone has also been found to encapsulate the sulfate ion in a 1:1 or 2:1 (host–guest) ratio, and some of them have been efficiently employed in sulfate-ion separation based on liquid-liquid anion-exchange technology or competitive crystallization techniques.[3] In recent review, Ghosh and co-worker give a nice account of sulfate recognition and extraction by various synthetic receptors.[4]

Another tetrahedral sulfur-containing oxyanion is thiosulfate, widely used (as the sodium salt) in different fields, for instance, the photographic industry, analytical chemistry (iodometric titration), paper making, gold extraction and also useful in a surprisingly broad range of clinical situations.[5] Moreover, sodium thiosulfate has been safely used as a therapeutic agent for a long time (almost 100 years). Nowadays it is widely used as an antidote for the treatment of cyanide poisoning,[5b] by converting cyanide to thiocyanate (excreted in the urine), catalyzed by the enzyme rhodanase and also found useful in prevention of the toxicity of cisplatin in cancer therapy. It reacts with free radicals (oxygen) to form a sodium sulfate compound which prevents the radicals from destroying or attacking the living cells. Additionally, it has also been used as potential remedy of renal diseases[5c] and anti-fungal (tinea versicolor) infections. These versatile applications of the thiosulfate anion make it an important target analyte for recognition. In this regard the slow release or transport of thiosulfate anion in the specific target site *via* encapsulation would be a promising approach in its clinical application.

This chapter describes the solid and solution state binding of two tetrahedral sulfur containing oxyanions (sulfate and thiosulfate) of a chloro-substituted tris(thiourea) receptor, **L_2** (Scheme 4.1). The solid state crystal structure of both the anions with **L_2** reveals that the anions are encapsulated within the dimeric capsular assembly of the receptor with optimal N–H···O and N–H···S hydrogen bonding coordination. The sizes of tight capsular assemblies for both anions are quite comparable, whereas the coordination mode of the anions and the hydrogen bonding parameters are noticeably varied. Moreover, the receptor anion solution state interactions are also studied in detail by NMR experiments in DMSO-d_6 at RT. Interestingly, in contradiction of 2:1 solid state binding, the results from solution state NMR experiments confirm that both the anions are bound within the pseudocavity of the receptor **L_2** with 1:1 binding stoichiometry.

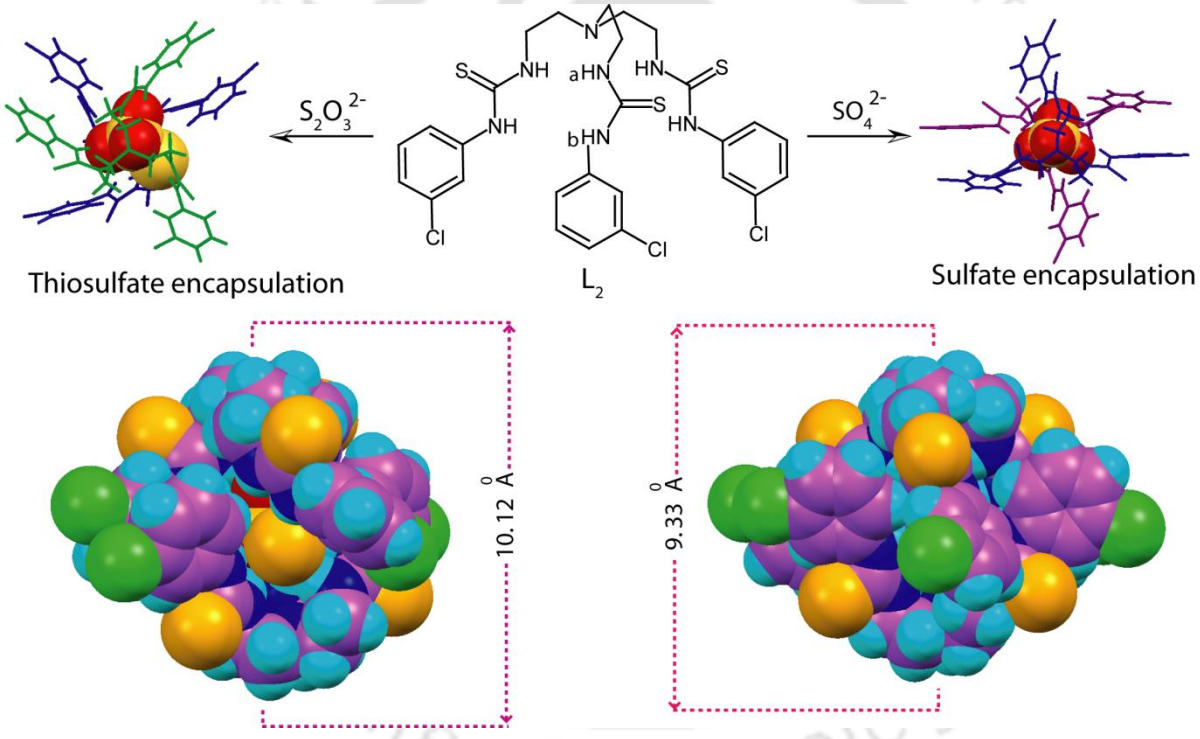

Scheme 4.1 Molecular structure of tripodal thiourea receptor, **L_2** and showing anion (Sulfate and Thiosulfate) induced dimeric capsular assembly formation.

4.2 Structural description of L_2

Needle shaped colorless single crystals of **L_2** suitable for XRD analysis were obtained from DMF, which crystallizes in triclinic space group *P21/c* with Z = 4 (Table 4.1). Structural analysis reveals that the receptor **L_2** forms a pseudocavity consisting of three arms, suitable for encapsulation of anionic guest molecule (Figure 4.1). Two arms of a single receptor molecule are assembled by π···π interactions of the *meta* substituted chloro phenyl rings (C1g···C3g=3.909Å), which certainly resists the opening of the tripodal side arms with a C_3

symmetry. Interestingly no intra receptor hydrogen bonding interaction is found between any two tripodal arms, although two nearby receptor molecules are connected through convergent N−H···S hydrogen bonding interaction with average donor-to-acceptor distance 3.52Å (Figure 4.1b), which eventually lead the formation of 1 D hydrogen bonded chain network structure along crystallographic b axis. Two such 1D hydrogen bonded chain network structures are further inter connected through C−H···Cl hydrogen bonding interactions and forming 2D layer structure along crystallographic b axis. The molecular structure along with packing diagram is shown in Figure. 4.1, whereas, the detailed hydrogen bond interactions involved in the crystal structure of **L_2** are provided in Annexure 4.

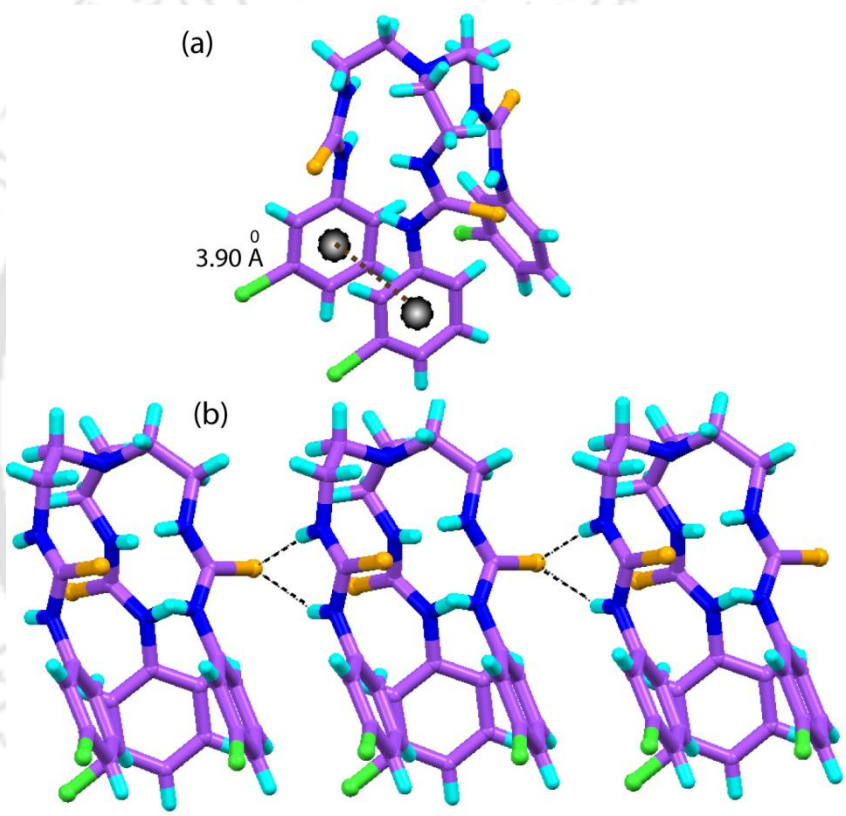

Figure 4.1 (a) X-ray structure of **L_2** depicting the intramolecular π···π interaction between the receptor side arms; (b) Intermolecular hydrogen bonding of the thiourea moieties forming 1D hydrogen bonded chain network structure along crystallographic b axis.

4.3 Structural aspects of anion binding with L_2

For a receptor to bind with the anionic guests, it should, in principle, possess preorganized directional H-bond donors tailored on a suitable platform/framework. Receptor **L_2** possesses a highly organized tripodal scaffold with three hydrogen-bonding thiourea functions appropriate for anion encapsulation *via* their optimal hydrogen bonding coordination. Efforts are made to find out the binding similarities and dissimilarities of receptor **L_2** towards two divalent tetrahedral oxyanions of sulfur (sulfate and thiosulfate) both in the solid and

solution state. From the viewpoint of anion coordination chemistry, crystallization has traditionally been a route to understand the structural details of the anion complexes formed, primarily by single-crystal XRD analysis. Fortunately, we were able to isolate single crystals of both sulfate and thiosulfate complexes of the receptor **L_2**, suitable for X-ray crystallographic analysis from individual solutions of **L_2** in presence of the respective anions. It is interesting to observe that both the anions are entrapped within the rigid supramolecular dimeric capsular assembly of the receptor **L_2** *via* N–H···anion interactions.

4.3.1 Structural description of SO_4^{2-}-encapsulated molecular capsule (2a)

We attempted to grow single crystal of complexes of **L_2** with both HSO_4^- and SO_4^{2-} by charging their excess n-TBA salt. Interestingly in both cases the colorless crystals of the sulfate complex of **L_2** crystallize with good yield. They crystallize in the triclinic space group *P-1*. Two identical symmetric molecules of **L_2** flipped inward toward each other in a face-to-face fashion (dN1···N1 = 9.334 (6) Å) form a micro-cavity that encapsulates a sulfate anion (disordered, eight half occupied oxygen atoms) in its centre *via* hydrogen bonding to the six thiourea groups (Figure 4.2a). The asymmetric unit of complex **2a** contains two symmetry-independent capsular units, exhibiting conformational isomorphism, their occurrence generally controlled by kinetic and thermodynamic crystal stability because these factors are mostly considered to be the consequences of interrupted crystallization. Both the capsular units are almost identical. In the first capsular unit the encapsulated sulfate anion is stabilized by a total of fifteen hydrogen bonding interactions between the twelve NH groups of two **L_2** moieties and four O atoms of SO_4^{2-}. Three out of the four oxygen atoms O1, O2 and O3 accept four hydrogen bonds each, while O4 accepts three hydrogen bonds in a trifurcated fashion. Apart from these hydrogen bonding interactions, there are also some weak C_{phenyl}–H···O interactions present, which give extra stabilization to the encapsulated sulfate anion. Moreover, a close inspection of the hydrogen-bond parameters, especially the N–H···O angle vs. H···O distances, reveal that in the strong hydrogen bonding interaction region of dH···O < 2.5 Å and dN···O ≤ 3.2 Å there are thirteen contacts (Figure 4.2b). The second capsular unit present in the crystal lattice is quite similar to the first one, only the receptor anion hydrogen bonding parameters are slightly varied (Table 4.2). A similar type of sulfate encapsulation in a metal free system by tripodal thiourea based receptors was previously reported by Gale and co-workers.[6] Interestingly, the sulfate-encapsulated dimeric cages are interlinked with one another through halogen-bonding interactions between the sulfur atom of the thiourea group and the meta-substituted chloride atom of the phenyl ring, with a separation distance of 3.482 (3) Å, and which subsequently form a 1D chain capsular

assembly along the crystallographic a axis. Two such 1D arrays of capsular assemblies are further interconnected with one another via TBA cations by C–H···S interactions, and generate hexagonal networks of sulfate-encapsulated dimeric cages around each capsular unit along the b axis (Figure 4.2d). These added interactions contribute to the high stability of **2a** (MP = 184). Moreover the presence of hydrogen bonded sulfate anions in complex **2a** has also been confirmed by solid-state FT-IR analysis. The stretching frequency of –NH in complex **2a** (ν 3277 cm^{-1}) shows a notable shift of 65 cm^{-1} with subsequent broadening of the peak in comparison to that of $\mathbf{L_2}$ (ν 3341 cm^{-1}), supporting the existence of strong N–H···O hydrogen bonds between $\mathbf{L_2}$ and the SO_4^{2-} anion. Furthermore, the presence of a moderate signal at 2873 cm^{-1} and a strong signal 1085 cm^{-1} in complex **2a** can be attributed to the C–H stretching frequencies of the TBA groups and symmetric stretching frequency of the sulfate anion (Annexure 4). Characteristically, the broad intense symmetric absorption band at ~1085 cm^{-1} is generally used to identify the presence of sulfate in individual

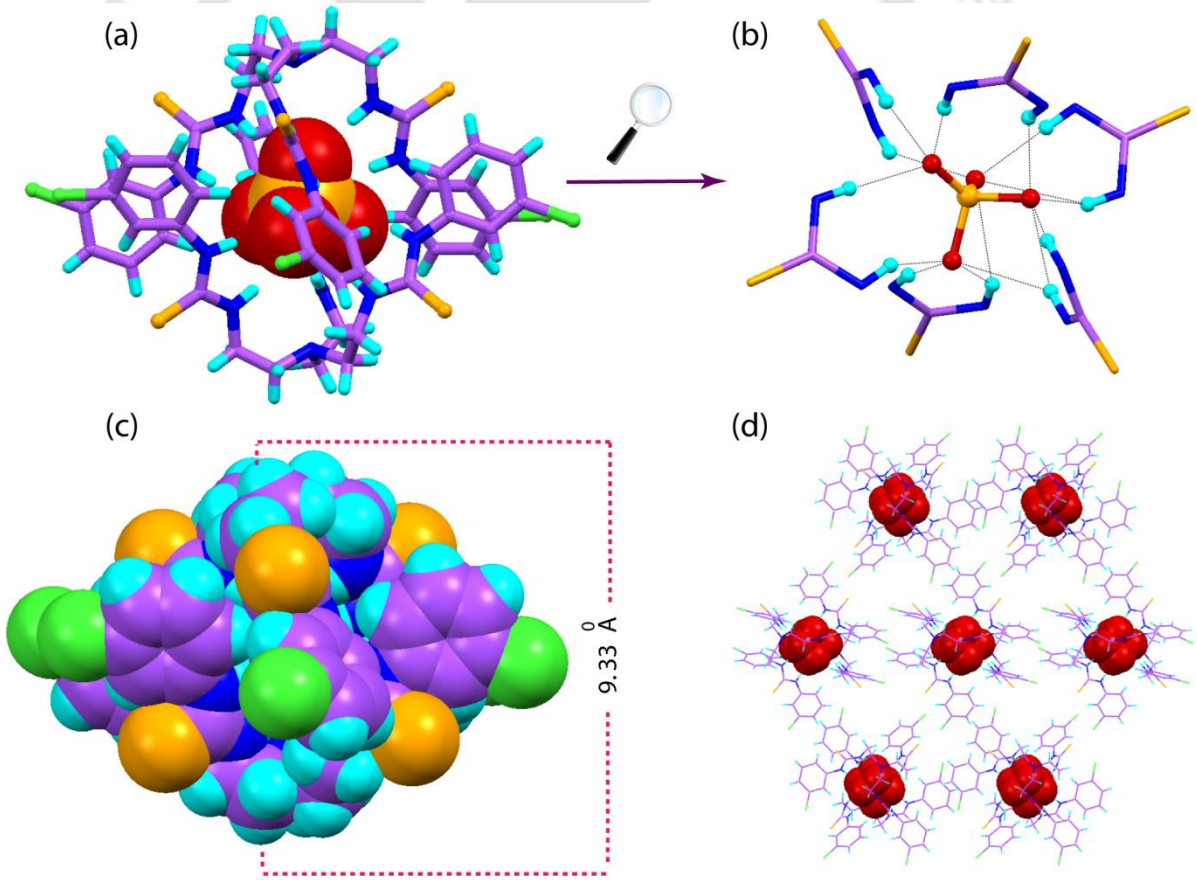

Figure 4.2 (a) Sulfate encapsulation by the crystalline self assembled capsules $\mathbf{L_2}$, Two molecules of $\mathbf{L_2}$, shown as stick models, and Sulfate anion is shown as a space-filling model; (b) Magnified view showing coordination of SO_4^{2-} with the 12 –NH groups of the dimeric capsule. TBA counter cations are omitted for clarity of presentation; (c) Space-filling representation depicting full encapsulation of the SO_4^{2-} anion; (d) Crystal packing in complex **2a**, as viewed down the crystallographic b axis.

-complexes. The powder X-ray diffraction studies on bulk crystals obtained from both in the presence of SO_4^- and HSO_4^- matches closely with the simulated diffraction pattern obtained from the single-crystal structure of complex **2a** suggesting that, even in the presence of HSO_4^-, the sulfate complex of the receptor $\mathbf{L_2}$ crystallizes (Figure 4.6a).

Moreover, the formation of the sulfate complex even in presence of HSO_4^- anions can be attributed to the coordination induced proton transfer between the free and bound anions; such solution-state deprotonations of the protonated state of an anion, *viz*., $H_2PO_4^-$, HCO_3^-, and HSO_4^- are quite well known in the literature.[6,7] Essentially the formation of several hydrogen- bonding interactions with the receptor significantly lowers the pK_a of the bound guest, which is eventually deprotonated by the free guest species present in solution.

4.3.2 Structural description of $S_2O_3^{2-}$ encapsulated molecular capsule (2b)

The complex **2b** was synthesized from the reaction between DMSO solutions of $\mathbf{L_2}$ and previously prepared aqueous mixture of TEACl and $Na_2S_2O_3$. Interestingly, the thiosulfate complex of $\mathbf{L_2}$ with a TEA counter cation was crystallized from slow evaporation of reaction mixture, suggesting geometric and electrostatic complementarity between $S_2O_3^{2-}$ and $\mathbf{L_2}$ that prefers the formation of a thiosulfate complex rather than a chloride complex. It is worth mentioning here that efforts were also made to crystallize an $S_2O_3^{2-}$ complex in presence of only $Na_2S_2O_3$, but these were not fruitful presumably because the thiosulfate encapsulated receptor segment does not prefer hydrophilic Na^+ or the hydrated Na^+ cation. This is also supported by the presence of a TEA counter cation instead of an Na^+ cation or hydrated Na^+ cation in the crystal lattice of complex **2b**, while, it was crystallized from the mixture of both the Na^+ and TEA cations. The complex **2b** crystallizes in the monoclinic system with centrosymmetric space group *C2/c*. Structural elucidation reveals two inversion-symmetric molecules of $\mathbf{L_2}$ are flipped inward toward each other in a face to face fashion [d(N1···N8) = 10.12 (1) Å; (Figure 4.3a), with one ligand coordinating in the axial mode and the other in the facial mode, and thereby creating a micro cage supramolecular structure that encapsulates a thiosulfate anion in its centre *via* N–H···O and N–H···S hydrogen bonds by the six thiourea groups and the two receptors are assembled by π···π interactions of the chloro-phenyl rings (C1g···C6g = 3.755 Å and C2g···C5g = 3.996 Å). The capsular size of complex **2b** (10.12 Å) is slightly larger (~0.8 Å) compared to complex **1a** (9.33 Å), which may attributed to the larger size and lower charge density of the thiosulfate anion compared to sulfate. In addition to this, close inspection of complex **2b** reveals that the N–H atoms of the thiourea functionalities are more directed towards three oxygen atoms of the encapsulated thiosulfate anion, resulting in the outer S8 atom of the thiosulfate anion being

slightly out of the capsular cage, probably due to the larger S7–S8 bond distance and the lower charge density over the S8 atom compared to the three oxygen atoms. The TEA counter cations of complex **2b** are disordered, and one TEA counter cation equally shares two positions in the asymmetric unit. There are thirteen N–H···O and four N–H···S hydrogen bonds of six thiourea groups that are responsible for stabilizing the encapsulated thiosulfate anion (Figure 4.3b). Two out of three oxygen atoms O1, and O2 accepts four hydrogen bonds each, while O3 accepts five hydrogen bonds. A correlation of the N–H···O angle vs. H···O distance (Figure 4.5b) shows that in the strong hydrogen bonding interaction region of dH···O < 2.5 Å and dN···O ≤ 3.2 Å, there are nine contacts stabilizing three oxygen atoms of the encapsulated thiosulfate anion. When compared to N–H···O interactions, the N–H···S interactions are relatively weak. The average values of the N···S distance and N–H···S angle

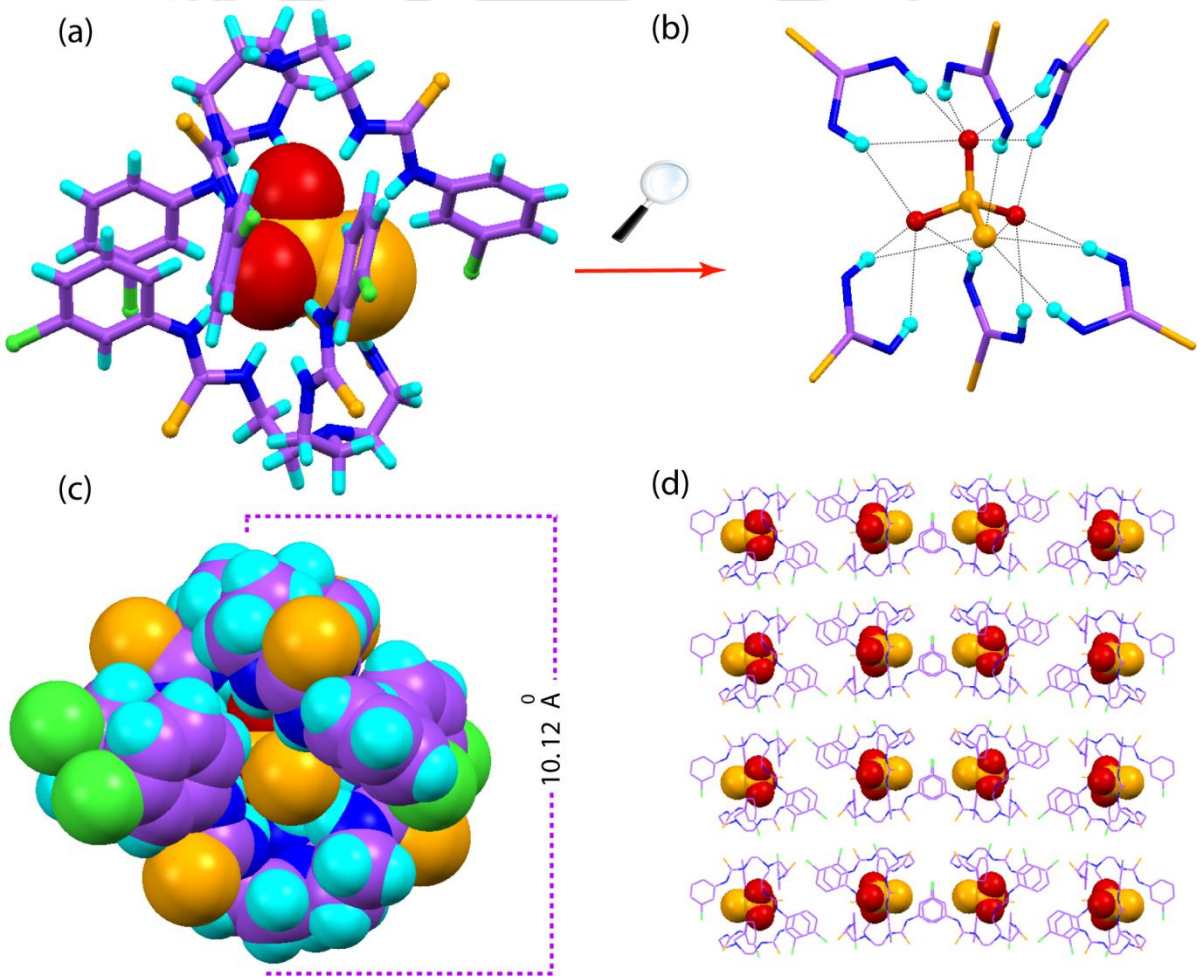

Figure 4.3 (a) Thiosulfate encapsulation by the crystalline self-assembled capsules $\mathbf{L_2}$, Two molecules of $\mathbf{L_2}$, shown as stick models, and thiosulfate anion is shown as a space-filling model; (b) Magnified view showing coordination of $S_2O_3^{2-}$ with the12 –NH groups of the dimeric capsule. TEA counter cations are omitted for clarity of presentation; (c) Space-filling representation depicting full encapsulation of the $S_2O_3^{2-}$ anion; (d) Crystal packing in complex **2b**, as viewed down the crystallographic bc plane (TEA cations are omitted for clarity).

are 3.43 Å and 148.2°, respectively. To the best of our knowledge this is the first report on the full encapsulation of thiosulfate anion within dimeric capsular assembly of a neutral receptor, although the first encapsulated thiosulphate complex within protonated cryptant host was previously reported by Nelson and co-workers.[8] The thiosulfate-encapsulated dimeric cages are interlinked with one another through Cl···Cl (3.31(1) Å) halogen bonding interactions, forming a 1D chain polymeric structure along the crystallographic a axis. Two such 1D arrays of capsular assemblies are further interconnected with one another by weak C–H···S interactions, forming a 2D layer structure along the crystallographic b axis (Figure 4.3d).

Moreover, the presence of a hydrogen bonded thiosulfate anion in complex **2b** has also been confirmed by solid-state FT-IR analysis. Analogous to complex **1a** here also a significant shift (55 cm^{-1}) with subsequent broadening in the –NH signal compared to that of $\mathbf{L_2}$ is observed, indicating the presence of strong N–H···anion interaction between the thiourea functionalities of $\mathbf{L_2}$ and the thiosulfate anion. Additionally, the presence of a moderate signal at 1075 cm^{-1} can be attributed to the stretching frequency corresponding to the thiosulfate anion (Annexure 4). As the complex **2b** crystallizes in presence of more than one anion, therefore, it is required to verify the homogeneity of the isolated bulk crystal. The powder X-ray diffraction studies on isolated bulk crystals match perfectly with the simulated diffraction pattern obtained from the single-crystal structure of complex **2b**, indicating the homogeneity of the isolated crystals of the thiosulfate capsules (Figure 4.6b).

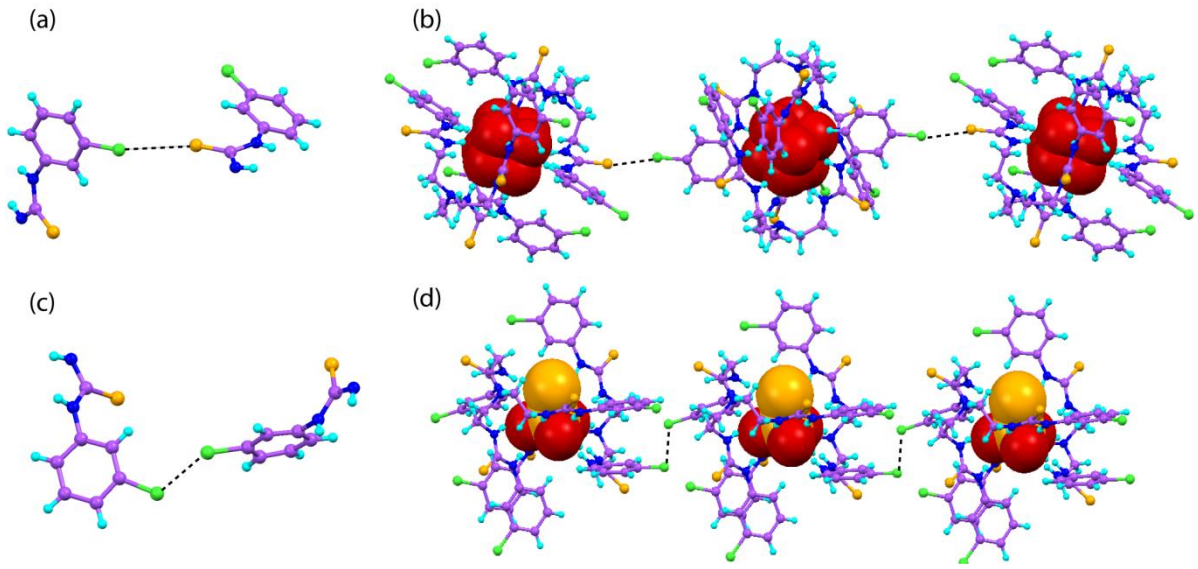

Figure 4.4 (a) The Cl···S halogen bonding interaction between two capsular units in complex **2a**; (b) Halogen bonding directed 1D capsular assembly along crystallographic a axis; (c) The Cl···Cl halogen bonding interaction between two capsular units in complex **2b**; (d) Halogen bonding directed 1D capsular assembly along the crystallographic a axis.

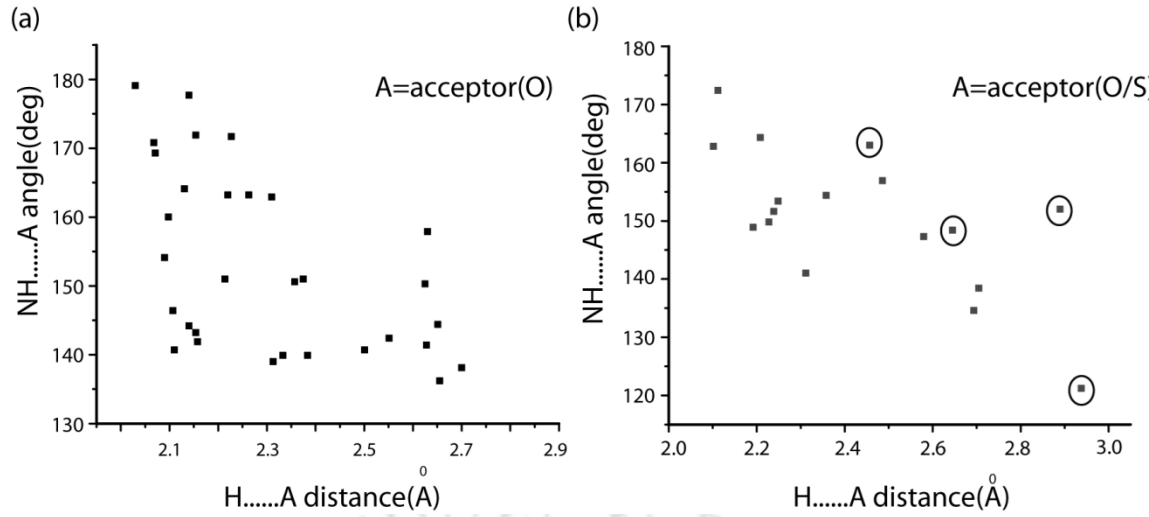

Figure 4.5 The scatter plot of the N–H···A angle vs. H···A distance of the hydrogen bonds for: (a) complex **2a**; and (b) complex **2b**. A = Acceptor (O\S); circled points indicate N–H···S interactions.

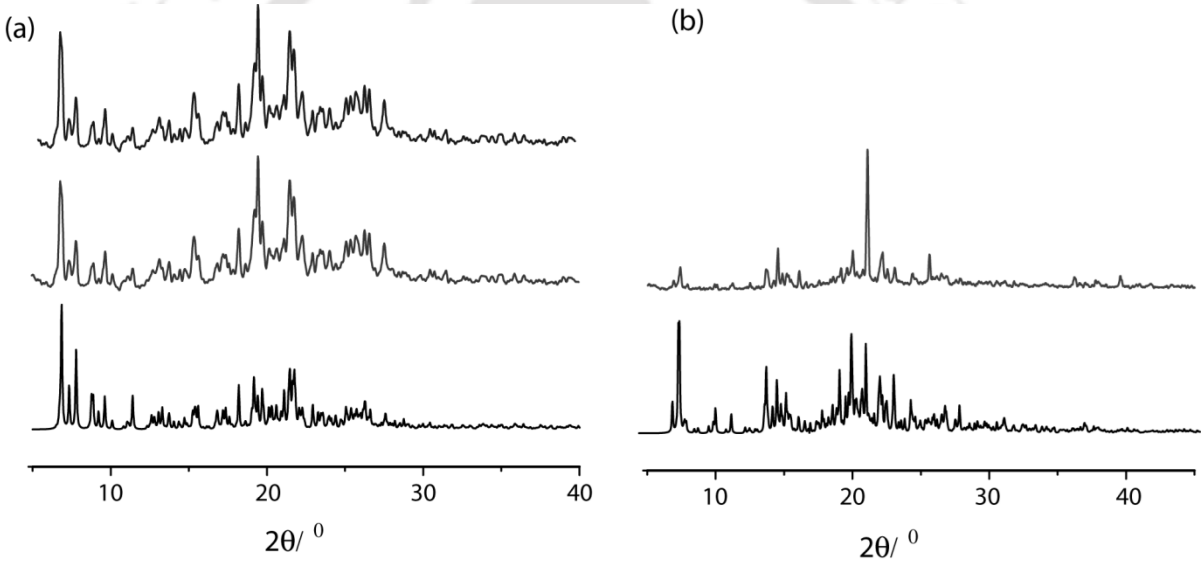

Figure 4.6 (a) Powder X-ray diffraction: simulated pattern from the single-crystal X-ray of complex **2a** (below), experimental pattern from the crystalline solid obtained in presence of sulfate anion (middle), experimental pattern from the crystalline solid obtained in presence of hydrogensulfate anion (top); (b) Powder X-ray diffraction: simulated pattern from the single-crystal X-ray of complex **2b** (bottom), experimental pattern from the crystalline solid of complex **2b** (top).

4.4 Sulfate and thiosulfate binding studies by ^{1}H NMR spectroscopy

It is now well known in the field of supramolecular chemistry that the behavior of molecules/receptors in dilute or very dilute solution is really quite dissimilar from their behavior in molecular capsules in the solid state. Therefore, to find the mode of receptor–anion interaction in solution we have carried out qualitative as well as quantitative ^{1}H NMR titration and NOESY experiments in DMSO-d_6 at RT. Figure 4.7 illustrates the qualitative test of both the anions, which shows the changes in chemical shift observed upon addition of 5 equivalents of each anion at once to the receptor $\mathbf{L_2}$ in DMSO-d_6 at RT. This preliminary

study reveals the most substantial shifts have been observed for the thiourea protons (–NH_a and –NH_b), indicating that the –NH functions of the thiourea groups provide suitable sites of interaction between the receptor and anions in solution. ^{1}H NMR titration of receptor **L_2** with [n-TBA]SO_4^{2-} shows that upon gradual addition of standard SO_4^{2-} solution a large downfield shift of thiourea –NH resonances (Δδ –NH_a = 1.666 ppm; Δδ –NH_b = 1.267 ppm) and a small but important change in the chemical shift with subsequent splitting of the aryl –CH protons Δδ = 0.227 ppm, could be explained by the fact that the sulfate anion also significantly interacts with the C–H protons in solution (Figure 4.11). The considerably larger shift of –NH_a (Δδ = 1.66 ppm) relative to –NH_b signals (Δδ = 1.267 ppm) indicates there is an obvious discrepancy between the –NH_a···sulfate and –NH_b···sulfate binding modes, whereas, no such binding discrepancy of –NH protons was found in the solid state structure of complex **2a**. The change in the chemical shift of the –NH resonances of the NMR spectra, as recorded with an increasing amount of sulfate anion in solution at room temperature, gave the best fit for a 1:1 binding model (log K = 4.54), which are well consistent with the report of Gale for fluoride-substituted tris(thiourea) receptors.[6] The 1:1 binding stoichiometry in DMSO-d_6 were further verified by the Job's plot analysis. The maximum change in the chemical shift during titrations for **L_2** is obtained when the mole fraction of sulfate anion has reached about 0.5, which suggests a host–guest binding in a 1:1 stoichiometry (Figure 4.11). Although the crystal structure obtained for complex **2a** revealed 2:1 complex stoichiometry. Furthermore, ^{1}H NMR titration of **L_2** with standard sodium thiosulfate solution also occurs downfield shift of thiourea –NH resonances (Δδ –NH_a = 1.18 ppm; Δδ –NH_b = 0.97 ppm). Interestingly the degree of downfield shift of both the –NH resonances is lesser compared to the sulfate anion (Figure 4.7). Here also there is a considerably larger shift of –NH_a (Δδ = 1.18 ppm) relative to the –NH_b signals (Δδ = 0.97 ppm), indicating –NH_a···anion interactions are more energetically favorable than NH_b···anion interactions (Figure 4.8). However, the solid state crystal structure of complex **2b** shows equal participation from both the thiourea protons toward the thiosulfate anion within the rigid dimeric capsular cage of **L_2**. Moreover, the significant shift with concomitant splitting of the aryl –CH protons indicates that thiosulfate induces a change of the electronic environment of the phenyl rings of the receptor **L_2**. The association constant (log K) of **L_2** with $S_2O_3^{2-}$ was calculated from quantitative titration experiment and found to be log K = 3.35 by considering the 1:1 binding model, because no data fit for the Job plot experiment was obtained due to complex precipitation during the titration experiment. The comparatively large Δδ values for thiourea protons and the higher binding constant value of

the sulfate anion can be attributed to the smaller size and higher charge density of sulfate anion compared to thiosulfate.

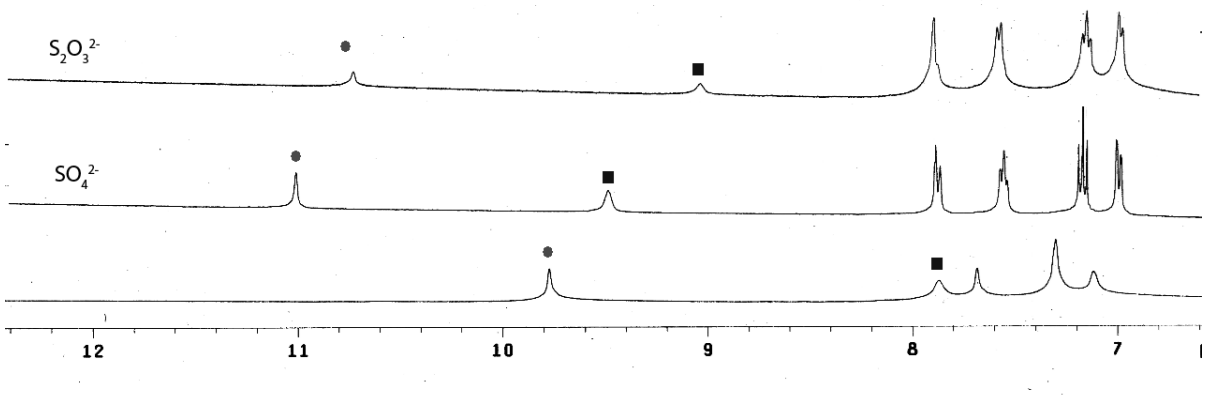

Figure 4.7 Partial ^{1}H NMR spectra (400 MHz, DMSO-d_6) of $\mathbf{L_2}$ and maximum observable shifts of thiourea –NH resonances upon the addition of excess (5 equiv.) SO_4^{2-} and $S_2O_3^{2-}$ anions.

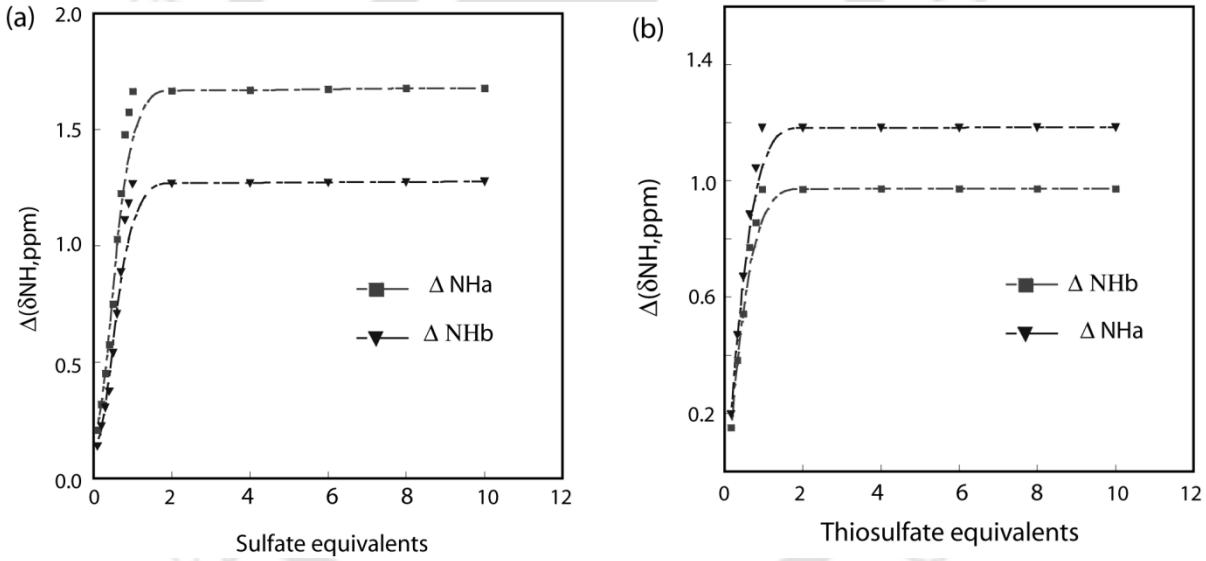

Figure 4.8 ^{1}H NMR titration curves of $\mathbf{L_2}$ with (a) SO_4^{2-} and (b) $S_2O_3^{2-}$ anions in DMSO-d_6 at RT. Net changes in the chemical shifts of –NH are shown against the increasing amount of anion. H_a = CH_2NHCS and H_b = CSNHAr.

The mode of receptor–anion interactions and the anion induced electronic and conformational changes of the receptor can be illustrated by the 2D NOESY NMR experiment, which is a traditional and useful tool in the field of supramolecular host–guest chemistry. Therefore, for improved understanding of the solution state binding nature of the receptor toward the anions, we have carried out 2D NOESY NMR experiments both for free receptor ($\mathbf{L_2}$) and anion complexes in DMSO-d_6 at RT (Figure 4.9). The free receptor molecule shows a significantly strong NOESY signal between the thiourea protons –NH_a and –NH_b. Interestingly, the through-space NOE signals are considerably weakened in both

complexes, and completely absent upon addition of one equivalent of the respective anions (sulfate and thiosulfate), indicating a conformational change of $\mathbf{L_2}$ due to encapsulation of the anions in a 1:1 binding stoichiometry. A similar type of anion encapsulation induced change in NOESY spectra was previously reported by Hossain and Schneider for tren-based (urea) receptors.[9] In contradiction of the 2:1 solid state binding, the results from NMR experiments confirm that in solution the studied anions are bound to the pseudocapsular cavity of $\mathbf{L_2}$ with 1:1 binding stoichiometry (Figure 4.10).

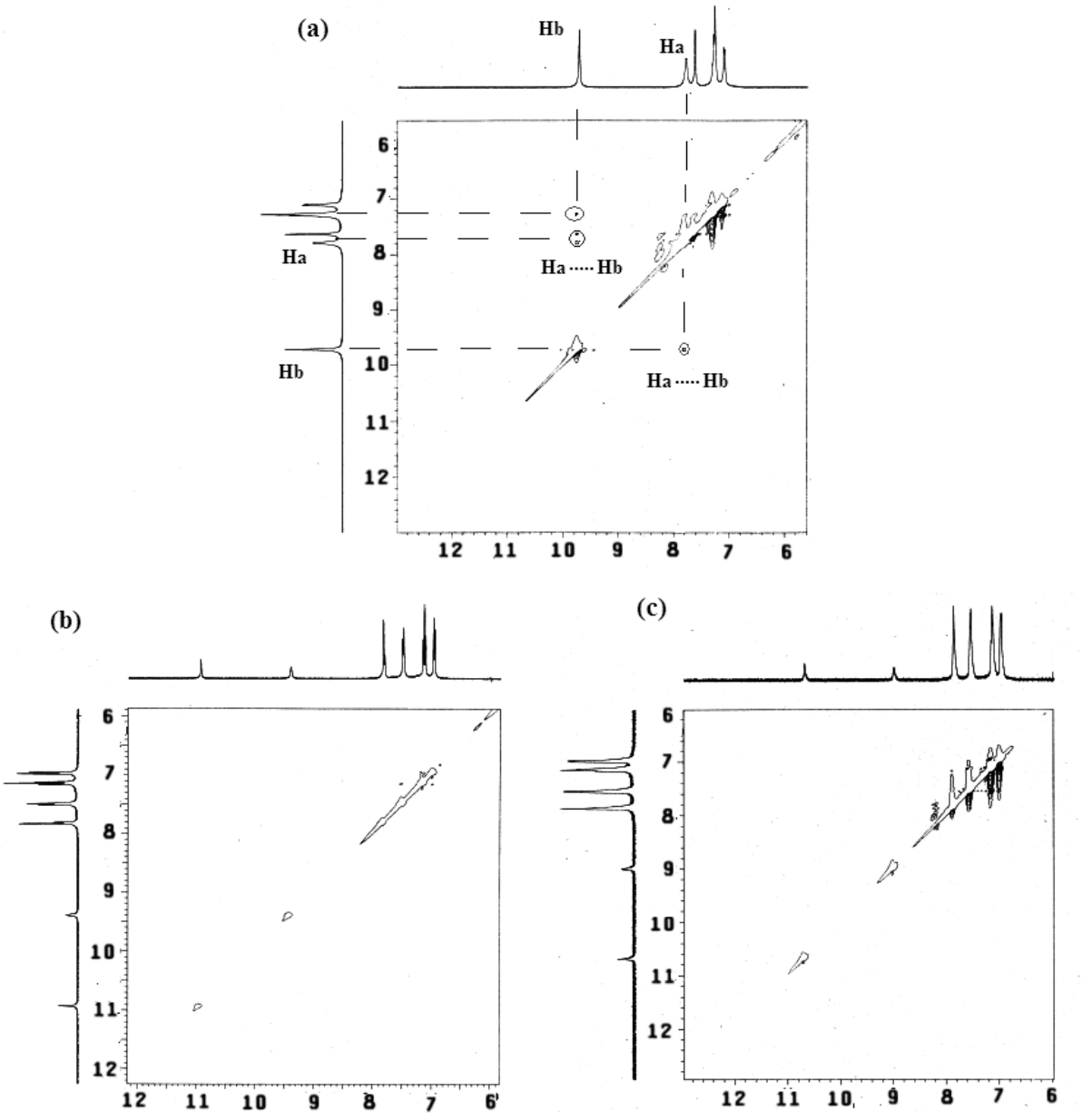

Figure 4.9 2D NOESY NMR experiments of: (a) Free receptor $\mathbf{L_2}$; (b) $\mathbf{L_2}$ in presence of 1 equiv. of sulfate anion; and (c) $\mathbf{L_2}$ in presence of 1 equiv. of thiosulfate anion. All the spectra are taken in DMSO-d_6 at 298K.

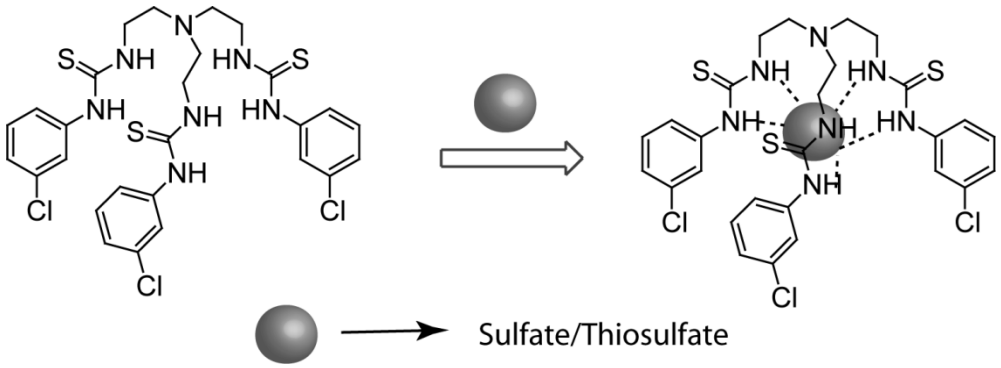

Figure 4.10 Proposed binding mode of the receptor $\mathbf{L_2}$ for sulfate and thiosulfate anion in solution

4.5 Conclusion

In conclusion, we have demonstrated the detailed solid and solution state binding comparison of two divalent oxyanions of sulfur with similar dimensionality (sulfate and thiosulfate) with a tris(thiourea) receptor $\mathbf{L_2}$. The solid state crystal structures for the anion complexes reveal that the SO_4^{2-} and $S_2O_3^{2-}$ are encapsulated within the dimeric capsular assembly of the receptor by satisfying their optimal coordination through N–H···O and N–H···S hydrogen bonds with 1:2 stoichiometries. It was found the mode of encapsulation and capsular sizes for both anion complexes are quite comparable. To the best of our knowledge, this is the first crystallographic evidence of the full encapsulation of thiosulfate anion within dimeric capsular assembly of a neutral receptor. The three-dimensional solid-state crystal packing of the capsular complexes are mainly governed by the Cl···Cl (for the thiosulfate complex) and Cl···S (for the sulfate complex) halogen bonding interactions, giving added stabilization to the anion complexes. The solution-state binding and encapsulation of oxyanions by N–H···anion hydrogen bonding has also been confirmed by quantitative ^{1}H NMR titration and 2D NOESY NMR experiments. The change in the chemical shifts of the thiourea –NH protons and the binding constant values suggests the receptor binds more strongly to sulfate anions compare to thiosulfate. Furthermore, the 2D NOESY NMR and Job's plot experiments suggest that in solution the anions SO_4^{2-} and $S_2O_3^{2-}$ are encapsulated in the pseudocapsular cavity of $\mathbf{L_2}$ with 1:1 binding stoichiometry, indicating an obvious disagreement of the binding mode from that observed in their solid state crystal structures.

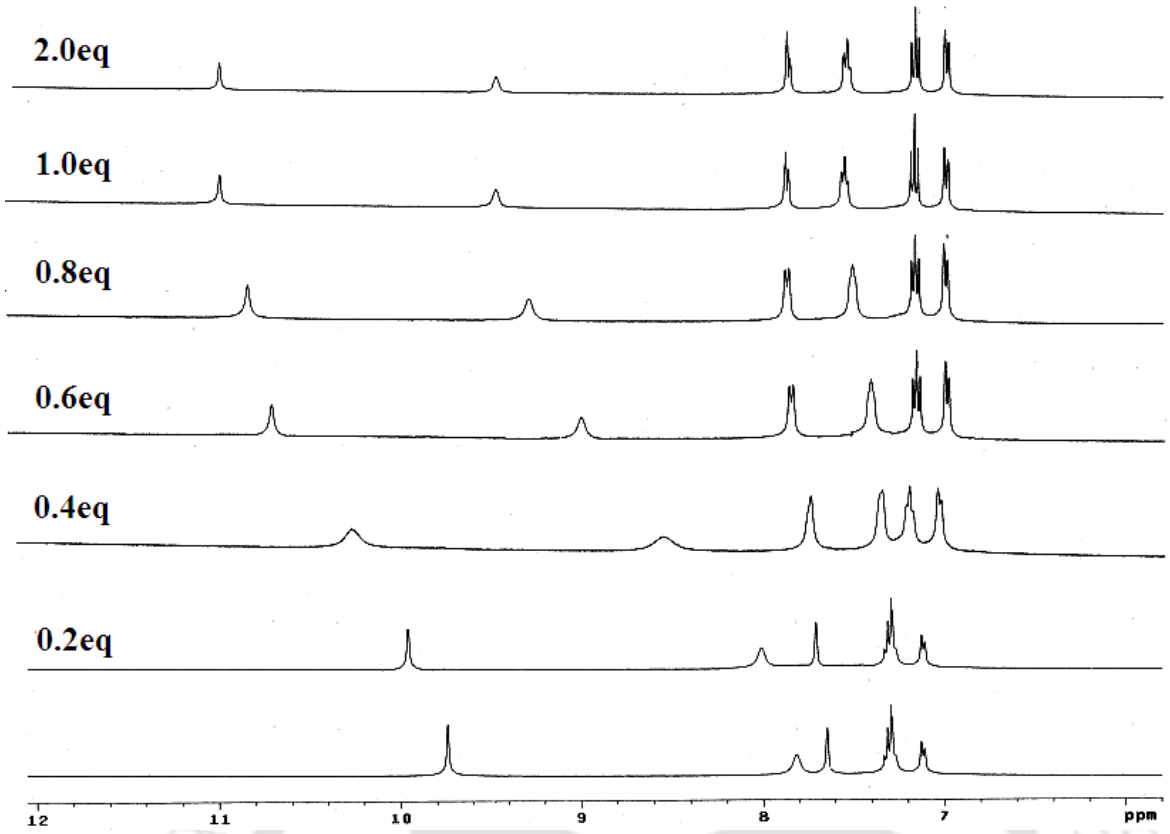

Figure 4.11 Partial ^{1}H NMR titration spectra of $\mathbf{L_2}$ with increasing concentration of $[n\text{-}Bu_4N^+]_2SO_4^{2-}$ in DMSO-d_6 at 298K.

.

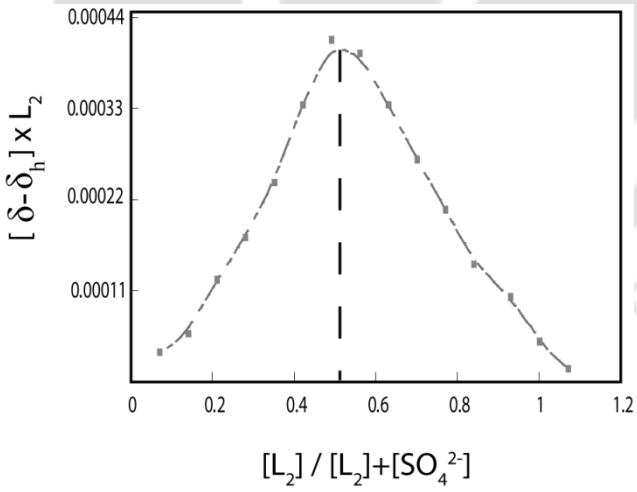

Figure 4.12 Job's plot for $\mathbf{L_2}$ with $[n\text{–}Bu_4N^+]_2SO_4^{2-}$ in DMSO-d_6 at 298K.

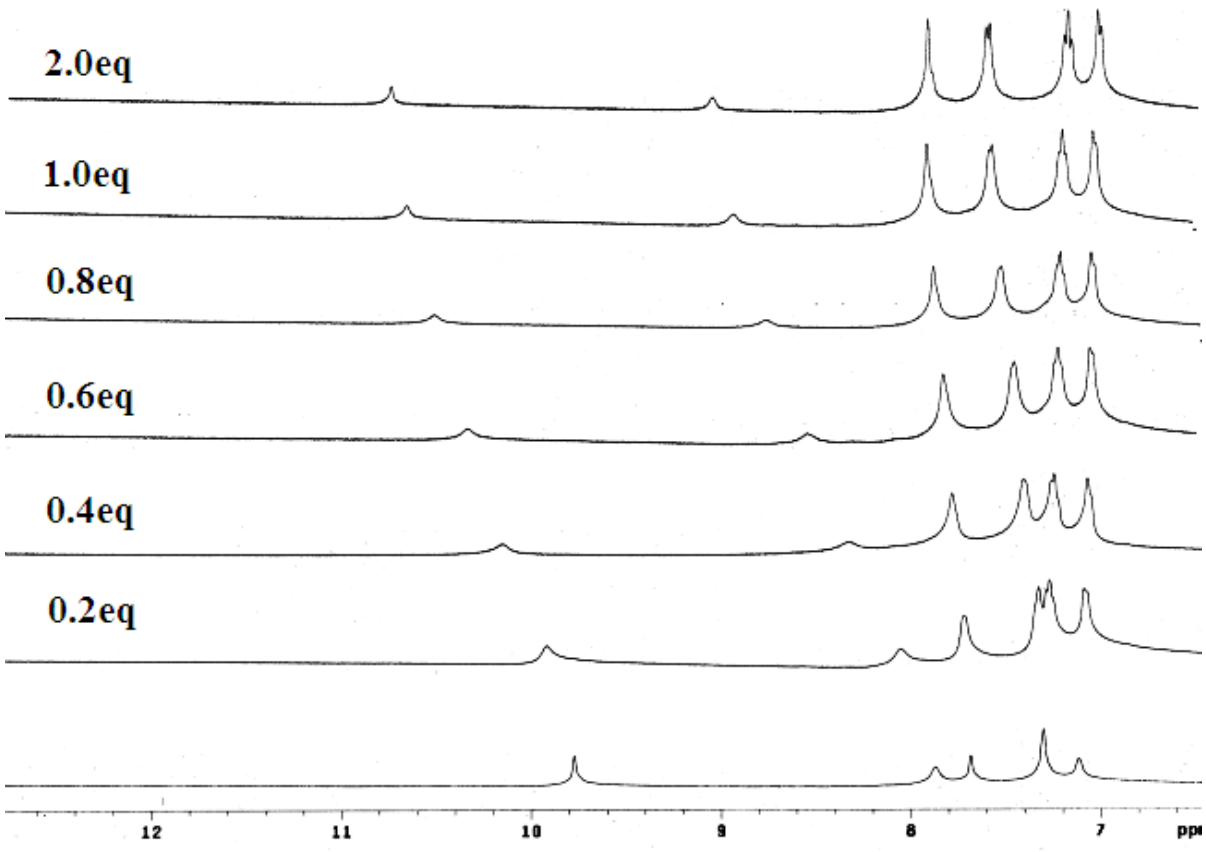

Figure 4.13 (a) Partial ^{1}H NMR titration spectra of $\mathbf{L_2}$ with increasing concentration of $Na_2S_2O_3$ in DMSO-d_6 at 298K.

Table 4.1 Crystallographic parameters and refinement details of receptor $\mathbf{L_2}$ and its anion-encapsulated complexes **2a** and **2b.**

Parameters	$\mathbf{L_2}$	**2a**	**2b**
Formula	$C_{27}\ H_{30}\ Cl_3\ N_7\ S_3$	$C_{86}\ H_{132}\ Cl_6\ N_{16}\ O_4\ S_7$	$C_{70}\ H_{100}\ Cl_6\ N_{16}\ O_3\ S_8$
Fw	655.14	1891.27	1682.92
Crystal system	Monoclinic	Triclinic	Monoclinic
Space group	*P 21/c*	*P-1*	*C*2/*c*
a/Å	19.9181(17)	13.8087(7)	13.7854(14)
b/Å	7.5424(7)	14.3169(7)	25.836(3)
c/Å	27.391(2)	26.6346(14)	48.851(5)
α/°	90.00	93.887(3)	90.00
β/°	98.195(2)	98.290(3)	95.818(6)
γ/°	90.00	97.087(3)	90.00
V/Å^3	3025.6(4)	5151.1(5)	17309(3)
Z	4	2	8
D_c/g cm^{-3}	1.438	1.130	1.292
μ Mo K_α/mm^{-1}	0.539	0.361	0.444
T/K	298(2)	298(2)	298(2)
Total reflections	35799	50188	83153
Independent reflections	7588	25686	21045
Observed reflections	7546	25645	20954
Parameters refined	361	1092	846
R1; wR2 (I > 2σ(I))	0.0525, 0.0981	0.0984, 0.2990	0.0945, 0.3113
R(int)	0.0595	0.0592	0.0788
GOF (F^2)	1.016	1.173	1.062

Table 4.2 Hydrogen bonding contacts on SO_4^{2-} and $S_2O_3^{2-}$ anion within the dimeric capsule of $\mathbf{L_2}$ in complexes **2a** and **2b.**

Complexes	D–H···A	*D*(H···A)/Å	*d*(D···A)/Å	∠D–H···A/°
2a	N3H···O1	2.313	3.016(9)	139.0(3)
	N4H···O1	2.209	3.007(8)	154.1(4)
	N5H···O1	2.63	2.977(9)	157.9(4)
	N6H···O1	2.384	3.09(1)	139.9(4)
	N2H···O2	2.628	3.343(9)	141.4(3)
	N5H···O2	2.286	3.010(9)	141.9(4)
	N6H···O2	2.651	3.388(9)	144.4(3)
	N7H···O2	2.071	2.92(1)	169.3(4)
	N2H···O3	2.551	3.275(9)	142.4(3)
	N3H···O3	2.068	2.92(1)	170.8(4)
	N4H···O3	2.501	3.21(1)	140.7(4)
	N2H···O4	2.333	3.041(9)	139.9(4)
	N4H···O4	2.023	2.923(9)	177.7(4)
	N6H···O4	2.22	3.05(1)	163.2(4)
2b	N4-H···O1	2.358	3.16(1)	154.4(6)
	N5H···O1	2.208	3.05(1)	164.3(7)
	N7H···O1	2.312	3.03(2)	141(1)
	N12H···O1	2.102	2.94 (1)	162.8(7)
	N3H···O2	2.112	2.97(7)	172.4(7)
	N5H···O2	2.694	3.36(1)	134.6(6)
	N2H···O2	2.580	3.34(1)	147.3(7)
	N14H···O2	2.239	3.02(1)	151.6(7)
	N9H···O3	2.228	3.00(1)	149.8(7)
	N11H···O3	2.192	2.96(1)	148.9(7)
	N12H···O3	2.705	3.40(1)	138.4(7)
	N13H···O3	2.249	3.04(1)	153.4(6)
	N14H···O3	2.645	3.41	148.4(7)
	N3H···S8	2.938	3.46(1)	121.2(7)

References

1. (*a*) J. L. Sessler, E. Katayev, G. D. Pantos and Y. A. Ustynyuk, *Chem. Commun*., 2004, 1276–1278; (*b*) L. R. Eller, M. Stepien, C. J. Fowler, J. T. Lee, J. L. Sessler and B. A. Moyer, *J. Am. Chem. Soc*., 2007, **129**, 11020–11021; (*c*) C. J. Fowler, T. J. Haverlock, B. A. Moyer, J. A. Shriver, D. E. Gross, M. Marquez, J. L. Sessler, M. A. Hossain and K. Bowman-James, *J. Am. Chem. Soc*., 2008, **130**, 14386–4387; (*d*) B. A. Moyer, L. H. Delmau, C. J. Fowler, A. Ruas, D. A. Bostick, J. L. Sessler, E. Katayev, G. D. Pantos, J. M. Llinares, M. A. Hossain, S. O. Kang and K. Bowman-James, *Adv. Inorg. Chem*., 2007, **59**, 175–204.

2. J. W. Pflugrath and F. A. Quiocho, *Nature*, 1985, **314**, 257−260.

3. (*a*) C. Jia, B. Wu, S. Li, X. Huang, Q. Zhao, Q.-S. Li and X.-J. Yang, *Angew. Chem., Int. Ed*., 2011, **50**, 486–490; (*b*) R. Custelcean, P. Remy, P. V. Bonnesen, D.-E. Jiang and B. A. Moyer, *Angew. Chem., Int. Ed*., 2008, **47**, 1866–1870; (*c*) B. Akhuli, I. Ravikumar and P. Ghosh, *Chem. Sci*., 2012, **3**, 1522–1530; (*d*)A. Rajbanshi, B. A. Moyer and R. Custelcean, *Cryst. Growth Des*., 2011, **11**, 2702–2706.

4. I. Ravikumar and P. Ghosh, *Chem. Soc. Rev*., 2012, **41**, 3077–3098.

5. (*a*) M. G. Aylmore and D. M. Muir, *Miner. Eng*., 2001, **14**, 135–174; (*b*) A. H. Hall, R. Dart and G. Bogda, *Ann. Emerg. Med*., 2007, **49**, 806–813; (*c*) J. S. Cicone, J. B. Petronis, C. D. Embert and D. A. Spector, *Am. J. Kidney Dis*., 2004, **43**, 1104–1108; (*d*) C. E. Araya, R. S. Fennell, R. E. Neiberger and V. R. Dharnidharka, *Clin. J. Am. Soc. Nephrol*., 2006, **1**, 1161–1166.

6. N. Busschaert, M. Wenzel, M. E. Light, P. Iglesias-Hernandez, R. Perez-Tomas and P. A. Gale, *J. Am. Chem. Soc*., 2011, **133**, 14136–14148.

7. I. Ravikumar, P. S. Lakshminarayanan, M. Arunachalam, E. Suresh and P. Ghosh, *Dalton Trans*., 2009, 4160–4168.

8. B. M. Maubert, J. Nelson, V. McKee, R. M. Town and I. Pál, *J. Chem. Soc., Dalton Trans*., 2001, 1395–1397.

9. (*a*) A. Pramanik, B. Thompson, T. Hayes, K. Tucker, D. R. Powell, P. V. Bonnesen, E. D. Ellis, K. S. Lee, H. Yu and M. A. Hossain, *Org. Biomol. Chem.*, 2011, **9**, 4444–4447; (*b*) F. Werner and H. J. Schneider, *Helv. Chim. Acta*, 2000, **83**, 465–478; (*c*) A. Pramanik, D. R. Powell, B. M. Wong and M. A. Hossain, *Inorg. Chem*., 2012, **51**, 4274–4284.

Chapter 5

Recognition of Anion/Anion-Water Cluster by a Tripodal Amide Receptor

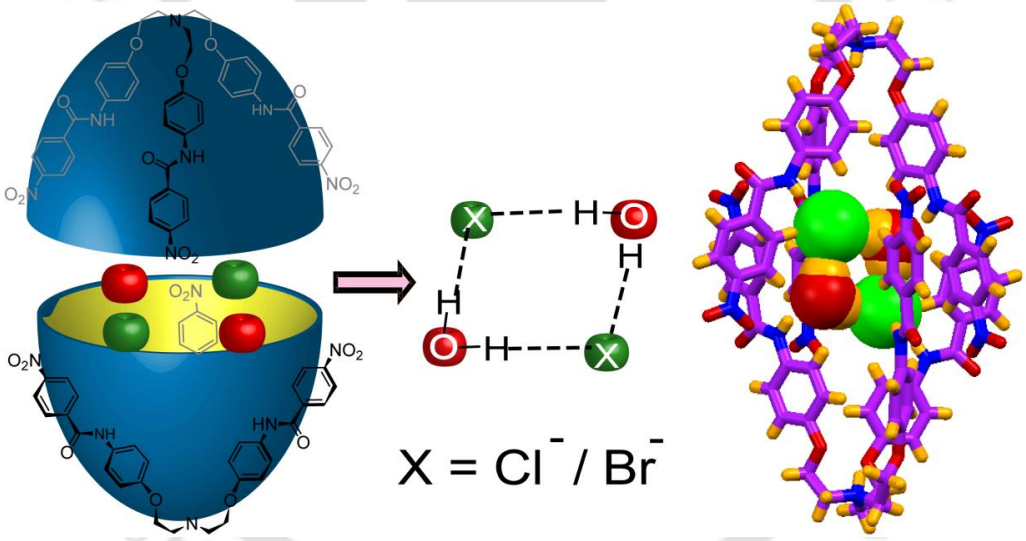

5.1 Background and focus of the chapter

Recently, recognition of hydrated anions has attracted a great deal of attention due to their occurrence in natural and biological environments such as marine water and various ecosystems. In particular, recognition of discrete ordered anion–water clusters is more challenging, because anions in their hydrated form are highly random and display a wide range of complicated interactions due to spontaneous formation of strong stable hydrogen bonds in an aqueous environment. The formation of ordered anion–water clusters within chemical receptors provides a unique opportunity to understand the detailed molecular interactions in these restricted environments.[1] A great deal of attention has especially been paid to understanding the water clusters in hydrophobic environments[2] due to their vast importance in chemical and biological interfaces.[3] The solid state structural characterization of anion–water clusters is important from the viewpoint of understanding the solvation mechanism, ion-mobilities in the bulk, ion translocation in water–membrane interfaces, and electrical phenomena in the troposphere and ionosphere.[4,5]

Among the various anions, aqueous solvation of halides has drawn much research attention due to their high abundance in nature. Thus, numerous theoretical calculations have predicted the existence of several hydrated halides $X(H_2O)_n$ in the recent past.[6] Although several hydrated anions have been characterized previously within lattices of organic hosts, or metal complexes,[7] examples of encapsulated discrete anion–water clusters by a dimeric assembly of synthetic acyclic receptors are rare.[8]

Acyclic receptors with a multi-armed hydrogen bonding functionality have often been found to coordinate with targeted anionic species *via* formation of capsular assemblies.[9] The most fascinating feature of molecular capsules is their unique ability to create a guest specific micro-cavity that isolates the encapsulated guest from the bulk of the solvent media.[10] Therefore, carefully designed multi-armed acyclic receptors having a convergent hydrogen bonding functionality can be utilized for the recognition of hydrated anions *via* self-assembly processes.[8]

In this chapter, we structurally demonstrate the encapsulation of a discrete cyclic halide–water tetrameric cluster $[X_2(H_2O)_2]^{2-}$ (where X = Cl^- / Br^-) inside the dimeric capsular assembly of a newly synthesized conformationally flexible, C_{3v} symmetric tripodal amide receptor, **L_3** (Scheme5.1). However, in the case of higher homologous iodide anions the receptor **L_3** prefers to adopt a non-capsular polymeric aggregation, which confirms the adaptability of flexible **L_3** as an anion receptor. Interestingly, crystallization of the receptor in presence of HF in glass container gives SiF_6^{2-} complex, and depending on crystallizing solvent the receptor forms both capsular and non capsular (polymeric) assemblies in

presence of SiF_6^{2-} anion. The thermal stability of the halide–water cluster in complexes has also been studied by thermo-gravimetric analysis, which indicates the strong hydrogen bonding between the anion–water cluster and the host molecules present in the complexes. Furthermore, detailed ^1H NMR titration and 2D-NOESY NMR experiments have also been carried out to validate the binding and encapsulation of halide and halide water cluster within the receptor scaffold.

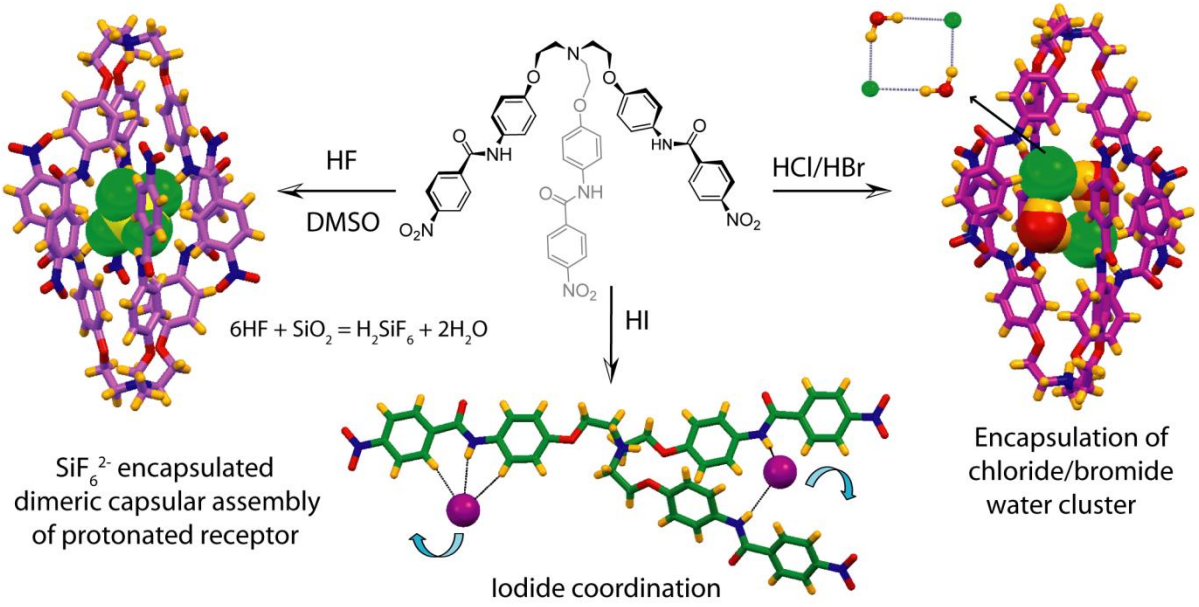

Scheme 5.1 Molecular structure of C_{3v} symmetric flexible tripodal amide receptor, $\mathbf{L_3}$ and schematic representation depicting the anion-water/anion induced capsular and polymeric assembly formation.

5.2 Structural aspects of anion binding with L_3

For a receptor to bind with the anionic guests, it should, in principle, possess preorganized directional H-bond donors tailored on a suitable platform/framework. Receptor $\mathbf{L_3}$ possesses three amide functions, suitable for recognizing anionic species through directional hydrogen bond formation. Moreover the strategically placed protonation site far apart from anion binding amide functions on highly organized tripodal scaffold appropriate for encapsulation of large anionic guest *via* hydrogen bonding coordination in its protonated form.

5.2.1 Structural description of chloride complex (3a)

Single crystals of the chloride complex $[(\mathbf{L_3H})^+\cdot Cl\cdot H_2O]$ (**3a**) were obtained by slow evaporation of a DMF solution of $\mathbf{L_3}$ in the presence of excess hydrochloric acid (HCl). It crystallizes in the triclinic space group *P 21/c* with Z = 2 (Table 5.1). The detail structural analysis of complex **3a** revealed that the protonated receptor molecule encapsulates a monohydrated chloride anion in its symmetric tripodal cleft, where all the three arms of

$\mathbf{L_3H^+}$ are projected in one direction. Each etheric O-atom of a $\mathbf{L_3H^+}$ unit is hydrogen bonded to the proton attached to the bridgehead N-atom that actually organizes the flexible arms in one direction. Two units of monohydrated chloride encapsulated $\mathbf{L_3H^+}$ are held together by two Cl···OH_2 hydrogen bonds to form a dimeric capsular assembly (dN1···N1 = 20.621(3) Å) that encapsulates the $[Cl_2(H_2O)_2]^{2-}$ cluster in its centre *via* hydrogen bonding interactions and the two receptors are assembled by weak π···π interactions of the nitro-phenyl rings (C1g···C3g = 3.717 Å). Probably the hydrogen bonding amidic functions of the receptor are

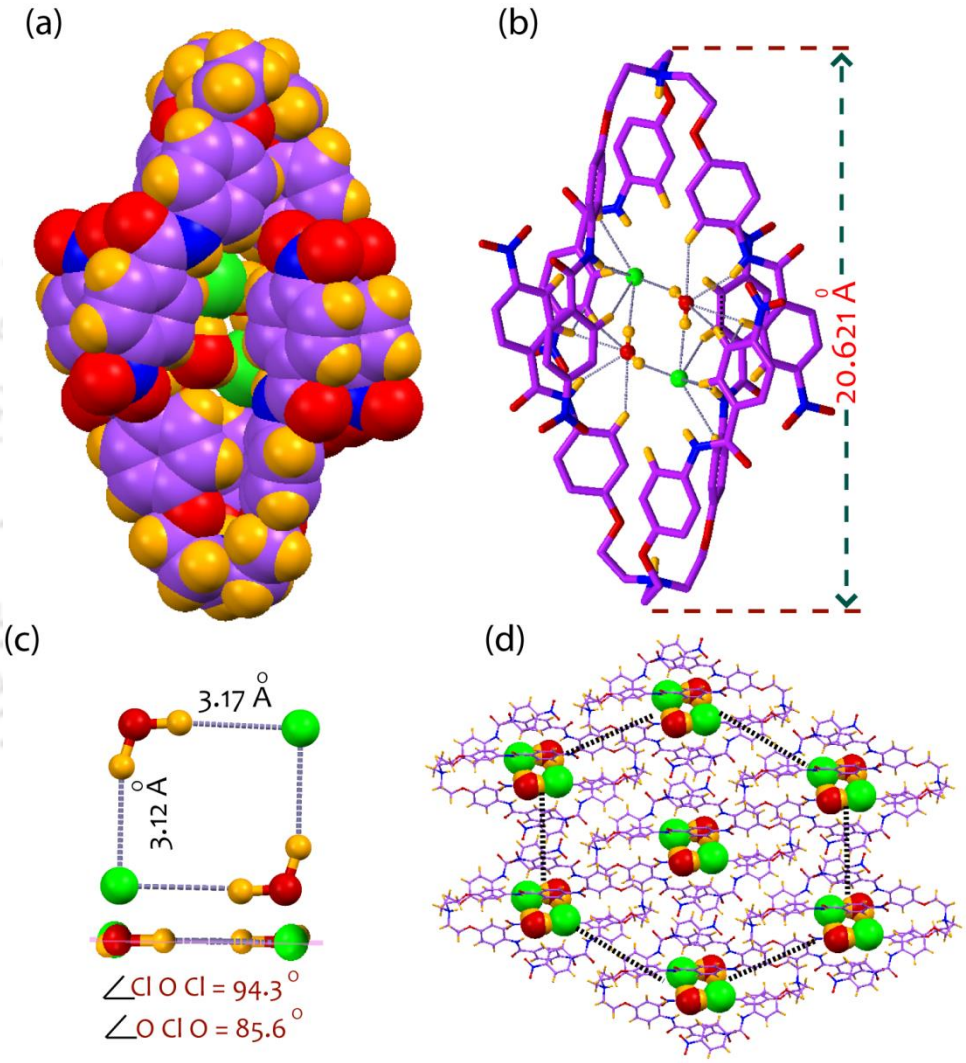

Figure 5.1 (a) Space-filling representation depicting complete encapsulation of the $[Cl_2(H_2O)_2]^{2-}$ cluster inside the dimeric capsule-like assembly of $\mathbf{L_3H^+}$; (b) The hydrogen bonding interactions of the $[Cl_2(H_2O)_2]^{2-}$ cluster with two $\mathbf{L_3H^+}$; (c) Close up view of the chloride water tetramer and the side view showing the perfect planar nature of $[Cl_2(H_2O)_2]^{2-}$; (d) Crystal packing of complex **3a** as viewed down along the crystallographic a axis.

-too widely placed to offer an appropriate binding pocket for a single chloride anion, resulting in the formation of the interesting $[Cl_2(H_2O)_2]^{2-}$ cluster encapsulated within a dimeric capsular assembly of a protonated receptor $\mathbf{L_3H^+}$ (Figure 5.1). The source of water in

the crystal could be from the HCl solution. Figure 5.1b and 5.1c show the hydrogen bonding pattern of the $[Cl_2(H_2O)_2]^{2-}$ cluster. The cluster is formed *via* strong chloride–water interactions and possesses a planar cyclic tetrameric arrangement where each chloride anion is hydrogen bonded with the two water molecules having hydrogen bonding distances of 3.127(2) Å and 3.277(2) Å. Close inspections of the distance and angle measurement values of the terameric water cluster confirmed it to be a perfect parallelogram (Figure 5.1c). The $[Cl_2(H_2O)_2]^{2-}$ cluster is completely enclosed by two protonated receptor units and stabilized by two N–H···Cl^-, two N–H···OH_2, four C–H···Cl^- and four C–H···OH_2 hydrogen bonds. These hydrogen bonds are the main driving forces in the formation of the dimeric capsular assembly. In this assembly, each chloride anion is stabilized by six hydrogen bonds in a octahedral geometry involving one –NH proton, two –OH protons (lattice water), and three aromatic –CH protons. The water molecules are also strongly held to the protonated receptors *via* one N–H···O and two C–H···O interactions (Figure 5.1b and Table 5.3). Interestingly, two out of six amidic –NH protons of two $\mathbf{L_3H}^+$ moieties are not involved in hydrogen bonding interactions with $[Cl_2(H_2O)_2]^{2-}$ in the capsular assembly. Instead, they form hydrogen bonds with the oxygen atom of the amide function from a neighboring capsular assembly and subsequently form a 1D chain of capsular assembly along the crystallographic b axis. Two such 1D arrays of capsular assemblies are further interconnected with one another *via* hydrogen bonds with the nitro group (C–H···O), and generate hexagonal networks of $[Cl_2(H_2O)_2]^{2-}$ encapsulated dimeric cages around each capsular unit along the a axis (Figure 5.1d).

5.2.2 Structural description of bromide complex (3b)

To understand the assembly process with higher homologous spherical anions, complexation with bromide has been carried out by protonating $\mathbf{L_3}$ in the presence of HBr. Single crystals of the chloride complex $[(\mathbf{L_3H})^+ \cdot Br \cdot H_2O]$ (**3b**) were obtained by slow evaporation of a DMF solution of $\mathbf{L_3}$ in the presence of excess hydrobromic acid (HBr). It crystallizes in the triclinic space group *P 21/c* with Z = 2 (Table 5.1). Interestingly, X-ray crystal structure analysis of the bromide complex **3b** established it to be isostructural with the chloride complex **3a**, and the receptor interacts with the bromide anion in an exactly identical fashion to that of the chloride anion in complex **3a** . Figure 5.2a represents the spacefill model of the $[Br_2(H_2O)_2]^{2-}$ encapsulated dimeric assembly of $\mathbf{L_3H}^+$, whereas, figure 5.2b and 5.2c show the hydrogen bonding pattern of the $[Br_2(H_2O)_2]^{2-}$ cluster. The capsular size (20.747 Å) and hydrogen bond distances (Table 5.3) of the bromide complex are somewhat greater than

those of the chloride complex (**3a**) due to the larger ionic radii and lower charge density of the bromide ion compared to chloride ion.

The presence of hydrogen bonded hydrated halides (Cl^- / Br^-) in complexes **3a** and **3b** have also been confirmed by solid-state FT-IR analysis. Both the complexes showed a distinct band at around ~ 3250 cm^{-1} that is assigned to the O–H stretching vibration of water in the complexes. Additionally the significant shift (~58 cm^{-1}) in the stretching frequency of the amidic –NH in the complexes in comparison to that of $\mathbf{L_3}$ (3326 cm^{-1}) further supports the existence of strong N–H····X^- (X = Cl / Br) hydrogen bonds between the amide functions of the protonated receptor ($\mathbf{L_3H^+}$) and halide anions in both the complexes (Annexure 5). The

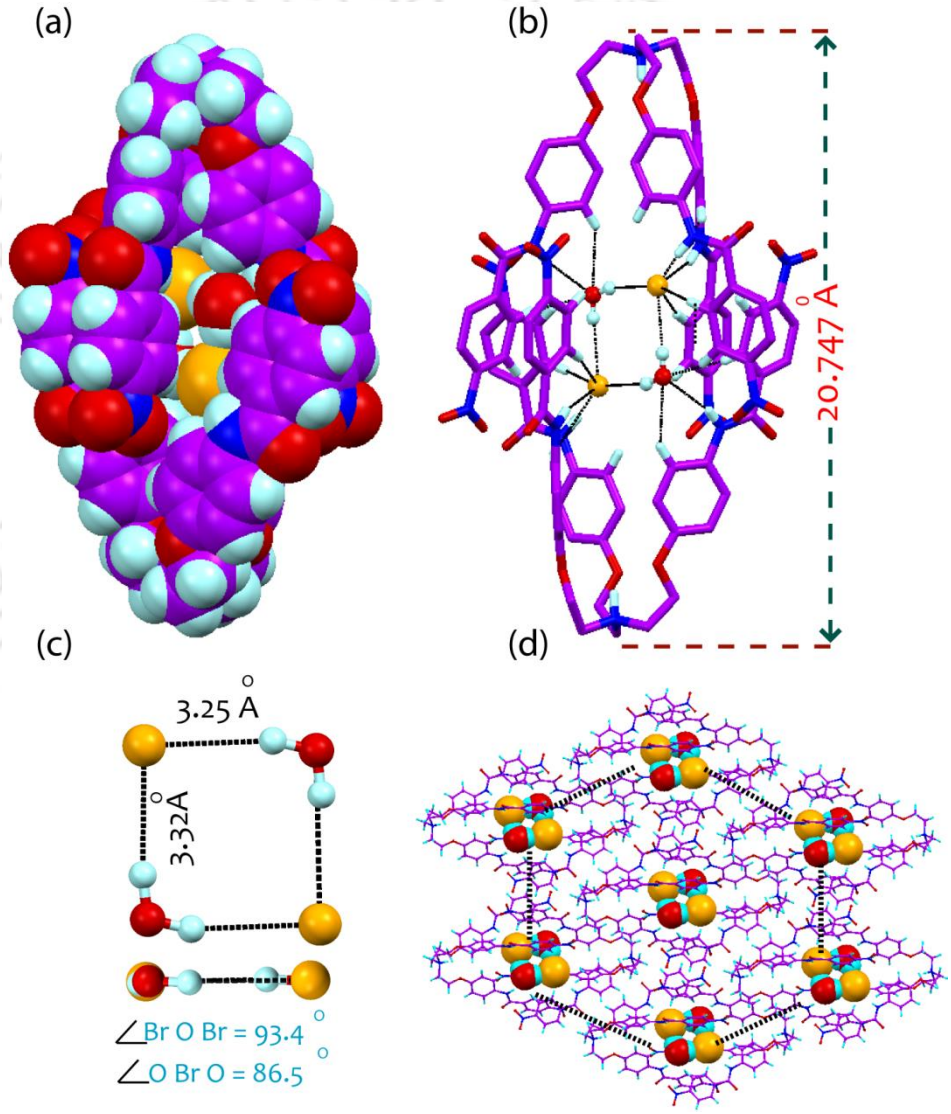

Figure 5.2 (a) Space-filling representation depicting complete encapsulation of the $[Br_2(H_2O)_2]^{2-}$ cluster inside the dimeric capsule-like assembly of $\mathbf{L_3H^+}$; (b) The hydrogen bonding interactions of the $[Br_2(H_2O)_2]^{2-}$ cluster with two $\mathbf{L_3H^+}$; (c) Close up view of the chloride water tetramer and the side view showing the perfect planar nature of $[Br_2(H_2O)_2]^{2-}$; (d) Crystal packing of complex **3b** as viewed down along the crystallographic a axis.

-thermal stability of the halide–water cluster in complexes **3a** and **3b** has further been studied by thermo-gravimetric analysis (TGA). Complex **3a** exhibits a first weight loss of 1.9% at a temperature of 193 °C, which corresponds to the water molecule, whereas complex **3b** loses water (1.8%) at 181 °C. These temperatures are well above 100 °C, which indicate the strong hydrogen bonding between the anion–water cluster and the host molecules for both complexes **3a** and **3b**. Figure 5.3a and 5.3b show the TGA analysis of complex **3a** and **3b** respectively.

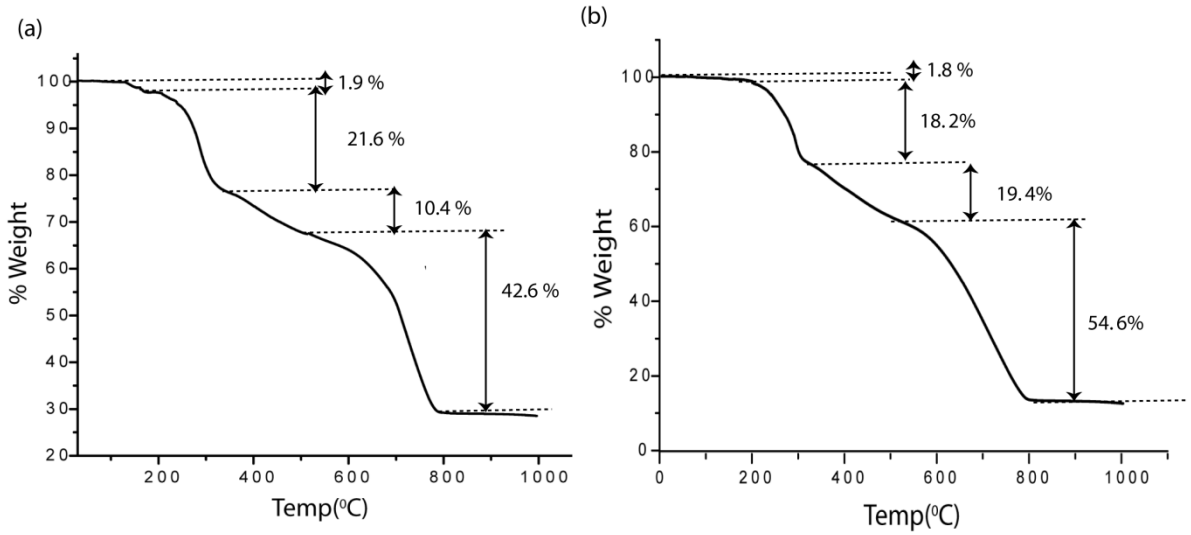

Figure 5.3 (a) Thermogram of complex **3a** shows TGA at the heating rate of 5 °C/min; (b) Thermogram of complex **3b** showing TGA at the heating rate of 5 °C/min.

5.2.3 Structural description of iodide complex (3c)

Single crystals of the iodide complex [$(\mathbf{L_3H})^{+}\cdot I^{-}$] (**3c**) were obtained by slow evaporation of a DMSO solution of $\mathbf{L_3}$ in the presence of excess hydroiodic acid (HI). It crystallizes in the monoclinic space group *P 21/c* with Z = 4 (Table 5.1). The single crystal X-ray structure analysis of the iodide complex **3c** revealed a non-capsular 1D polymeric assembly of the protonated receptors upon iodide coordination (Figure 5.4). In complex **3c** there is a significant change in conformation of the receptor ($\mathbf{L_3H^{+}}$) observed, where one arm of the protonated tripodal receptor is directed opposite to the other two arms, in contrast to complexes **3a** and **3b** (where all three arms are unidirectional). Probably the larger size and lower charge density of the iodide ion is responsible for this conformational change of the receptor in complex **3c**. This change in conformation of $\mathbf{L_3H^{+}}$ indeed helps the formation of the 1D polymeric structure upon iodide coordination in the crystalline solid state. Interestingly, in contrast to complex **3a** and **3b** (where the protonated bridgehead nitrogen atom is stabilized *via* hydrogen bonding interaction with O-atoms of each aliphatic branch)

here in complex **3c** the protonated bridgehead nitrogen atom is stabilized *via* hydrogen bonding interaction with a nitro group of a neighboring receptor unit. The iodide anion in complex **3c** is stabilized by five hydrogen bonds involving three amide NH protons and two aromatic –CH protons (one from nitro phenyl ring and the other one from phenyl ring attached to ethereal oxygen atom). Figure 5.4a represents molecular structure of iodide complex; whereas, figure 5.4b and 5.4c represent coordination environment of iodide anion and iodide coordination induce formation of 1D polymeric assembly respectively. The detail hydrogen bonding interactions are given in table 5.3.

It is important to mention here that efforts were also made to crystallize the fluoride complex of the receptor $\mathbf{L_3}$ but in spite of several attempts we were unable to grow good quality single crystals.

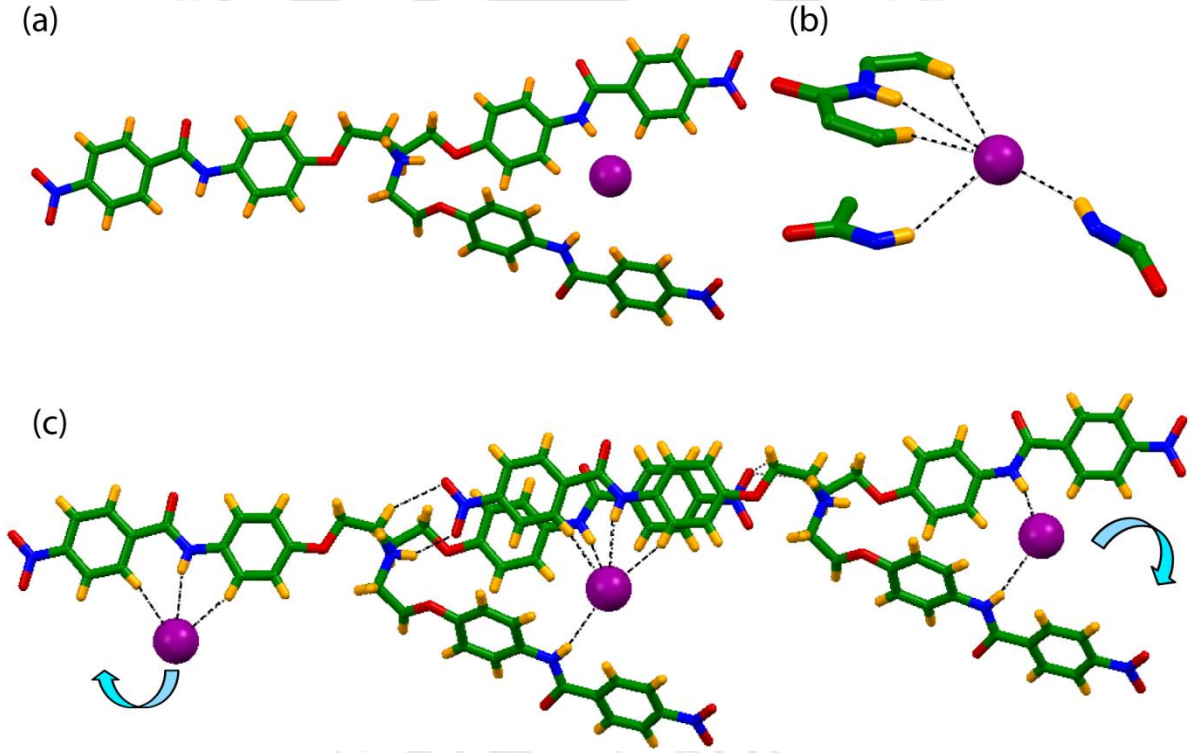

Figure 5.4 (a) Showing molecular structure of complex **3c** where the protonated receptor $\mathbf{L_3H^+}$ is shown in stick model, and iodide anion is shown in spacefill model; (b) Magnified view showing coordination of iodide anion with two $\mathbf{L_3H^+}$ in complex **3c**; (c) Showing formation of polymeric aggregation upon iodide coordination along crystallographic c axis.

5.2.4 Structural description of hexafluorosilicate complex (3d)

Silicon hexafluoride salt **3d** was obtained on reaction of the tripodal ligand $\mathbf{L_3}$ with HF in DMSO, presumably as a result of glass corrosion (eq 1). The complex crystallizes in trigonal crystal system with centrosymmetric space group *R-3* with Z = 3 (Table 5.2). Structural elucidation reveals that two units of protonated receptor $\mathbf{L_3H^+}$ which are flipped inward toward each other in a face-to-face fashion (dN1···N1 = 19.330 (8) Å) with both the

receptors coordinating hexafluorosilicate SiF_6^{2-} anion exactly identical fashion and thereby, creating a caged supramolecular structure. Figure 5.5a and 5.5c represents SiF_6^{2-}

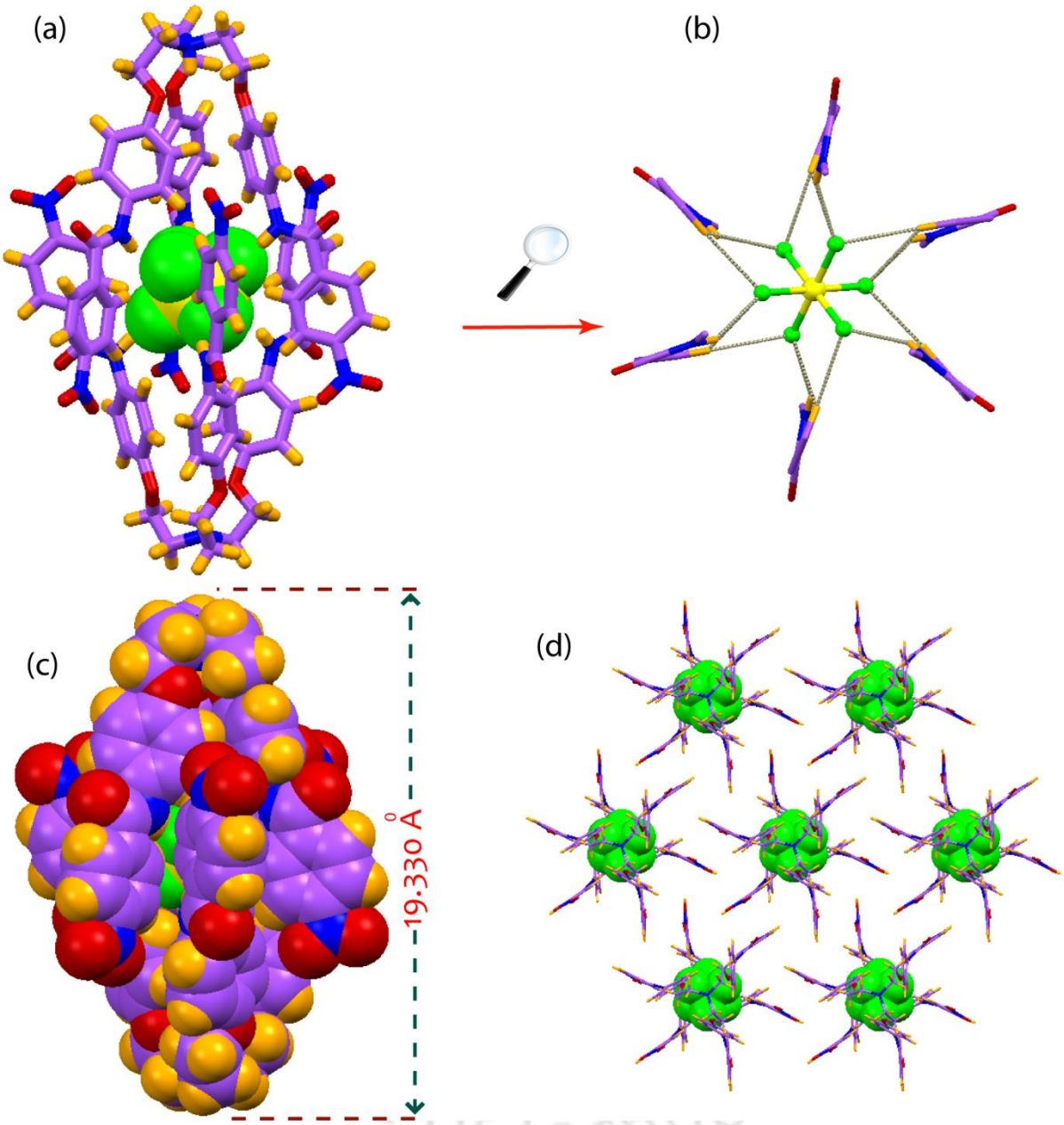

Figure 5.5 (a) Hexafluorosilcate encapsulation by the crystalline self assembled capsules $\mathbf{L_3H^+}$, Two molecules of $\mathbf{L_3H^+}$, shown as stick models, and hexafluorosilcate anion is shown as a space-filling model; (b) Magnified view showing coordination of SiF_6^{2-} with six amide –NH and C−H···F (ortho aryl hydrogen of nitro phenyl ring) within the dimeric capsule; (c) Space-filling representation depicting full encapsulation of the SiF_6^{2-} anion; (d) Crystal packing in complex **3c**, as viewed down the crystallographic c axis.

encapsulation within dimeric assembly of $\mathbf{L_3H^+}$ having a capsule length of 19.330 Å and Figure 5.5b shows the hydrogen bonding interactions of SiF_6^{2-} anion with the capsular assembly of $\mathbf{L_3H^+}$. In complex **3d** all the three arms of the protonated receptor ($\mathbf{L_3H^+}$) are

projected in one direction. The O-atoms of each aliphatic branch are equidistant (~2.71Å) from centrally bridged N-atom, indicative of hydrogen-bonding interactions between the

$$6HF + SiO_2 = H_2SiF_6 + 2H_2O \quad \text{.....eq (1)}$$

proton attached to central N-atom and O-atoms of each aliphatic branch. These hydrogen bonding interactions actually organizes the flexible arms in one direction. One ortho hydrogen atom of the aromatic ring attached to ethereal oxygen atom of each branch are connected to similar aromatic ring of neighbouring arm through C−H···π interactions in a twisted edge-to-face fashion. The unidirectional arms of $\mathbf{L_3H^+}$ creates a C_3 symmetric tripodal cavity and two symmetry independent molecules of $\mathbf{L_3H^+}$ with opposite orientation form a capsular nanocavity that encapsulates a divalent hexafluorosilicate anion in its centre *via* eighteen H-bonds (Figure 5.5b). Hydrogen-bonding interactions [d(D···A) < 3.20 Å] on SiF_6^{2-} shows that, the anion is completely engulfed within a highly symmetrical dimeric assembly of $\mathbf{L_3H^+}$ with an array of 18 strong hydrogen-bonds comprised of six N–H···F and twelve C–H···F bonds from the six tripodal side arms (Figure 5.5b). Each fluoride atoms of hexafluorosilicate anion behaves as a trifurcated hydrogen bond acceptor and each tripodal arm donates one N−H···F and two C−H···F (from ortho aryl hydrogen of nitro phenyl ring) hydrogen bonds resulting in eighteen H-bonds with an average donor-to-acceptor distance of 3.112 Å (Table 5.4). Interestingly, the hexafluorosilicate encapsulated dimeric cages are interlinked with one another through hydrogen-bonding interactions between the oxygen atom of a nitro group and one of the aryl hydrogen atoms of the phenyl ring attached to ethereal oxygen, with a separation distance of 2.48 Å, and which subsequently form a 1D chain capsular assembly along the crystallographic b axis. Two such 1D arrays of capsular assemblies are further interconnected with one another *via* similar C−H···O (nitro) interactions, and generate hexagonal networks of hexafluorosilicate encapsulated dimeric cages around each capsular unit along the c axis (Figure 5.5d)

5.2.5 Structural description of hexafluorosilicate complex (3e)

Interestingly, another SiF_6^{2-} complex with different cell parameter was grown from DMF solvent. Complex **3e** crystallizes in the triclinic space group *P-1* with two protonated receptor moieties along with one hexafluorosilicate anion, and two DMF and four water molecules as the solvents of crystallization (Table 5.2). The structural elucidation reveals a 2:1 receptor−anion stoichiometric salt formation confirming the SiF_6^{2-} complex of protonated $\mathbf{L_3}$. Although, all the three arms of the protonated receptor ($\mathbf{L_3H^+}$) are projected in one direction, but the protonated receptor does not able to create C_3 symmetric tripodal cavity, which is evident from the difference in basal N···N distances of nitro groups

(N3···N5=6.93Å, N5···N7=12.09Å, and N3···N7= 17.46Å) and, the SiF_6^{2-}anions in complex **3e** is located outside the tripodal cavity and stabilized mainly by N−H···F and C−H···F

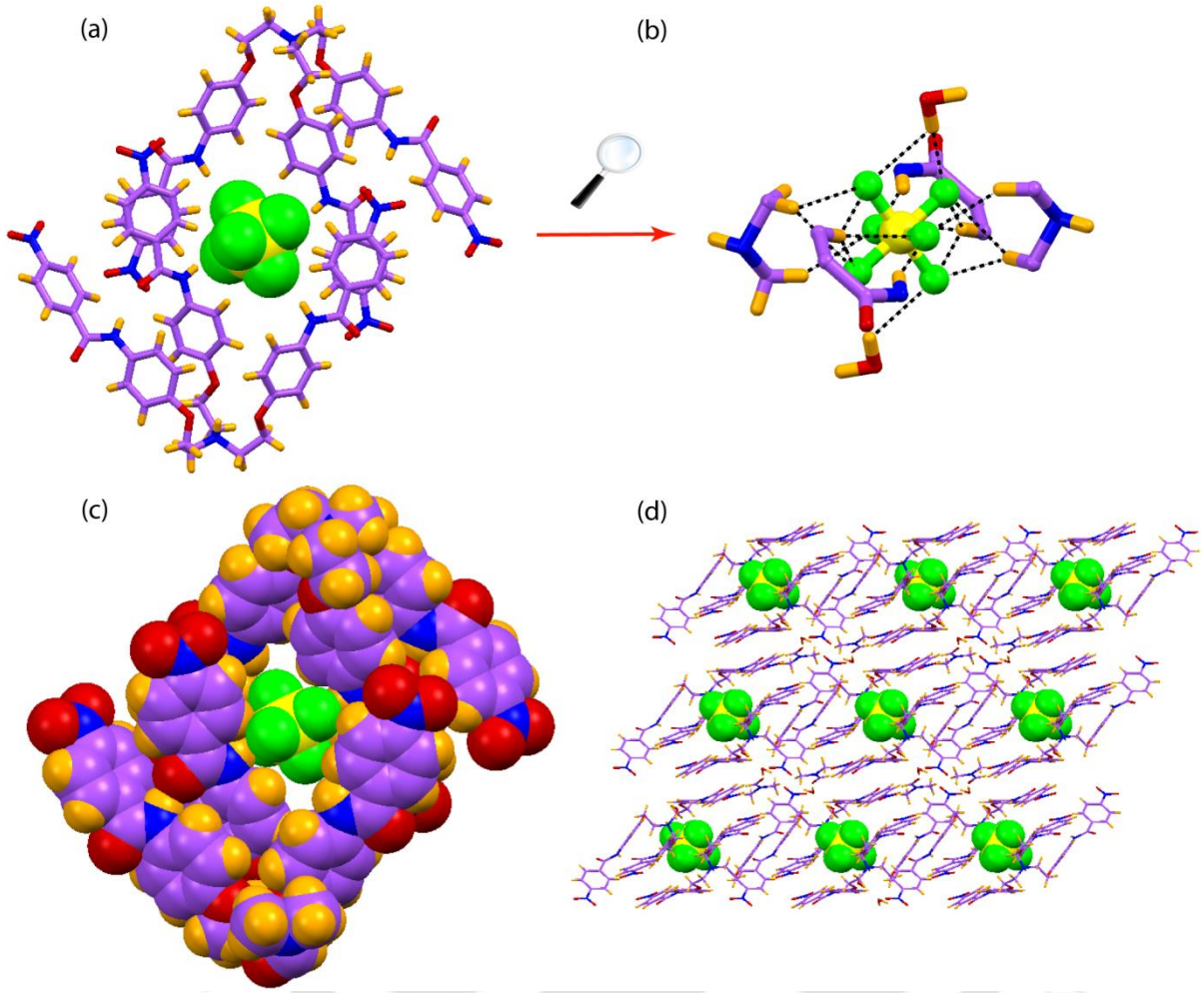

Figure 5.6 (a) Showing molecular structure of hexafluorosilcate complex **3e**.Two molecules of $\mathbf{L_3H^+}$, shown as stick models, and hexafluorosilcate anion is shown as a space-filling model; (b) Magnified view showing coordination of SiF_6^{2-} with four $\mathbf{L_3H^+}$ (only the interacting parts of the protonated receptors are shown) and two lattice water molecules ; (c) Space-filling representation of complex **3e** depicting side cleft binding of SiF_6^{2-} anion; (d) Crystal packing in complex **3e**, as viewed down the crystallographic c axis.

-hydrogen bonds from the four receptor cations. Apart from these hydrogen bonds with the receptor cations, the hexafluorosilicate anion also forms O−H···F hydrogen bonds with two lattice water molecules. The coordination environment of the SiF_6^{2-} in complex **3e** is shown in a part of Figure 5.6. The detail coordination environment of SiF_6^{2-} suggests that, it is stabilized *via* eighteen hydrogen bonding interactions with four receptor cations and two crysllizing water molecules, comprised of two N–H···F, four O–H···F (lattice water), 6 C_{Ar}–H···F (ortho hydrogen of the nitro phenyl ring) and 6 C_{Alp}–H···F (from the acidic −CH2 group, adjacent to the bridgehead protonated nitrogen atom of two receptors) bonds having

an average donor-to-acceptor distance of 3.18 Å (Table 5.4). It is important to note both the SiF_6^{2-}complexes (**3d** and **3e**) the SiF_6^{2-} anion is stabilized *via* 18 H-bonds, therefore it can be concluded that the optimal coordination number for SiF_6^{2-} is 18 H-bonds. Interestingly, one out of three amidic –NH protons of a $\mathbf{L_3H^+}$ moiety is not involved in hydrogen bonding interactions with SiF_6^{2-}in the complex **3e**. Instead, it forms hydrogen bonds with the oxygen atom of a crystallizing water molecule. Probably insertion of crystallizing solvent molecule in complex **3e** prevents the formation of SiF_6^{2-} encapsulated dimeric capsular assembly of protonated receptor $\mathbf{L_3H^+}$.

Thus, by a mere change of crystallizing solvent, we have been able to isolate two structurally different SiF_6^{2-} complexes (**3d** and **3e**). In complex **3d** SiF_6^{2-} anion is encapsulated encapsulated with in highly symmetric dimeric capsular assembly of $\mathbf{L_3H^+}$. Whereas in case of **3e** the SiF_6^{2-} anion is located outside the tripodal cavity and stabilized mainly by N−H···F and C−H···F hydrogen bonds from the urea functions of four receptor cations.

5.3 Anion-binding studies by ^{1}H NMR spectroscopy

The binding properties of $\mathbf{L_3H^+}ClO_4^-$ with halides in solution are investigated by performing ^{1}H NMR experiments in DMSO-d_6 by using $(n\text{-}Bu)_4N^+$ salts of different halides at room temperature. Figure 5.7 shows the chemical shift changes found upon addition of different halides (excess 10 equivalent) to the receptor $\mathbf{L_3H^+}ClO_4^-$ in DMSO-d_6 at RT.

^{1}H NMR titration of $\mathbf{L_3H^+}ClO_4^-$ with $(n\text{-}Bu)_4N^+F^-$ shows that upon gradual addition of standard fluoride solution, no downfield shift is observed for the amide NH peak until the addition of 1 equivalent of fluoride anion. However, the aliphatic –CH protons are shifted upfield and remain almost unchanged after further addition of fluoride anions. This observation suggests that the centrally bridged N-atom is deprotonated after addition of 1 equivalent of fluoride anion and thus, in solution fluoride complexation is not possible with the protonated receptor ($\mathbf{L_3H^+}$). Whereas the disappearance of amide NH signals beyond addition of 1 equivalent of fluoride anion is due to the binding (with neutral receptor) induced broadening of the −NH signals rather than deprotonation. In the case of $(n\text{-}Bu)_4N^+Cl^-$ a significant downfield shift 0.1 ppm of amide NH proton resonance is observed and subsequently the binding constant with chloride anions is determined from titration experiments and was found to be $118M^{-1}$. However, addition of $(n\text{-}Bu)_4N^+Br^-$ produces a very slight downfield shift (0.02 ppm) of the amide –NH proton resonance of the protonated receptor. Unfortunately, accurate binding constant value with bromide anion could not be obtained from small and inconsistent changes during titration experiment. Interestingly, no

notable change in the chemical shift of the amide NH proton resonance is observed in the case of $(n\text{-}Bu)_4N^+I^-$ indicating the hydrogen-bonding interactions between receptor and the iodide anion are energetically not favorable. Although solid state crystal structure of the iodide complex (**3c**) shows presence of weak hydrogen bonding interactions between amide functions of $\mathbf{L_3H^+}$ and iodide anion.

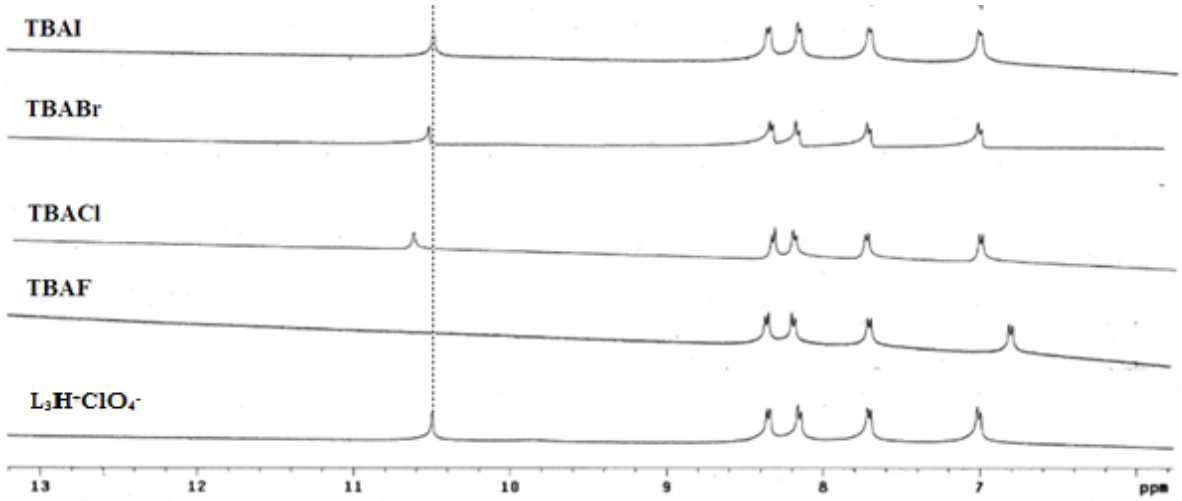

Figure 5.7 (a) ^{1}H NMR spectra (400 MHz, DMSO-d_6, 298 K) of $\mathbf{L_3H^+}ClO_4^-$ and change of amide −NH resonance upon addition of excess (10 equivalent) F^-, Cl^-, Br^-, and I^- as their tetrabutylammonium salts.

The mode of receptor–anion interactions and the anion induced electronic and conformational changes of the receptor can be illustrated by the 2D NOESY NMR experiment, which is a traditional and very useful tool in the field of supramolecular host–guest chemistry. Therefore, for improved understanding of the solution state binding nature of the receptor toward the anions, we have carried out 2D NOESY NMR experiments both for free receptor ($\mathbf{L_3}$) and anion complexes in DMSO-d_6 at RT. The NOESY spectra of both the chloride and bromide (**3a** and **3b**) complexes show significantly strong NOE coupling between the amide NH protons and water (H–O–H), whereas, no such type (N–H···H–O–H) of interaction is observed in the case of the free receptor ($\mathbf{L_3}$) and complex **3c** (iodide complex). Figure 5.8 shows partial NOESY spectra of free receptor ($\mathbf{L_3}$) and its halide complexes (**3a**, **3b** and **3c**). These results imply that for complexes **3a** and **3b** the receptor ($\mathbf{L_3H^+}$) encapsulates hydrated halide anion(s) (Cl^- or Br^-) *via* hydrogen bonding interactions inside its tripodal cavity. We have also taken the NOESY spectra of both the SiF_6^{2-} complexes (**3d** and **3e**) to correlate solid and solid and solution state binding behavior of SiF_6^{2-} anion, but even after careful evaluation of the experimental (noesy) results it is hard to

give any concluding remarks, because NOESY spectra of both the complexes are almost identical (Annexure 5).

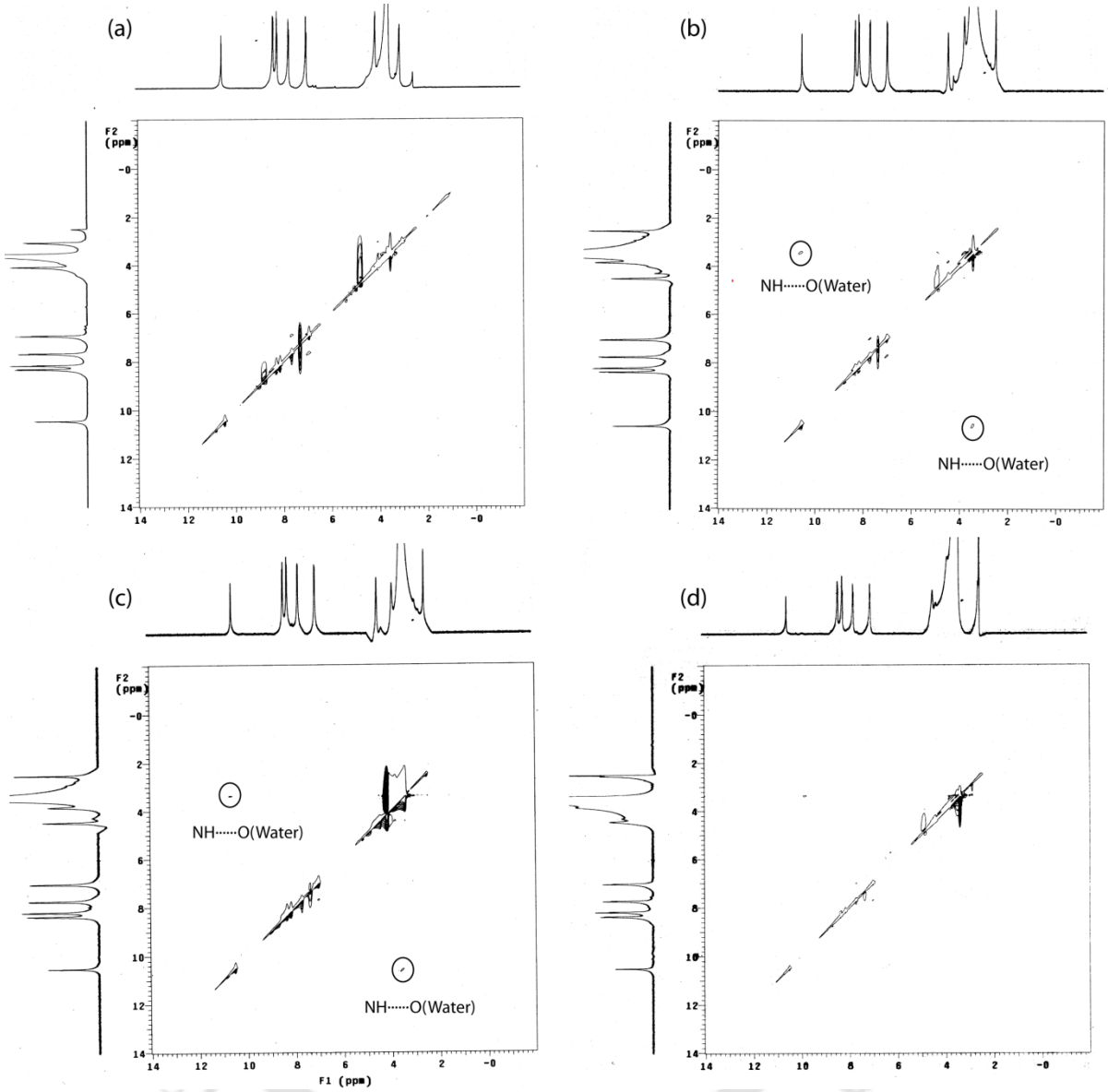

Figure 5.8 2D NOESY NMR experiments of (a) receptor, $\mathbf{L_3}$; (b) $[Cl_2(H_2O)_2]^{2-}$ encapsulated complex, **3a**; (c) $[Br_2(H_2O)_2]^{2-}$ encapsulated complex, **3b** and (d) iodide complex[$(\mathbf{L_3H})^+ \cdot I^-$] **3c.** All the spectra were taken in DMSO-d_6 at RT.

5.4 Conclusion

In summary, we have demonstrated we have shown the encapsulation of a planar cyclic tetrameric halide water cluster $[X_2(H_2O)_2]^{2-}$ X = Cl^-/Br^- within the dimeric capsular assembly of a conformationally flexible tripodal amide receptor, where $[X_2(H_2O)_2]^{2-}$ X = Cl^- /Br^- has acted as a template in the formation of the dimeric capsular complexes. The clusters are formed *via* strong halide (X = Cl^- / Br^-)–water interactions and possesses a planar cyclic tetrameric arrangement where each halide(X = Cl^- / Br^-) anion is hydrogen bonded with the two water molecules. Close inspections of the distance and angle measurement values of

these terameric water clusters confirmed that they are perfect parallelogram. However, in the case of higher homologous iodide anions the receptor changes its conformation and adopts noncapsular polymeric aggregation upon iodide coordination. Probably the larger size and lower charge density of the iodide ion is responsible for this conformational change in the receptor which indeed helps the formation of the 1D polymeric structure upon iodide coordination. The thermal stability of the halide–water cluster in complexes **3a** and **3b** has been studied by thermo-gravimetric analysis, which shows both the complexes are stable beyond 150 °C indicating strong hydrogen bonding between the anion–water cluster and the host molecules. The solution state receptor-hydrated halide (Cl^- and Br^-) interaction in complexes **3a** and **3b** has further been confirmed using 2D-NOESY NMR experiments. The NOESY spectra of both the complexes show significantly strong NOE coupling between the amide NH protons and water (H–O–H), suggesting encapsulation of hydrated halide anion(s) (Cl^- or Br^-) *via* hydrogen bonding interactions inside its tripodal cavity. Additionally, crystallization of the receptor in presence of HF in glass container gives SiF_6^{2-} complex. The formation of SiF_6^{2-} instead of fluoride complex in presence of HF is presumably as a result of glass corrosion. Interestingly, depending on solvent of crystallization the receptor forms two different SiF_6^{2-} complexes **3d** and **3e**. In **3d** the SiF_6^{2-} anion is encapsulated within dimeric capsular assembly of the protonated receptor, where in **3e** SiF_6^{2-} anion is located outside the tripodal cavity and stabilized mainly by N−H···F and C−H···F hydrogen bonding interactions with four receptor cations.

Table 5.1 Crystallographic parameters and refinement details of halide complexes **3a**, **3b** and **3c**.

Parameters	**3a**	**3b**	**3c**
Formula	$C_{45}H_{42}ClN_7O_{13}$	$C_{45}H_{42}BrN_7O_{13}$	$C_{45}H_{40}IN_7O_{12}$
Fw	924.31	968.76	997.74
Cry. system	Triclinic	Triclinic	Monoclinic
Space group	*P-1*	*P-1*	*P 21/c*
a/Å	9.3971(5)	9.4231(11)	8.0650(5)
b/Å	14.8204(7)	14.9240(12)	41.706(2)
c/Å	17.5829(9)	17.6464(15)	15.0999(8)
α/°	69.237(3)	68.839(8)	90.00
β/°	75.363(3)	74.960(9)	97.283(6)
γ/°	83.377(3)	83.360(8)	90.00
V/Å^3	2214.51(19)	2234.3(4)	5038.0(5)
Z	2	2	4
D_c/g cm^{-3}	1.386	1.440	1.315
μ (mm^{-1})	0.161	0.992	0.699
T/°K	298(2)	298(2)	298(2)
Total reflns	27999	18093	24379
Ind. reflns	10812	11412	12947
Obs. reflns	4793	4794	6479
Parameters	614	614	587
R1; wR2 (I > 2σ(I))	0.0568, 0.1856	0.0830, 0.2748	0.1000, 0.3292
R(int)	0.0415	0.0770	0.0532
GOF (F^2)	0.861	0.988	1.120

Table 5.2 Crystallographic parameters and refinement details of hexafluorosilicate complexes **3d** and **3e.**

Parameters	**3d**	**3e**
Formula	$C_{90}H_{80}F_6N_{14}O_{24}Si$	$C_{96}H_{102}F_6N_{16}O_{30}Si$
Fw	1883.77	968.76
Cry. system	Trigonal	Triclinic
Space group	*R -3*	*P-1*
a/Å	13.3641(7)	13.1197(5)
b/Å	13.3641(7)	13.1321(6)
c/Å	45.517(3)	15.7929(6)
α/^{o}	90.00	108.655(2)
β/^{o}	90.00	105.033(2)
γ/^{o}	120.00	92.632(2)
V/Å^3	7040.2(6)	2464.94(17)
Z	3	1
D_c/g cm^{-3}	1.333	1.416
μ (mm^{-1})	0.118	0.125
T/^{o}K	298(2)	298(2)
Total reflns	10351	30365
Ind. reflns	3736	11455
Obs. reflns	2030	9244
Parameters	206	708
R1; wR2 (I > 2σ(I))	0.0987, 0.3140	0.0608, 0.1831
R(int)	0.0472	0.1291
GOF (F^2)	1.057	0.830

Table 5.3 Important hydrogen bonding contacts in complexes **3a**, **3b** and **3c**.

Complexes	D–H···O	*d*(H···O)/Å	*d*(D···O)/Å	∠D–H···O/^{o}
3a	N6H···Cl1	2.51	3.330(3)	162.9(3)
	C11H···Cl1	2.76	3.544(4)	147.2(2)
	C35H···Cl1	2.88	3.567(3)	131.7(2)
	C41H···Cl1	2.81	3.684(3)	155.8(2)
	O13HA···Cl1	2.30	3.127(2)	162.3(1)
	O13HB···Cl1	2.32	3.177(2)	174.9(1)
	C20H···O13	2.57	3.374(3)	145.0(2)
	N4H···O13	2.07	2.92(1)	160.7(3)
	C26H···O13	2.40	3.252(4)	152.2(2)
	C12H···O13	2.71	3.551(4)	150.1(2)
3b	N6H···Br1	2.66	3.481(4)	159.9(3)
	C11H···Br1	2.76	3.638(7)	143.2(4)
	C35H···Br1	2.98	3.669(5)	131.3(3)
	C41H···Br1	2.88	3.789(5)	163.3(3)
	O13HA···Br1	2.42	3.250(5)	164.4(3)
	O13HB···Br1	2.48	3. 326 (4)	172.7(3)
	C20H···O13	2.57	3.374(6)	144.5(2)
	N4H···O13	2.23	3.058(6)	161.6(3)
	C26H···O13	2.42	3.227(7)	145.1(4)
	C12H···O13	2.81	3.634 (4)	148.0(4)
3c	N2H···I1	3.08	3.795(5)	141.9(3)
	N4H···I1	2.97	3.776(7)	155.2(4)
	N6H···I1	3.11	3.919(5)	156.2(3)
	C45H···I1	2.95	3.847(6)	161.9(3)
	C37H···I1	3.15	3.978(6)	147.7(4)
	N1H···O11	2.27	3.084(7)	148.0(3)

Table 5.4 Important hydrogen bonding contacts in complexes **3d** and **3e**.

Complexes	D–H···O	*d*(H···O)/Å	*d*(D···O)/Å	∠D–H···O/°
3d	N2H···F1	2.07	2.847(6)	148.8(3)
	C15H··· F1	2.41	3.210(8)	144.0(4)
	C15H··· F1	2.51	3.290(1)	140.9(0)
3e	N4H···F1	2.08	2.820(4)	156.0(3)
	C30HA···F1	2.65	3.511(4)	152.9(2)
	C30HA···F3	2.47	3.306(5)	148.8(2)
	C30HA···F2	2.66	3.424(4)	139.3(2)
	C31HA···F1	2.50	3.371(3)	149.1(2)
	C16HA···F2	2.25	3.057(4)	139.3(2)
	C16HA···F3	2.60	3. 364 (5)	135.3(2)
	O14H15O···F2	2.46	2.974(3)	114.0(4)
	O14H15O···F3	2.07	3.010(4)	171.0(5)

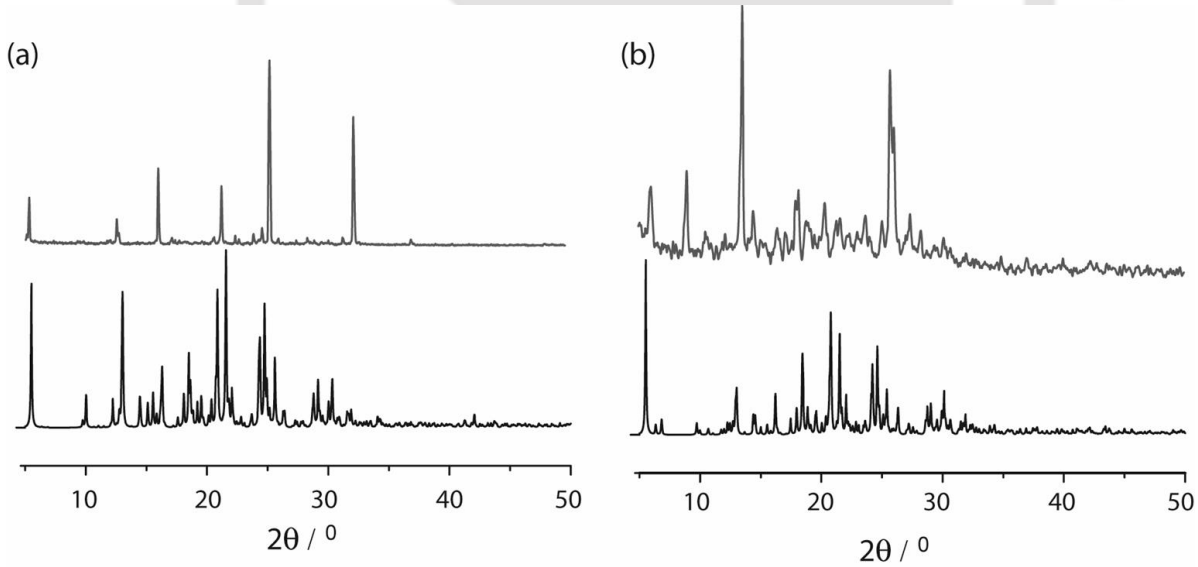

Figure 5.9 (a) Powder X-ray diffraction: simulated pattern from the single-crystal X-ray of complex **3a** (bottom), experimental pattern from the crystalline solid **3a** (top); (b) Powder X-ray diffraction: simulated pattern from the single-crystal X-ray of complex **3b** (bottom), experimental pattern from the crystalline solid of complex **3b** (top).

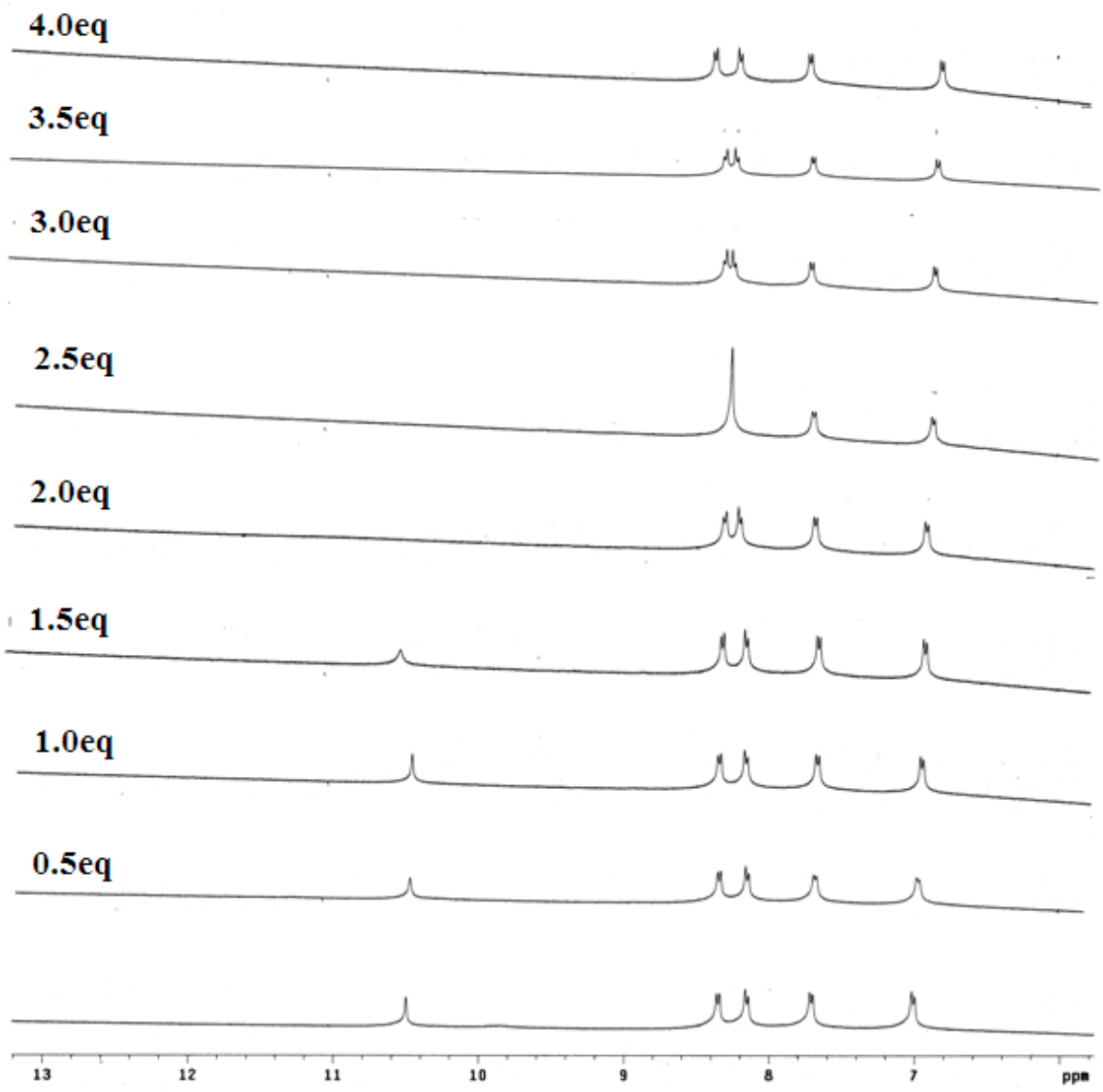

Figure 5.10 (a) Change in chemical shift of –NH resonances of $\mathbf{L_3H^+}.ClO_4^-$ with increasing concentration of standard fluoride solution in DMSO-d_6 at 298

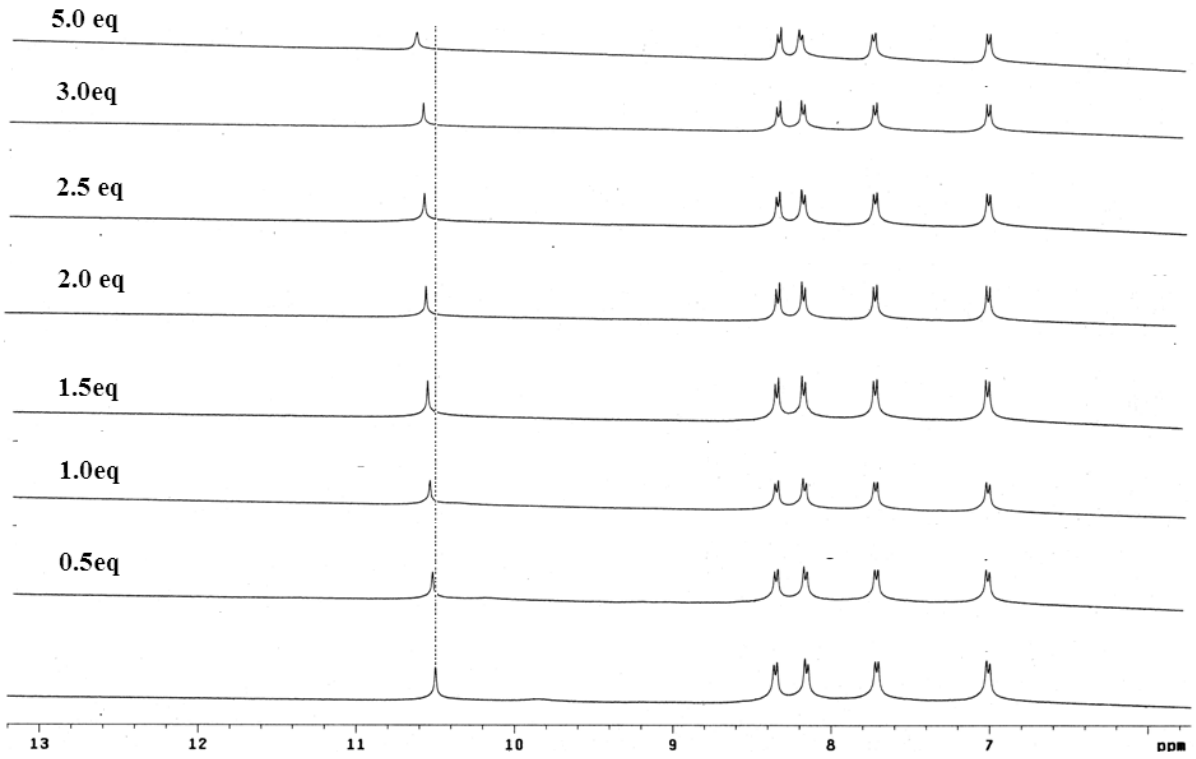

Figure 5.11 (a) Change in chemical shift of –NH resonances of $\mathbf{L_3H^+}.ClO_4^-$ with increasing concentration of standard chloride solution in DMSO-d_6.

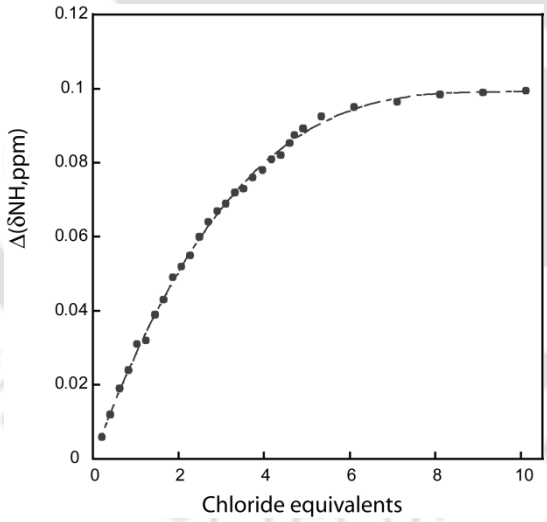

Figure 5.12 ^{1}H NMR titration curves of $\mathbf{L_3H^+}.ClO_4^-$ with Cl^- in DMSO-d_6 at RT. Net changes in the chemical shifts of amidic –NH is shown against the increasing amount of chloride anion.

References

1 (*a*) M. Cametti and K. Rissanen, *Chem. Commun*., 2009, 2809; (*b*) T.W. Hudnall, C.-W. Chiu and F. P. Gabbai, *Acc. Chem. Res*., 2009, **42**, 388; (*c*) M. Cametti and K. Rissanen, *Chem. Soc. Rev*., 2013, **42**, 2016.

2 (*a*) L. R. MacGillivray and J. L. Atwood, *J. Am. Chem. Soc*., 1997, **119**, 2592; (*b*) M. Zuhayra, W. U. Kampen, E. Henze, Z. Soti, L. Zsolnai, G. Huttner and F. Oberdorfer, *J. Am. Chem. Soc*., 2006, **128**, 424; *(c*) B.-Q. Ma, H.-L. Sun and S. Gao, *Chem. Commun*., 2004, 2220; (*d*) J. L. Atwood, L. J. Barbour, T. J. Ness, C. L. Raston and P. L. Raston, *J. Am. Chem. Soc*., 2001, **123**, 7192; (*e*) L. J. Barbour, G. W. Orr and J. L. Atwood, *Nature*, 1998, **393**, 671; (*f*) M. Mascal, L. Infantes and J. Chisholm, *Angew. Chem., Int. Ed*., 2006, **45**, 32; (g) B.-Q. Ma, H.-L. Sun and S. Gao, *Angew. Chem., Int. Ed*., 2004, **43**, 1374; (*h*) S. O. Kang, D. Powell, V. W. Day and K. Bowman-James, *Cryst. Growth Des*., 2007, **7**, 606; (*i*) Y. Li, L. Jiang, T.-B. Feng and X.-L. Lu, *Cryst. Growth Des*., 2008, **8**, 3689; (*j*) M. Yoshizawa, T. Kusukawa, M. Kawano, T. Ohhara, I. Tanaka, K. Kurihara, N. Niimura and M. Fujita, *J. Am. Chem. Soc*., 2005, **127**, 2798; (*k*) M. A. Saeed, B. M. Wong, F. R. Fronczek, R. Venkatraman and M. A. Hossain, *Cryst. Growth Des*., 2010, **10**, 1486; (*l*) C. Massera, M.Melegari, F. Ugozzoli and E. Dalcanale, *Chem. Commun*., 2010, **46**, 88.

3 (*a*) J. Peters, W. Baumeister and A. Lupas, *J. Mol. Biol*., 1996, **257**, 1031–1041; (*b*) H. Yin, G. Hummer and J. C. Rasaiah, *J. Am. Chem. Soc*., 2007, **129**, 7369–7377; (*c*) Z. Otwinowski, R. W. Schevitz, R.-G. Zhang and P. B. Sigler, *Nature*, 1988, **335**, 321–329; (*d*) S. H. Sleigh, J. R. H. Tame, E. J. Dodson and A. J. Wilkinson, *Biochemistry*, 1997, **36**, 9747–9748.

4 H. Ohtaki and T. Radnai, *Chem. Rev*., 1993, **93**, 1157–1204.

5 D. T. Richens, *The Chemistry of Aqua Ions*, Wiley, Chichester, 1987.

6 (*a*) R. A. Bryce, M. A. Vincent and I. H. Hillier, *J. Phys. Chem. A*, 1999, **103**, 4094–4100; (*b*) P. Weis, P. R. Kemper, M. T. Bowers and S. S. Xantheas, *J. Am. Chem. Soc*., 1999, **121**, 3531–3532; (*c*) H. M. Lee, D. Kim and K. S. Kima, *J. Chem. Phys*., 2002, **116**, 5509–5520; (*d*) D. D. Kemp and M. S. Gordon, *J. Phys. Chem. A*, 2005, **109**, 7688–7699; (*e*) C. P. Kelly, C. J. Cramer and D. G. Truhlar, *J. Phys. Chem. B*, 2006, **110**, 16066–16081; (*f*) S. Lima, B. J. Goodfellow and J. J. C. Teixeira-Dias, *J. Inclusion Phenom. Macrocyclic Chem*., 2006, **54**, 35–40; (*g*) W. H. Robertson and M. A. Johnson, *Annu. Rev. Phys. Chem*., 2003, **54**, 173–213.

7 (*a*) J. R. Butchard, O. J. Curnow, D. J. Garrett and R. G. A. R. Maclagan, *Angew. Chem., Int. Ed*., 2006, **45**, 7550; (*b*) Q.-Q. Wang, V. W. Day and K. Bowman-James, *J. Am. Chem. Soc*., 2013, **135**, 392; (*c*) Q.-Q.Wang,V. W. Day and K. Bowman-James, *Angew. Chem., Int. Ed*., 2012, **51**, 2119; (*d*) M. A. Saeed, A. Pramanik, B.M.Wong, S. A. Haque, D. R. Powell, D. K. Chandd and M. A. Hossain, *Chem. Commun*., 2012, **48**, 8631; (*e*) M. A. Hossain, M. A. Saeed, A. Pramanik, B. M. Wong, S. A. Haque and D. R. Powell, *J. Am. Chem. Soc*., 2012, **134**, 11892; (*f*) A. Bakhoda, H. R. Khavasi and N. Safari, *Cryst. Growth Des*., 2011,**11**, 933; (*g*) K. K. Bisht, A. C. Kathalikkattil and E. Suresh, *Cryst. Growth Des*., 2012, **12**, 556; (*h*) R. Custelcean and M. G. Gorbunova, *J. Am. Chem. Soc*., 2005, **127**, 16362;

8 (*a*) M. Arunachalam and P. Ghosh, *Chem. Commun*., 2011, **47**, 6269; (b) M. Arunachalam and P. Ghosh, *Chem. Commun*., 2009, 5389; (*c*) M. Arunachalam and P. Ghosh, *Inorg. Chem*., 2010, **49**, 943; (*d*) D. A. Jose, D. K. Kumar, B. Ganguly and A. Das, *Inorg. Chem*.,2007, 46, 5817.

9 (*a*) N. Busschaert, M. Wenzel, M. E. Light, P. Iglesias-Hernandez, R. Perez-Tomas and P. A. Gale, *J. Am. Chem. Soc*., 2011, **133**, 14136; (*b*) B. Akhuli, I. Ravikumar and P. Ghosh, *Chem. Sci*., 2012, **3**, 1522; (*c*) A. S. Singh and S.-S. Sun, *Chem. Commun*., 2011, **47**, 8563; (*d*) A. Basu and G. Das, *Dalton Trans*., 2012, **41**, 10792; (*e*) S. K. Dey, R. Chutia and G. Das, *Inorg. Chem*., 2012, **51**, 1727.

10 (*a*) Y. Yamauchi and M. Fujita, *Chem. Commun*., 2010, **46**, 5897; (*b*) K. Ikemoto, Y. Inokuma and M. Fujita, *Angew. Chem., Int. Ed*., 2010, **49**, 5750; (*c*) M. Yoshizawa, J. K. Klosterman and M. Fujita, *Angew. Chem., Int. Ed*., 2009, **48**, 3418; (*d*) J. Rebek Jr., *Chem.Commun*., 2000, 637.

Chapter 6

A Heteroditopic Tripodal Urea Receptor for Recognition of Ion-pairs

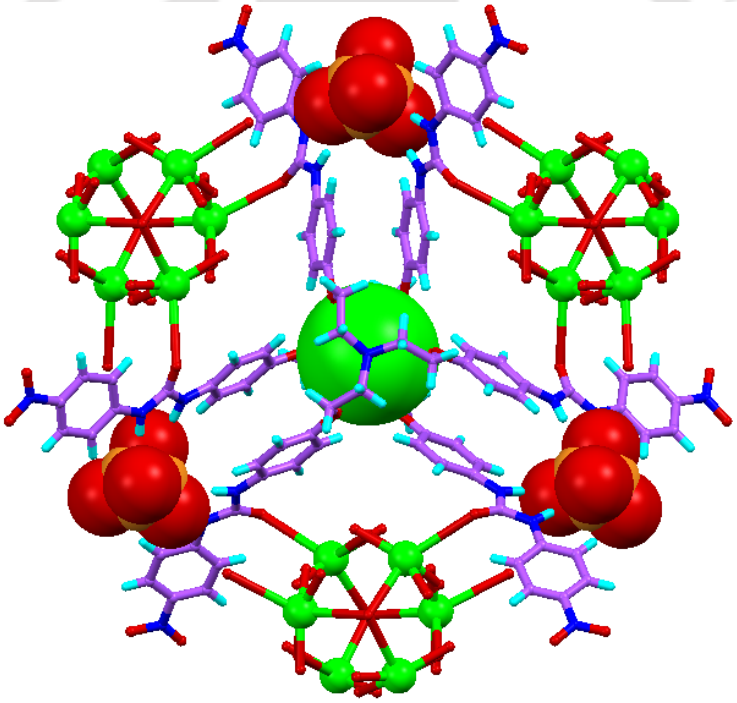

6.1 Background and focus of the chapter

Given the interest in the anion recognition chemistry of the tetrahedral oxyanions especially sulfate and phosphate[1] in the synthetic, healthcare, environmental, or energy related problems, sulfate and phosphate salts with alkali metal cations have emerged as desirable targets for molecular recognition.[2] This is largely motivated by the pivotal roles these salts play in environmental and biological processes. These anions (sulfate and phosphate) are also elusive guests for selective recognition particularly in polar hydrophilic solvents due to the large hydration energy compared to other anions.[1a,b]

Acyclic receptors with multi-armed hydrogen bonding functionality have often been found to coordinate with targeted anionic species *via* formation of capsular assemblies.[3] In this regard tren-based tris urea or thiourea ligands represent a class of receptors that has proven particularly useful for recognition and separation of tetrahedral oxyanions (sulfate and phosphate) through encapsulation.[3b] The TREN scaffold has been vastly used in anion coordination chemistry, either in its protonated form or as a part of more complicated receptors. On the other hand, tetrahedral oxyanion (sulfate and phosphate) encapsulation can also be constructed with the help of metal coordination. Metal complexes allow for the pre-orientation of the building blocks according to the metal coordination geometry to offer a complementary binding environment for anions.[4]

Considering, these facts we have developed an elongated C_{3v} symmetric N-bridgehead flexible tripodal urea receptor **L_4** by deliberately positioning the cation binding site far apart from anion binding site. Detail ^{1}H NMR spectroscopic investigations in solution and solid-state crystallographic analysis shows that the **L_4** is able to act as a potential receptor for both anion and ion-pair. As detailed below, ^{1}H NMR spectroscopic studies revealed that receptor **L_4** moderately and weakly binds the hydrogensulfate and di-hydrogenphosphate anions respectively. However, in presence of Group I metal ions, (Li^+ (1eq), Na^+(1eq) and K^+(0.5eq), as their perchlorate salts in DMSO-d_6/D_2O) the receptor **L_4** exhibited a dramatic enhancement of anion binding property. Interestingly, in presence of one equivalent K^+ the receptor shows negative cooperative binding with both the HSO_4^- and $H_2PO_4^-$ anions. The receptor forms sulfate complex (**4a**) in its protonated form, which is structurally characterized and shows encapsulation of single DMF solvent molecule in the tripodal cavity of the protonated receptor, and the SO_4^{2-} anion is located outside the tripodal cavity and stabilized by N−H···O hydrogen bonds from the urea functions of four receptor cations. Whilst, in case of $TBAHSO_4$ the receptor forms an unusual contact ion-pair complex (**4b**), in which both the TBA cation and SO_4^{2-} anion are encapsulated in the distorted C_{3v} symmetric tripodal cleft of the protonated receptor. The protonation of the receptor suggests HSO_4^- to

receptor proton transfer phenomena. Further, the receptor also forms a remarkable C_{3v} symmetric charge separated ion-pair complex (**4c**) with potassium cation and hydrgenphosphate anion *via* formation of dimeric capsular assembly of the receptor, where three nearby K^+ encapsulated dimeric capsular assemblies interdigitate to form a cavity to encapsulate the HPO_4^{2-} by six urea groups (Scheme 6.1).

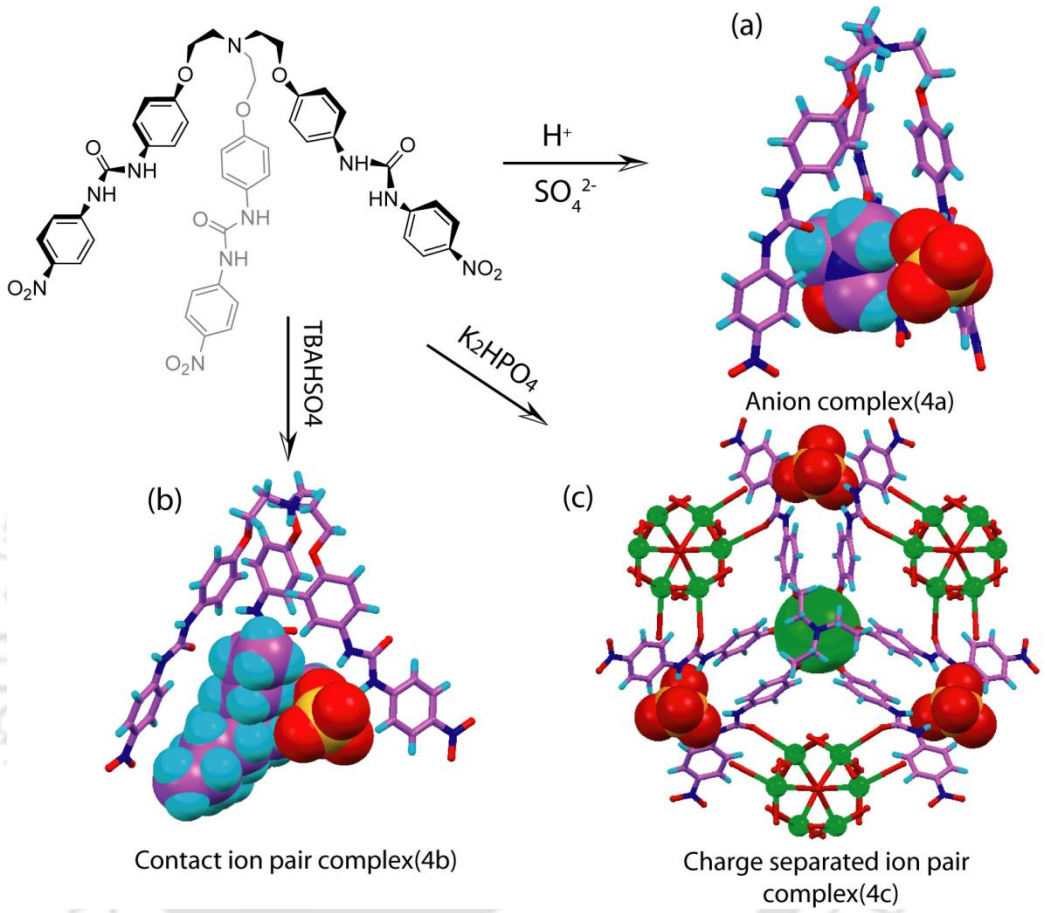

Scheme 6.1 Molecular structure of heteroditopic tripodal urea receptor $\mathbf{L_4}$ and schematic representation depicting the anion and ion-pair complexes of $\mathbf{L_4}$: (a) SO_4^{2-}complex of protonated receptor $\mathbf{L_4}$; (b) Showing formation of contact ion-pair complex with $TBAHSO_4$; (d) Showing formation of charge separated ion-pair complex with K_2HPO_4.

6.2 Structural description of L_4

Single crystals of $\mathbf{L_4}$ suitable for XRD analysis were obtained by slow evaporation of DMF solution, which crystallizes in triclinic space group *P-1* with Z = 4. The asymmetric unit contains two symmetry-independent receptor molecules (Z´ = 2) with four crystallizing DMF and two water molecules. The molecular structure of the receptor $\mathbf{L_4}$ is shown in figure 6.1. In supramolecular chemistry, the presence of more than one molecular conformer in the same crystal structure has been described by the term conformational isomorphism and their occurrence is accounted by thermodynamic and kinetic crystal stability because these are

considered to be results of interrupted crystallization process. Crystal structure analysis of **L_4** shows that the three tripodal side arms of both conformational isomorphs (C1 and C2) are directed in three different directions with absence of any intramolecular interactions, suggesting un-preorganized nature of the tripodal receptor **L_4** in guest (anion/cation) free condition. Probably the absence of intramolecular interactions makes the receptor flat and un-preorganized (Figure 6.1a). For both the conformer (C1 and C2) two urea functions form similar bifurcated hydrogen bonds with the oxygen atoms of two DMF molecules individually, whereas, the third urea function forms bifurcated hydrogen bonds with the lattice water molecule which is further hydrogen bonded with the bridgehead nitrogen atom and the oxygen atom of a urea function of neighboring receptor molecules (Figure 6.1b). The donor acceptor distances of these hydrogen bonds are <3.0 Å and the details of hydrogen-bonding interactions involved in the crystal structure of **L_4** are provided in (Table 6.2).

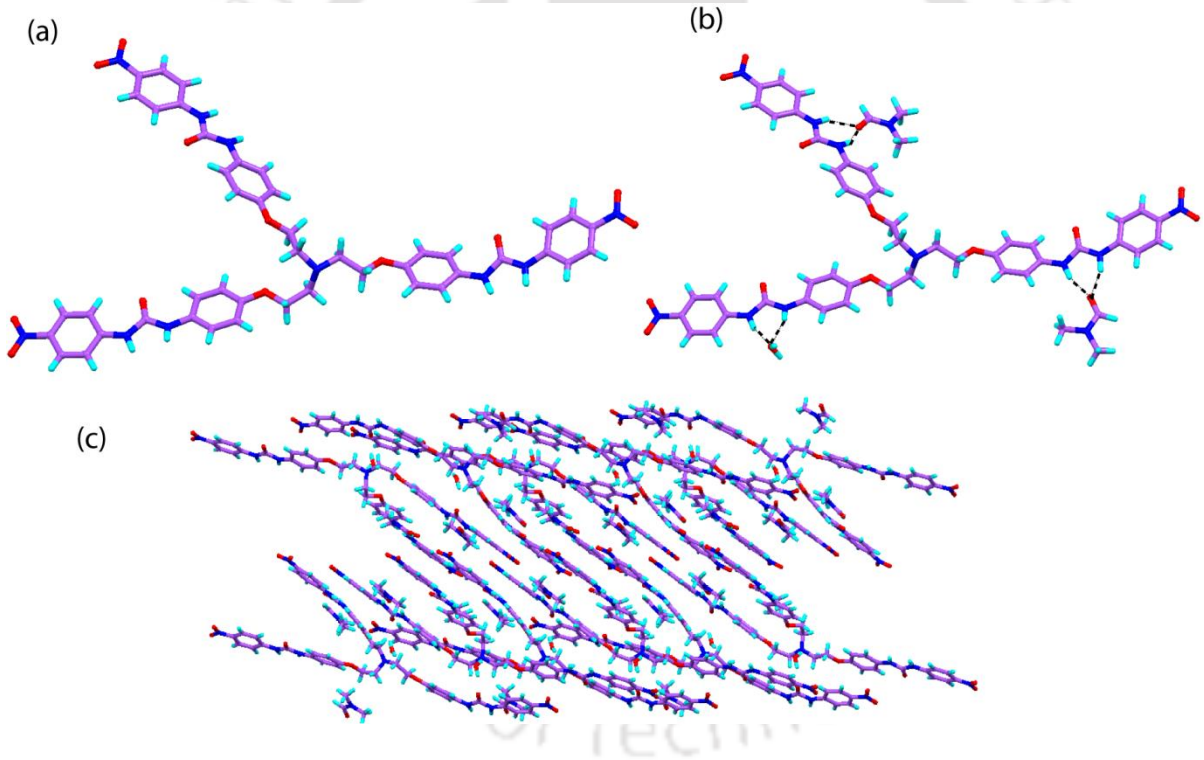

Figure 6.1 (a) Unpreorganized molecular structure of receptor **L_4**. The other unit in the asymmetric unit and solvent molecules are omitted for clarity; (b) Showing hydrogen bonding interactions between urea functions of the receptor **L_4** and crystallizing solvent molecules (DMF and water); (c) Showing packing diagram of **L_4** along a axis.

Furthermore, each receptor unit is linked to another adjacent unit of different symmetry *via* intermolecular C−H···O hydrogen bonding interactions, donated from aromatic C−H protons to the oxygen atoms of the urea functions of adjacent molecule. The three dimensional

crystal packing as viewed down the crystallographic a axis, shows layered assembly formation (Figure 6.1c).

6.3 Structural aspects of anion and ion-pair binding with L_4

Structural information obtained from single crystal X-ray analyses of the anion and ion-pair complexes can provide insight into the proper binding topology of different guests (anion, cation or both) with **L_4**. From the viewpoint of supramolecular chemistry, crystallization has traditionally been a route to understand the structural insights of the complexes, and the acquired knowledge can then be used to correlate solution state binding.

6.3.1 Structural description of complex 4a

Complex **4a** crystallizes in the triclinic space group *P-1* with two protonated receptor moieties along with one sulfate anion, and four DMF and two water molecules as the solvents of crystallization (Table 6.1). The structural elucidation reveals a 2:1 receptor−anion stoichiometric salt formation confirming the SO_4^{2-} complex of protonated **L_4**. All the three arms of the protonated receptor (**L_4H^+**) are projected in one direction. The O-atoms of each aliphatic branch are nearly equidistant (~2.74Å) from centrally bridged N-atom, indicative of hydrogen-bonding interactions between the proton attached to central N-atom and O-atoms of each aliphatic branch. These hydrogen bonding interactions actually organizes the flexible arms in one direction. One ortho hydrogen atom of the aromatic ring attached to ethereal oxygen atom of each branch are connected to similar aromatic ring of neighboring arm through C−H···π interactions (Figure 6.2a) in a twisted edge-to-face fashion. The unidirectional arms of **L_4H^+** creates a tripodal cavity, which encapsulates DMF solvent in its centre, and the encapsulated DMF molecule is stabilized by the C−H···O hydrogen bonding interactions with two inwardly directed C=O groups of the two urea functions of **L_4H^+** (Figure 6.2b). The distance measured between the bridgehead nitrogen atom of protonated receptor (**L_4H^+**) and the nitrogen atom of the encapsulated DMF solvent is 10.53Å. The oxygen atom of the encapsulated DMF molecule is hydrogen bonded with the crystallizing water molecule which is further hydrogen bonded with a urea function of **L_4H^+** and next DMF molecule. The SO_4^{2-} anions in complex **4a** is located outside the tripodal cavity and stabilized mainly by N−H···O hydrogen bonds from the urea functions of four receptor cations. The coordination environment of the SO_4^{2-} in complex **4a** is shown in a part of Figure 6.2. The detail coordination environment of SO_4^{2-} suggests that, it is involved in side-cleft binding with four receptor cations *via* twelve hydrogen bonding interactions comprised of ten N–H···O and two C–H···O bonds having an average donor-to-acceptor distance of

3.058 Å (Table 6.2). A correlation of N–H···O angle vs. N–H···O distance shows that eight out of ten N–H hydrogen bonds are in the strong hydrogen-bonding interaction region of d(H···O) < 2.5 Å, d(N···O) < 3.2 Å and N–H···O > 140°. Apart from these hydrogen bonds with the receptor cations, the sulfate anion also forms weak C−H···O hydrogen bonds with encapsulated DMF molecule.

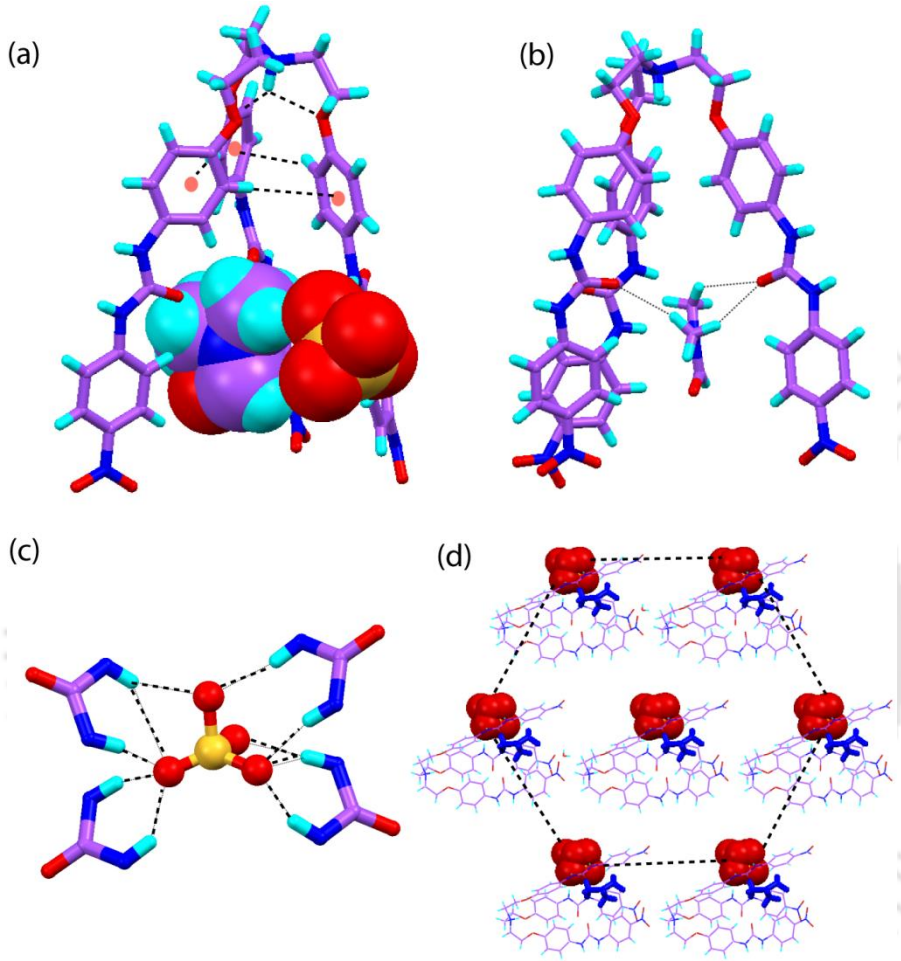

Figure 6.2 (a) X-ray structure of complex **4a**, where the receptor molecule is shown in stick model and encapsulated DMF molecule and sulfate anion is shown in spacefill model; The DMF and water molecules positioning outside the capsule are omitted for clarity of presentation; (b) Hydrogen bonding interactions between encapsulated DMF molecule with protonated receptor $\mathbf{L_4H^+}$ in complex **4a**; (c) Magnified view showing coordination of SO_4^{2-} with the 8 –NH groups in complex **4a**; (d) Crystal packing in complex 4a, as viewed down the crystallographic a axis. Sulfate anion is shown in spacefill model and encapsulated DMF molecule is shown in bold stick model (blue).

6.3.2 Structural description of complex 4b

After several attempts we were able to isolate single crystals for $\mathbf{L_4}$ with $TBAHSO_4$. Complex **4b** crystallized in a triclinic crystal system with the *P-1* space group. Single crystals of complex **4b** were grown from acetone solvent with moderate yield upon very slow evaporation of a solution of $\mathbf{L_4}$ in the presence of excess $TBAHSO_4$. The asymmetric

unit of complex **4b** has a distorted C_{3v} symmetric cavity, which is evident from the difference in basal N···N distances of nitro groups (N4···N7=17.17Å, N7···N10=10.63Å, and N10···N4= 9.58Å). Close inspection of the crystal structure of the complex **4b** reveals the receptor is protonated. Along with three crystallizing water molecules, the asymmetric unit of complex **4b** contains one protonated receptor $\mathbf{L_4H^+}$, one SO_4^{2-} anion and one TBA counter cation to balance the overall charge. The solution-state deprotonation of HSO_4^- can be explained by the formation of multiple hydrogen-bonding interactions with neutral receptor $\mathbf{L_4}$. Consequently the pK_a of the bound HSO_4^- is lowered and it is deprotonated by bridgehead nitrogen atom of the receptor molecule $\mathbf{L_4}$, which in turn becomes protonated. To the best of our knowledge, crystallographic evidence for proton transfer phenomena from hydrogenated anion to receptor is not reported. Although, solution-state deprotonation of the protonated state of an anion *viz*. $H_2PO_4^-$, HCO_3^- and HSO_4^- and subsequent formation of complex with deprotonated anion in solid state is not uncommon.[2d-f] As similar to complex **4b** here also all the three arms of $\mathbf{L_4H^+}$ are projected in one direction and each ethereal O-atom of a $\mathbf{L_4H^+}$ unit is hydrogen bonded to the proton attached to the bridgehead N-atom that actually arranges the flexible arms in one direction. The unidirectional tripodal arms of $\mathbf{L_4H^+}$ create a distorted C_{3v} symmetric tripodal cavity, which encapsulate fully TBA cation and partially the SO_4^{2-} anion as a contact ion-pair in its centre (Figure 6.3a). The encapsulated TBA cation is stabilized by C−H···π, C−H···O and cation···π interactions with the phenyl rings and the urea functions of two side arms of the protonated tripodal receptor $\mathbf{L_4H^+}$ (Annexure 6). The distance measured between the bridgehead nitrogen atoms of $\mathbf{L_4H^+}$ and the TBA counter cation is 11.616Å. The detail coordination environment of SO_4^{2-} suggests it is stabilized by 14 hydrogen bonds involving seven N−H···O (three urea functions) two O−H···O (lattice water molecules) two C−H···O (aryl –CH of nitrophenyl ring) and three C−H···O (TBA cation) (Figure 6.3b and 6.3c). Moreover, the detail analysis of the hydrogen-bond parameters, especially the N–H···O angle vs. H···O distances, reveal that in the strong hydrogen bonding interaction region of dN···O ≤ 3.2 Å there are eight contacts. The detailed hydrogen-bonding parameters are given in the Table 6.2.

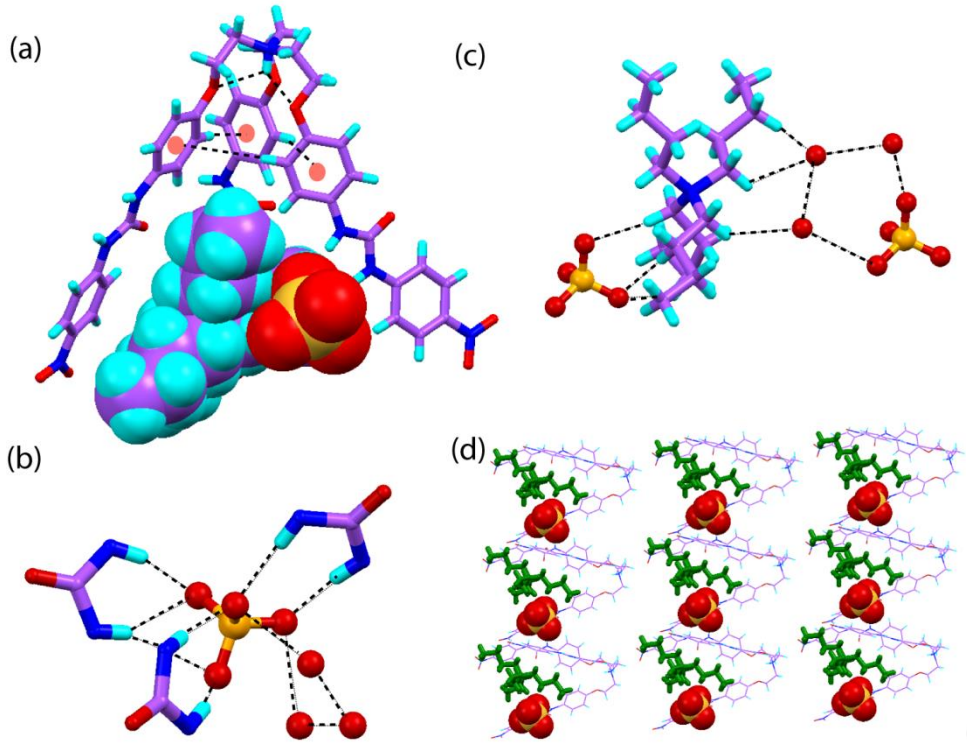

Figure 6.3 (a) X-ray structure of complex **4b**, where the receptor molecule is shown in stick model and recognized TBA cation sulfate anion is shown in spacefill model; (b) Hydrogen bonding interactions of the sulfate anion with the urea functions of three receptor cations and with crystallizing water molecules; (c) Showing presence of both contact ion-pair and solvent separated ion-pair interactions between TBA cation and sulfate anion in complex **4b**; (d) Crystal packing in complex **4b**, as viewed down the crystallographic *c* axis. Sulfate anion shown in spacefill model and encapsulated TBA cation shown in bold stick model (dark green color).

6.3.3 Structural description of complex 4c

Reaction of K_2HPO4 with $\mathbf{L_4}$ in 2:1 DMSO-H_2O binary mixture afforded the complex **4c**, as determined by X-ray diffraction. Complex **4c** crystallizes in the trigonal system with centrosymmetric space group *P-3₁c* (Table 6.1). A symmetric molecular structure of complex **4c** is shown in figure 6.4a. The crystal structure of **4c** shows the two potassium cations (K_1^+ and K_2^+) are present in different environments. The K_1^+ is encapsulated by two receptor molecules, where two same symmetric receptor molecules flipped inward toward each other in a face-to-face fashion (dN1···N1´ = 5.794 Å) and each receptor coordinating the K_1^+ *via* three ethereal oxygen atoms and bridgehead nitrogen atom with O···K_1^+ and N···K_1^+ distances 2.962Å and 2.899Å respectively (Figure 6.4b). The two receptors in this capsular assembly are assembled by weak π···π interactions of phenyl rings (C1g···C1´g = 3.579 Å) attached to the ethereal oxygen atoms. Whereas, K_2^+ is coordinated with oxygen atoms of urea function and five water molecules (disordered). Two out of five water molecules are further coordinated to next similar potassium cations and eventually forms C_3 symmtric $[K_6(H_2O)_5]^{6+}$ cluster (Figure 6.4a). Notably the receptor not recognizing the K_2^+ in

convincing fashion, therefore, the presence of K_2^+ in the crystal lattice of complex **4c** is only due to balance of the overall charge of the complex. The K_1^+ encapsulated dimeric capsular

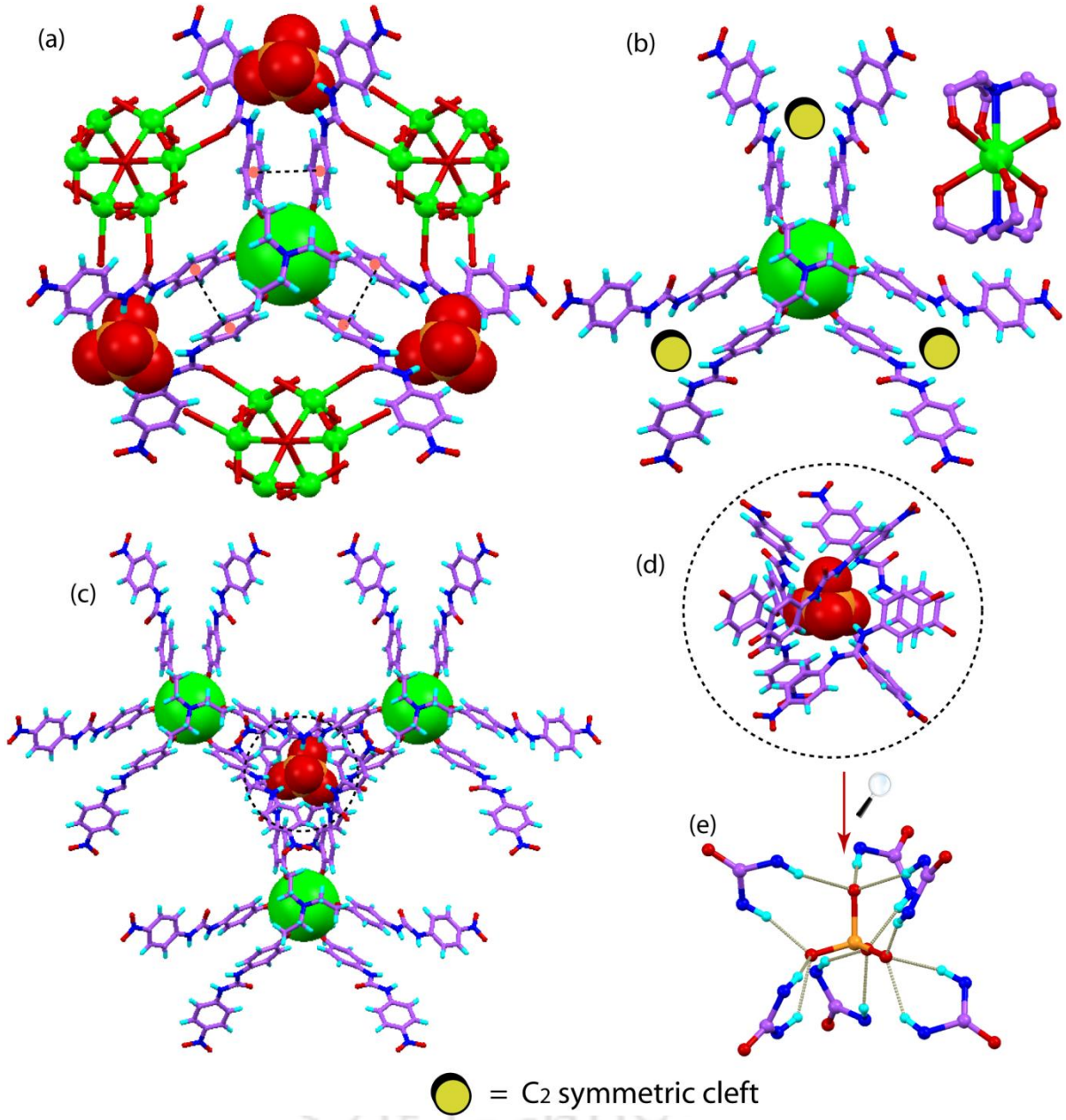

Figure 6.4 (a) A C_{3v} Symmetric X-ray structure of complex **4c**, where two receptor molecules are shown in stick, mono-hydrogen phosphate anion and encapsulated potassium cation shown in space fill model and the potassium cation bind to oxygen atom of urea function is shown as ball and stick model; (b) Showing encapsulation of K_1^+ within a dimeric capsular assembly of two symmetry-identical molecules of $\mathbf{L_4}$ and generation of three C_2 symmetric clefts, Inset shows the coordination mode of encapsulated potassium cation with two receptor molecules; (c) Showing three nearby K_1^+ encapsulated dimeric capsular assemblies interdigitate to form a precise cavity to encapsulate HPO_4^{2-} anion; (d) Encapsulation of hydrogen phosphate anion by six urea functions; (e) Magnified view showing coordination 12−hydrongen-bonding interactions between six urea functions and hydrogen phosphate anion.

assembly of the receptor forms three C_2-symmetric clefts (Figure 6.4b). Three such clefts of three nearby K_1^+ encapsulated dimeric capsular complexes are aligned in such a way to create an anion specific microcavity that further encapsulates a HPO_4^{2-} anion in its center *via* hydrogen bonding participation of six urea functions (Figure 6.4c), which eventually leads to the formation of 2D polymeric structure (Annexure 6). Notably, the hydrogenphosphate anion is disordered over two positions, with the eight half occupied O atoms, and due to disorder, it was not possible to locate the hydrogen atom on phosphate anion. Interestingly, all the six urea arms within a capsule participate in hydrogen bonding with the encapsulated hydrogenphosphate ion (Figure 6.4d). There are total of twelve hydrogen bonding interactions between six urea functions of **L_4** moieties and four O atoms of one HPO_4^{2-} ion. Each oxygen atom of hydrogenphosphate anion behaves as a trifurcated hydrogen bond acceptor and each NH group donates one N–H···O bond, resulting in twelve hydrogen bonds with an average donor-to-acceptor distance of 2.811 Å (Table 6.2). Moreover, several weaker interactions involving aryl –CH protons could be added to the encapsulated HPO_4^{2-} anion when the donor-to-acceptor distance is limited to <3.5 Å for hydrogen-bonding, which provide additional stability for hydrogenphosphate binding. As the urea functions of the K_1^+ encapsulated dimeric capsular assembly of the receptor forms strong hydrogen bonding interactions with hydrogenphosphate anion therefore, the formation of capsular assembly of the tripodal receptor **L_4** is not solely due to potassium cation coordination, rather than it is a combined coordination effect of potassium cation (encapsulated) and hydrogen phosphate anion. Thus, the receptor **L_4** forms ion-pair induced capsular assembly. It is important to mention here that efforts were also made to crystallize sulfate and phosphate complexes of other alkali metals, but in spite of several attempts we were unable to crystallize.

The ideal binding mode for tetrahedral oxyanion (sulfate and phosphate) is encapsulation of the anion *via* 12 optimally arranged binding sites.[1a,3b,5] The detail crystallographic analysis of complexes (**4a**, **4b** and **4c**) show that the metal free receptor (in case of complex **4a** and **4b**) is not able to provide ideal binding site for these tetrahedral oxyanions (Figure 6.5). Whereas in case of complex **4c** the K_1^+ coordinated preorganized receptor provides almost ideal binding site for tetrahedral oxyanion through assembly process. Therefore, from structural analysis it can be predicted, that in solution the metal (K^+) coordinated preorganized receptor may render enhance anion binding property compare to metal free receptor.

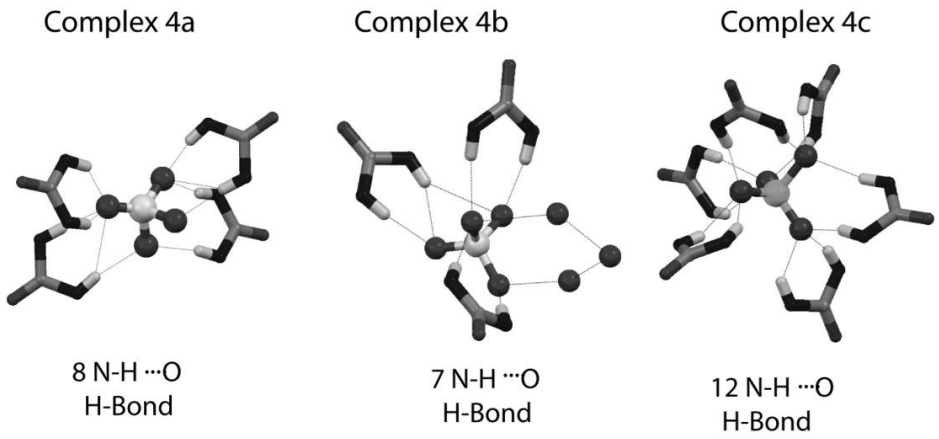

Figure 6.5 Comparison of hydrogen bonding interactions in the complexes (**4a**, **4b** and **4c**).

6.4 Solution-state ^{1}H NMR binding studies

Receptor $\mathbf{L_4}$ was intentionally designed to simultaneously bind cations and anions such that the presence of co-bound alkali metal cations (Li^+, Na^+ and K^+) would enhance the strength of anion binding *via* favorable cooperative electrostatic interactions and/or preorganisation effects. Titration experiments of $\mathbf{L_4}$ with hydrogensulfate and di-hydrogenphosphate anions were conducted both in the absence and presence of lithium, sodium and potassium cations, added as their perchlorate salts, because perchlorate is a bulky anion with a lower charge density and does not interfere with the binding of other strong hydrogen bond acceptor anions. Whereas, in these titration experiments the anions were added as their TBAX salts (X= HSO_4^- and $H_2PO_4^-$), in which tetrabutylammonium (TBA) is a bulky non-coordinating or weakly-coordinating cation. The anion and alkali metal ion induce anion coordination properties of $\mathbf{L_4}$ in solution were investigated by ^{1}H NMR titration experiments in 98:2 DMSO-d_6–D_2O binary solvent mixtures.

The addition of perchlorate salts of alkali metal cations (Li^+, Na^+ and K^+) to the receptor $\mathbf{L_4}$ caused small but significant upfield perturbations of aliphatic–CH protons in the individual ^{1}H NMR-spectra. Unfortunately, accurate binding constant values for these cations could not be obtained from these small and inconsistent changes.

It is important to note that while evaluating the cation cooperative anion binding of a particular ditopic receptor, the presence of cation equivalents with respect to receptor during titration experiments with anions is vital, because presence of excess metal ions may lead to ion-pairing outside of the receptor, which eventually lead to significant amount of error during binding constant calculation. Taking this into account the coordination mode of the receptor $\mathbf{L_4}$ with sodium and lithium cation was confirmed from ESI mass spectroscopic analysis. Electrospray mass spectrometry (ESIMS) experiments confirm that the receptor forms 1:1 complex with both Na^+ and Li^+ cation (Annexure 6). While, in case of K^+

Electrospray mass spectrometry (ESIMS) experiment reveals the formation of both 1:1 and 2:1 L/K^+ complex in solution. Significantly, the solid state crystal structure of complex **4c** shows 2:1 binding for large K^+ cation. This binding discrepancy is due to larger size and higher coordination number of K^+ compared to sodium and lithium cation. Notably, this type of binding discrepancy for alkali metal cations for ion-pair receptors is previously known in literature.[6]

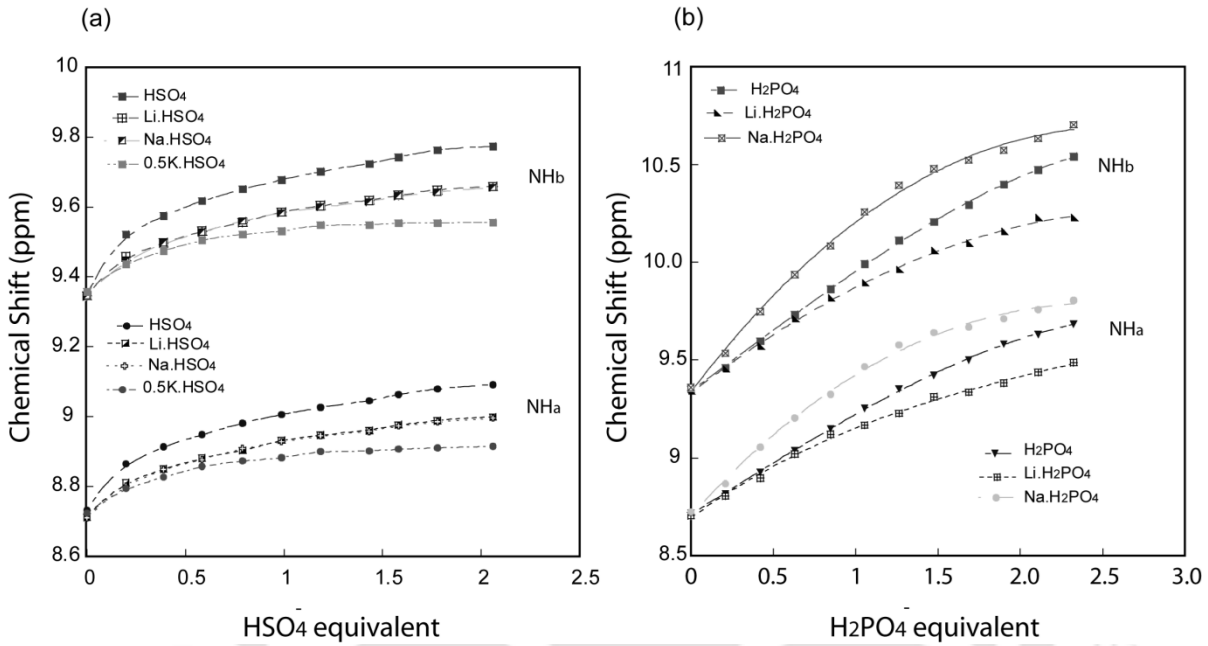

Figure 6.6 (a) Changes in chemical shift for urea protons of $\mathbf{L_4}$ during ^{1}H NMR titration for $\mathbf{L_4}$, $\mathbf{L_4}\cdot Li^+$, $\mathbf{L_4}\cdot Na^+$ and $\mathbf{L_4}\cdot 0.5K^+$ upon gradual addition of hydrogensufate anion in 98:2 DMSO-d_6–D_2O at 298K; (b) Changes in chemical shift for urea protons of $\mathbf{L_4}$ during ^{1}H NMR titration for $\mathbf{L_4}$ and $\mathbf{L_4}\cdot Li^+$, $\mathbf{L_4}\cdot Na^+$, upon gradual addition of hydrogensufate anion in 98:2 DMSO-d_6–D_2O at 298K.

The stability constant values for anion binding in the presence and absence of alkali metal cations (1eq Li^+, 1eq Na^+, 0.5eq K^+ and 1eq K^+) were determined by EQNMR[7] analysis (Annexure 6) of the titration curves, monitoring the downfield shifts of urea protons of the receptor $\mathbf{L_4}$.

^{1}H NMR titration of $\mathbf{L_4}$ with tetrahedral oxyanions (hydrogensulfate and di-hydrogenphosphate) demonstrated that it binds anions with modest stability constant values and stronger association occurs with HSO_4^- (K=170M^{-1}) compared to $H_2PO_4^-$ (K=24 M^{-1}). Titrations of $\mathbf{L_4}\cdot Li^+$ with HSO_4^- and $H_2PO_4^-$ gave same trend, compared to the metal-free system, but gave 1.31 and 2.75 fold increases in association constants for HSO_4^- and $H_2PO_4^-$, respectively. Although, the $\mathbf{L_4}\cdot Na^+$ complex trended likewise with the $\mathbf{L_4}\cdot Li^+$ complex, but notably anion binding affinities increased 2 and 12 fold in comparison to the metal free receptor (Table 6.3). The enhancement in HSO_4^- and $H_2PO_4^-$ binding

demonstrates the ability of Li^+ and Na^+ metals to cooperatively affect anion binding of the receptor **L_4** (Figure 6.6). The coordination of M^+ (Li^+ and Na^+) with three ethereal oxygen atoms and the bridgehead nitrogen atom of the receptor generate a suitable anion binding tris-urea cavity, as illustrated in Scheme 6.2.

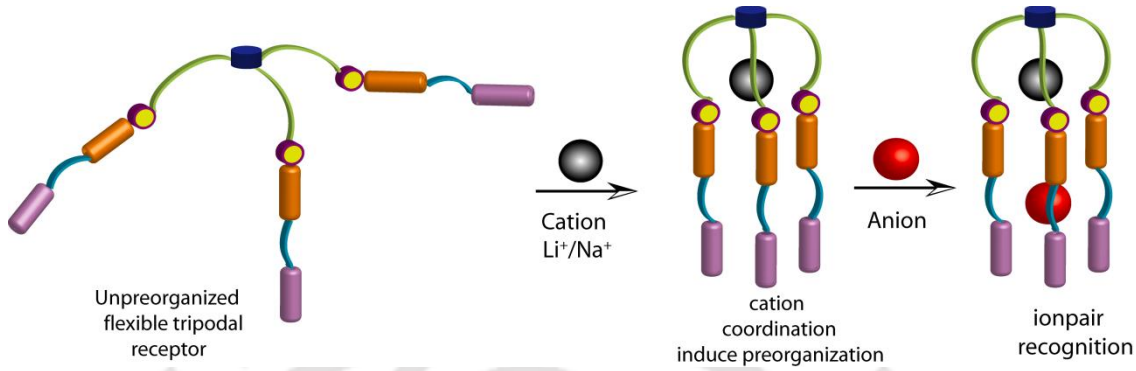

Scheme 6.2 Schematic representation of sodium or lithium cation induces preorganization of the receptor for anion recognition.

Table 6.3 Association constants, $K(M^{-1})$, of **L_4** with HSO_4^- and $H_2PO_4^-$ (added as the tetrabutylammonium salts) in the absence and presence of 1eq Li^+, 1 eq Na^+, 0.5 eq K^+ and 1eq K^+cation (added as the perchlorate salt) in DMSO-d_6 at 298 K. All association constants are calculated using WinEQNMR2, and associated errors are <15%

	HSO_4^-	$H_2PO_4^-$
L_4	170	24
L_4+Li^+	224	66
L_4+Na^+	338	269
L_4+ 0.5 K^+	4074	−a
L_4+ 0.5 K^+	11	14

[a] New peaks due to deprotonation of bound $H_2PO_4^-$ and subsequent binding of HPO_4^{2-}.

It is noteworthy that the receptor **L_4** in presence of 0.5eq of K^+ results in dramatic enhancement (~24 fold) of association constant for HSO_4^-, which is well consistent with our prediction from solid state structure. The association with $H_2PO_4^-$ could not be accurately determined due to the appearance of new peak during titration experiments (Figure 6.7).[3d] The generation of new peak is due to strong multipile hydrogen bonding interactions between K^+ coordinated preorganized receptor and $H_2PO_4^-$ anion, which indeed lower the pKa of the bound $H_2PO_4^-$ to the extent that it probably undergoes deprotonation and form HPO_4^{2-} complex (Figure 6.7).[3d-f] The generation of new peak during $H_2PO_4^-$ titration experiment with **L_4**·0.5K^+ further suggest that K^+ coordination induced preorganized receptor binds $H_2PO_4^-$ strongly compared to metal free receptor and Li^+/Na^+ coordinated

preorganized receptor, where no new peaks was found during titration experiments with $H_2PO_4^-$ anion.

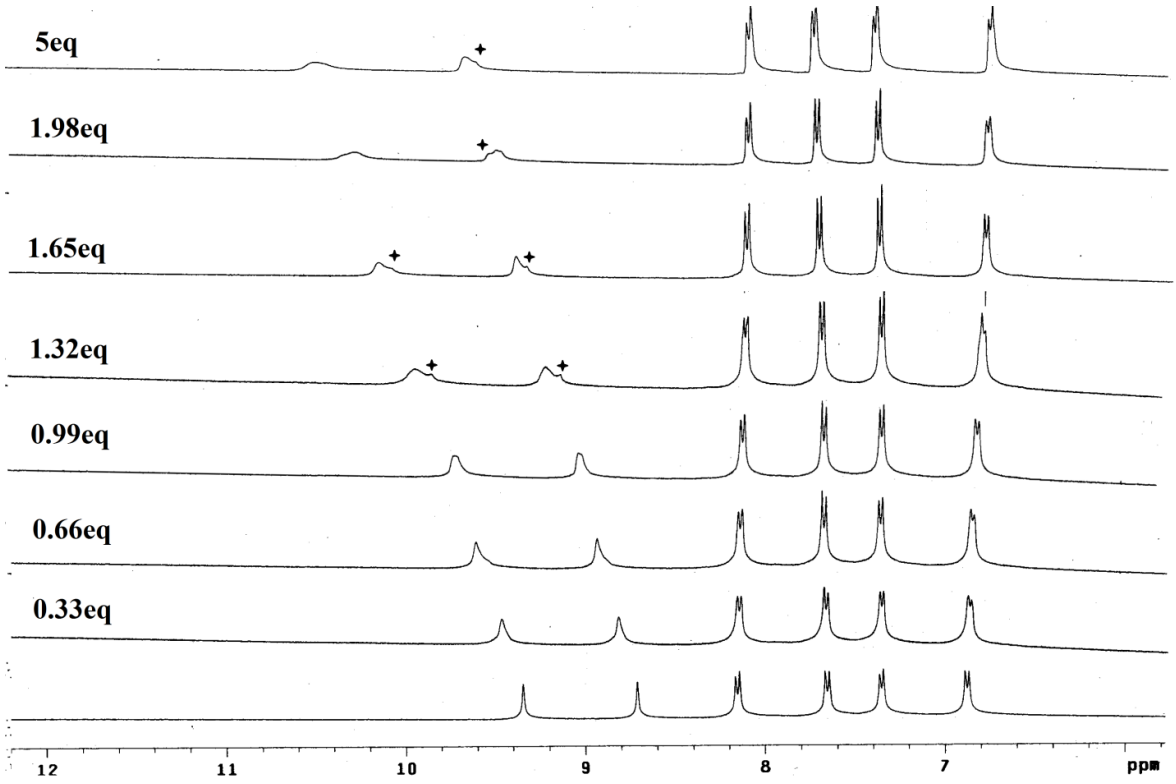

Figure 6.7 Stack plot of the ^{1}H NMR spectra of receptor $0.5K^+ \cdot \mathbf{L_4}$ in the presence of increasing amounts of $[TBA]H_2PO_4$ recorded in 98:2 DMSO-d_6:D_2O at 298 K. The asterisk sigh shows the generation of new peak.

We have also carried out the ^{1}H NMR titration experiments of $\mathbf{L_4}$ with both HSO_4^- and $H_2PO_4^-$ in presence of one equivalent K^+. The titration experiments show minimal downfield shift of urea NH protons in both the occasions and the subsequent calculation of binding constant values suggest that the presence of one equivalent K^+ decreases the anion (HSO_4^- and $H_2PO_4^-$) binding strength of the receptor $\mathbf{L_4}$ (Table 6.3). This is due to the formation of weakly bound 1:1 receptor–K^+ complex, which allows ion-pairing outside of the receptor that actually prevents the anions (HSO_4^- and $H_2PO_4^-$) to interact directly with the receptor $\mathbf{L_4}$. Moreover, potassium cation selective significant enhancement of binding is due to 2:1 receptor K^+ cation complex formation which generates precise binding pocket for tetrahedral oxyanions (hydrogensulfate and di-hydrogenphophate/hydrogenphosphate) that actually stabilizes the anion *via* fulfilling its optimal hydrogen bonding coordination, as observed in the crystal structure of complex **4c**.

6.5 Conclusion

A new C_{3v} symmetric flexible N bridgehead heteroditopic tripodal urea receptor **L_4** contains both cation and anion binding sites, capable of recognizing both anions and ion-pairs through respective binding modes of tripodal unit, has been prepared and characterized. ^{1}H NMR spectroscopic studies revealed that the free receptor **L_4** moderately and weakly binds the hydrogensulfate and di-hydrogenphosphate anions respectively. In presence of the Group I metal ions such as Li^+(1 eq), Na^+(1eq) and K^+ (0.5eq) the receptor **L_4** shows remarkable enhancement of binding property with hydrogensulfate and di-hydrogenphosphate anions compared to metal free receptor, reiterating the ditopic nature of this receptor. Whereas, interestingly the receptor (**L_4**) in presence of one equivalent K^+ shows negative cooperative binding with both the HSO_4^- and $H_2PO_4^-$ anions. This is due to the formation of weakly bound 1:1 receptor–K^+ complex, which allows ion-pairing outside of the receptor. In general the anion (HSO_4^- and $H_2PO_4^-$) binding property of **L_4** greatly depends on nature and stoichiometry of metal ion used (where M = Li^+, Na^+ and K^+). The significant enhancement of HSO_4^- binding with **L_4** in presence of 0.5eq of K^+ is due to is due to 2:1 receptor K^+ complex formation which possibly generates exact binding pockets for tetrahedral oxyanions. The crystal structure analysis of the ion-pair complexes of **L_4** demonstrate that, in case of complex **4b** one TBA cation and a sulfate anion is encapsulated as a contact ion-pair in the distorted C_{3v} symmetric tripodal cavity of the protonated receptor. While for complex **4c** the receptor forms highly symmetric charge separated ion-pair complex with potassium cation and hydrogen phosphate anion *via* formation of dimeric capsular assembly of the receptor, where three C_2 clefts of K^+ encapsulated dimeric capsular assemblies interdigitate to form a microcavity that further encapsulates the hydrogen phosphate anion *via* hydrogen bonding interactions with six urea groups, and subsequently generates 2D polymeric assembly of capsular complexes. Our findings could motivate researcher to develop new generation tripodal receptors for recognition of ion-pairs.

Table 6.1 Crystallographic parameters and refinement details of receptor $\mathbf{L_4}$ and its complexes **4a**, **4b** and **4c.**

Parameters	$\mathbf{L_4 \cdot 2DMF \cdot H_2O}$	**4a**	**4b**	**4c**
Formula	$C_{51}\,H_{58}\,N_{12}\,O_{15}$	$C_{102}\,H_{118}\,N_{24}\,O_{34}\,S$	$C_{61}\,H_{79}\,N_{11}\,O_{19}\,S$	$C_{90}\,H_{84}\,K_2\,N_{20}\,O_{51}\,P$
Fw	1079.09	2256.27	1302.42	2369.36
Cry. system	Triclinic	Triclinic	Triclinic	Trigonal
Space group	*P*-1	*P*-1	*P*-1	*P-31c*
a/Å	12.8085(4)	11.4144(6)	11.3397(10)	17.3549(9)
b/Å	15.4038(5)	16.9099(11)	18.6819(17)	17.3549(9)
c/Å	28.8727(12)	17.2091(11)	18.7690(16)	22.6324(12)
α/^{o}	84.217(3)	115.692(7)	103.700(3)	90.00
β/^{o}	82.467(3)	100.539(5)	106.612(3)	90.00
γ/^{o}	87.202(3)	98.828(5)	98.493(3)	120.00
V/Å^3	5615.0(3)	2839.4(3)	3601.4(6)	5903.4(5)
Z	4	1	2	2
D_c/g cm^{-3}	1.276	1.319	1.201	1.334
μ (mm^{-1})	0.096	0.118	0.118	0.192
T/^{o}K	298(2)	298(2)	298(2)	298(2)
Total reflns	52642	23096	27840	16209
Ind. reflns	28571	14395	17883	5125
Obs. reflns	18021	6871	8201	2213
Parameters	1465	760	827	244
R1; wR2 (I > 2σ(I))	0.0762, 0.2479	0.0838, 0.3383	0.0880, 0.2755	0.0966,2740
R(int)	0.0386	0.0278	0.2158	0.0992
GOF (F^2)	0.934	1.052	1.067	1.034

Table 6.2 Hydrogen bonding contacts on anions with receptor $\mathbf{L_4}$ in complexes **4a-4c.**

Species	D–H···A	*D*(H···A)/Å	*d*(D···A)/Å	∠D–H···A/°
$\mathbf{L_4}$	N3H···O1	2.313	3.016(9)	139.0(3)
	N13H···O25	1.96	2.790(1)	161.5(8)
	N18H···O28	2.10	2.870(2)	156.9(1)
	N19H···O28	2.10	2.880(2)	159.9(1)
	N8H···O30	2.09	2.900(1)	157.0(8)
	N9H···O30	1.90	2.860(1)	163.1(2)
	N15H···O29	2.17	2.990(1)	159.2(7)
	N16H···O29	2.12	2.950(1)	161.2(7)
	N3H···O26	1.90	2.810(2)	161.1(2)
	N2H···O26	2.00	2.880(2)	158.1(2)
	N5H···O27	1.90	2.840(2)	155.5(1)
	O30H(W)···N11	2.10	2.890(1)	163.1(2)
	O30H(W)···O2	1.84	2.720(1)	144.2(1)
	O29H(W)···N11	2.10(3)	2.890(2)	139.3(2)
	O29H(W)···O14	2.30	3.060(2)	138.3(7)
4a	N2H···O14	2.06	2.829(9)	148.6(3)
	N3H···O14	2.03	2.757(9)	141.6(3)
	N9H···O14	2.12	2.918(7)	153.2(3)
	N8H···O14	2.68	3.410(1)	143.8(3)
	N9H···O13	2.03	2.875(8)	164.6(3)
	N8H···O15	2.04	2.847(9)	155.6(3)
	N2H···O15	2.11	2.965(9)	167.6(3)
	N9H···O15	2.55	3.234(8)	136.8(3)
	N8H···O16	2.12	2.926(5)	154.2(3)
	N3H···O16	2.06	2.914(6)	170.4(3)
4b	N9-H···O13	2.05	2.875(8)	158.7(3)

	N3H···O13	2.69	3.454(6)	147.6(3)
	N5H···O14	2.08	2.935(4)	168.9(3)
	N6H···O15	2.08	2.912(4)	162.6(3)
	N8H···O15	2.06	2.897(6)	163.2(2)
	N2H···O16	1.97	2.805(7)	161.5(3)
	N3H···O16	2.24	3.027(7)	151.5(3)
4c	N3H···O5	2.11	2.955(5)	165.6(4)
	N2H···O6	1.93	2.766(6)	165.3(4)
	N2H···O6	1.93	2.739(9)	154.6(4)
	N3H···O6	2.07	2.770(6)	138.0(4)

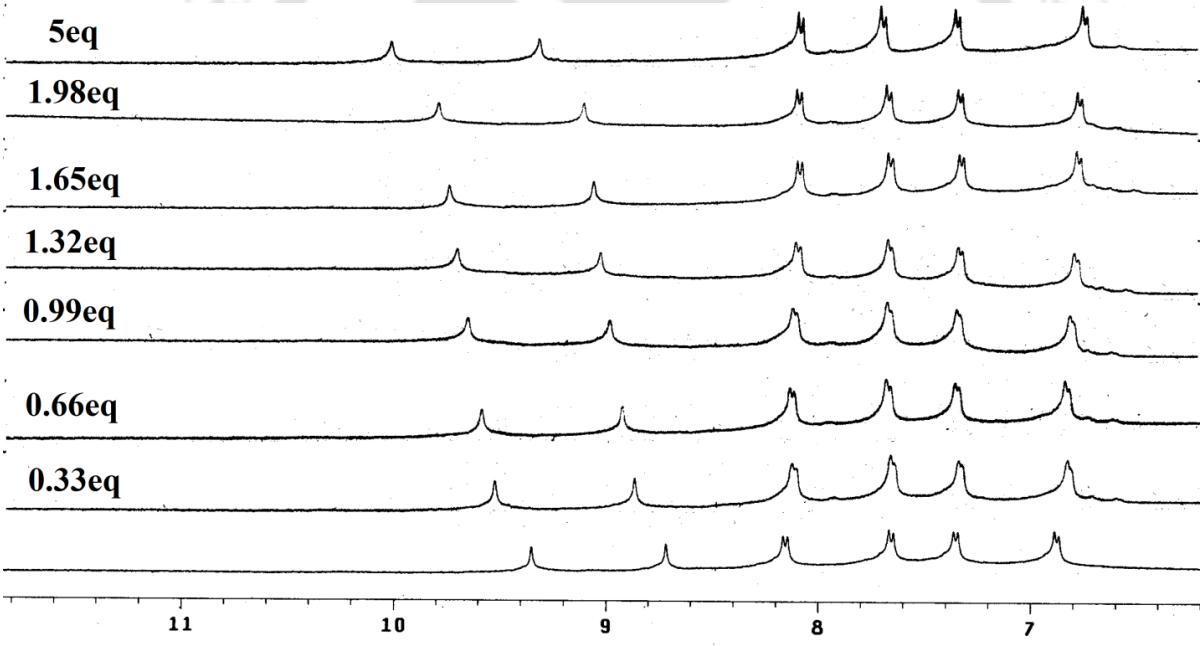

Figure 6.8 Stack plot of the ^{1}H NMR spectra of receptor **L_4** in the presence of increasing amounts of $[n\text{-}Bu_4N^+]HSO_4^-$ recorded in 98:2 DMSO-d_6–D_2O at 298 K.

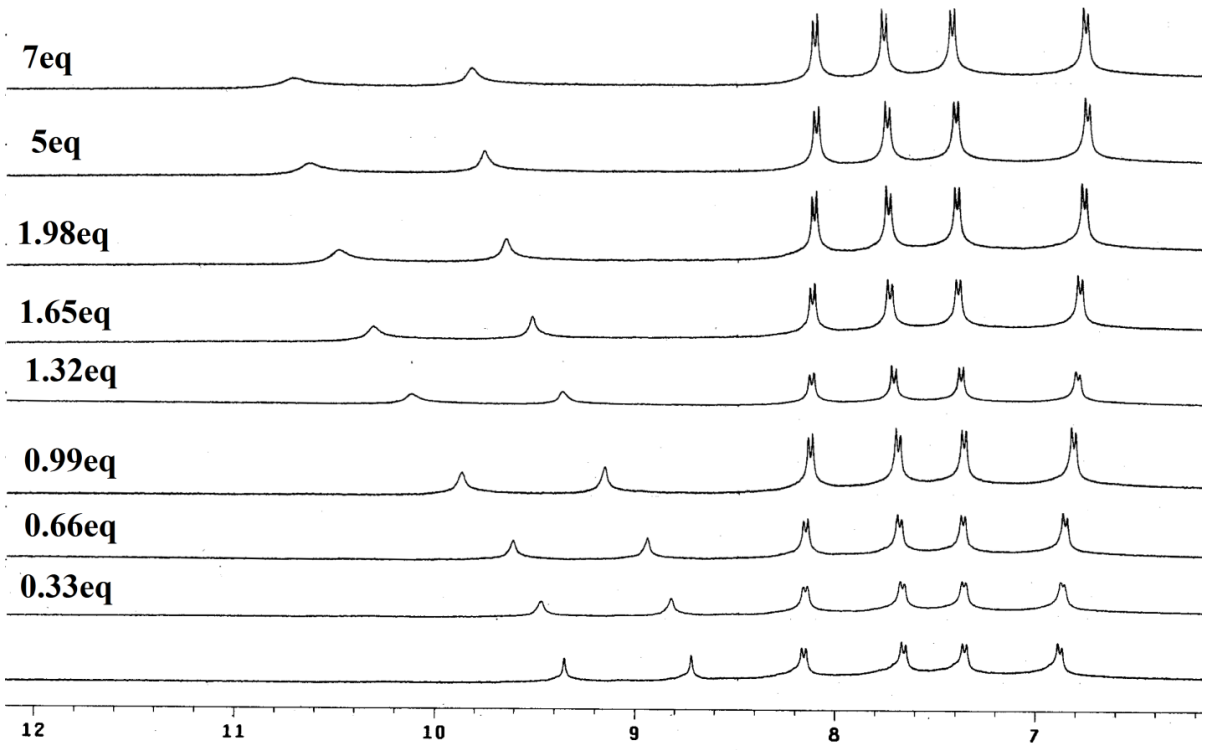

Figure 6.9 Stack plot of the ^{1}H NMR spectra of receptor **L$_4$** in the presence of increasing amounts of [n-Bu$_4$N$^+$]H$_2$PO$_4^-$ recorded in 98:2 DMSO-d$_6$–D$_2$O at 298 K.

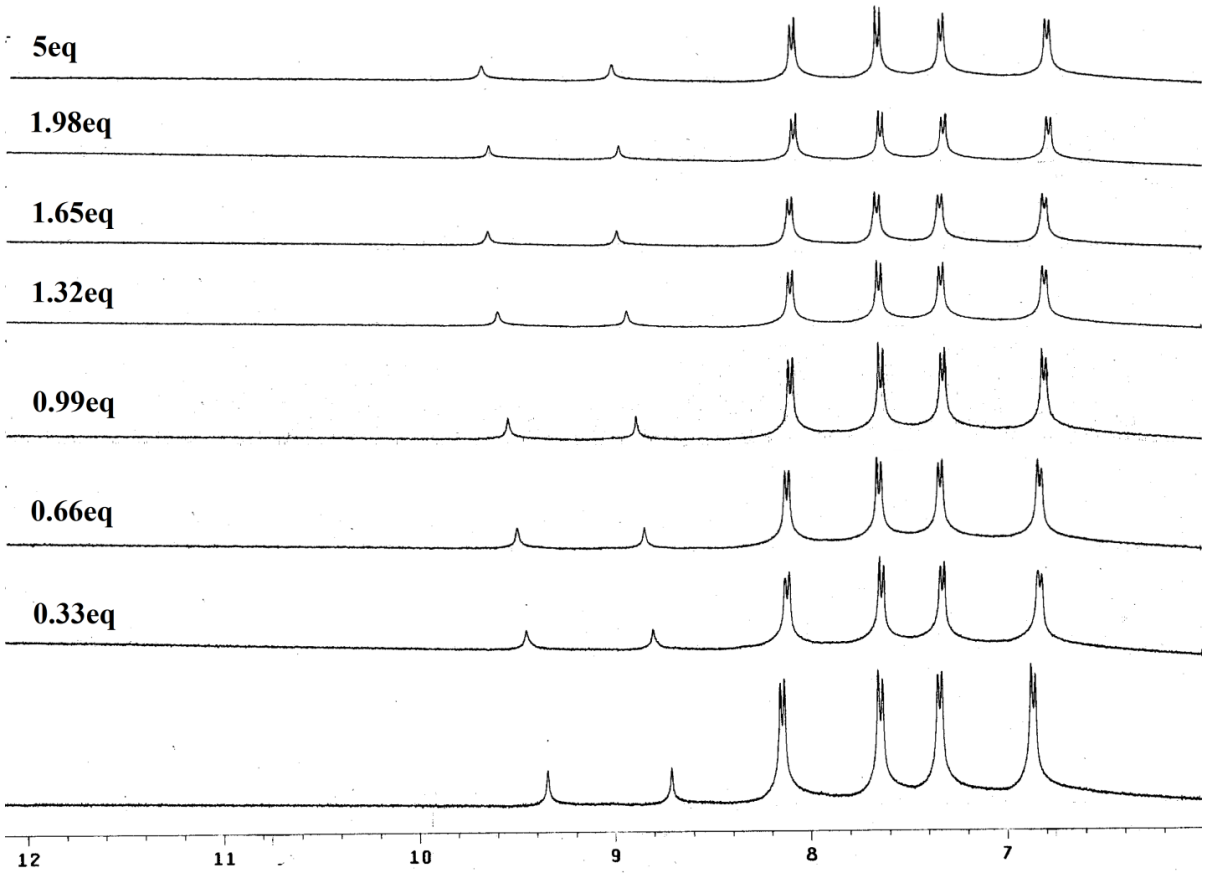

Figure 6.10 Stack plot of the ^{1}H NMR spectra of receptor Li$^+$·**L$_4$** in the presence of increasing amounts of [n-Bu$_4$N$^+$]HSO$_4^-$ recorded in 98:2 DMSO-d$_6$–D$_2$O at 298 K.

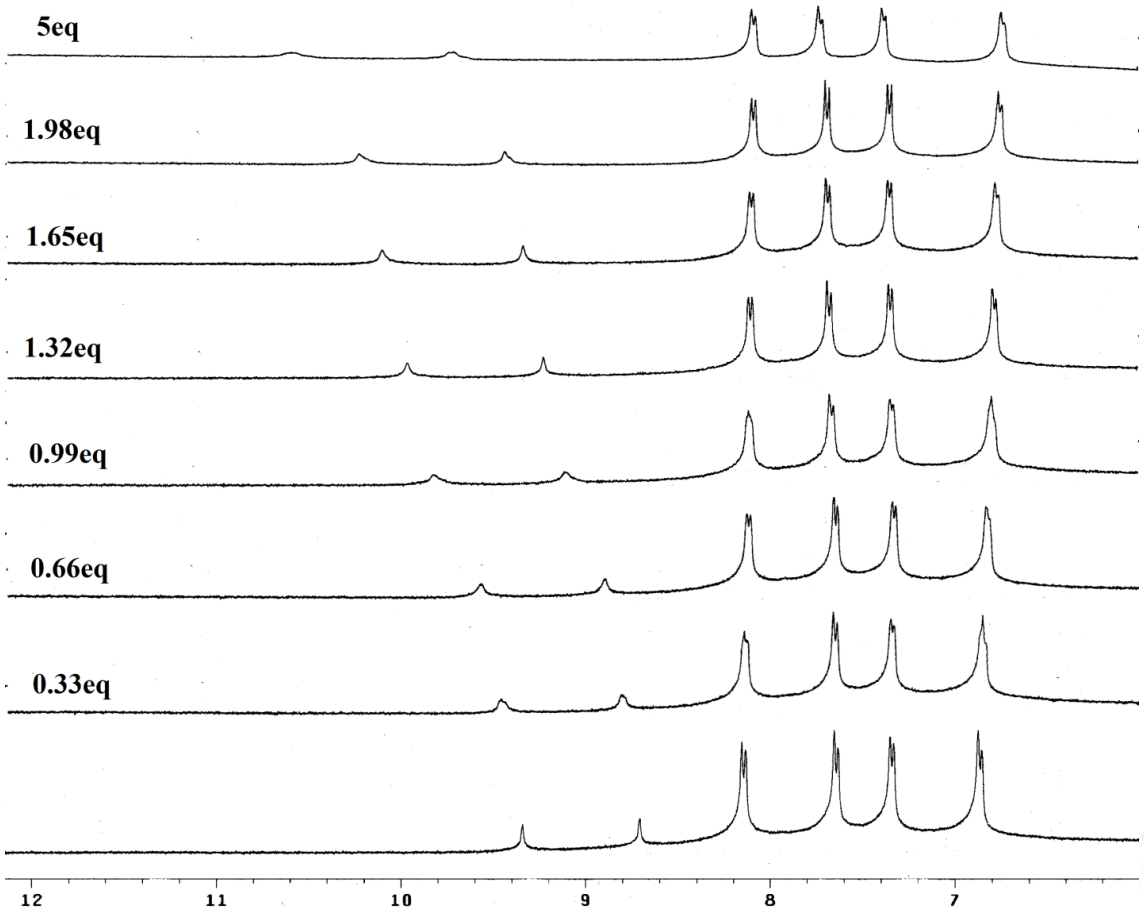

Figure 6.11 Stack plot of the ^{1}H NMR spectra of receptor $Li^{+}\cdot\mathbf{L_4}$ in the presence of increasing amounts of $[n\text{-}Bu_4N^{+}]H_2PO_4^{-}$ recorded in 98:2 DMSO-d_6–D_2O at 298 K.

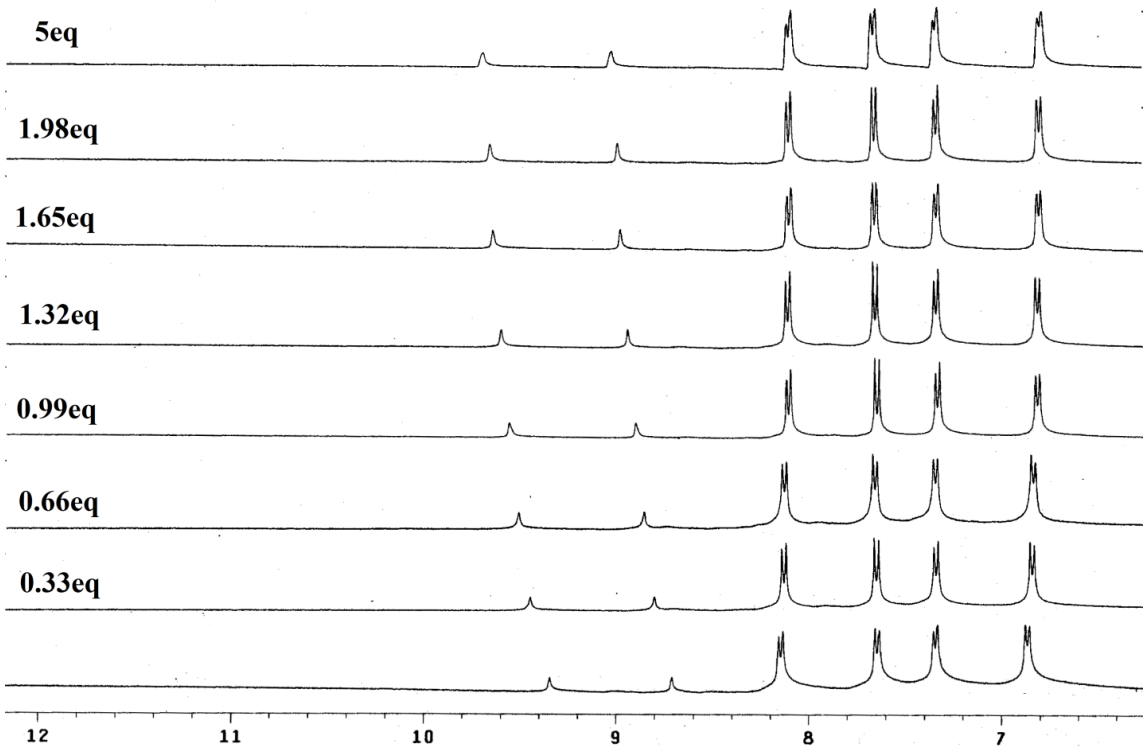

Figure 6.12 Stack plot of the ^{1}H NMR spectra of receptor $Na^{+}\cdot\mathbf{L_4}$ in the presence of increasing amounts of $[n\text{-}Bu_4N^{+}]HSO_4^{-}$ recorded in 98:2 DMSO-d_6–D_2O at 298 K.

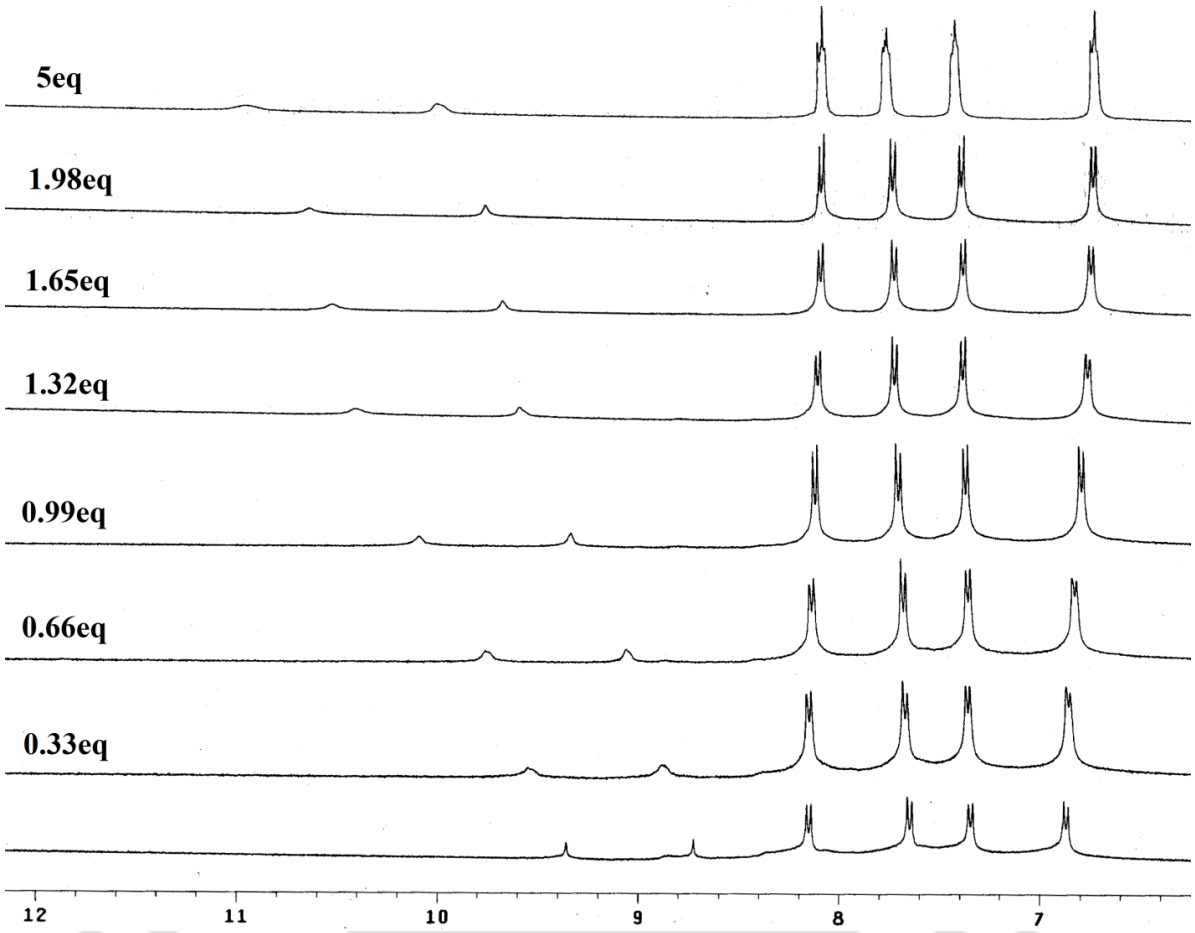

Figure 6.13 Stack plot of the ^{1}HNMR spectra of receptor $Na^{+}\cdot\mathbf{L_4}$ in the presence of increasing amounts of $[n\text{-}Bu_4N^{+}]H_2PO_4^{-}$ recorded in 98:2 DMSO-d_6–D_2O at 298 K.

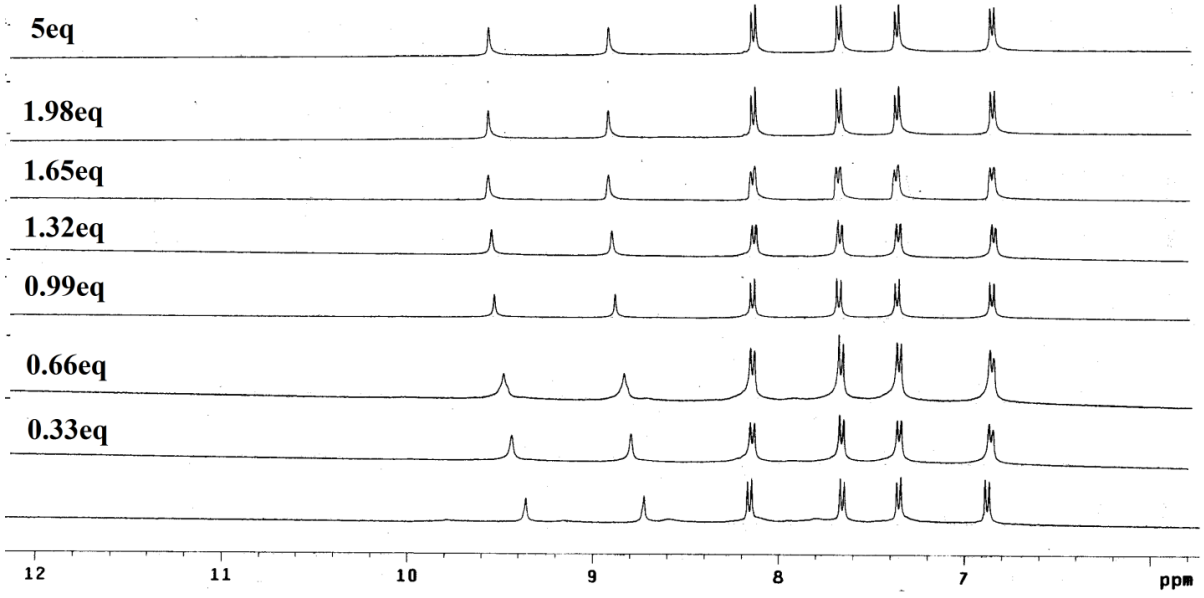

Figure 6.14 Stack plot of the ^{1}H NMR spectra of receptor $0.5K^{+}\cdot\mathbf{L_4}$ in the presence of increasing amounts of $[n\text{-}Bu_4N^{+}]HSO_4^{-}$ recorded in 98:2 DMSO-d_6–D_2O at 298 K.

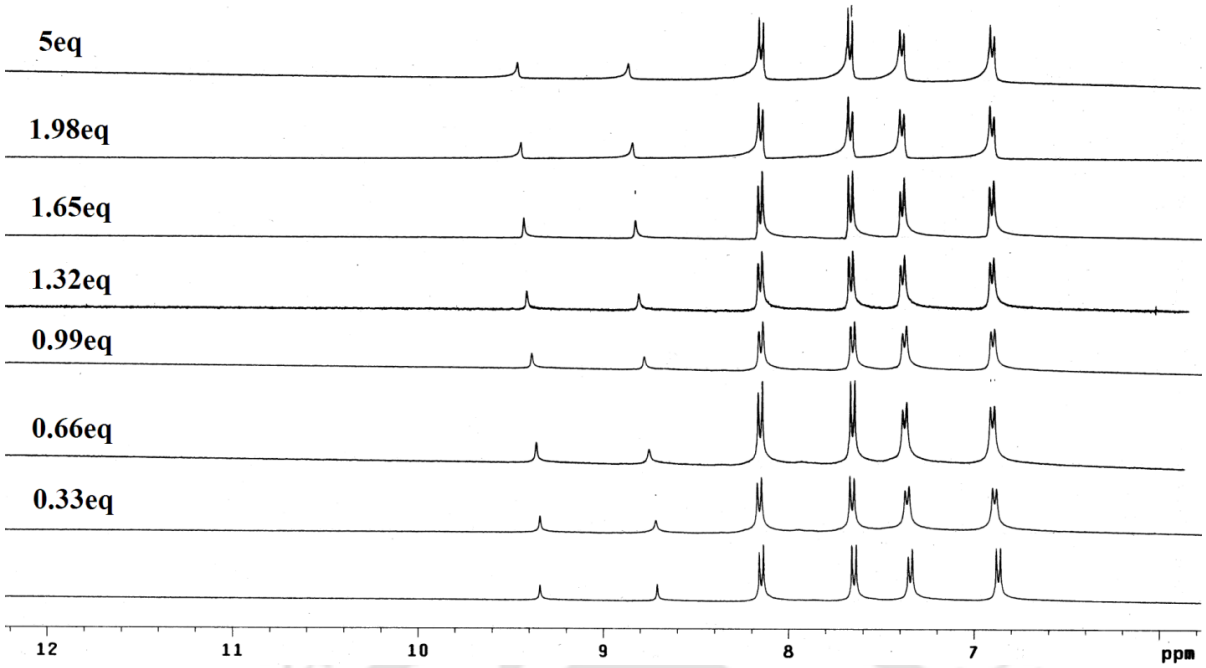

Figure 6.15. Stack plot of the ^{1}HNMR spectra of receptor $K^{+}\cdot\mathbf{L_4}$ in the presence of increasing amounts of [n-Bu_4N^{+}]HSO_4^{-} recorded in 98:2 d_6-DMSO:D_2O at 298 K.

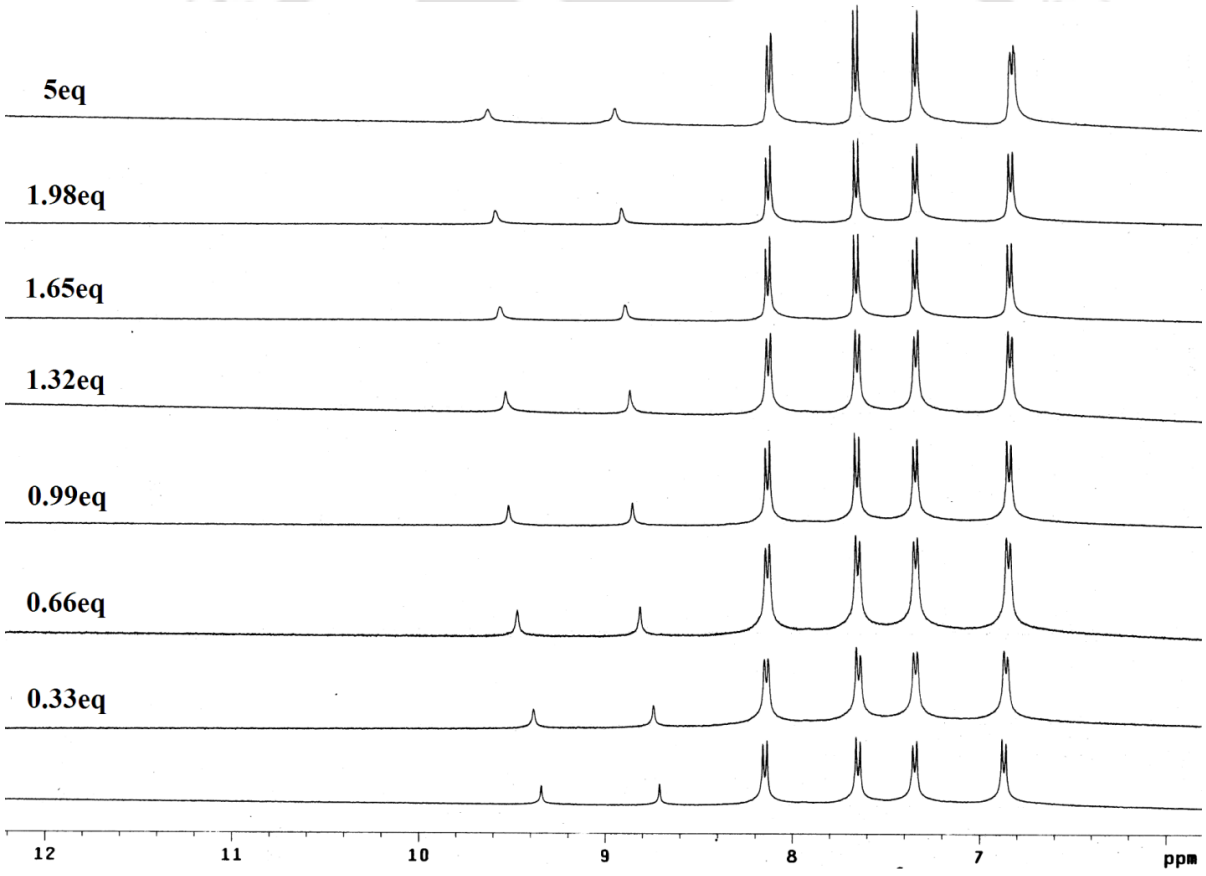

Figure 6.16 Stack plot of the ^{1}HNMR spectra of receptor $K^{+}\cdot\mathbf{L_4}$ in the presence of increasing amounts of [n-Bu_4N^{+}]$H_2PO_4^{-}$ recorded in 98:2 d_6-DMSO: D_2O at 298 K. The asterisk sigh shows the generation of new peak.

References

1. (*a*) I. Ravikumar and P. Ghosh, *Chem. Soc. Rev.*, 2012, **41**, 3077−3098; (*b*) C. Jia, Biao Wu, S. Li, X. Huang, Q. Zhao, Q-S. Li and X-J. Yang, *Angew. Chem. Int. Ed*., 2011, **50**, 486–490; (*c*) R. Custelcean, A. Bock and B. A. Moyer, *J. Am. Chem. Soc*., 2010, **132**, 7177–7185; (*d*) B. Wu, J. Liang, J. Yang, C. Jia, X.- J. Yang, H. Zhang, N. Tang and C. Janiak, *Chem. Commun*., 2008, 1762–1764; (*e*) P. S. Lakshminarayanan, I. Ravikumar, E. Suresh and P. Ghosh, *Chem. Commun*. 2007, 5214–5216; (*f*) S. Dey and G. Das, *Dalton Trans*. 2011, **40**, 12048–12051; (*g*) S. Dey and G. Das, *Dalton Trans*., 2012, **41**, 8960−8972; (*h*) B. Akhuli, I. Ravikumar and P. Ghosh, *Chem. Sci*., 2012, **3**, 1522–1530.

2. A. Rajbanshi, B. A. Moyer and R. Custelcean, *Cryst. Growth Des*., 2011, **11**, 2702–2706.

3. (*a*) M. Arunachalam and P. Ghosh, *Chem. Commun*., 2011, **47**, 8477–8492; (*b*) R. Custelcean, *Chem. Commun*., 2013, **49**, 2173−2182; (*c*) P. A. Gale, *Acc. Chem. Res*., 2006, **39**, 465– 475; (*d*) N. Busschaert, M. Wenzel, M. E. Light, P. Iglesias-Hernandez, R. Perez-Tomas and P. A. Gale, *J. Am. Chem. Soc*., 2011, **133**, 14136−14148; (*e*) A. Basu and G. Das, *Dalton Trans*., 2012, **41**, 10792−10802; (*f*) S. K. Dey, R. Chutia and G. Das, *Inorg. Chem*., 2012, **51**, 1727−1738; (*g*) M. Arunachalam and P. Ghosh, *Org. Lett*., 2010, **12**, 328–331; (*h*) M. Arunachalam, B. N. Ahamed and P. Ghosh, *Org. Lett*., 2010, **12**, 2742–2745; (*i*) A. Basu and G. Das, *Chem. Commun*., 2013, **49**, 3997−3999.

4 (*a*) S. R. Seidel and P. J. Stang, *Acc. Chem. Res*., 2002, **35**, 972–983; (*b*) Z. Yang, B. Wu, X. Huang, Y. Liu, S. Li, Y. Xia, C. Jiaac and X-J. Yanga, *Chem. Commun.*, 2011, **47**, 2880–2882; (*c*) B. Akhuli and P. Ghosh, *Dalton Trans.*, 2013, **42**, 5818-5825; (*d*) D. R. Turner, M. B. Hursthouse, M. E. Light and J. W. Steed, *Chem. Commun*., 2004, 1354−1355; (*e*) R. Custelcean, P. V. Bonnesen, B. D. Roach and N. C. Duncan, *Chem. Commun.*, 2012, **48**, 7438−7440; (*f*) S. Li, C. Jia, B. Wu, Q. Luo, X. Huang, Z. Yang, Q.-S. Li and X.-J. Yang, *Angew. Chem., Int. Ed*., 2011, **50**, 5721−5724; (*g*) R. Custelcean, P. V. Bonnesen, N. C. Duncan, X. Zhang, L. A. Watson, G. V. Berkel, W. B. Parson and B. P. Hay, *J. Am. Chem. Soc.*, 2012, **134**, 8525−8534.

5. B. P. Hay, T. K. Firman and B. A. Moyer, *J. Am. Chem. Soc*., 2005, **127**, 1810-1819.

6. A. J. Evans and P. D. Beer, *Dalton Trans*., 2003, 4451−4456

7. M. J. Hynes, *J. Chem. Soc. Dalton Trans.*, 1993, 311–312.

To conclude, this thesis provides some significant results in the domain of 'supramolecular chemistry of anions and ion-pairs, where the anions and/or ion-pairs binding capability of some newly synthesized acyclic receptors (**H_2L_1** and **L_2-L_4**) were explored in the solid-state and in solution as well. In general the present findings provide evidence of anion and ion-pair induced formation of capsular, pseudo-capsular and polymeric assembly of the studied receptor molecules. Each receptor has shown an interesting property in presence of a specific anion or a set of ionic guests.

The receptor **H_2L_1** has been shown to selectively detect F^- ion *via* formation of H-bonded complex and subsequent stepwise deprotonation of two N−H groups, which can be visually monitored by a change in colour from yellow to blue *via* pink. Additionally, the receptor also forms halide (Cl^- and Br^-) induced polymeric architecture in crystalline solid state. The presence of a rigid thiadiazole spacer presumably opens up enough space for capturing two halide anions by a single receptor molecule, where the coordinated −NH protons are pointed in the same direction with respect to the spacer and eventually favour formation of halide (Cl^- and Br^-) induced polymeric architecture, although no obvious chloride or bromide-directed polymeric assembly is found in solution.

The multi armed tris-(thiourea) receptor **L_2** has been shown to encapsulate large sulfate and thiosulfate anions within the rigidified dimeric capsular assembly of **L_2**. The solid state crystal structure of both the anions with **L_2** shows that the encapsulated anions are stabilized *via* N–H···O and N–H···S hydrogen bonding coordination. The sizes of tight capsular assemblies for both anions are quite comparable. Interestingly, in contradiction of 2:1 solid state binding, the results from solution state NMR experiments confirm that both the anions are bound within the pseudocavity of the receptor **L_2** with 1:1 binding stoichiometry.

The newly synthesized tripodal amide receptor **L_3** has been established as a competent hydrogen bonding scaffold for encapsulation of halide water cluster within rigidified molecular capsules, assembled by aromatic π-stacking interactions between the receptor side arms. However, in the case of higher homologous iodide anions the receptor **L_3** prefers to adopt a non-capsular polymeric aggregation. Interestingly, crystallization of the receptor in presence of HF in glass container gives SiF_6^{2-} complex, and depending on crystallizing solvent the receptor forms both capsular and non-capsular (polymeric) assemblies in presence of SiF_6^{2-} anion, which confirms the adaptability of flexible **L_3** as an anion receptor.

In contrast, the urea receptor **L_4** has been shown to efficiently form complex with ion-pairs and also gave rise significant enhancement of binding property with hydrogensulfate (HSO_4^-) and di-hydrogenphosphate ($H_2PO_4^-$) in presence of Group I metal ions (Li^+, Na^+ and K^+) compared to free receptor. The solid state crystal structure of sulfate complex shows encapsulation of single DMF solvent molecule in the tripodal cavity of the protonated receptor, and the SO_4^{2-} anion is located outside the tripodal cavity and stabilized by N−H···O hydrogen bonds from the urea functions of four receptor cations. Whilst, in case of $TBAHSO_4$ the receptor forms an unusual contact ion-pair complex, in which both the TBA cation and SO_4^{2-} anion are encapsulated in the distorted C_{3v} symmetric tripodal cleft of the protonated receptor. Interestingly, the receptor forms a remarkable C_{3v} symmetric charge separated ion-pair complex with potassium cation and hydrgenphosphate anion *via* formation of dimeric capsular assembly of the receptor, where three nearby K^+ encapsulated dimeric capsular assemblies interdigitate to form a precise cavity to encapsulate the HPO_4^{2-} by six urea groups.

Thus, the thesis demonstrates some of the core and erratic concepts of supramolecular chemistry and versatility of the acyclic receptors as efficient building block for the generation of molecular assembly. The recognition of anions and ion-pairs with in molecular assembly/molecular cavity in solid state is definitely a field which can expand considerably and bring immense advances in specialized applications such as drug delivery, membrane transport, salt solubilization, extraction, catalysis *etc*. However, for these applications to reach their prospective, basic work in tuning anion, hydrated anion and ion-pair binding inside the molecular capsules or molecular assembly is highly appreciated. Although the results included in this thesis are extremely useful from a fundamental viewpoint, there is other challenging aspects in supramolecular chemistry that need to be developed, basically from an applicative approach. Research in these areas with a focus on technological and biomedical applications, based upon the remarkable anion and ion-pair binding molecular assembly appear to be forthcoming.

List of Publications

1. Encapsulation of discrete cyclic halide water tetramer $[X_2(H_2O)_2]^{2-}$, $X=Cl^-/Br^-$ within dimeric capsular assembly of tripodal amide receptor **Arghya Basu** and Gopal Das, ***Chem. Comun***., 2013 2013**,49,** 3997-3999.

2. Amidothiourea based colorimetric receptors for basic anions: evidence of anioninduced deprotonation of amide –NH proton and hydroxide induced anion···π interaction with the deprotonated receptors. **Arghya Basu** and Gopal Das, ***RSC Adv.***, 2013. **3**, 6596-6605.

3. Selective fluorescence sensor for Al^{3+} and Pb^{2+} in physiological condition by a benzene based tripodal receptor. Barun Kumar Datta, Chirantan Kar, **Arghya Basu** and Gopal Das, ***Tetrahedron Lett.***, 2013, **54**, 771−774.

4. Benzimidazole functionalized tripodal receptor for selective recognition of iodide. Chirantan Kar**, Arghya Basu** and Gopal Das ***Tetrahedron Lett.***, 2012, **53**, 4754−4757.

5. Encapsulation of divalent tetrahedral oxyanions of sulfur within rigidified dimeric capsular assembly of tripodal receptor: First crystallographic evidence of thiosulfate encapsulation. **Arghya Basu** and Gopal Das, ***Dalton Trans.***, 2012, **41**, 10792−10802.

6. Cyclic pentameric puckered hybrid chloride-water cluster $[Cl_3(H_2O)_4]^{3-}$ in hydrophobic architecture, Md. Najbul Hoque, **Arghya Basu** and Gopal Das, ***Cryst. Growth Des***, 2012, **12**, 2153−2157

7. Amidothiourea as a potential receptor for organic bases by resonance assisted low barrier hydrogen bond formation: Structure and Hirshfeld surface analysis **Arghya Basu** and Gopal Das, ***CrystEngComm***., 2012, **14**, 3306−3314.

8. A neutral acyclic anion receptor with thiadiazole spacer: halide binding study and halide-directed self-assembly in the solid state **Arghya Basu** and Gopal Das, ***Inorg. Chem.***, 2012, **51**, 2012−2019.

9. Oxidative cyclization of thiosemicarbazone: an optical and turn-on fluorescent chemodosimeter for Cu(II) **Arghya Basu** and Gopal Das ***Dalton Trans.***, 2011, **40**, 2837−2843.

10. Zn(II) and Hg(II) complexes of naphthalene based thiosemicarbazone: Structure and spectroscopic studies **Arghya Basu** and Gopal Das, ***Inorg. Chim. Acta.***, 2011, **372**, 394–399.

11. Coordination assembly of *p*-substituted aryl azo imidazole complexes: Influences of electron donating substitution and counter ions Avijit Pramanik, **Arghya Basu** and Gopal Das, ***Polyhedron***, 2010, **29**, 1980−1989.

12. A C_{3v} Symmetric Heteroditopic Tripodal Urea Receptor: Evidences of Alkali Metal Cation Cooperative Anion Recognition and Ion Pair Induced Formation of Molecular Capsule **Arghya Basu** and Gopal Das, Manuscript under communication.

Contents for Annexure

	Page No.
Annexure 1	**A – 1**
Annexure 2	**A – 5**
Annexure 3	**A – 31**
Annexure 4	**A – 35**
Annexure 5	**A – 38**
Annexure 6	**A – 41**

Annexure 1

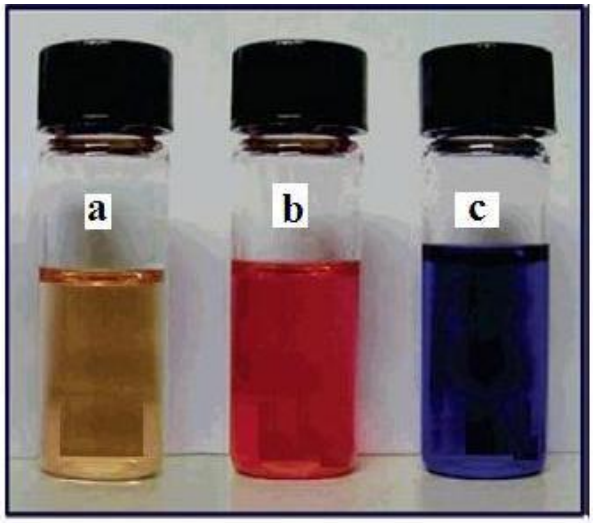

Figure A1.1 Color changes observed on addition of $[Bu_4N^+]F^-$ to a DMSO solution of receptor 1 (a): no addition (species present only receptor **1**); (b) plus 5 equiv of $[Bu_4N^+]F^-$ (dominant species, mono deprotonated receptor); (b) plus 40 equiv of $[Bu_4N^+]F^-$ (doubly deprotonated receptor).

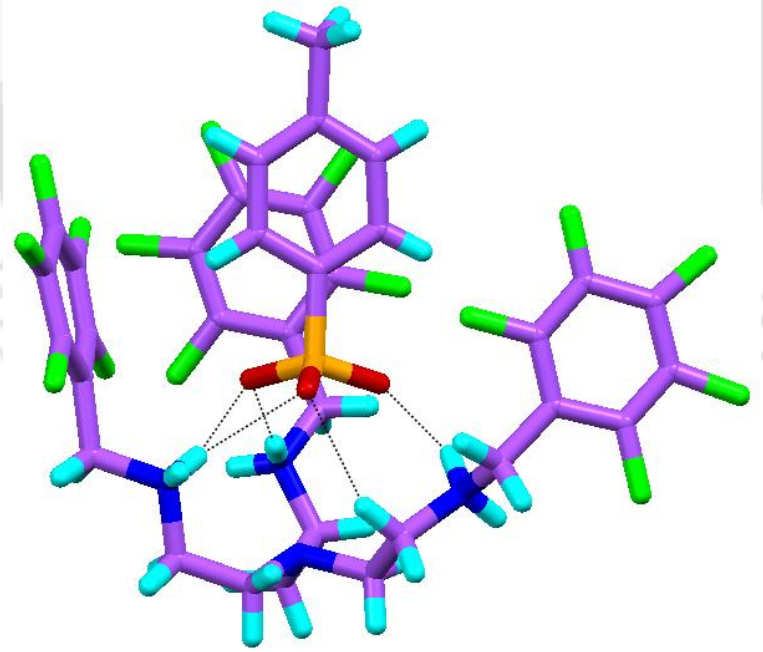

Figure A1.2 Binding and pseudo-encapsulation of a p-toluene sulfonate anion by protonated **4a** in complex $[(H_3\mathbf{4a})(OTs^-)_3]$.

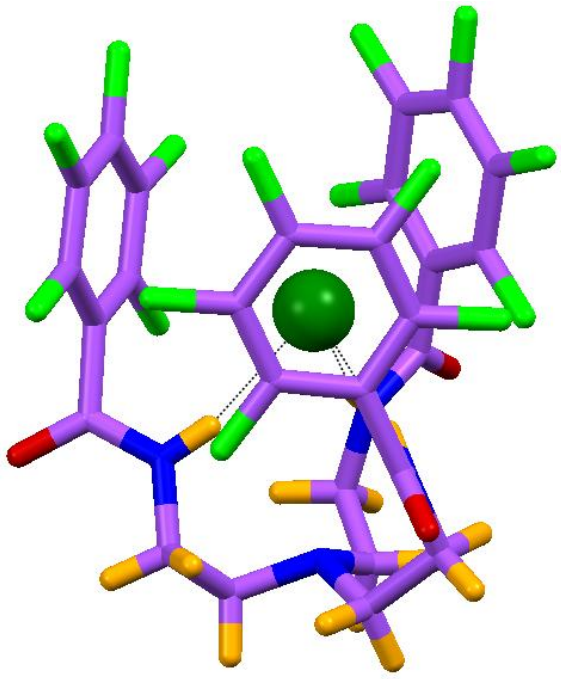

Figure A1.3 Chloride encapsulation within the receptor cavity of **5a**.

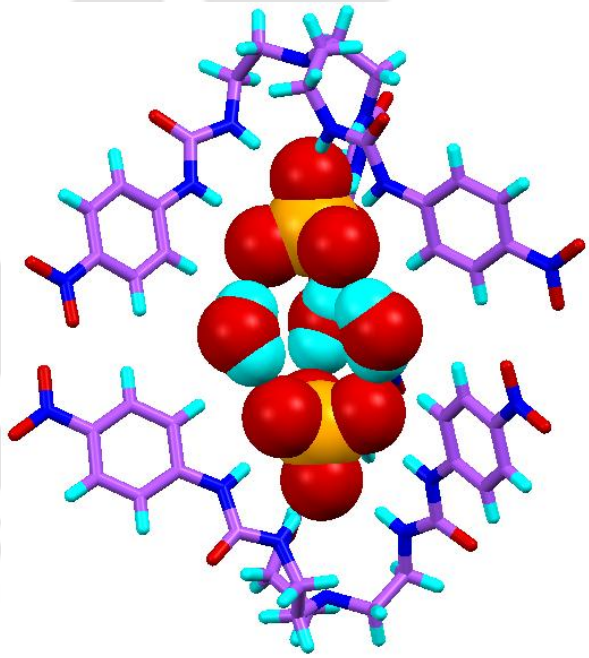

Figure A1.4 encapsulation of a SO_4^{2-}–$(H_2O)_3$–SO_4^{2-}adduct within a pseudo-dimeric capsular assembly of receptor **6e**.

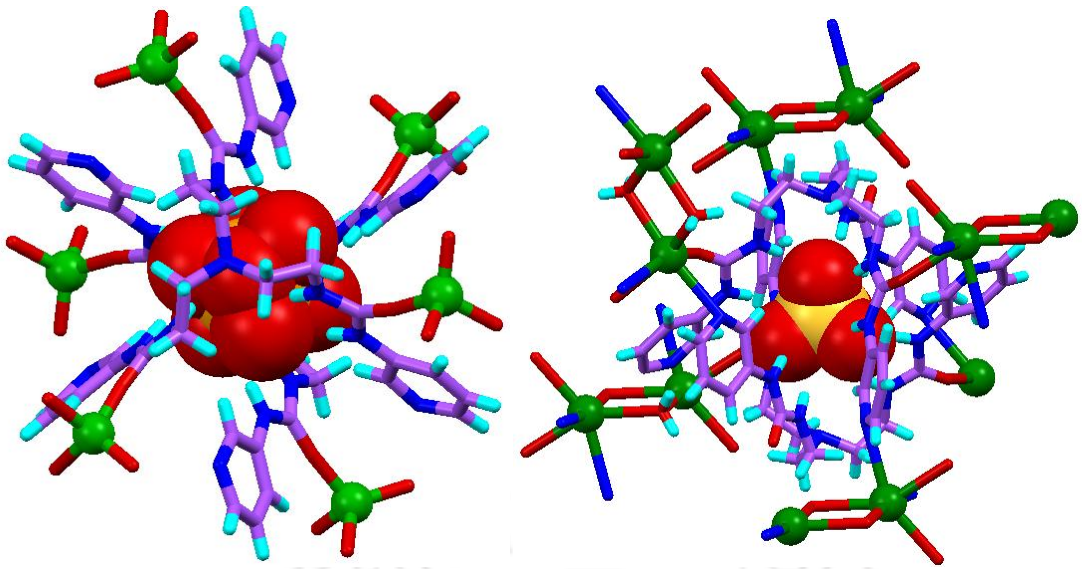

Figure A1.5 Crystallization of the sulfate capsule of **6h** with $Na_2(H_2O)_4^{2+}$ (left), and $K_2(H_2O)_2^{2+}$ (right) counter cations.

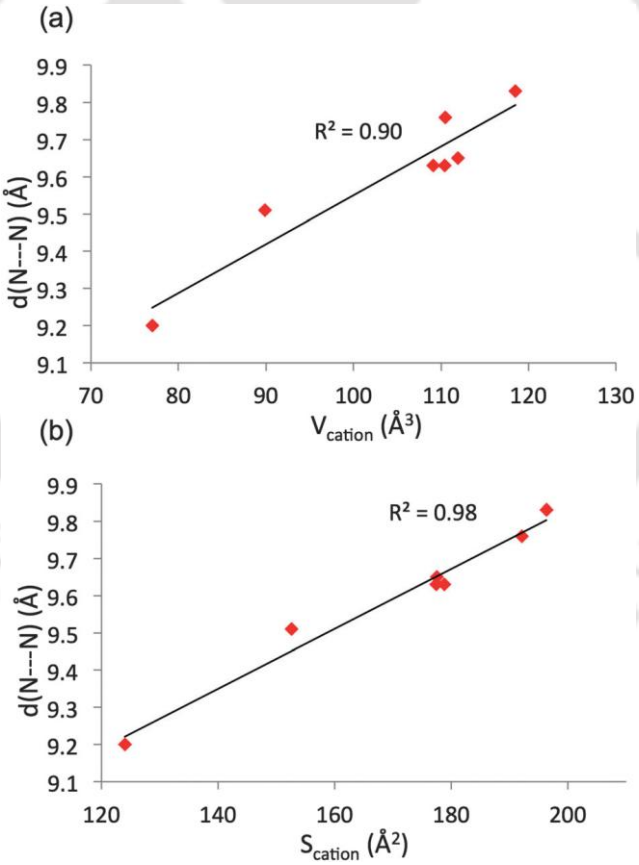

Figure A1.6 Correlation between the height of the capsules and the volume (a) or surface area (b) of sulfate complexes of **6h**.

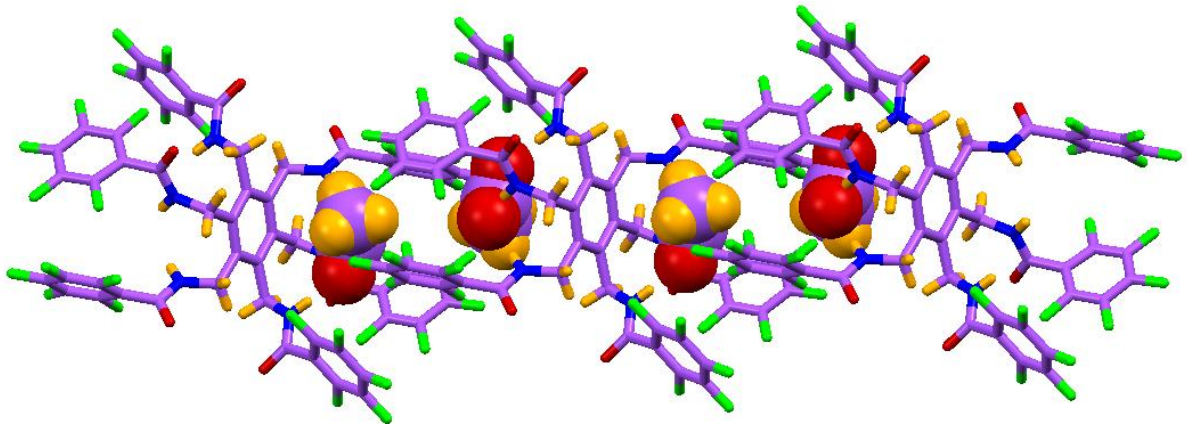

Figure A1.7 Packing diagram of acetate complex of **9a** showing two tripodal clefts from two receptors holding two acetate ions in the pseudo cage.

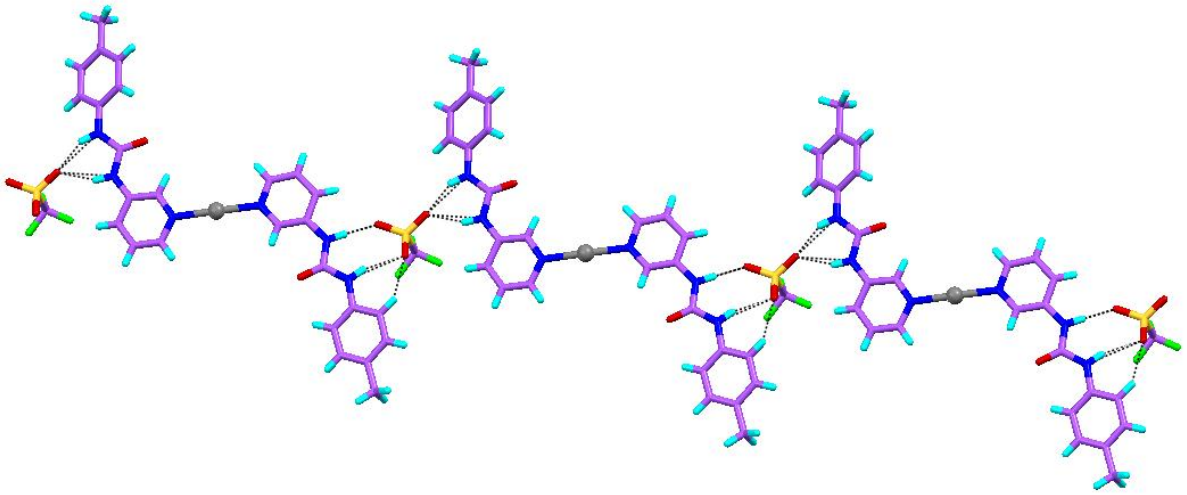

Figure A1.8 Formation of stable extended polymeric structures of **10b** upon complexation with $AgCF_3SO_3$.

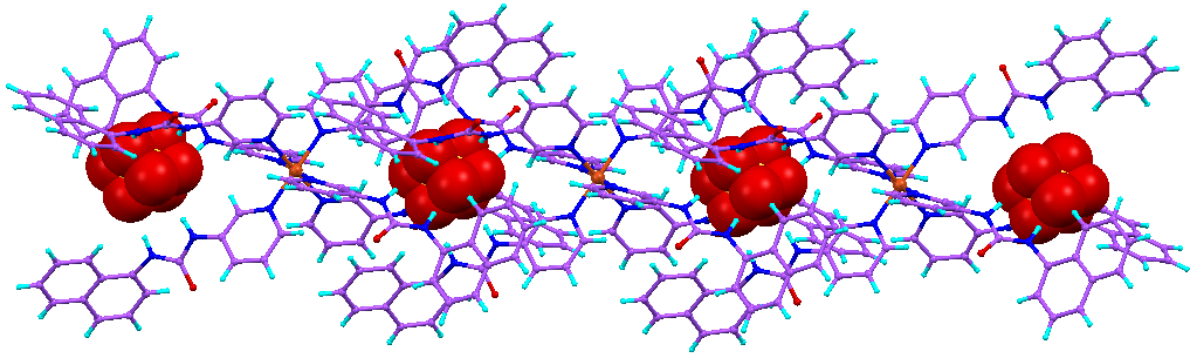

Figure A1.9 Infinite 1D hydrogenbonded chain linked by sulfate encapsulation in $CuSO_4$ complex of **10b**.

Annexure 2

Characterization data of receptors, H_2L_1 and L_2-L_4:

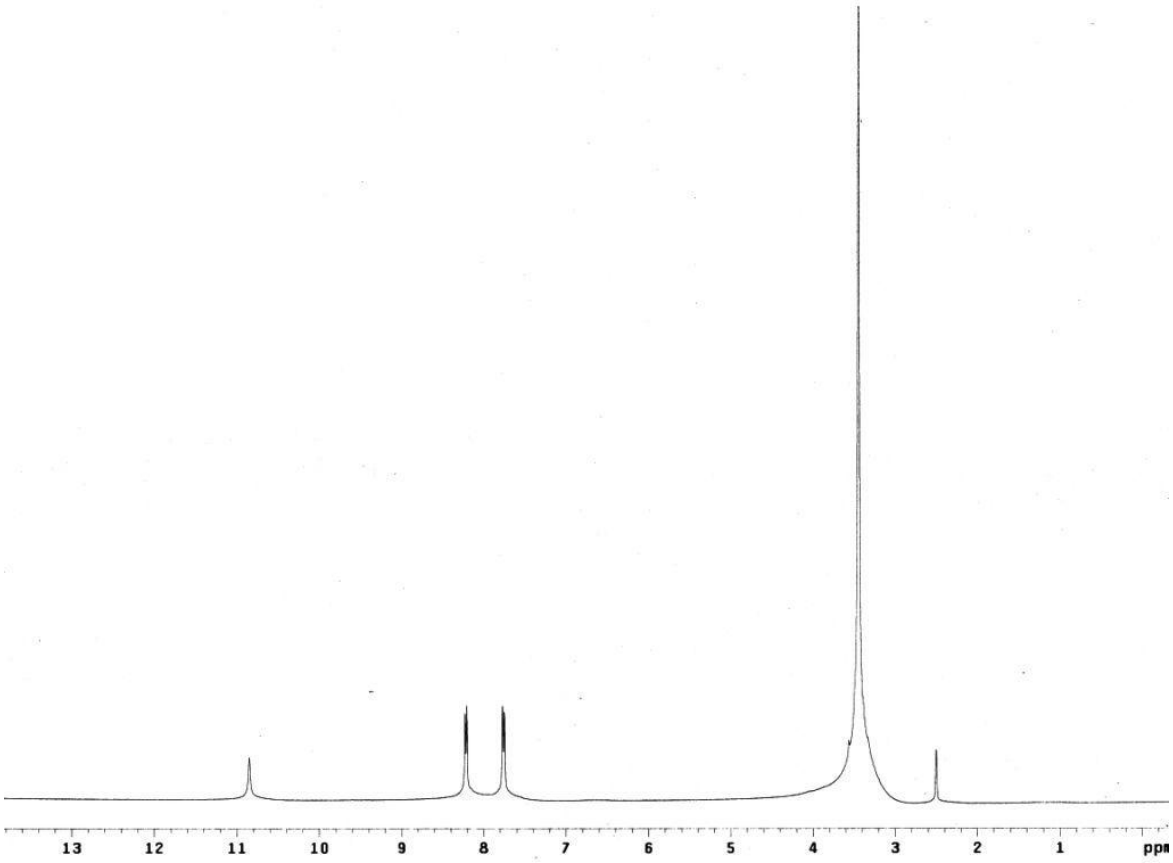

Figure A2.1 ^{1}H NMR spectrum of receptor $\mathbf{H_2L_1}$ (400 MHz, DMSO-d_6).

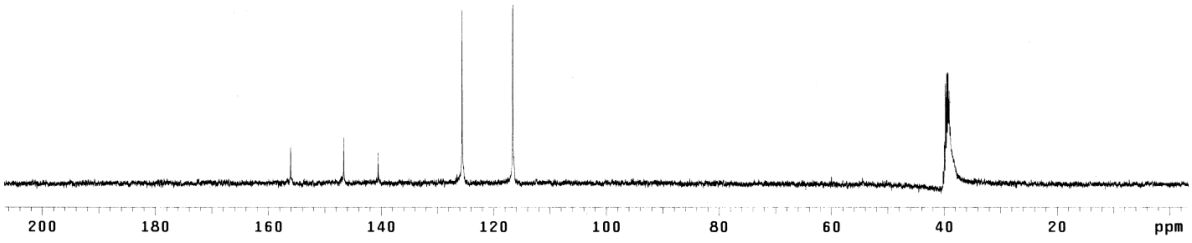

Figure A2.2 ^{13}C NMR spectrum of receptor $\mathbf{H_2L_1}$ (100 MHz, DMSO-d_6).

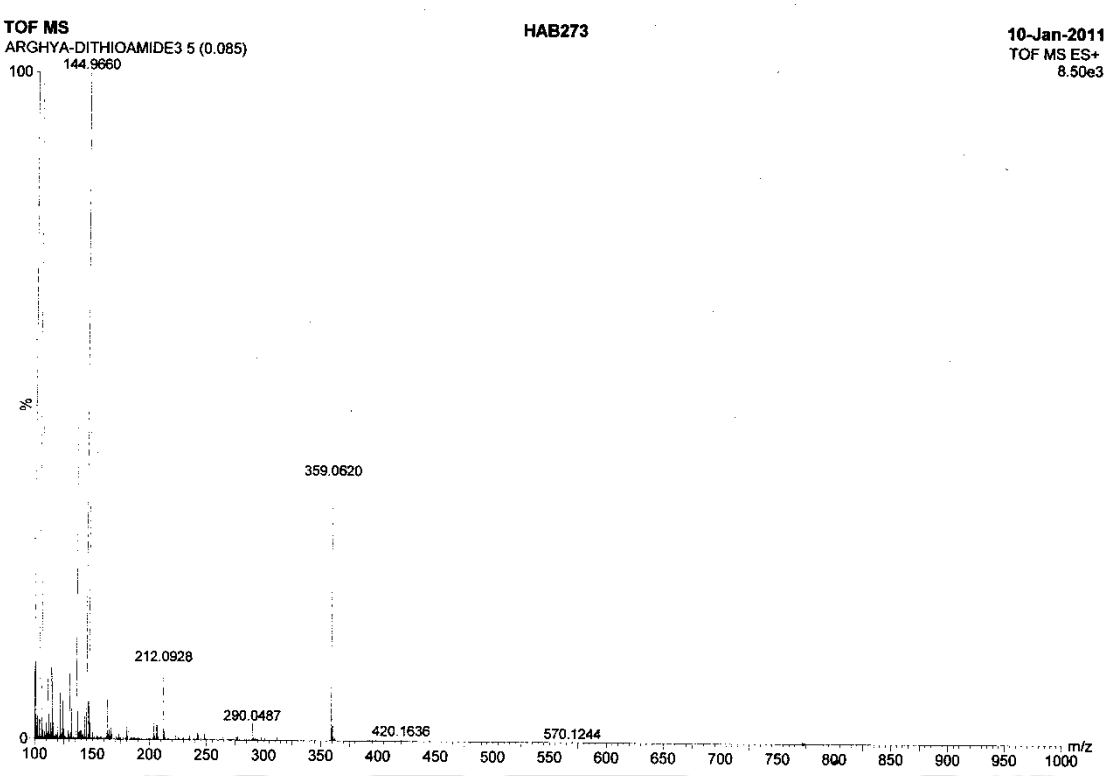

Figure A2.3 ESI-Mass spectrum of receptor of $\mathbf{H_2L_1}$ in acetonitrile.

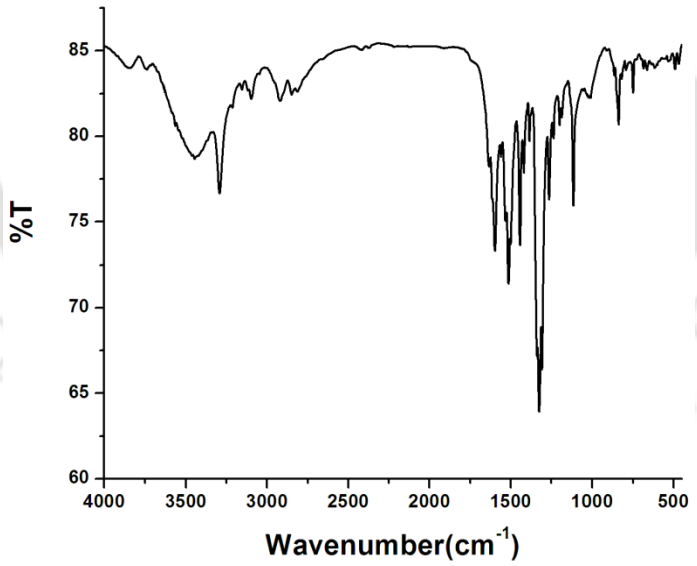

Figure A2.4 FT-IR spectrum of $\mathbf{H_2L_1}$ recorded in KBr pellet.

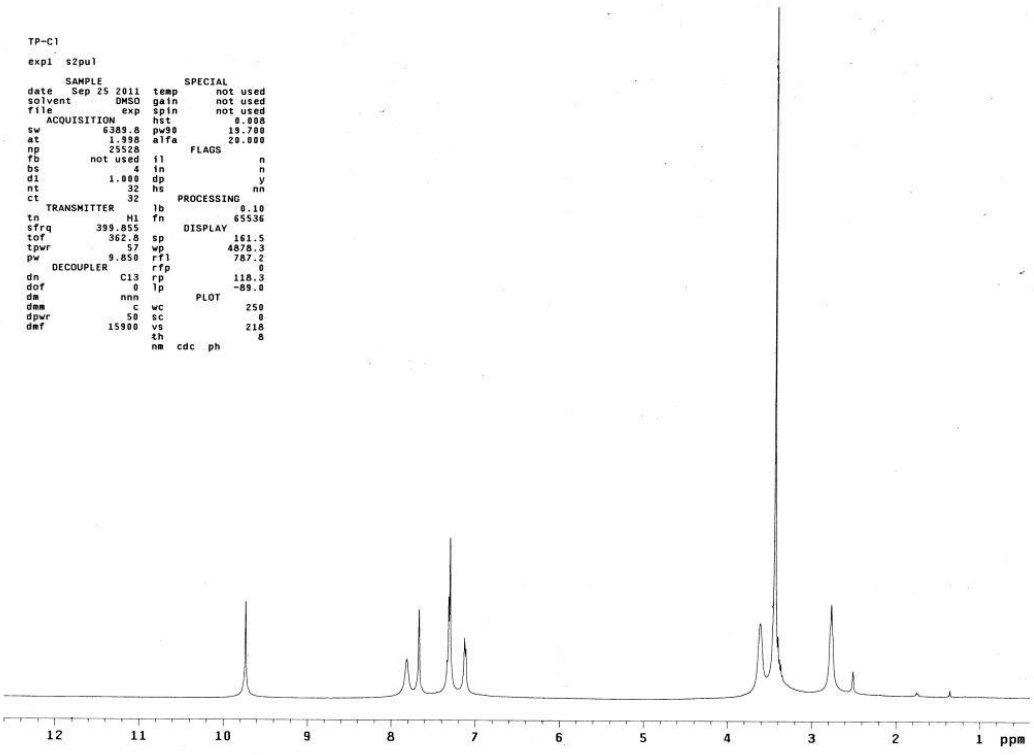

Figure A2.5 ^{1}H NMR spectrum of receptor $\mathbf{L_2}$ (400 MHz, DMSO-d_6).

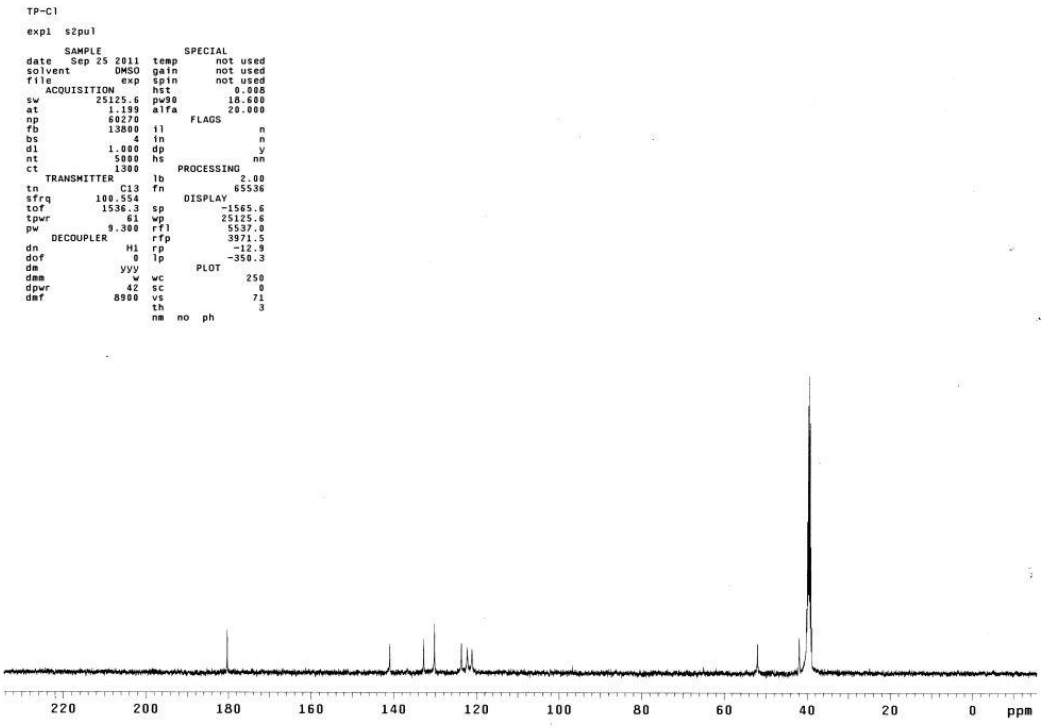

Figure A2.6 ^{13}C NMR spectrum of receptor $\mathbf{L_2}$ (100 MHz, DMSO-d_6).

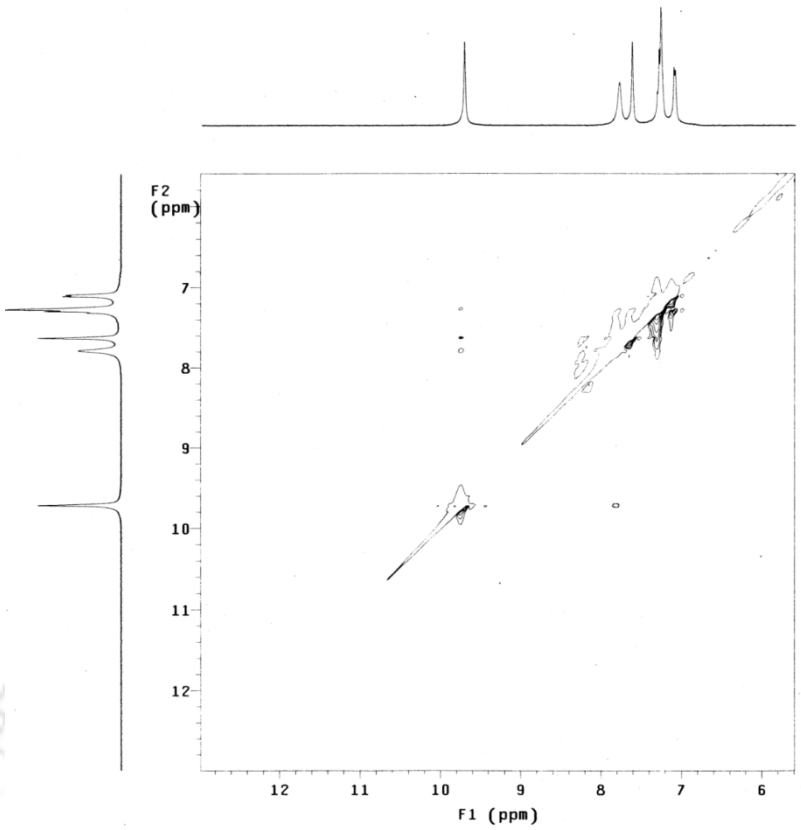

Figure A2.7 NOESY spectrum of $\mathbf{L_2}$ (400 MHz, DMSO-d_6).

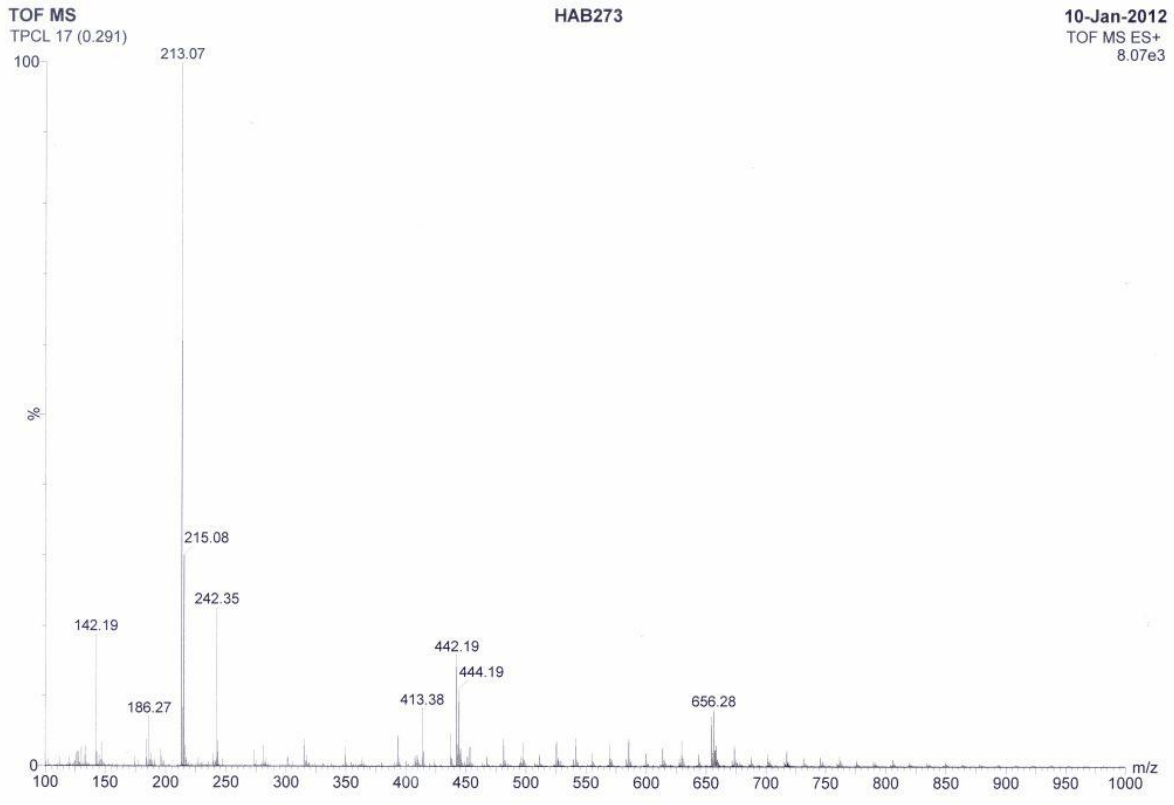

Figure A2.8 ESI-Mass spectrum of receptor $\mathbf{L_2}$ in acetonitrile.

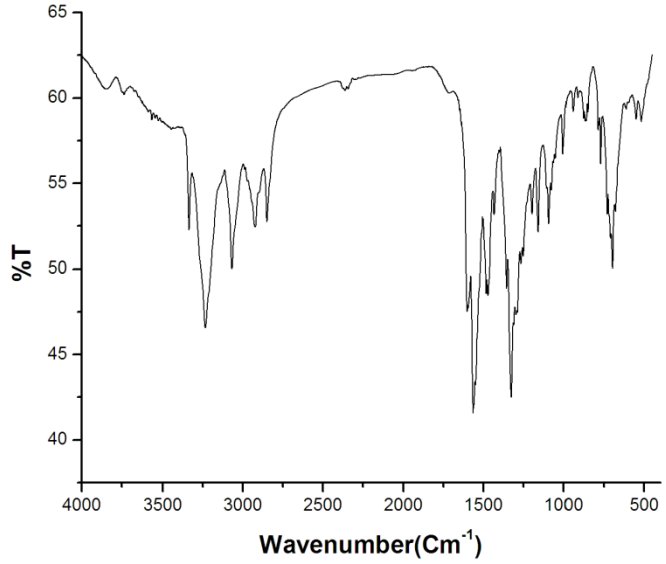

Figure A2.9 FT-IR spectrum of $\mathbf{L_2}$ recorded in KBr pellet.

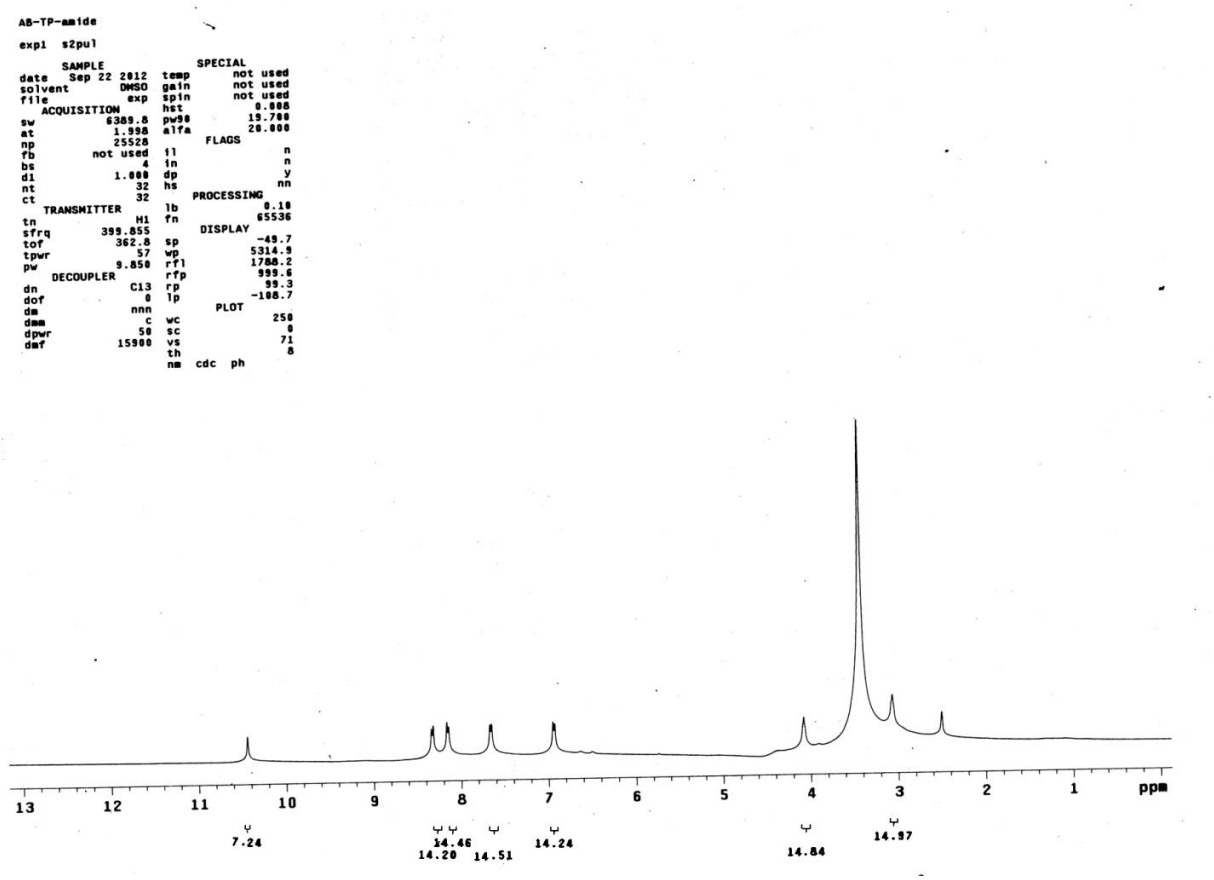

Figure A2.10 ^{1}H NMR spectrum of receptor $\mathbf{L_3}$ (400 MHz, DMSO-d_6).

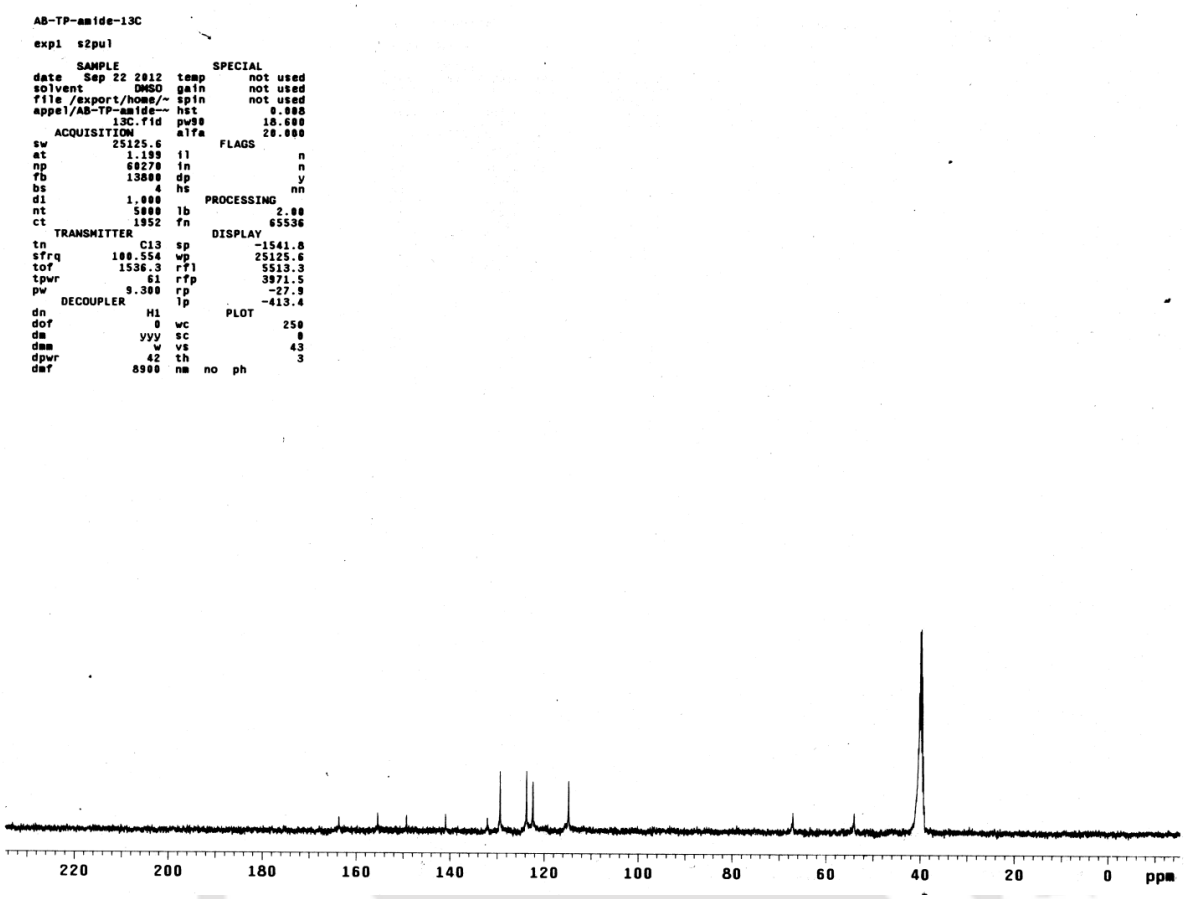

Figure A2.11 ^{13}C NMR spectrum of receptor $\mathbf{L_3}$ (100 MHz, DMSO-d_6).

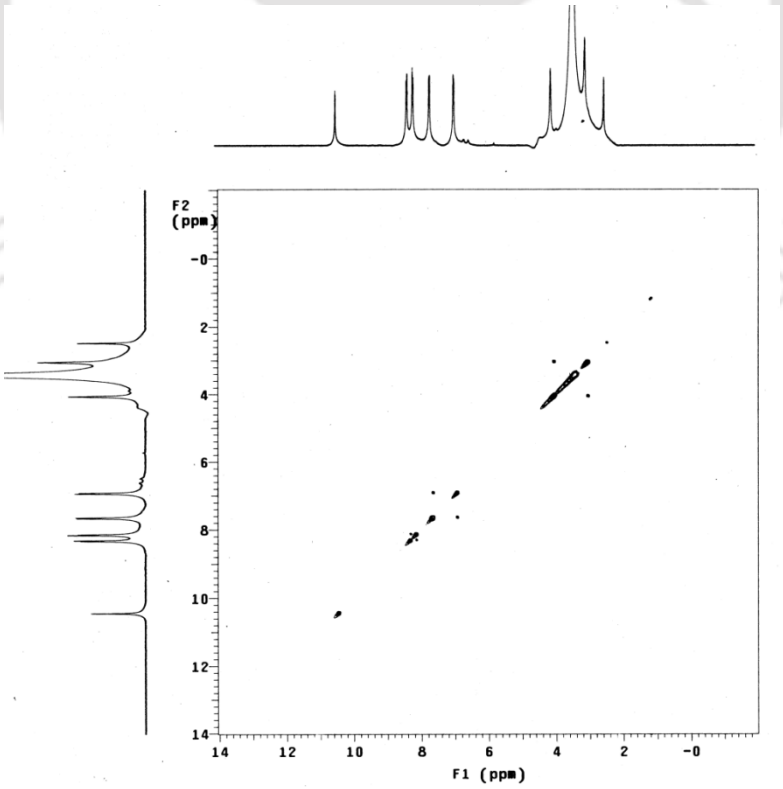

Figure A2.12 COSY spectra of $\mathbf{L_3}$ (400 MHz, DMSO-d_6).

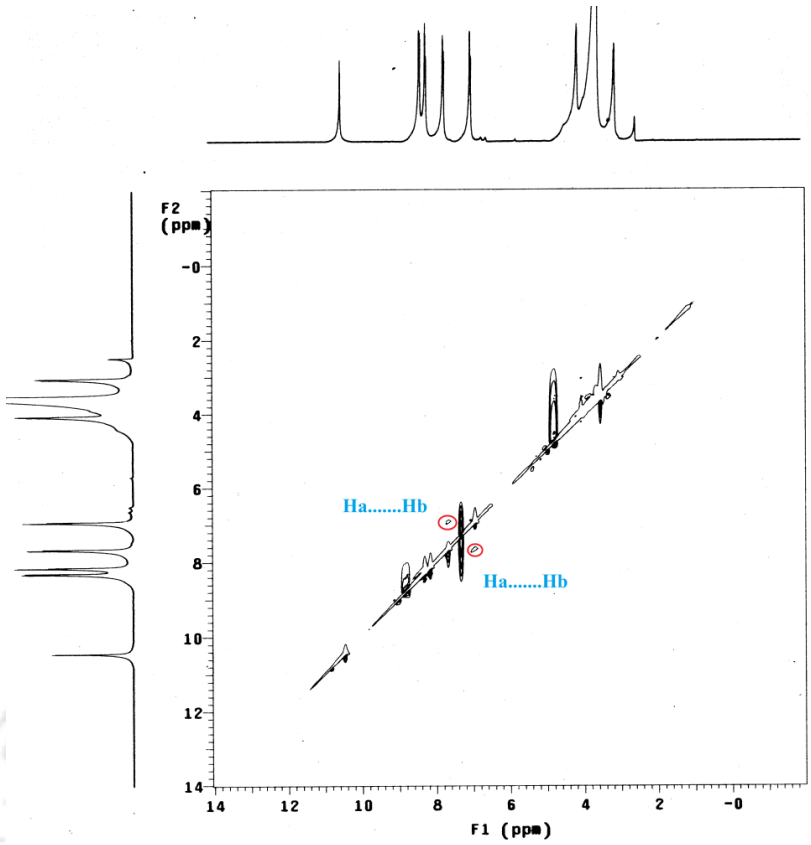

Figure A2.13 NOESY spectrum of $\mathbf{L_3}$. (400 MHz, DMSO-d_6).

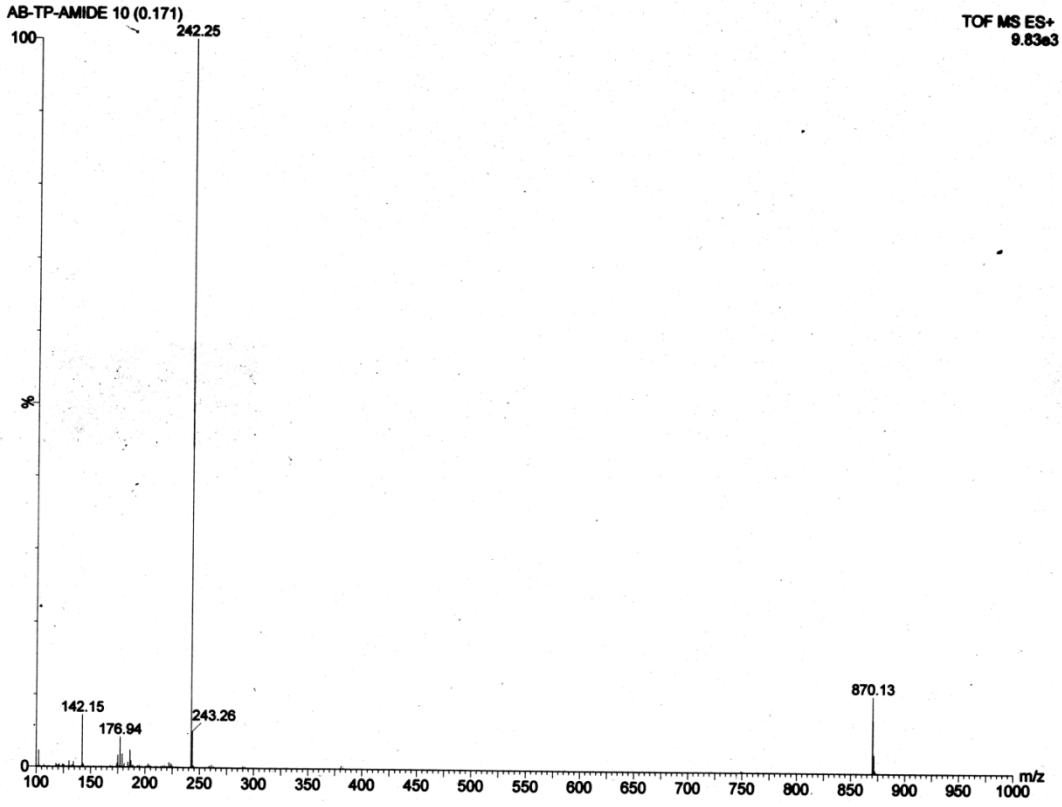

Figure A2.14 ESI-Mass spectrum of receptor $\mathbf{L_3}$ in acetonitrile.

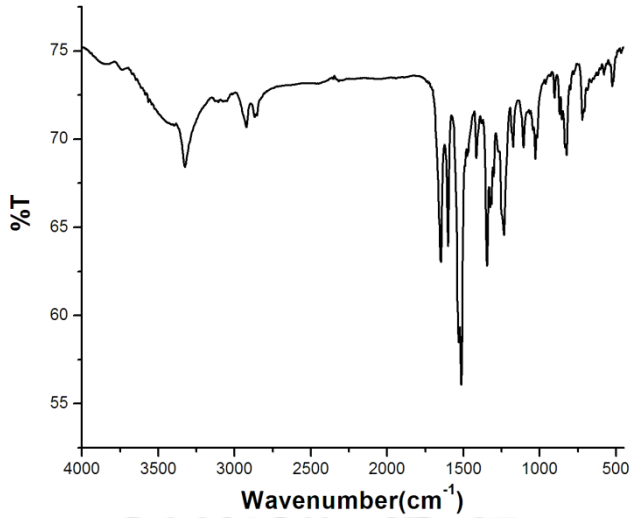

Figure A2.15 FT-IR spectrum of $\mathbf{L_3}$ recorded in KBr pellet.

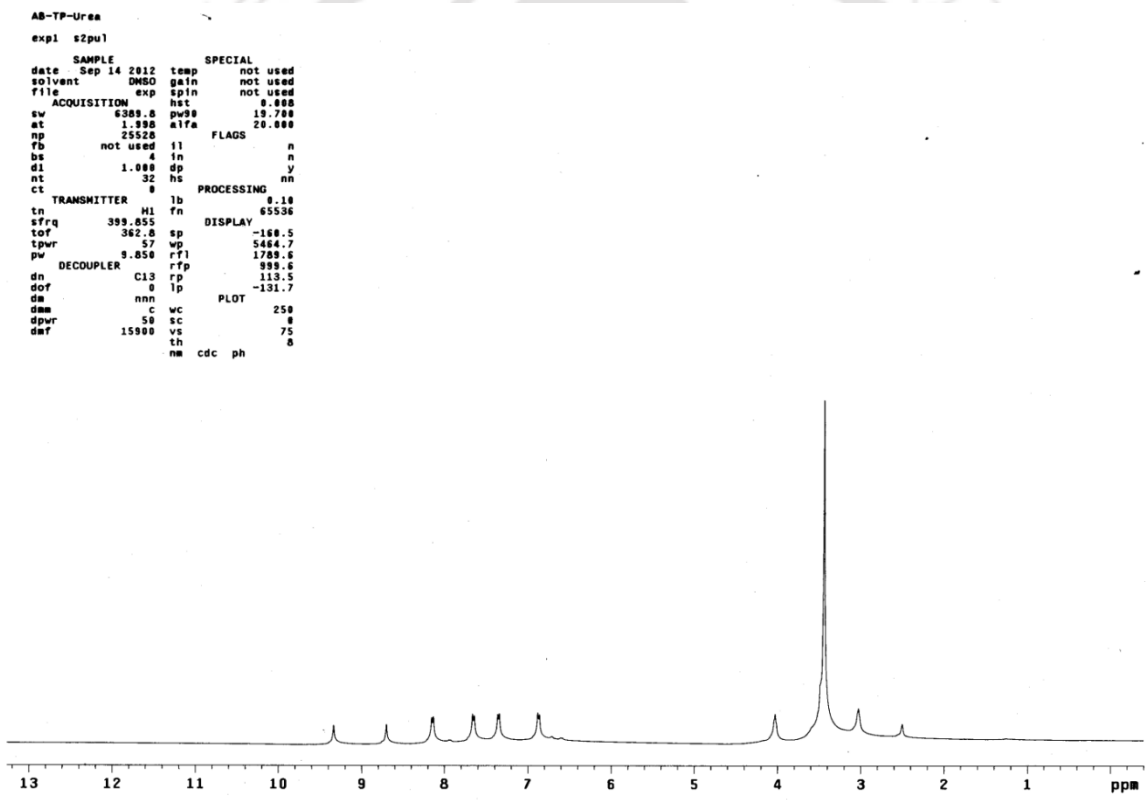

Figure A2.16 ^{1}H NMR spectrum of receptor $\mathbf{L_4}$ (400 MHz, DMSO-d_6).

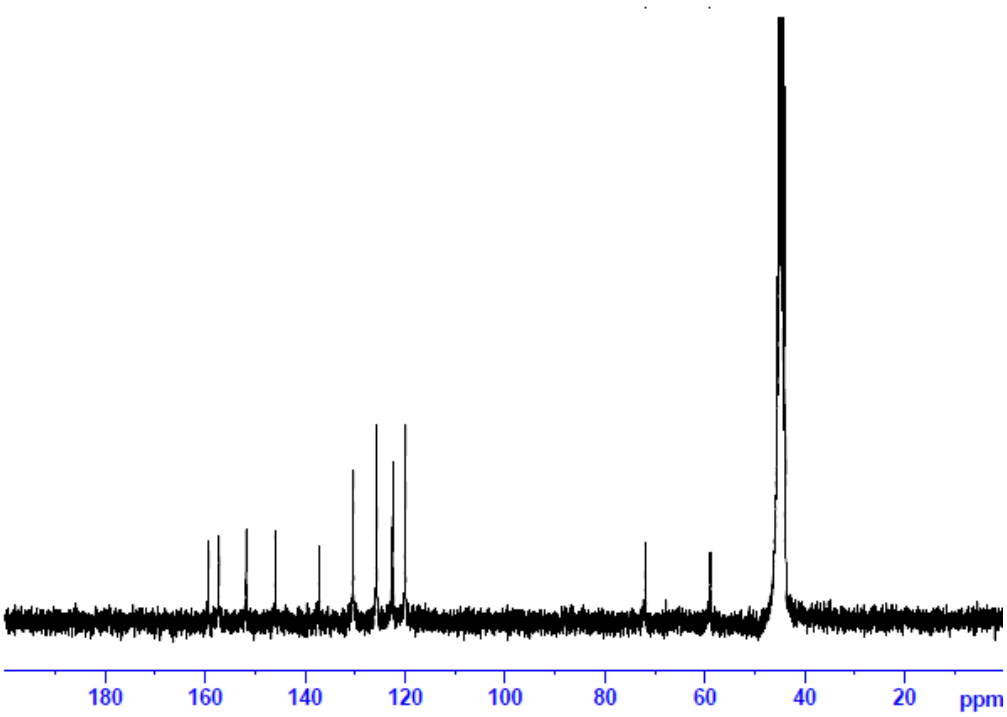

Figure A2.17 ^{13}C NMR spectrum of receptor **L$_4$** (100 MHz, DMSO-d$_6$).

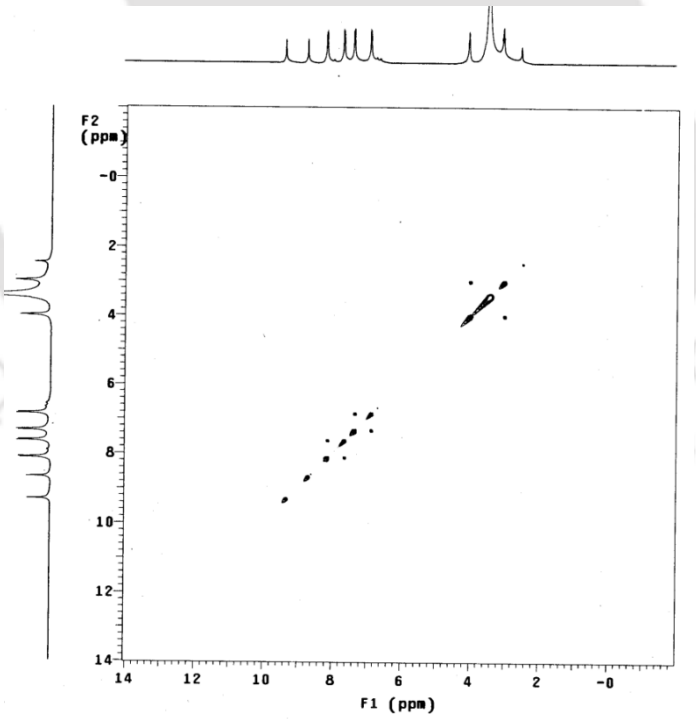

Figure A2.18 COSY spectra of **L$_4$** (400 MHz, DMSO-d$_6$).

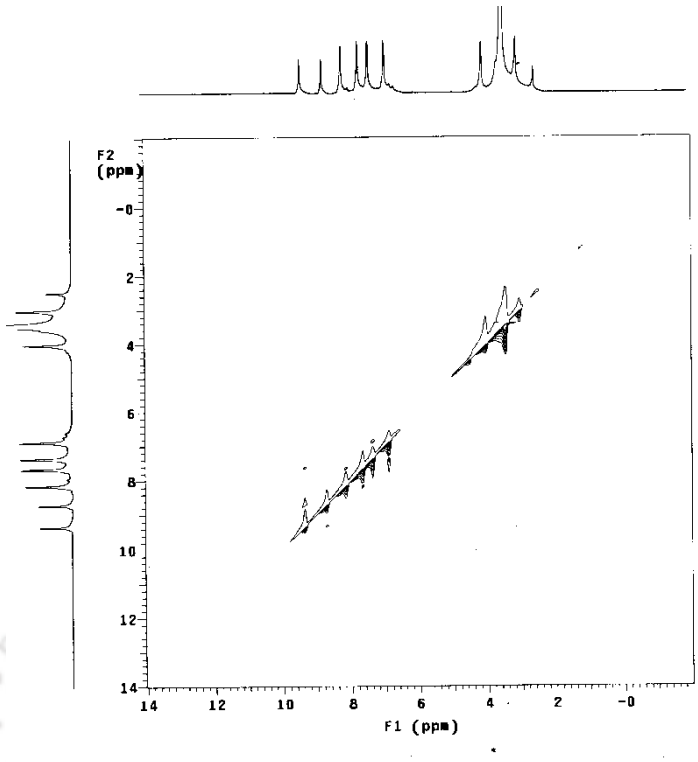

Figure A2.19 NOESY spectrum of $\mathbf{L_4}$ (400 MHz, DMSO-d_6).

Sample Name	Unavailable	**Position**	Unavailable	**Instrument Name**	Unavailable	**User Name**	Unavailable
Inj Vol	Unavailable	**InjPosition**	Unavailable	**SampleType**	Unavailable	**IRM Calibration Status**	Success
Data Filename	AB-5.d	**ACQ Method**		**Comment**	Sample information is unavailable	**Acquired Time**	Unavailable

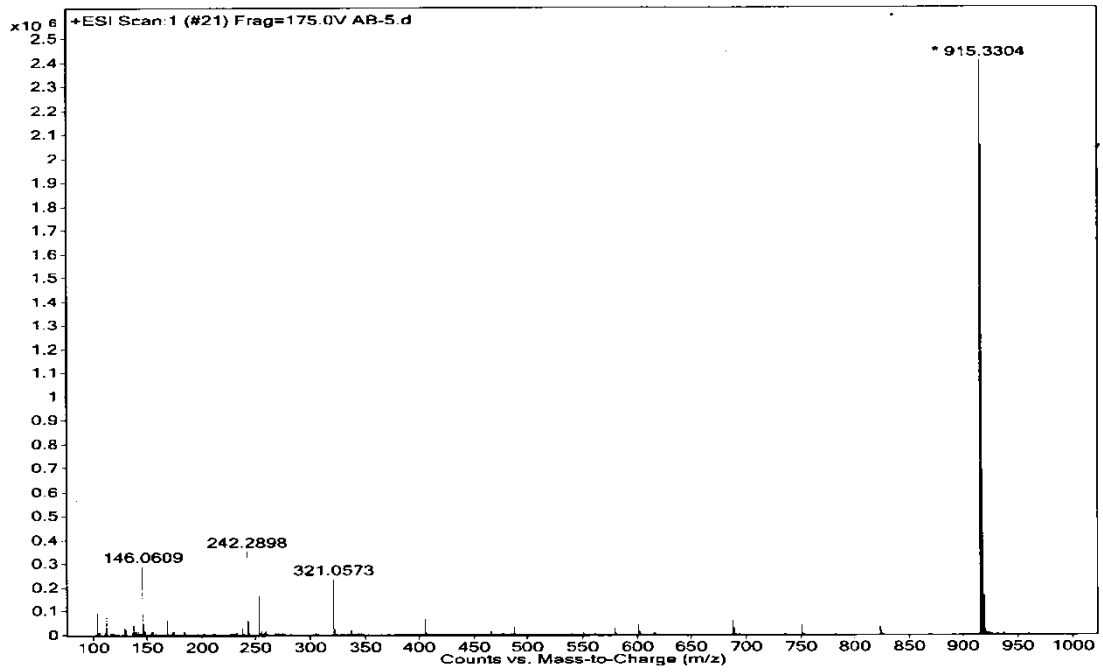

Figure A2.20 ESI-mass spectrum of $\mathbf{L_4}$ in acetonitrile.

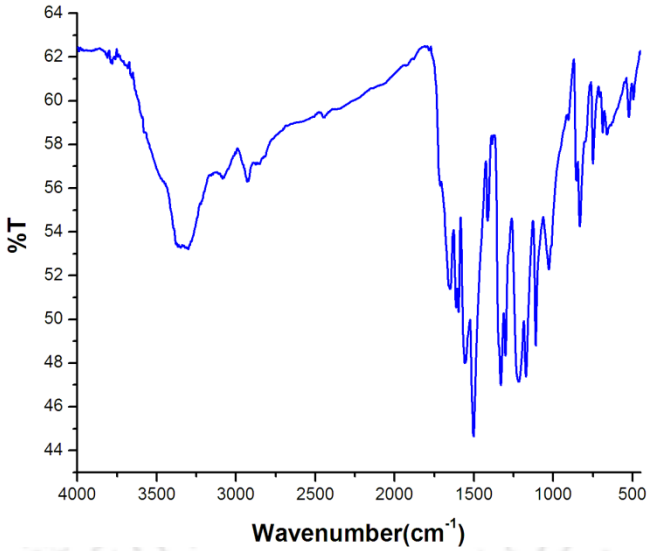

Figure A2.21 FT-IR spectrum of $\mathbf{L_4}$ recorded in KBr pellet.

Characterization data of anion complexes of L_1 (1a-1e):

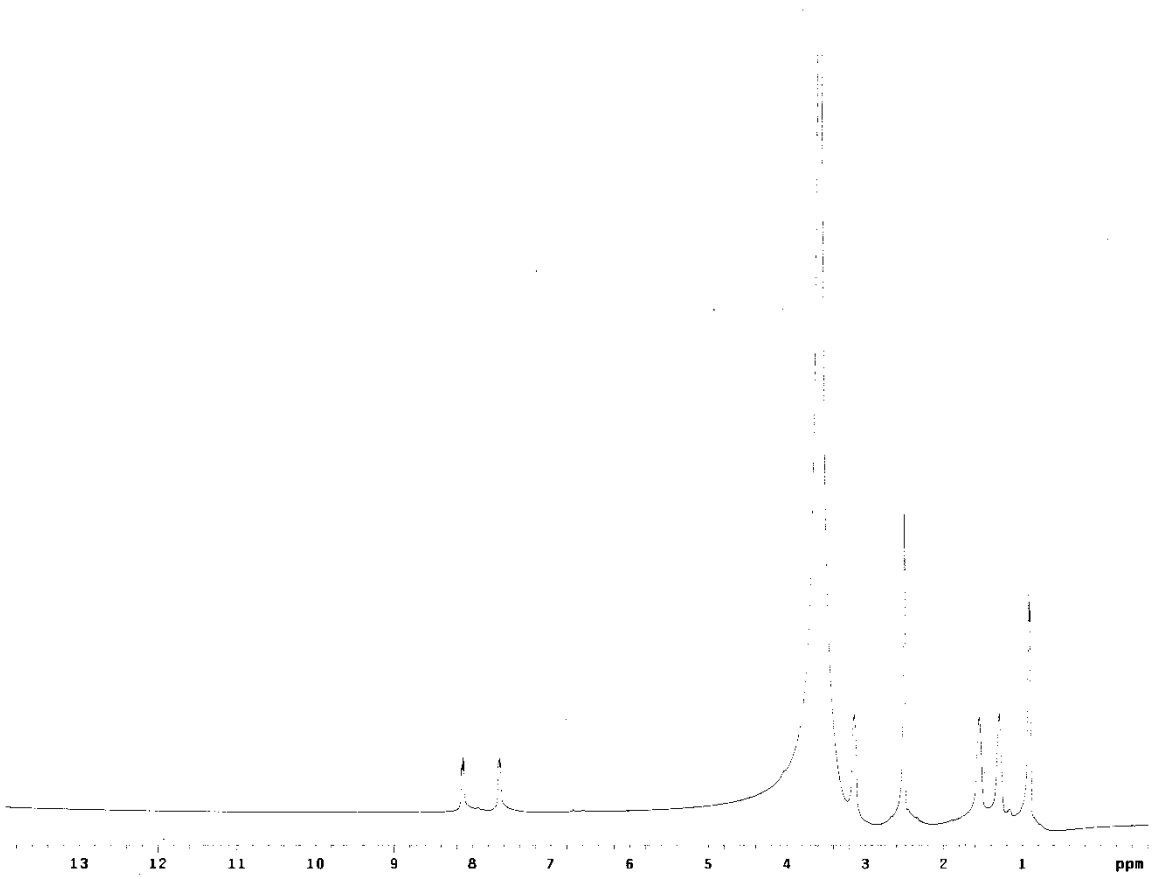

Figure A2.22 ^{1}H NMR spectrum of complex $(TBA)^+_2[\mathbf{HL_1}(F^-)]$, **1a** (400 MHz, DMSO-$d_6$).

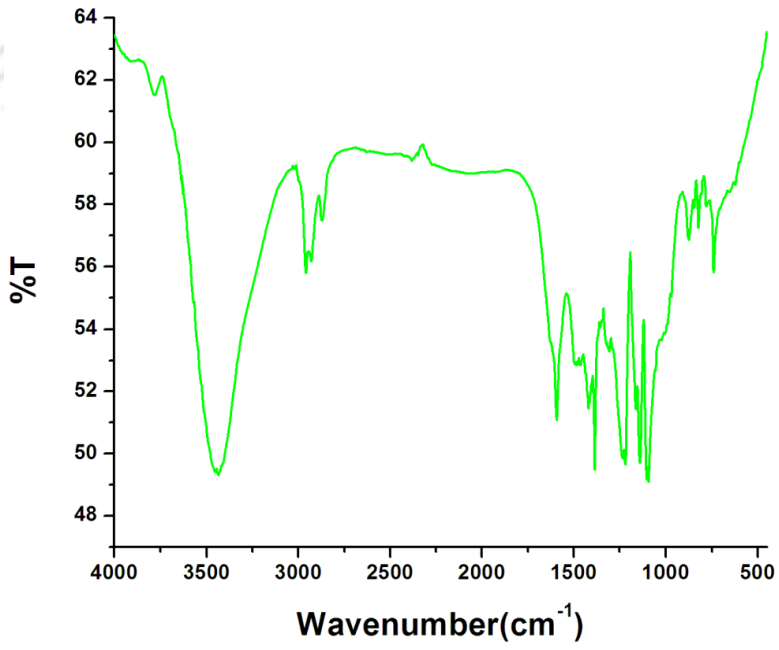

Figure A2.23 FT-IR spectrum of $(TBA)^+_2[\mathbf{HL_1}(F^-)]$, **1a** recorded in KBr pellet.

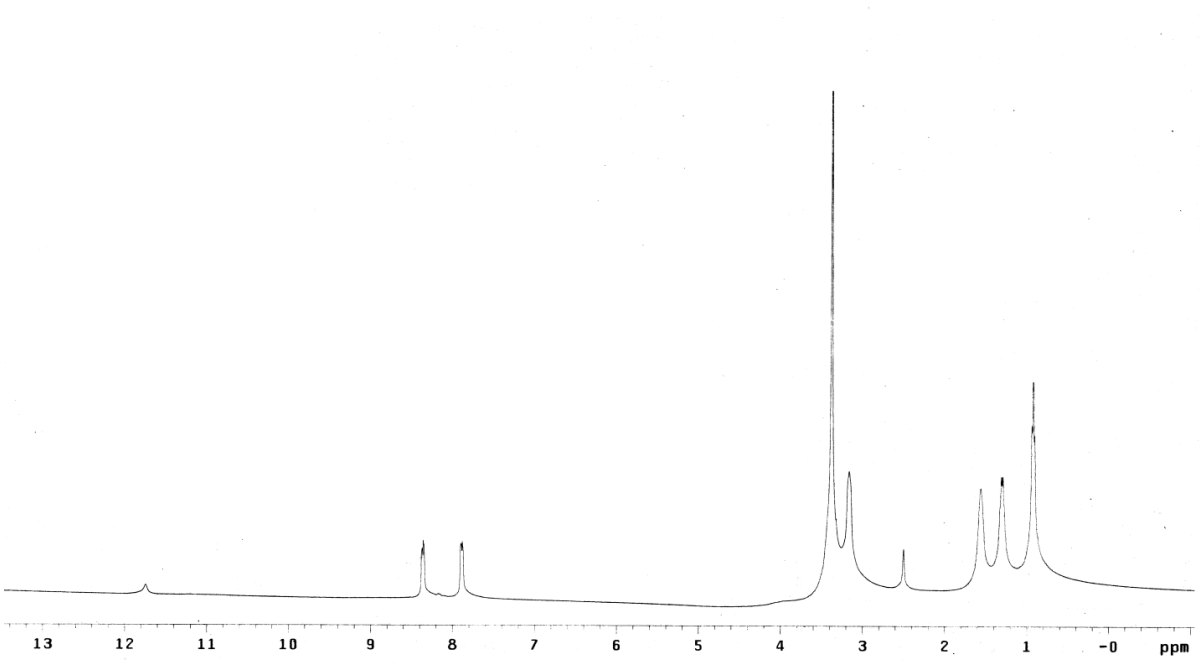

Figure A2.24 ^{1}H NMR spectrum of complex $(TBA)^{+}_{2}[\mathbf{H_2L_1}(Cl^{-})_2]\cdot H_2O$, **1b** (400 MHz, DMSO-$d_6$).

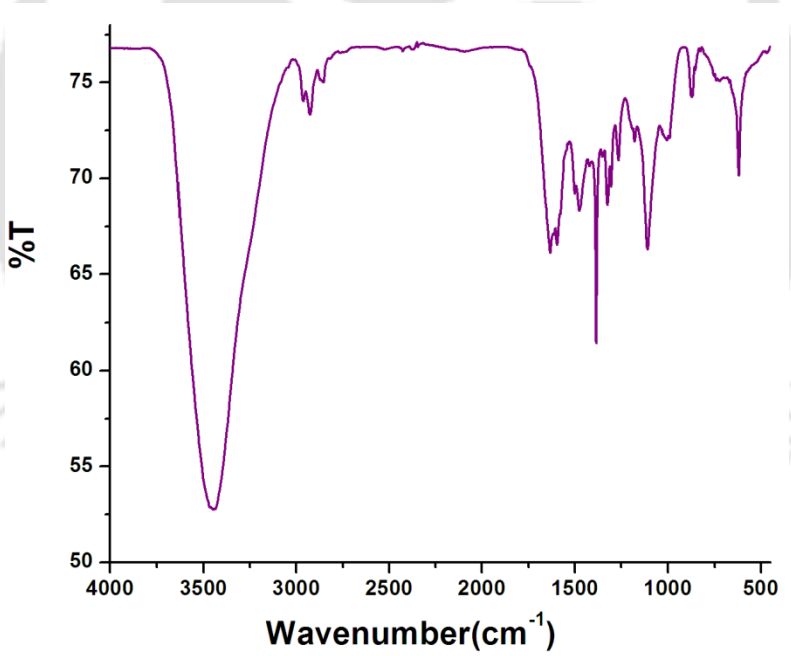

Figure A2.25 FT-IR spectrum of complex $(TBA)^{+}_{2}[\mathbf{H_2L_1}(Cl^{-})_2]\cdot H_2O$, **1b** recorded in KBr pellet.

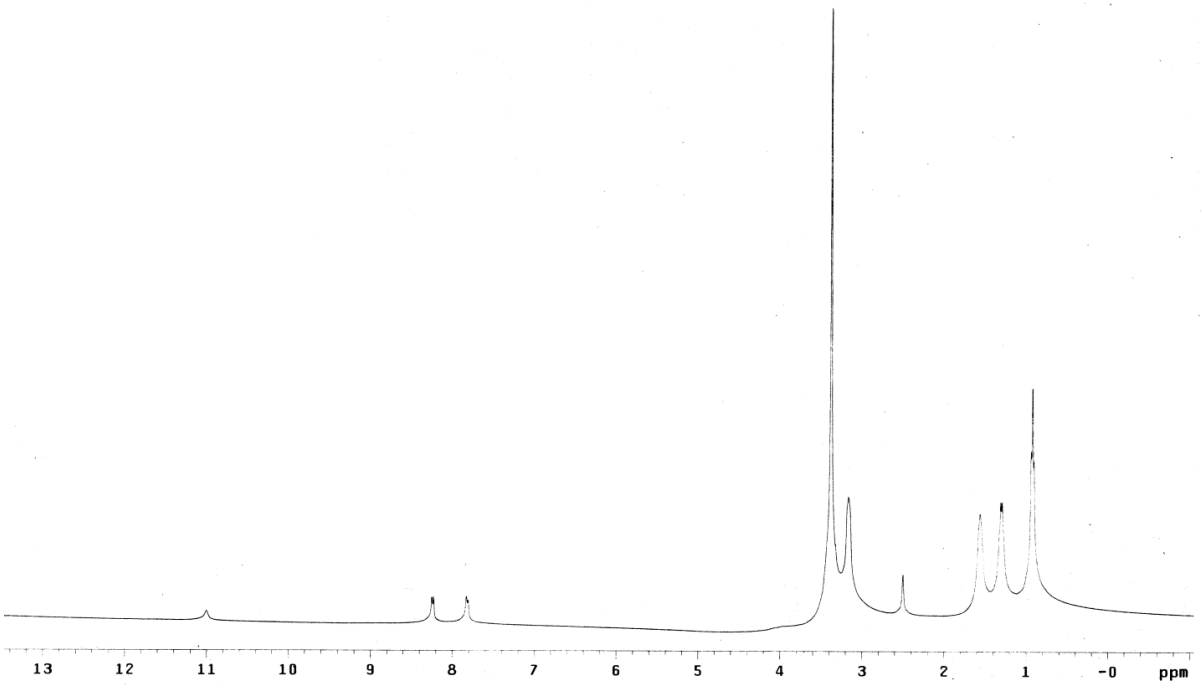

Figure A2.26 ^{1}H NMR spectrum of complex $(TBA)^{+}_{2}[\mathbf{H_2L_1}(Br^{-})_2]\cdot H_2O$, **1c** (400 MHz, DMSO-$d_6$).

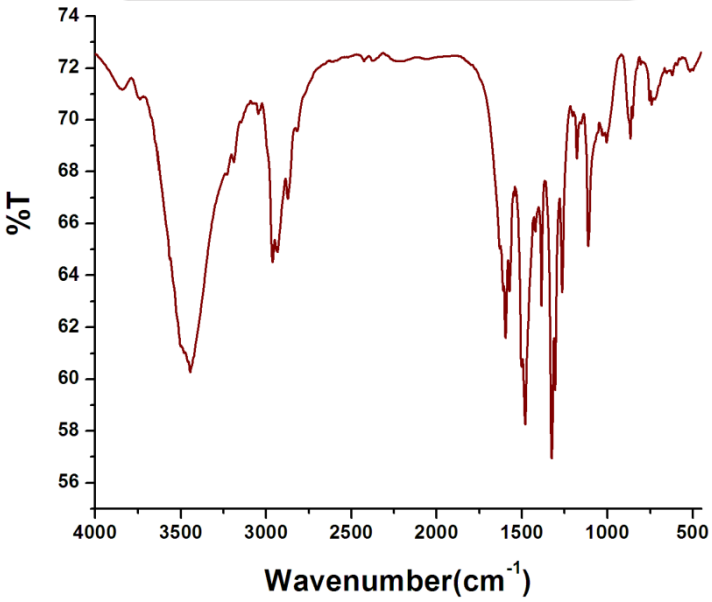

Figure A2.27 FT-IR spectrum of complex $(TBA)^{+}_{2}[\mathbf{H_2L_1}(Br^{-})_2]\cdot H_2O$, **1c** recorded in KBr pellet.

Characterization data of anion complexes of L_2 (2a-2b):

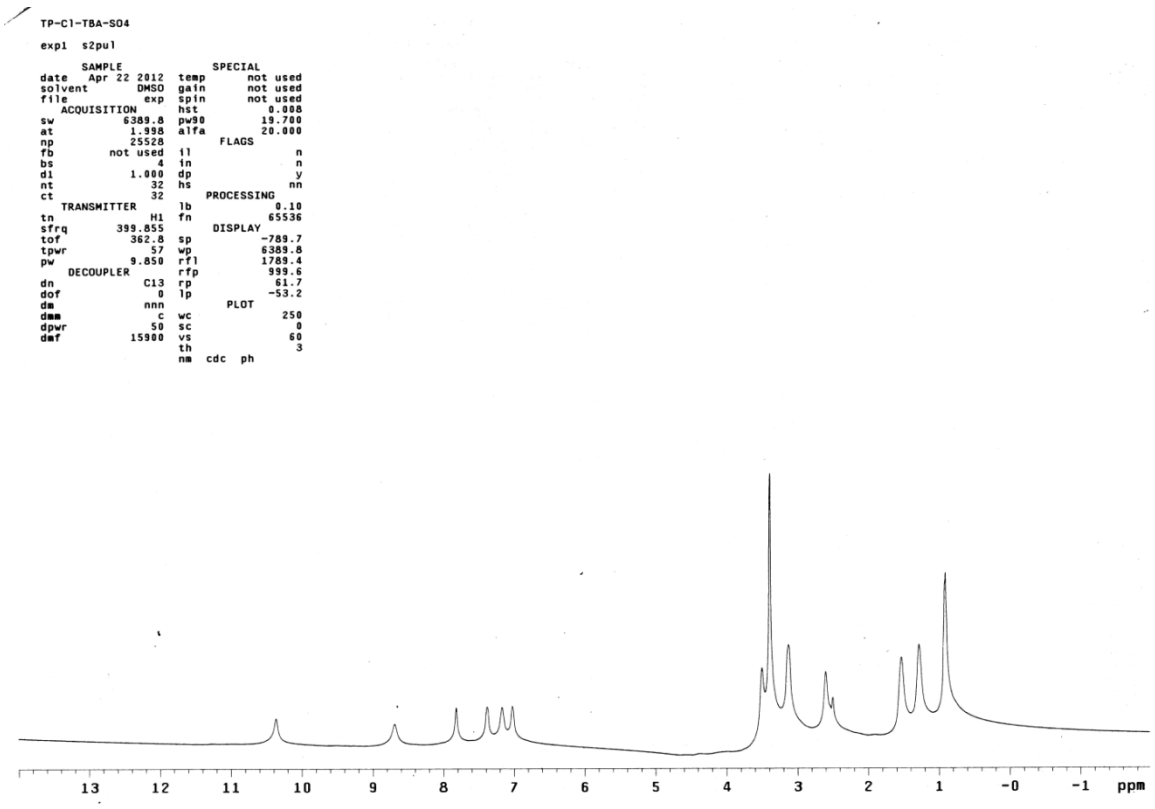

Figure A2.28 ^{1}H NMR spectrum of complex 2TBA^{+}[2$\mathbf{L}_2$(SO_4^{2-})], **2a** (400 MHz, DMSO-d_6).

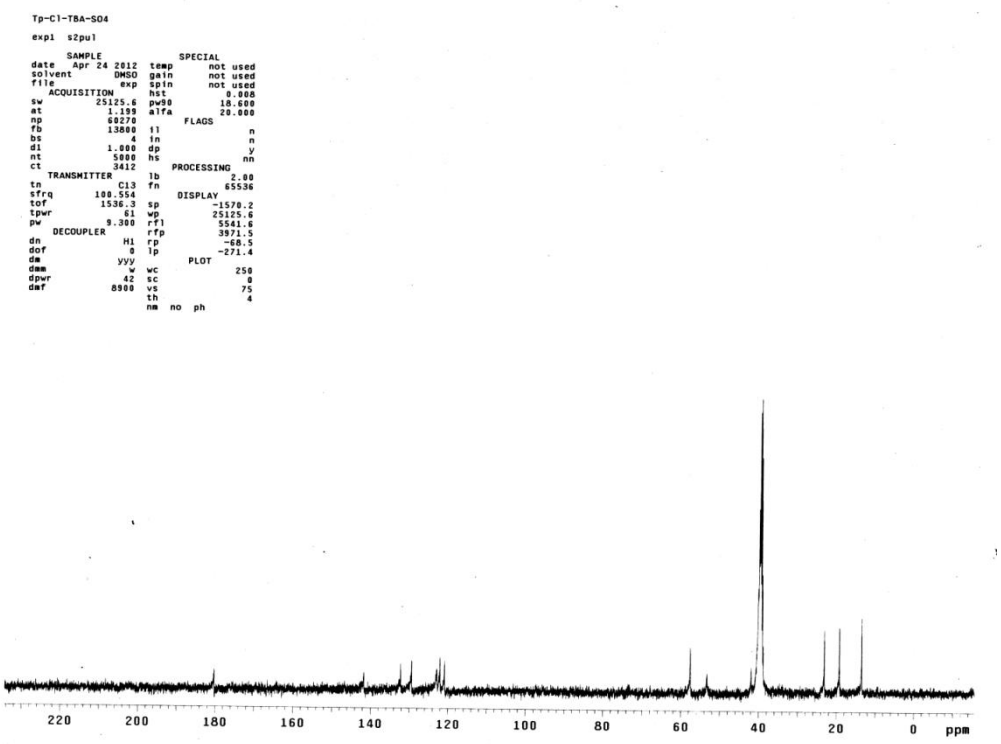

Figure A2.29 ^{13}C NMR spectrum of complex 2TBA^{+}[2$\mathbf{L}_2$(SO_4^{2-})], **2a** (100 MHz, DMSO-d_6).

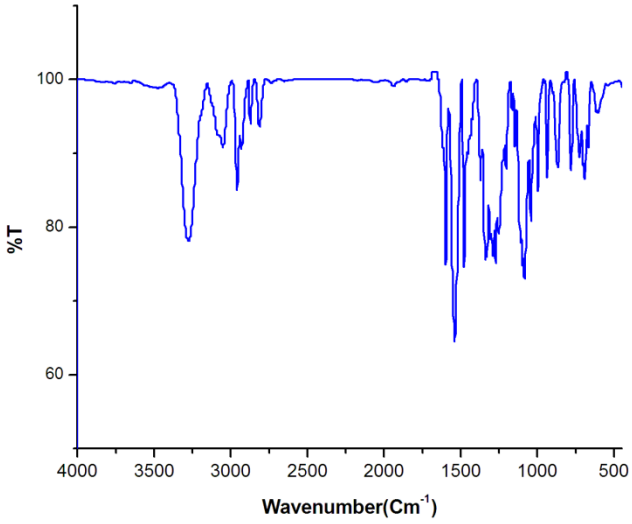

Figure A2.30 FT-IR spectrum of complex $2TBA^{+}[2\mathbf{L}_2(SO_4^{2-})]$, **2a** recorded in KBr pellet.

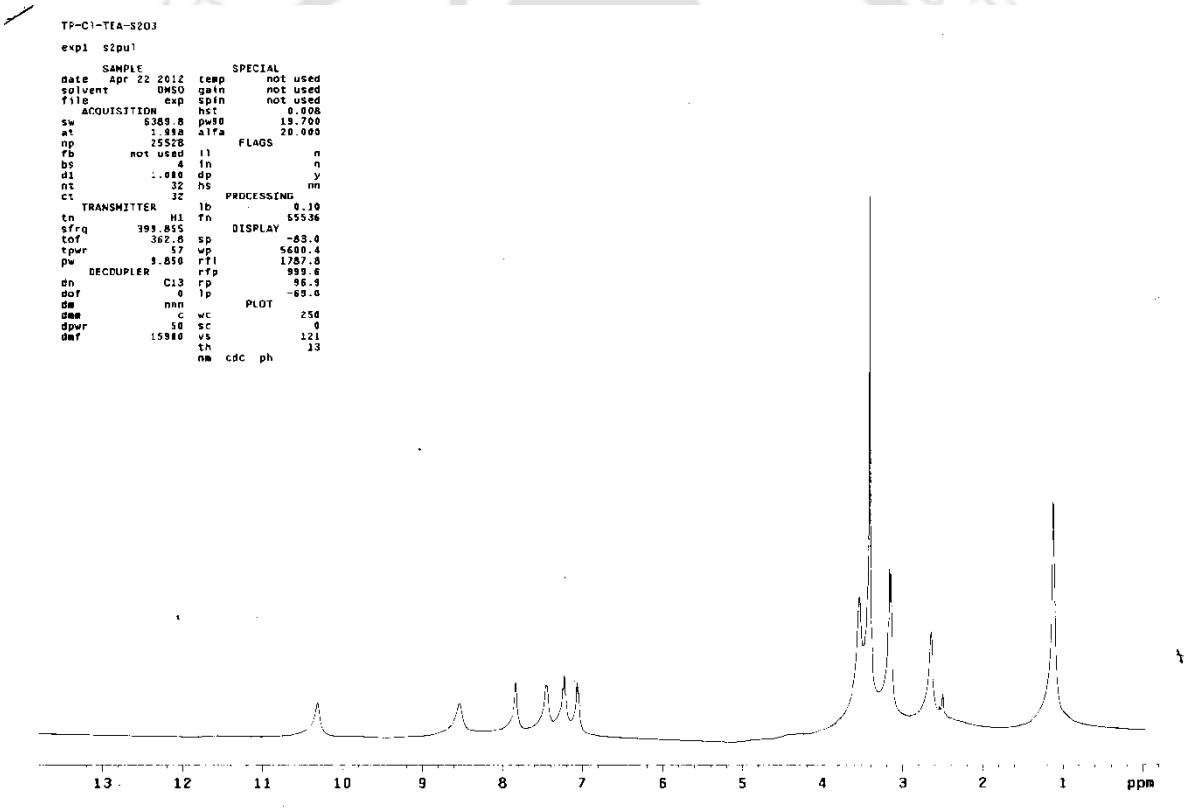

Figure A2.31 ^{1}H NMR spectrum of complex $2TEA^{+}[2\mathbf{L}_2(S_2O_3^{2-})]$, **2b** (400 MHz, DMSO-$d_6$).

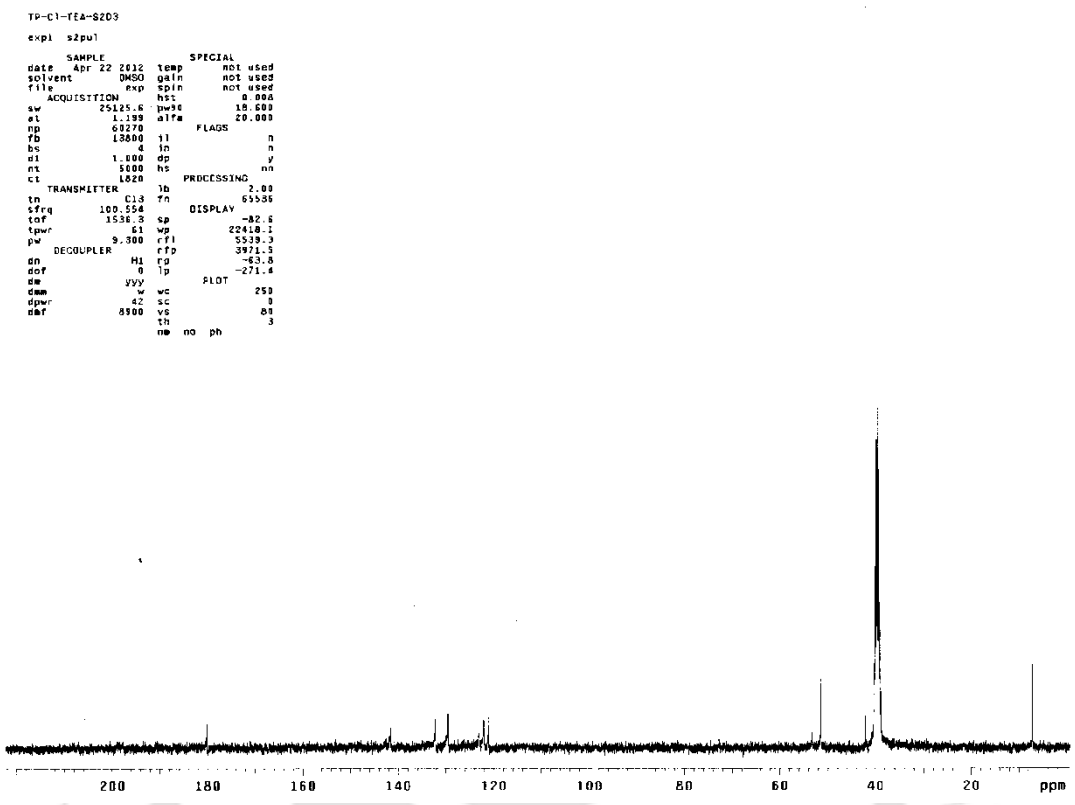

Figure A2.32 ^{13}C NMR spectrum of complex 2TEA^{+}[2**L**$_2$($S_2O_3^{2-}$)], **2b** (100 MHz, DMSO-d_6).

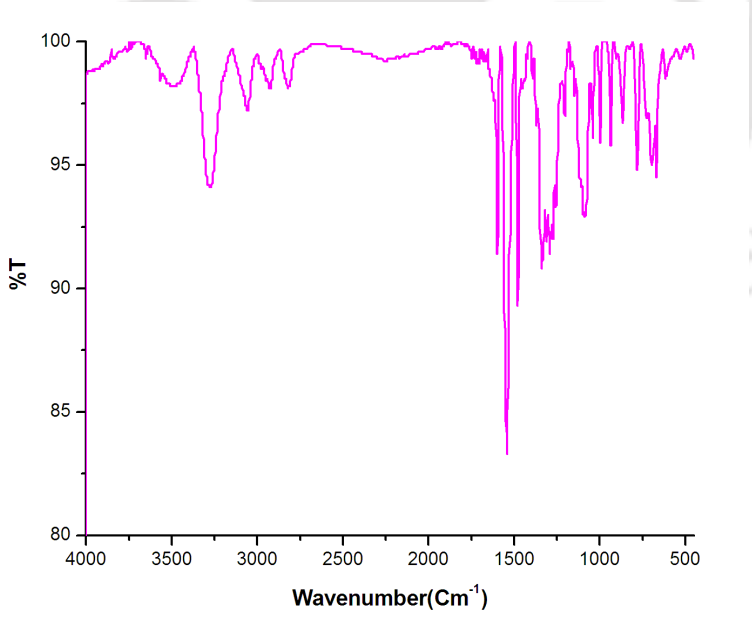

Figure A2.33 FT-IR spectrum of 2TEA^{+}[2**L**$_2$($S_2O_3^{2-}$)], **2b** recorded in KBr pellet.

Characterization data of anion complexes of L_3 (3a-3f):

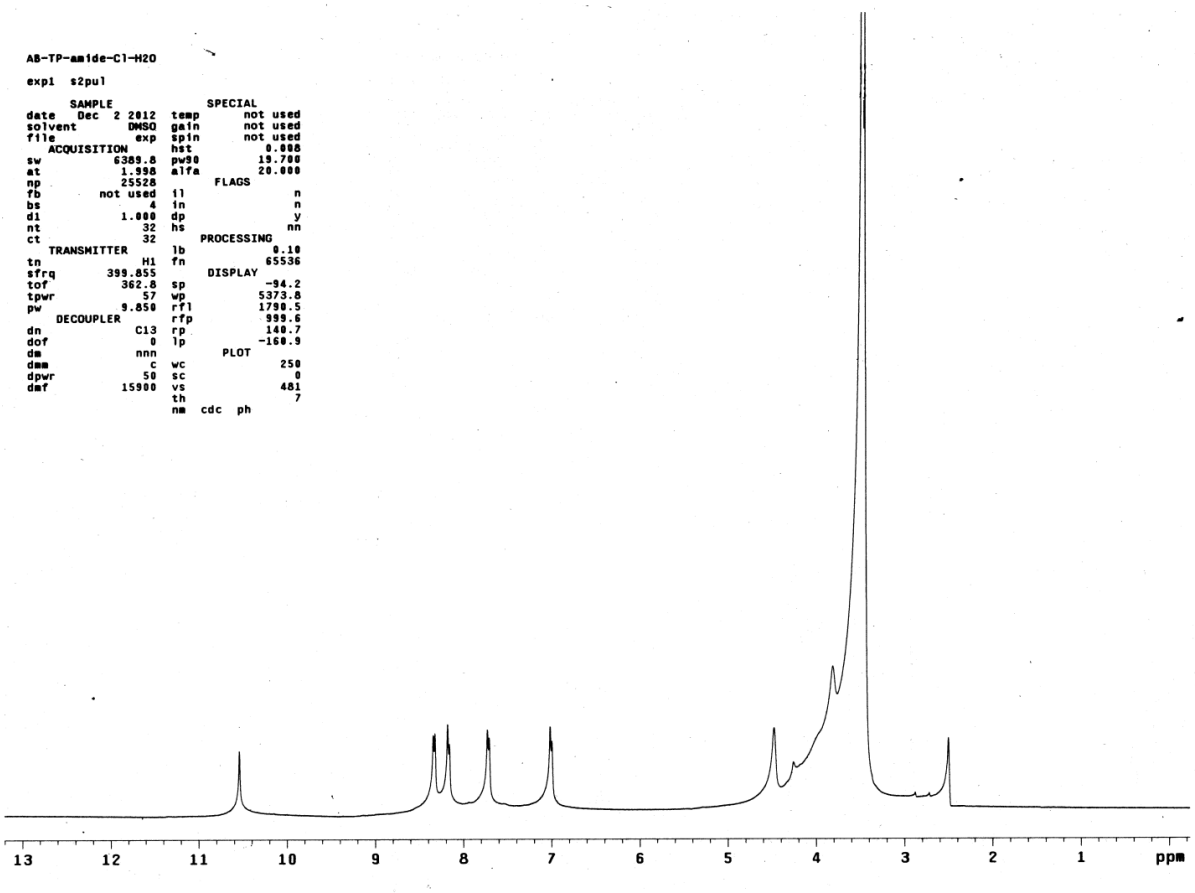

Figure A2.34 ^{1}H NMR spectrum of complex $[(\mathbf{L_3H})^+.Cl^-].H_2O$, **3a** (400 MHz, DMSO-$d_6$).

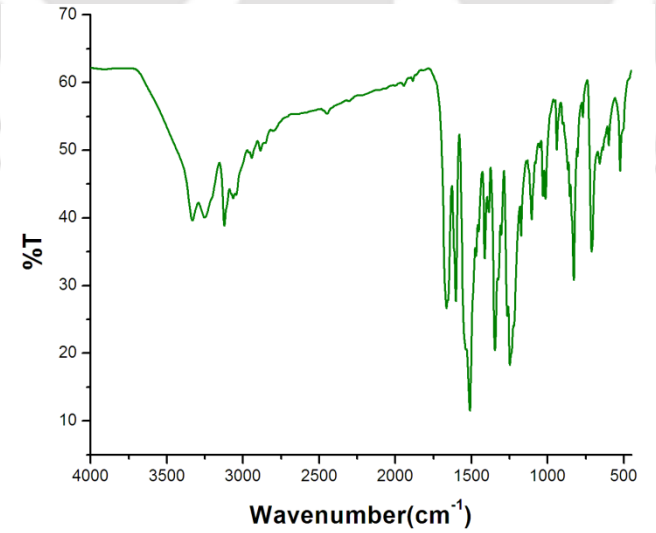

Figure A2.35 FT-IR spectrum of complex $[(\mathbf{L_3H})^+.Cl^-].H_2O$, **3a** recorded in KBr pellet.

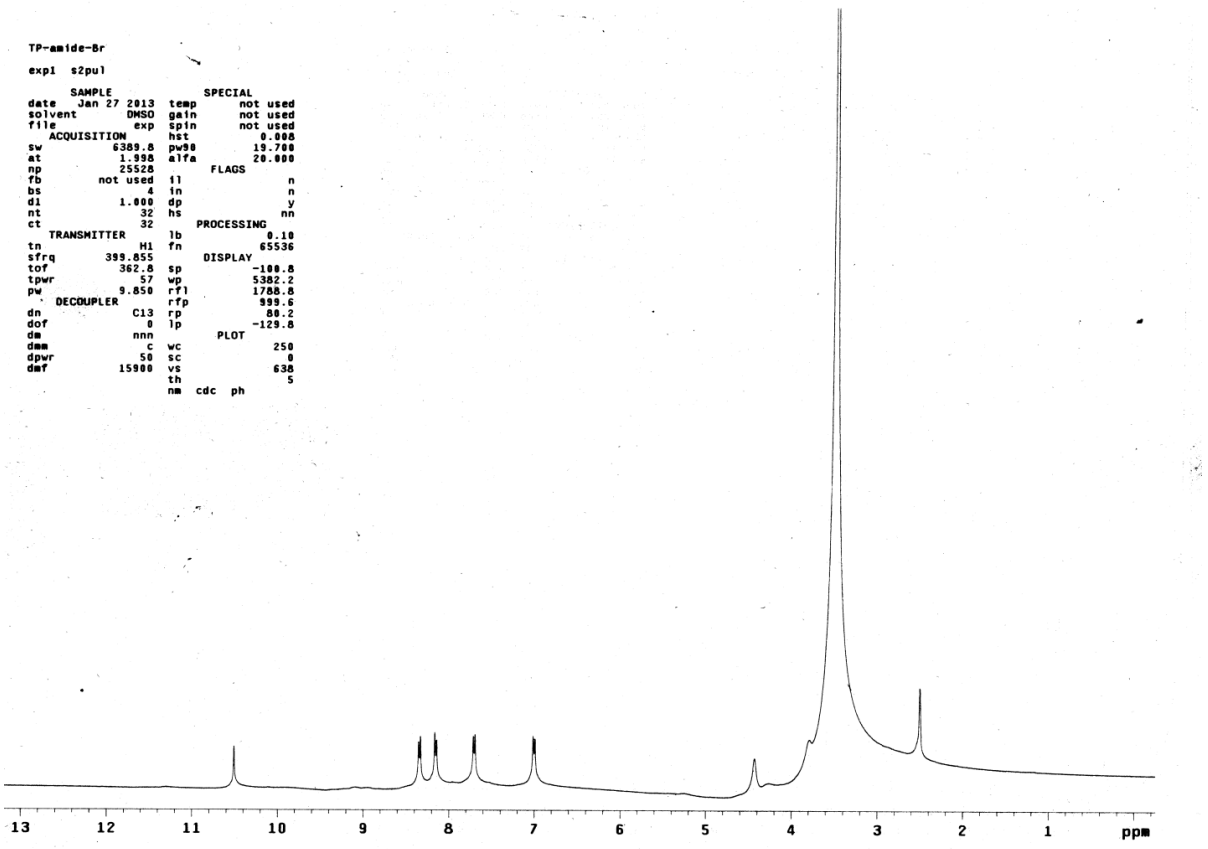

Figure A2.36 ^{1}H NMR spectrum of complex [(**L$_3$H**)$^+$.Br$^-$].H$_2$O, **3b** (400 MHz, DMSO-d$_6$).

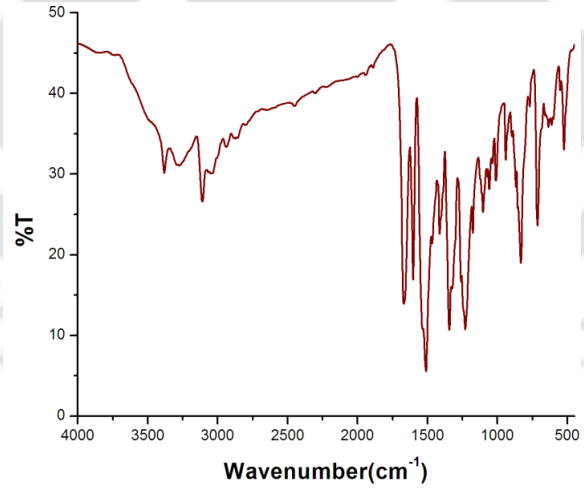

Figure A2.37 FT-IR spectrum of complex [(**L$_3$H**)$^+$.Br$^-$].H$_2$O, **3b** recorded in KBr pellet.

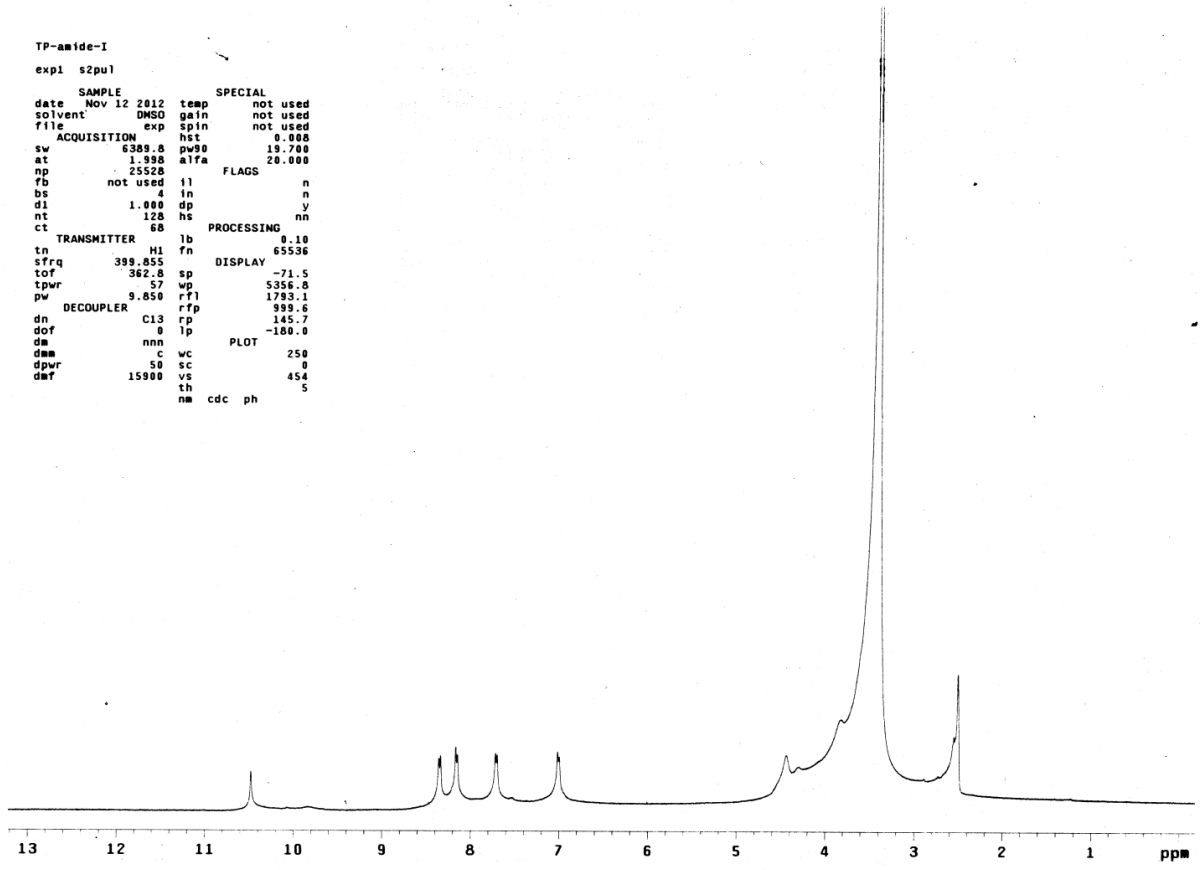

Figure A2.38 ^{1}H NMR spectrum of complex $[(\mathbf{L_3H})^{+}.I^{-}]$, **3c** (400 MHz, DMSO-$d_6$).

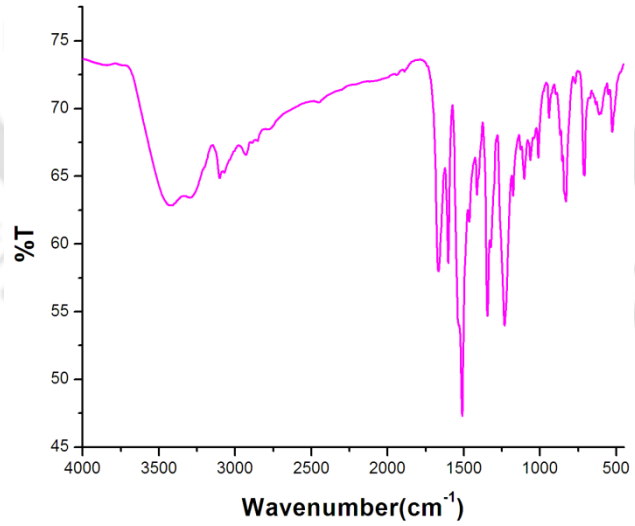

Figure A2.39 FT-IR spectrum of complex $[(\mathbf{L_3H})^{+}.I^{-}]$, **3c** recorded in KBr pellet.

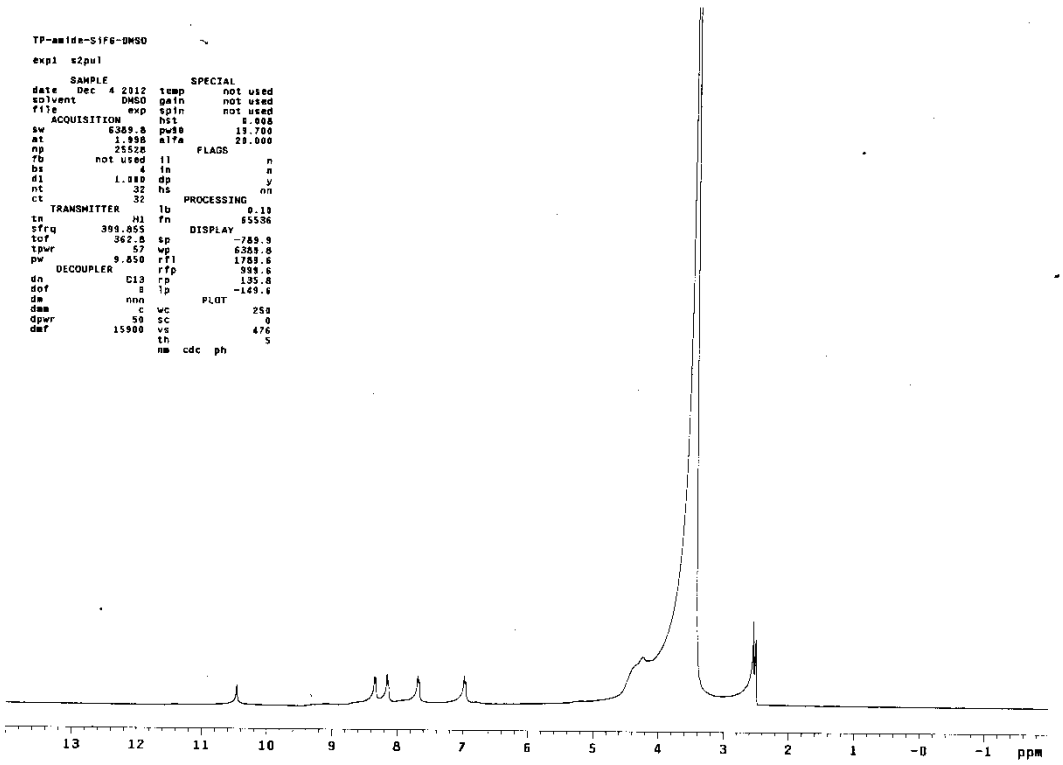

Figure A2.40 ^{1}H NMR spectrum of complex $[(\mathbf{L_3H})_2^{+}.SiF_6^{2-}]$, **3d** (400 MHz, DMSO-$d_6$).

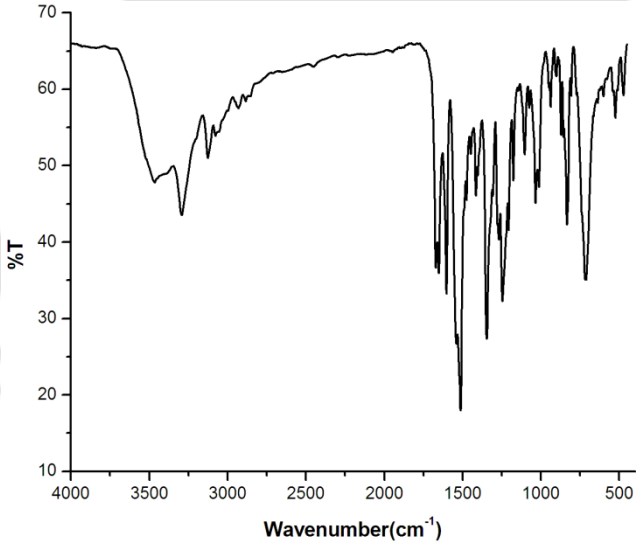

Figure A2.41 FT-IR spectrum of complex $[(\mathbf{L_3H})_2^{+}.SiF_6^{2-}]$, **3d** recorded in KBr pellet.

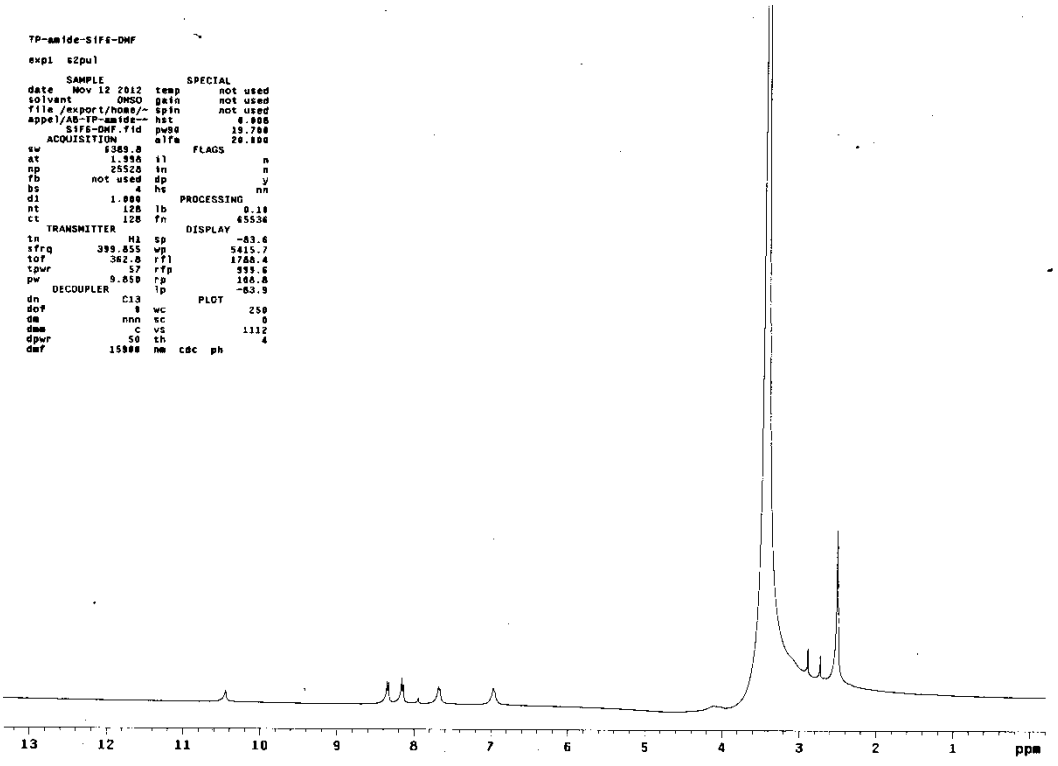

Figure A2.42 ^{1}H NMR spectrum of complex $[(\mathbf{L_3H})_2^{+}.SiF_6^{-}]\cdot 2DMF,4H_2O$, **3e** (400 MHz, DMSO-$d_6$).

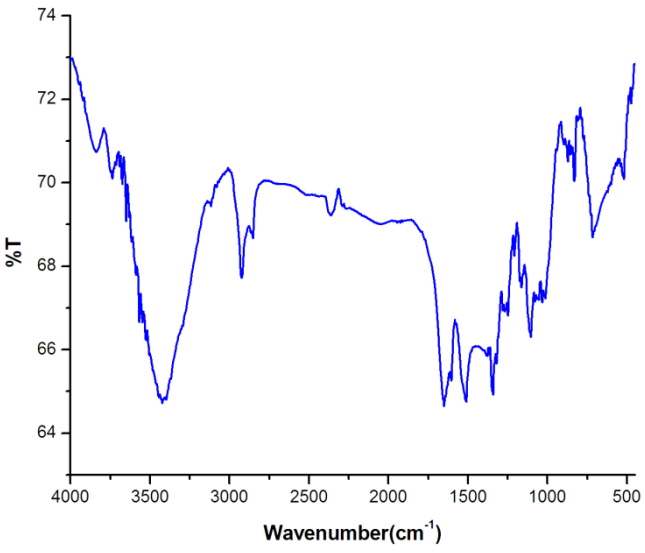

Figure A2.43 FT-IR spectrum of complex $[(\mathbf{L_3H})_2^{+}.SiF_6^{-}]\cdot 2DMF,4H_2O$, **3e** recorded in KBr pellet.

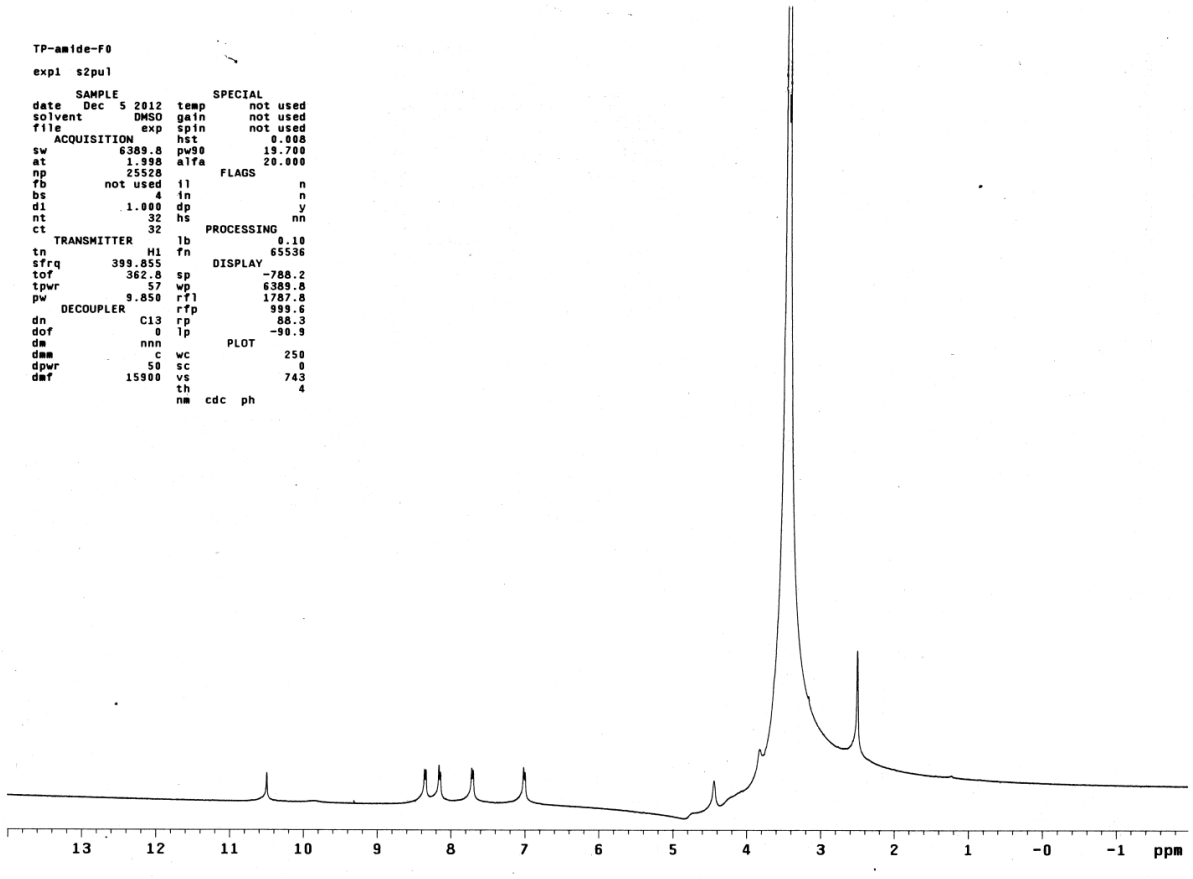

Figure A2.44 ^{1}H NMR spectrum of complex [(**L$_3$H**)$^{+}$.(ClO_4)$^{-}$], **3f** (400 MHz, DMSO-d_6).

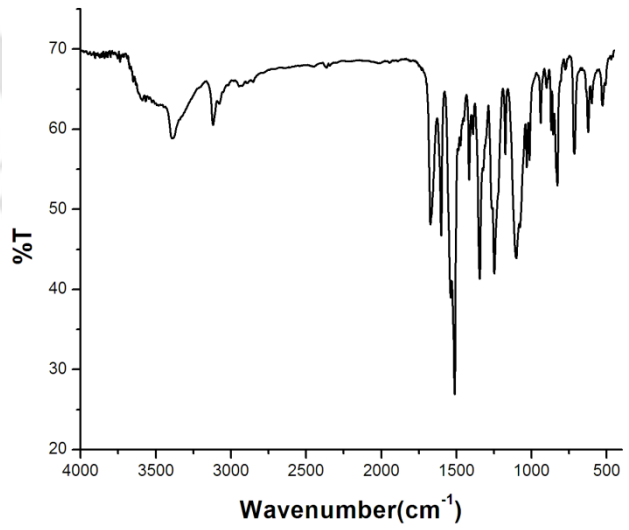

Figure A2.45 FT-IR spectrum of complex [(**L$_3$H**)$^{+}$.(ClO_4)$^{-}$], **3f** recorded in KBr pellet.

Characterization data of anion complexes of L_4 (4a-4c):

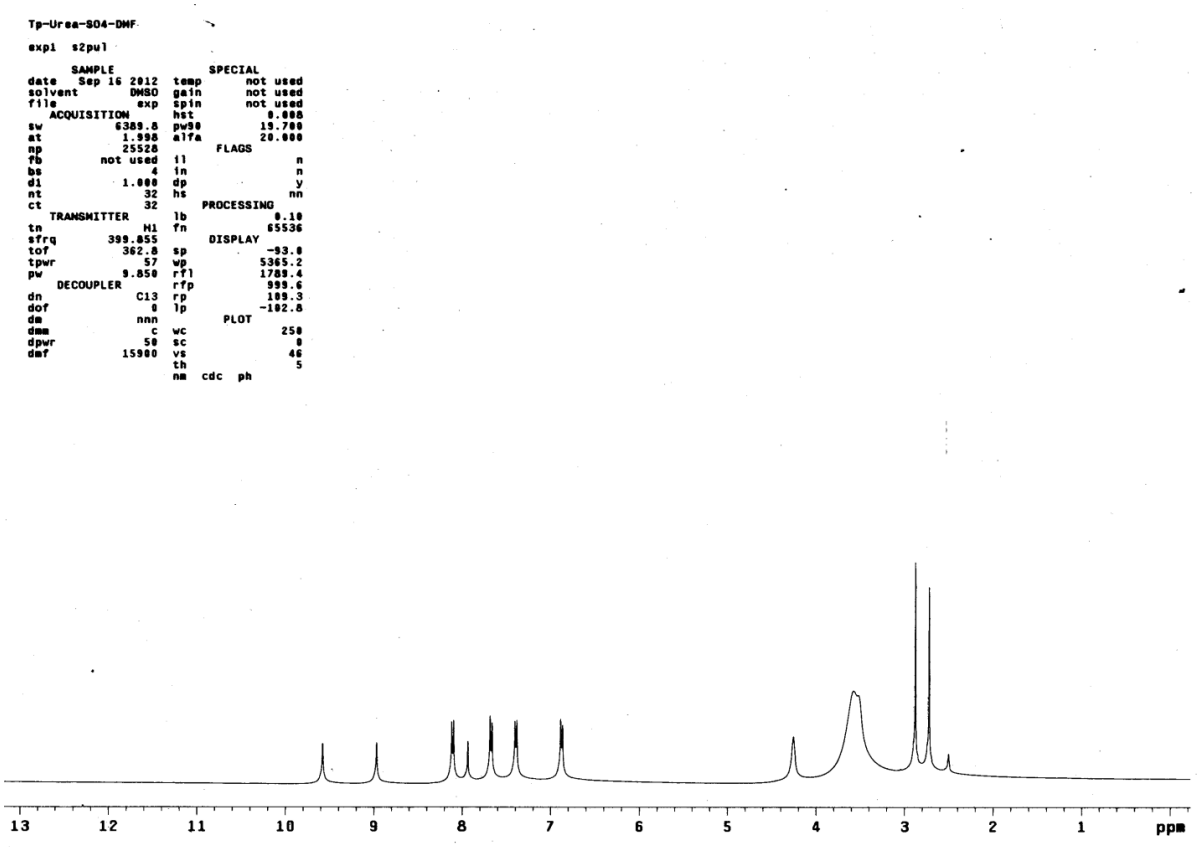

Figure A2.46 ^{1}H NMR spectrum of complex $[(\mathbf{L_4H})_2^+.(SO_4)^{2-}]\cdot 4DMF,2H_2O$, **4a** (400 MHz, DMSO-$d_6$).

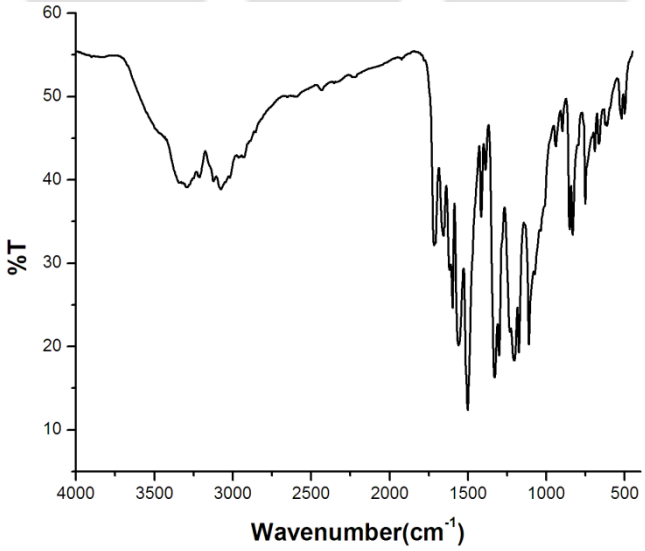

Figure A2.47 FT-IR spectrum of complex $[(\mathbf{L_4H})_2^+.(SO_4)^{2-}]\cdot 4DMF,2H_2O$, **4a** recorded in KBr pellet.

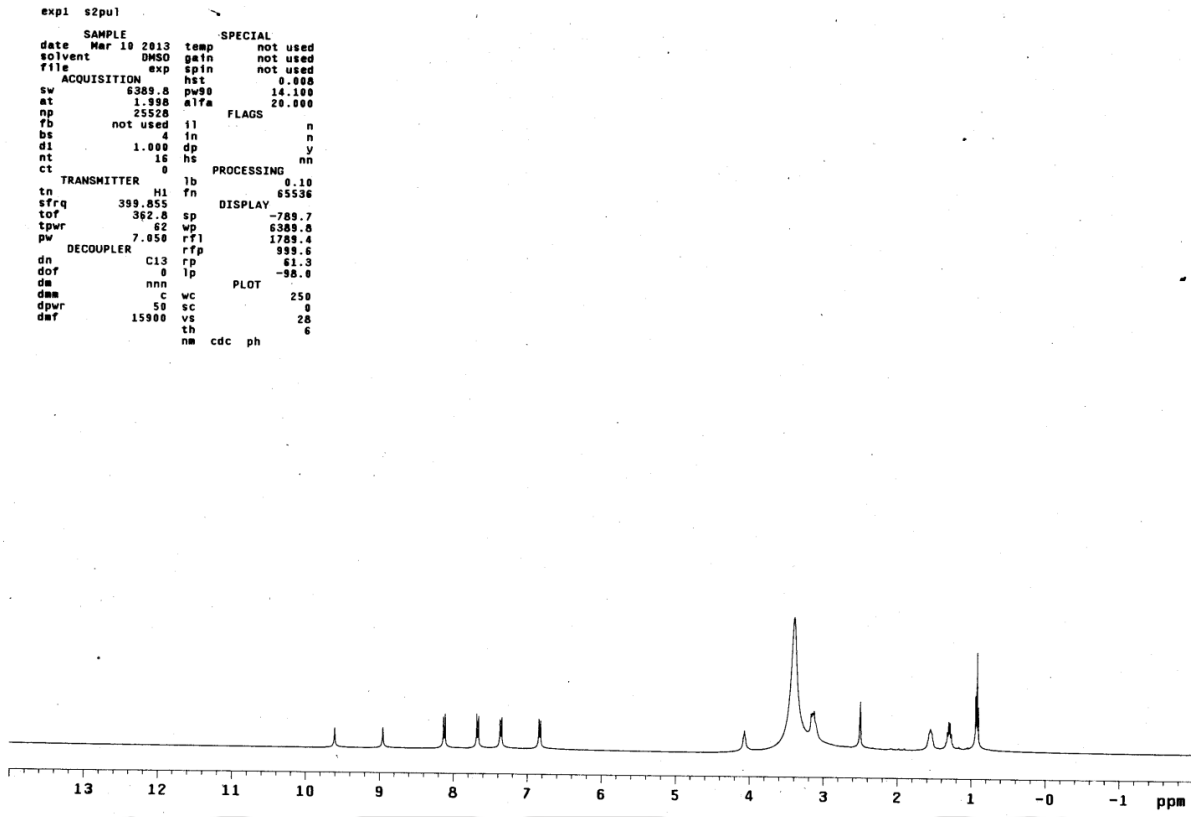

Figure A2.48 ^{1}H NMR spectrum of complex TBA^{+}[(**L$_4$H**)$^{+}$(SO_4^{2-})]·3H_2O, **4b** (400 MHz, DMSO-d_6).

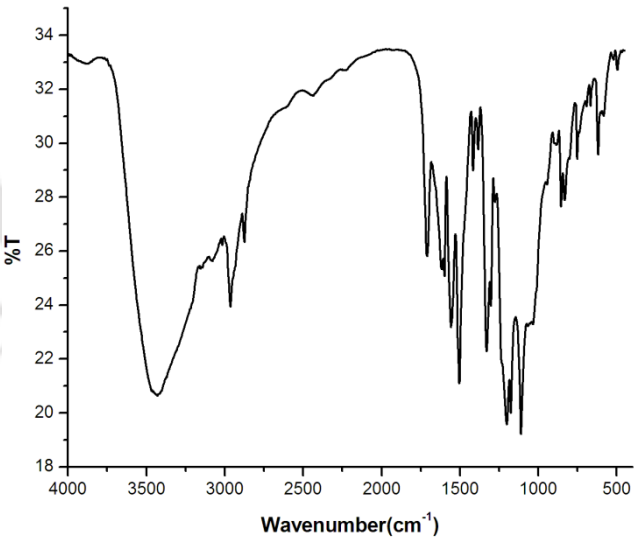

Figure A2.49 FT-IR spectrum of complex [(**L$_4$H**)$_2^{+}$.$(SO_4)^{2-}$]·4DMF,2H_2O, **4a** recorded in KBr pellet.

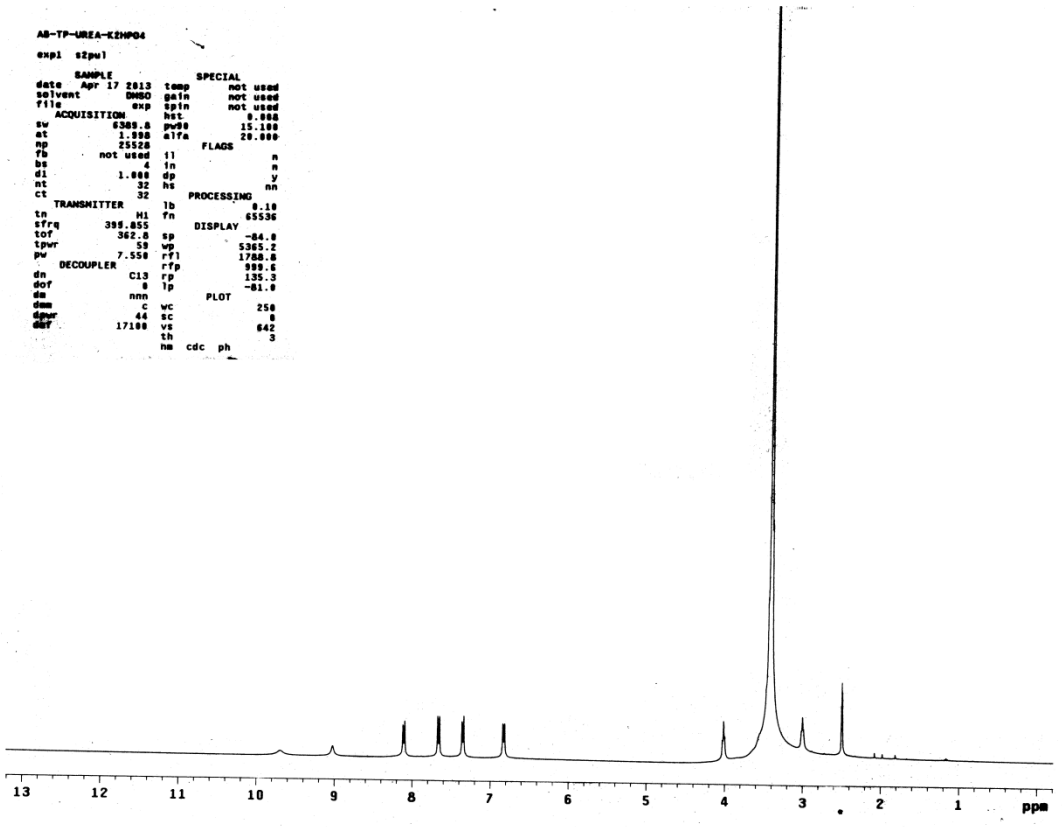

Figure A2.50 ^{1}H NMR spectrum of complex $K^{+}[K^{+}(\mathbf{L_4})_2(HPO_4)^{2-}]\cdot 23H_2O$, **4c** (400 MHz, DMSO-$d_6$).

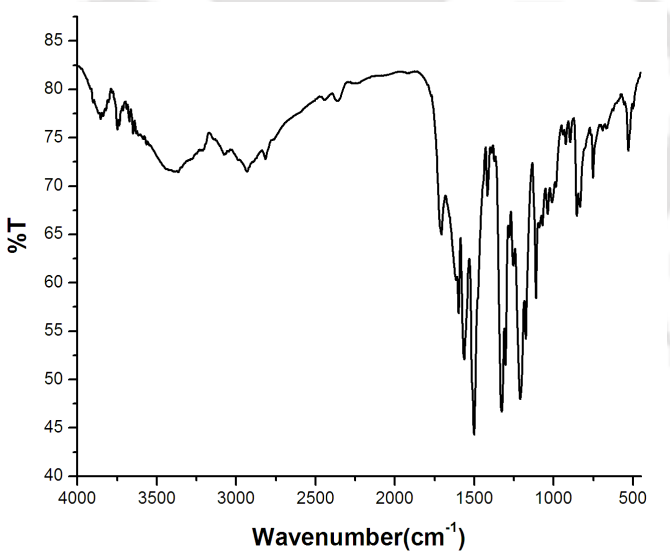

Figure A2.51 FT-IR spectrum of complex $K^{+}[K^{+}(\mathbf{L_4})_2(HPO_4)^{2-}]\cdot 23H_2O$, **4c** recorded in KBr pellet.

Annexure 3

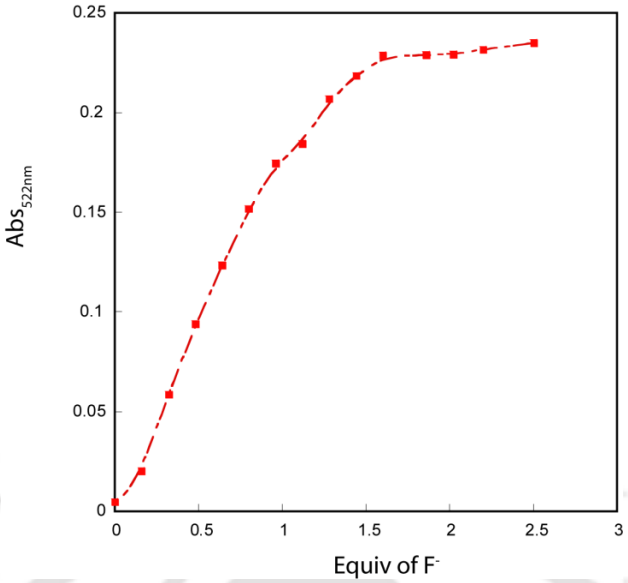

Figure A3.1 Absorbance changes for $\mathbf{H_2L_1}$ at 522 nm on addition of different equiv. of [*n*-Bu_4N^+]F^-.

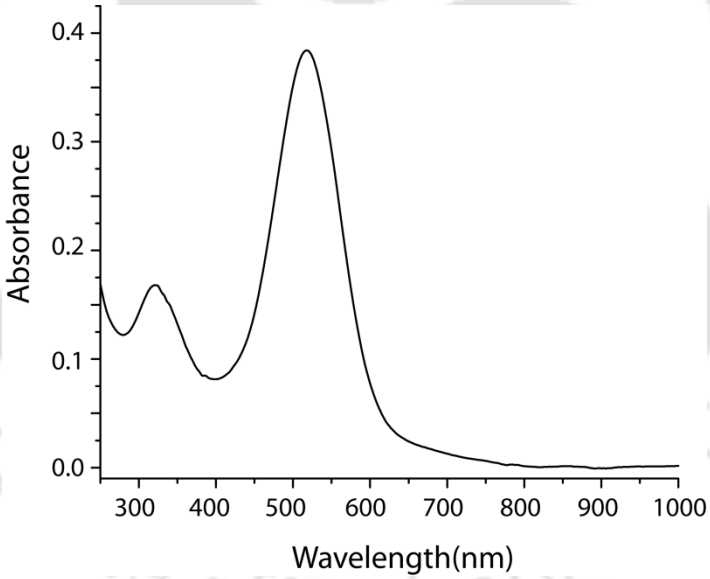

Figure A3.2 UV/Vis spectrum of the isolated single crystals of fluoride complex(**1a**) in acetonitrile.

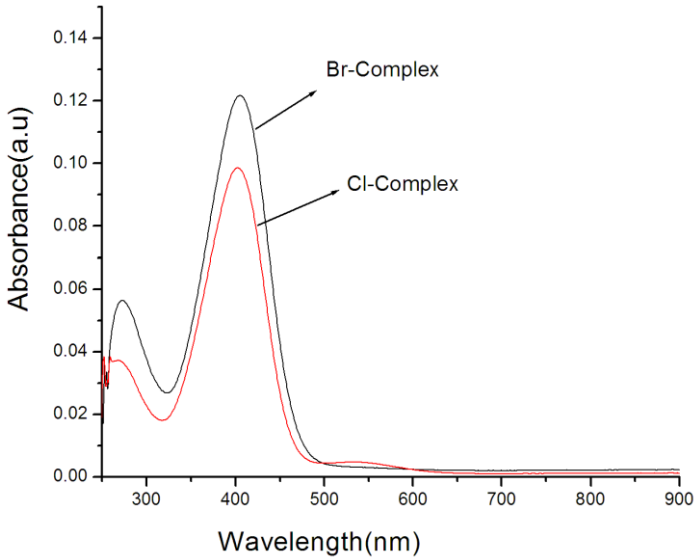

Figure A3.3 UV/Vis spectra of chloride complex (**1b**) and bromide complex (**1c**) in CH_3CN.

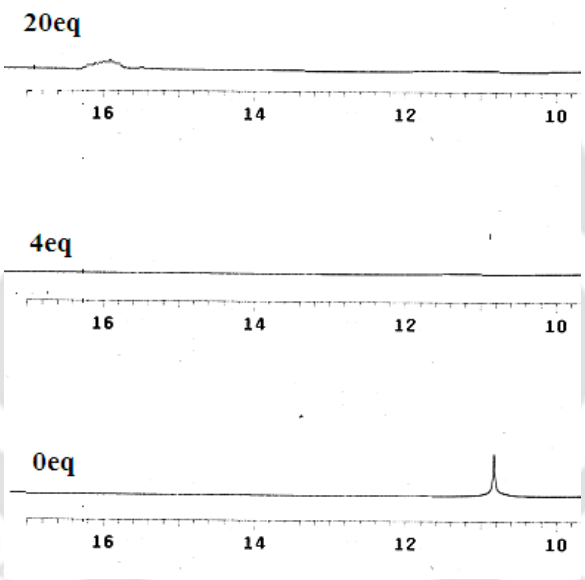

Figure A3.4 ^{1}H-NMR (400 MHz) spectra in DMSO-d_6 of $\mathbf{H_2L_1}$ upon incremental addition of [*n*-Bu_4N^+]F^- at RT.

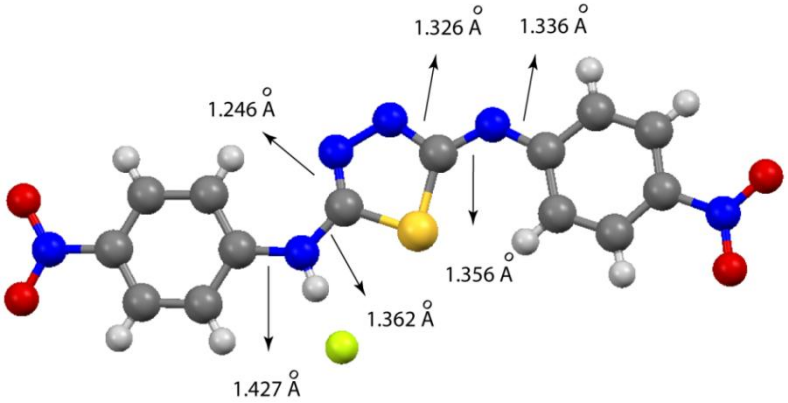

Figure. A3.5. Crystal structure of fluoride complex highlighting the significant bond lengths of the receptor ($\mathbf{HL_1^-}$).

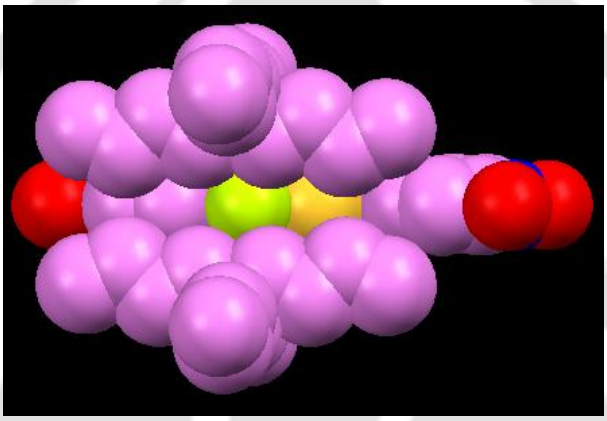

Figure A3.6. Showing the fluoride anion is exactly sandwiched between two tetrabutylammonium groups in **1a**.

Table A3.1 Step wise binding constants of the receptor $\mathbf{H_2L_1}$ with chloride and bromide anions.

Anion	**logK_1**	**logK_2**
Cl^-	1.37	2.55
Br^-	0.96	1.91

Table A3.2 Selected bond lengths comparison table of the receptor in the halide complexes (**1a-1c**).

Bonds	**Distances (Å)**		
	Chloride Complex(1b)	**Bromide Complex(1c)**	**Fluoride Complex(1a)**
C1-N2	1.385	1.380	1.427
N2-C7	1.378	1.376	1.362
C7-S1	1.736	1.705	1.733
C7-N3	1.281	1.312	1.246
N3-N4	1.399	1.401	1.386
N4-C8	1.279	1.252	1.326
C8-S1	1.731	1.714	1.764
C8-N5	1.388	1.372	1.356
N5-C9	1.373	1.362	1.336

Annexure 4

Table A4.1 Hydrogen-Bonding parameters for $\mathbf{L_2}$.

D—H····O	H····O	D····O	D−H….O(deg)
L3			
N6-H····S1	2.54	3.404(3)	171.7(2)
N7-H····S1	2.84	3.649(2)	156.7(2)
C11-H11A····S1	2.93	3.784(3)	147.0(2)

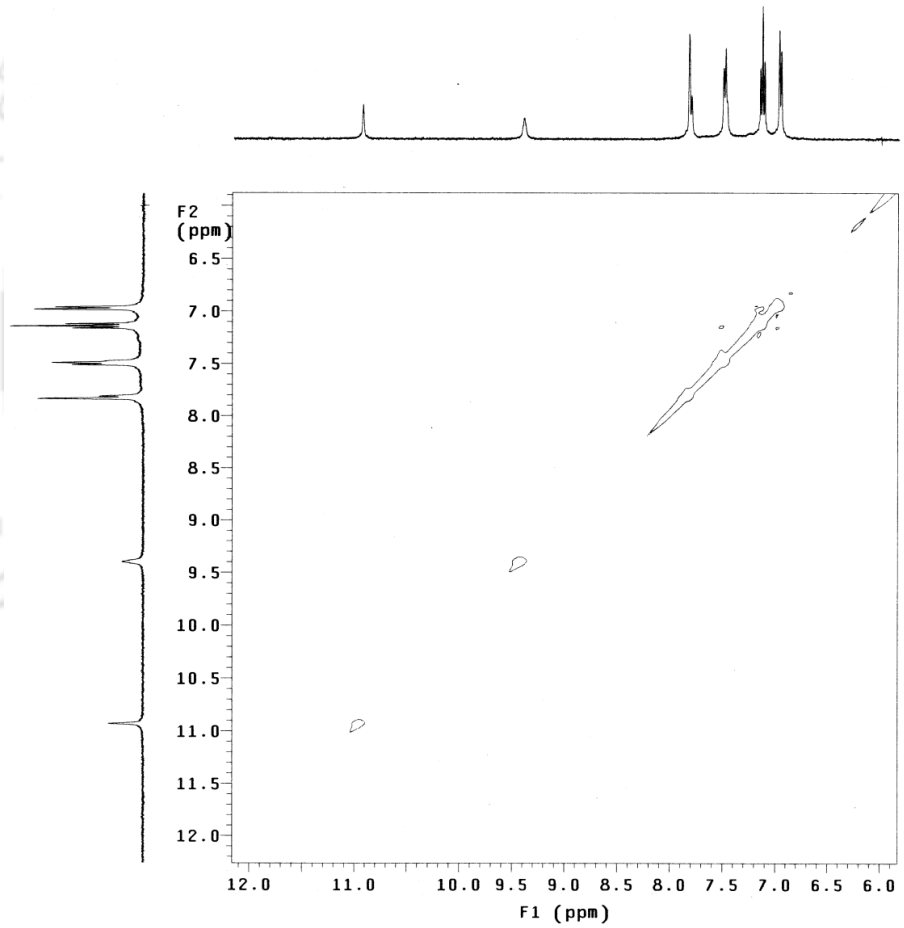

Figure A4.1 NOESY spectrum of $\mathbf{L_2}$ in presence of one equivalent SO_4^{2-} anion recorded in DMSO-d_6 at 298 K.

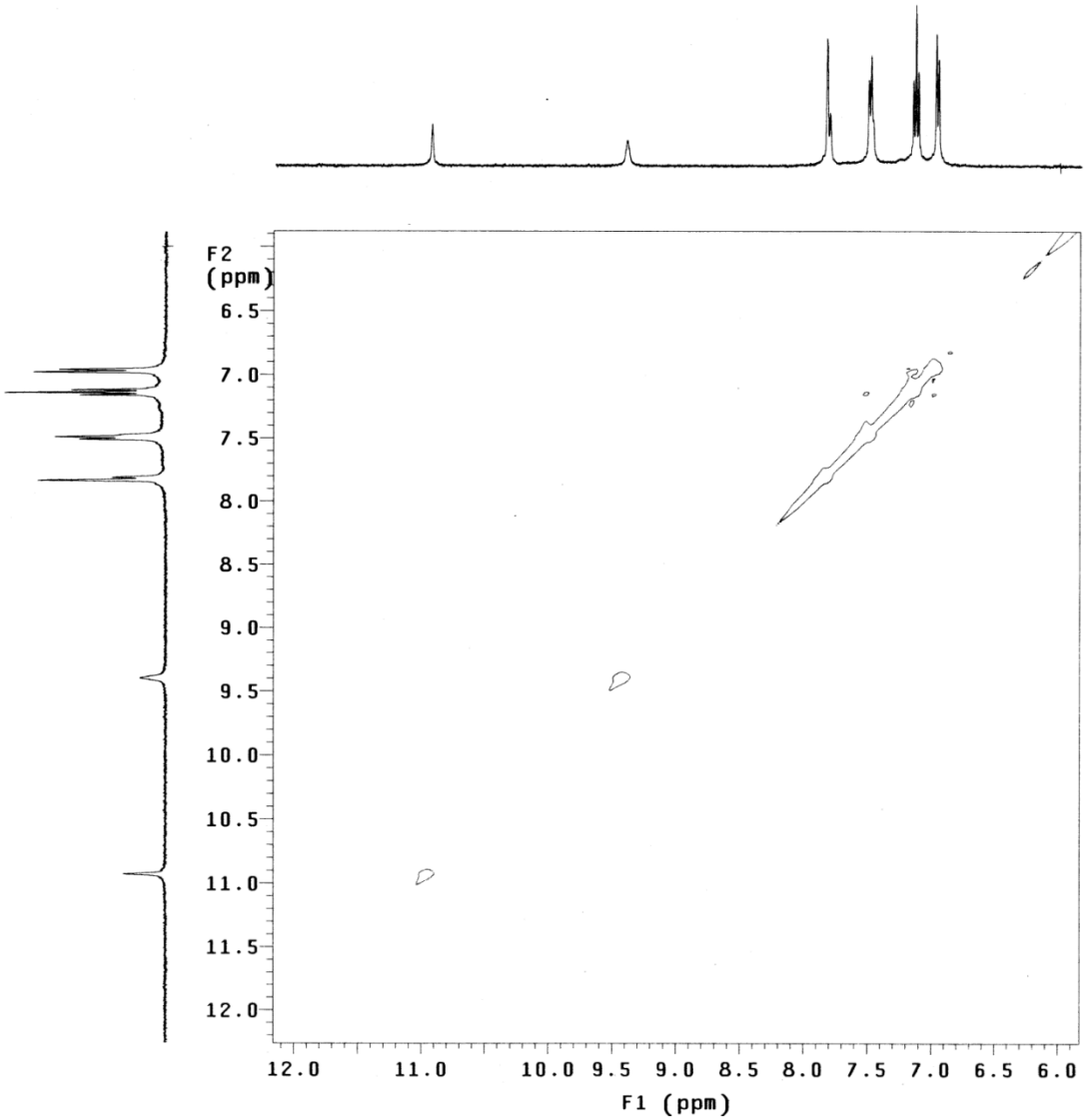

Figure A4.2 NOESY spectrum of $\mathbf{L_2}$ in presence of one equivalent $S_2O_3^{2-}$ anion recorded in DMSO-d_6 at 298 K.

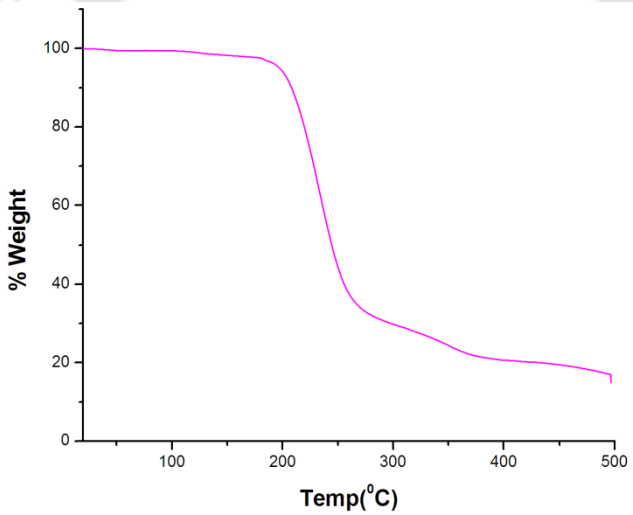

Figure A4.3 Thermogravimetricanalysis (TGA) curve of complex **2a** at a heating rate of 10°C per min.

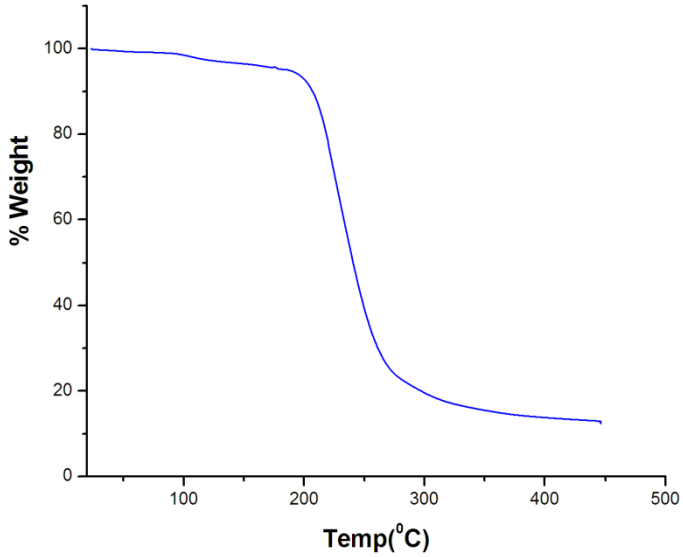

Figure A4.4 Thermogravimetricanalysis (TGA) curve of complex **2b** at a heating rate of 10°C per min.

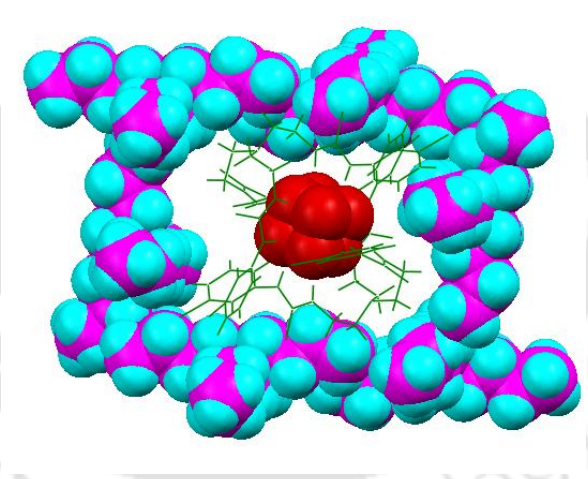

Figure A4.5 Depicting sulfate encapsulated receptor segment is present in the hydrophobic pocket of TBA counter cations in complex **2a**.

Annexure 5

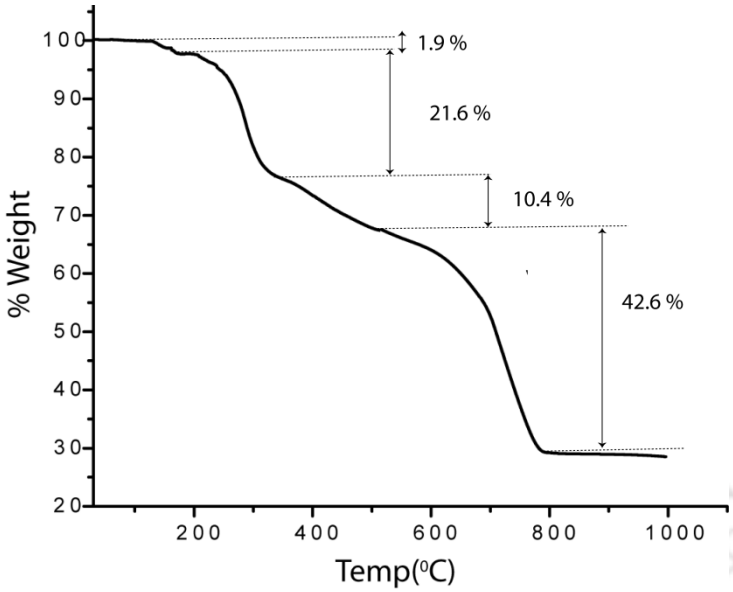

Figure A5.1 Thermo gravimetric (TGA) curve of complex **3a** obtained at a heating rate of 5°C/min in N_2 atmosphere.

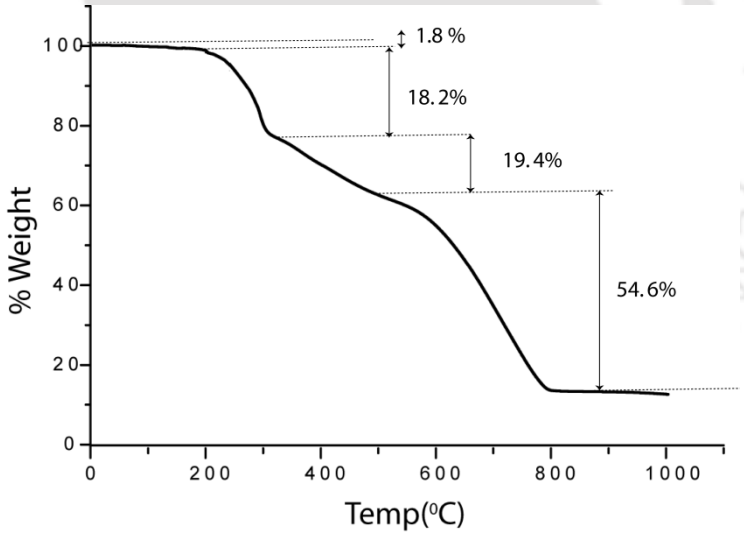

Figure A5.2 Thermo gravimetric (TGA) curve of complex **3b** obtained at a heating rate of 5°C/min in N_2 atmosphere.

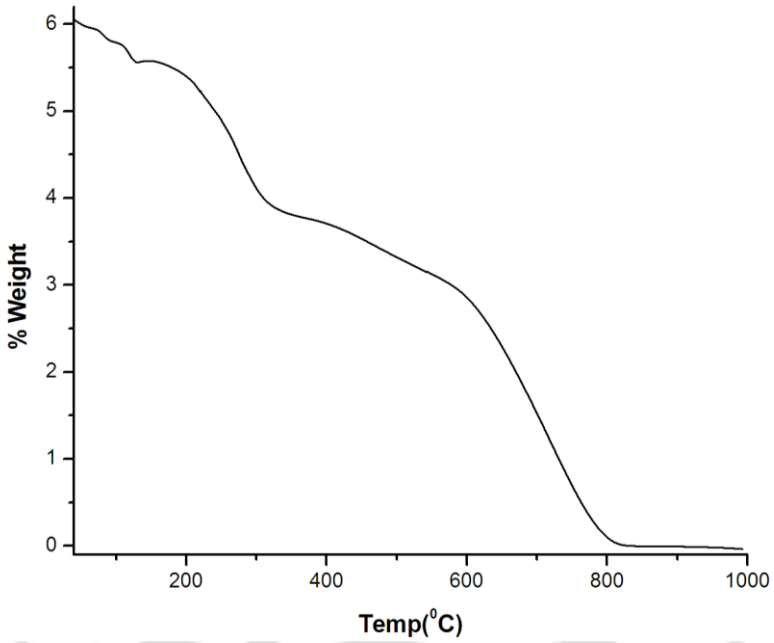

Figure A.5.3 Thermo gravimetric (TGA) curve of complex **3c** obtained at a heating rate of 5°C/min in N_2 atmosphere.

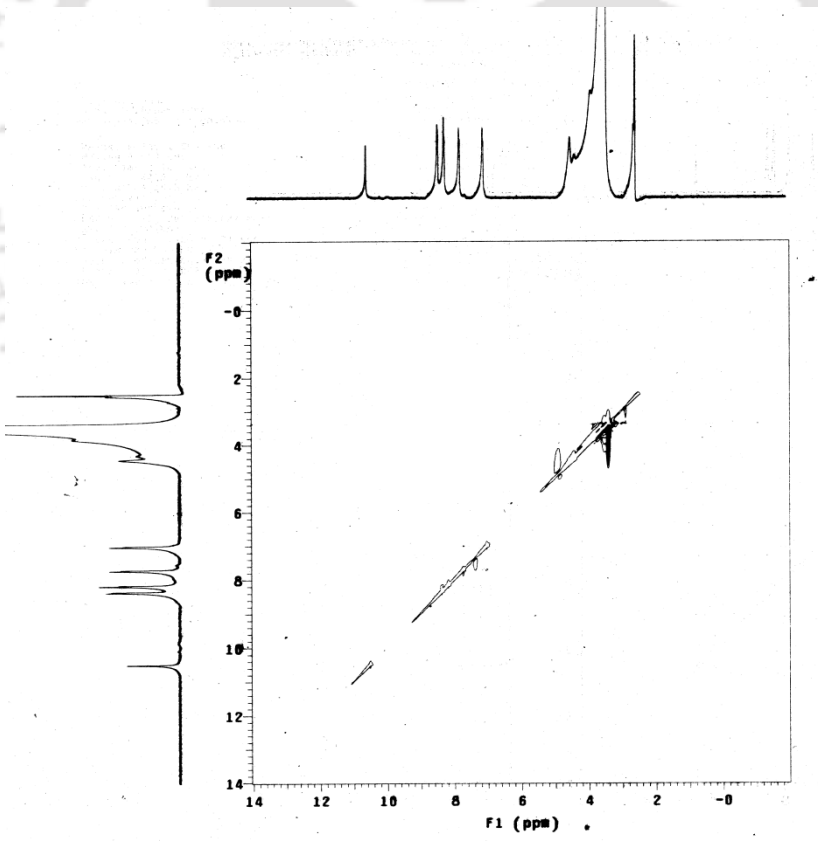

Figure A.5.4 NOESY spectrum of complex **3d** in DMSO-d_6 at 298 K.

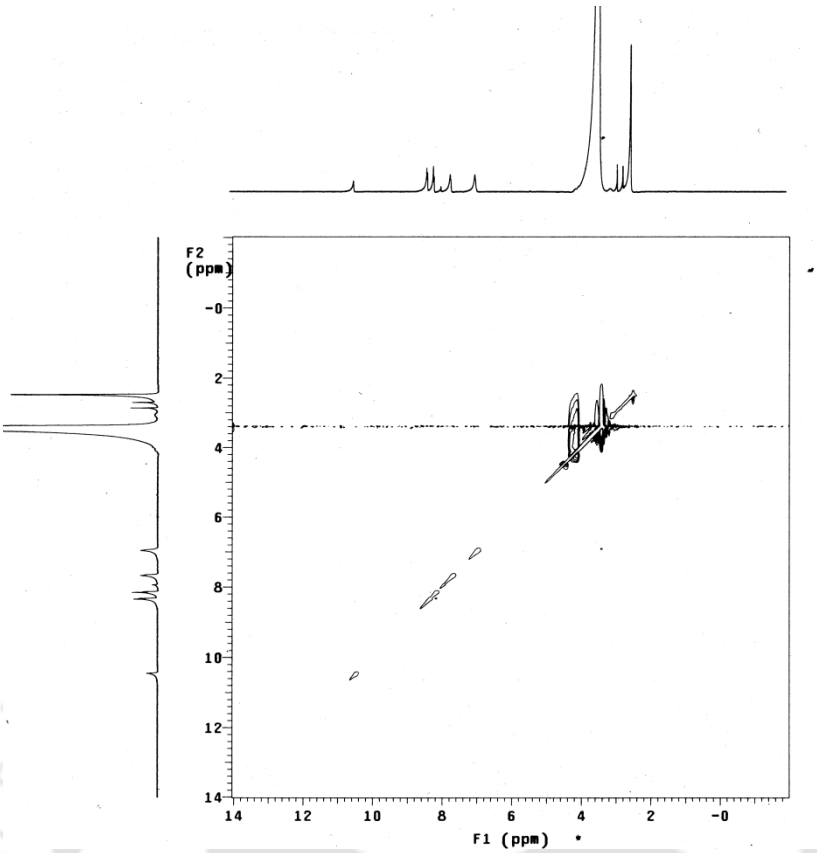

Figure A.5.5 NOESY spectrum of complex **3e** in DMSO-d_6 at 298 K.

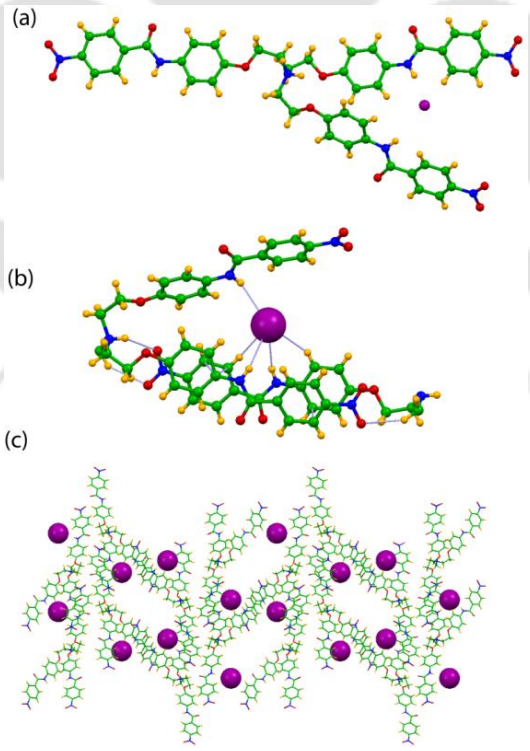

Figure A5.6 Ball and stick representation of molecular structure **3c**;(b)Hydrogen-bonding interactions of Iodide anions with $\mathbf{L_3H^+}$ in complex **3c**;(c) Crystal packing of complex **3c**, as viewed down the crystallographic '*a*' axis.

Annexure 6

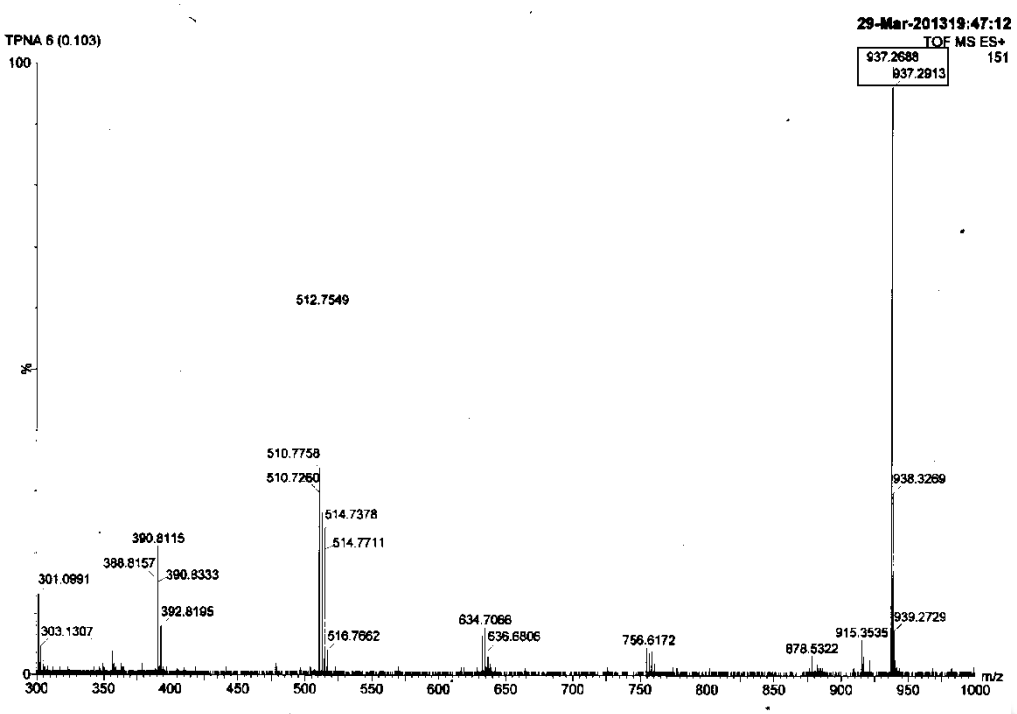

Figure A6.1 Mass spectrum of $\mathbf{L_4}$ in presence of Lithium cation (Li^+).

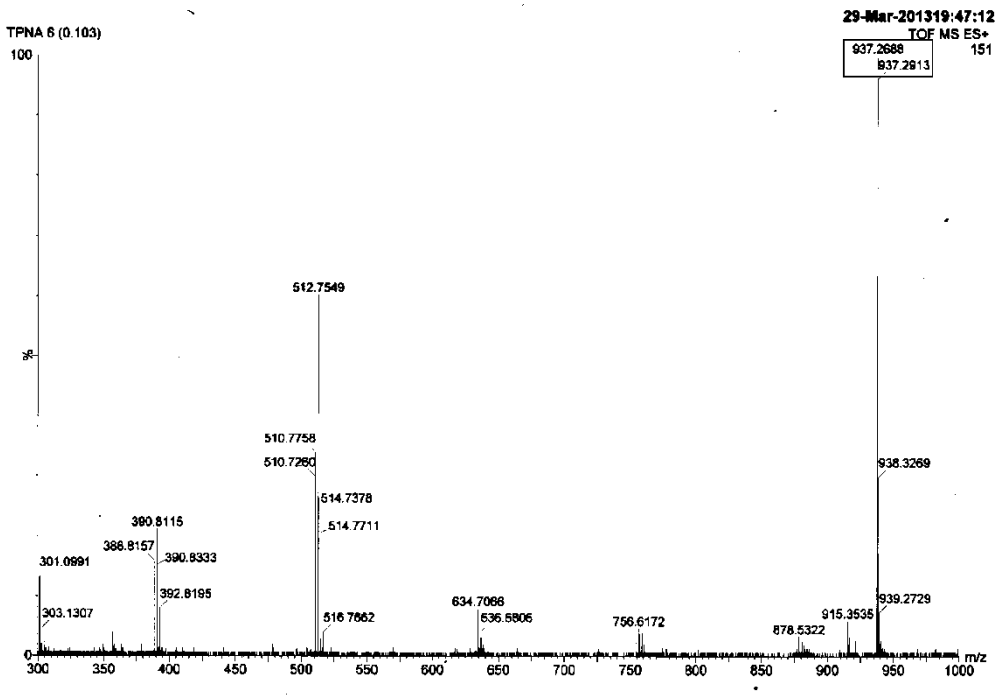

Figure A6.2 Mass spectrum of $\mathbf{L_4}$ in presence of Sodium cation (Na^+).

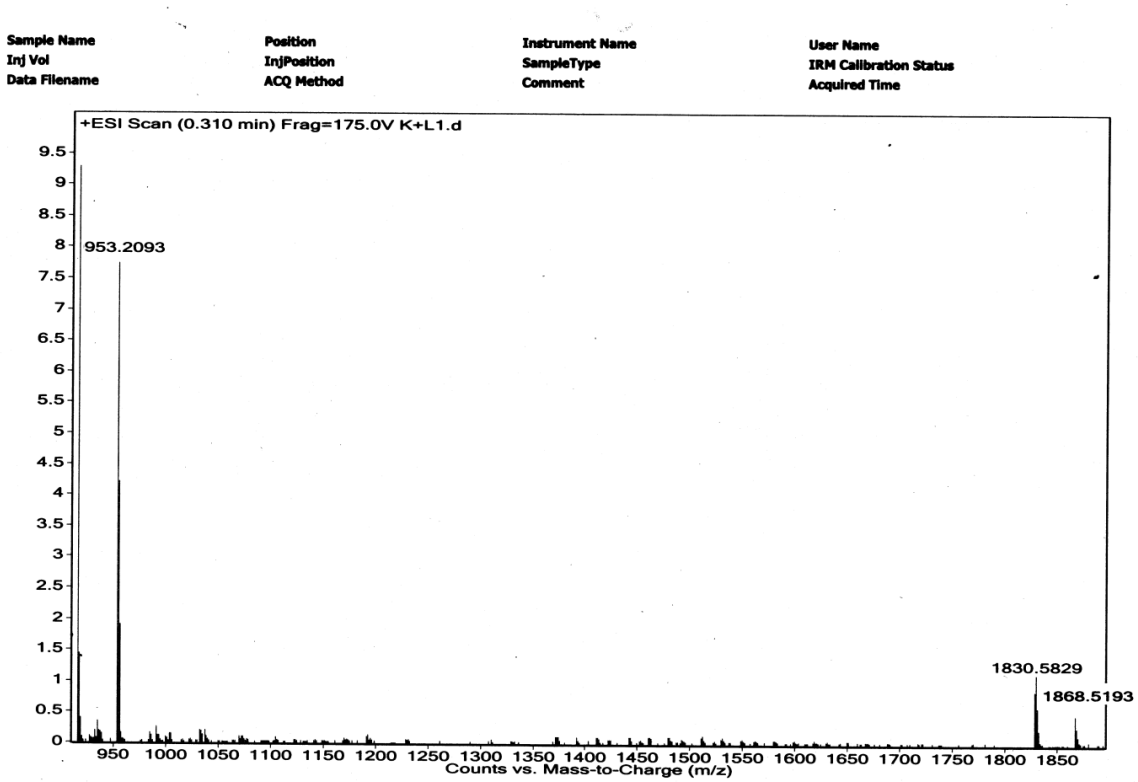

Figure A6.3 Mass spectrum of $\mathbf{L_4}$ in presence of Potassium cation (K^+).

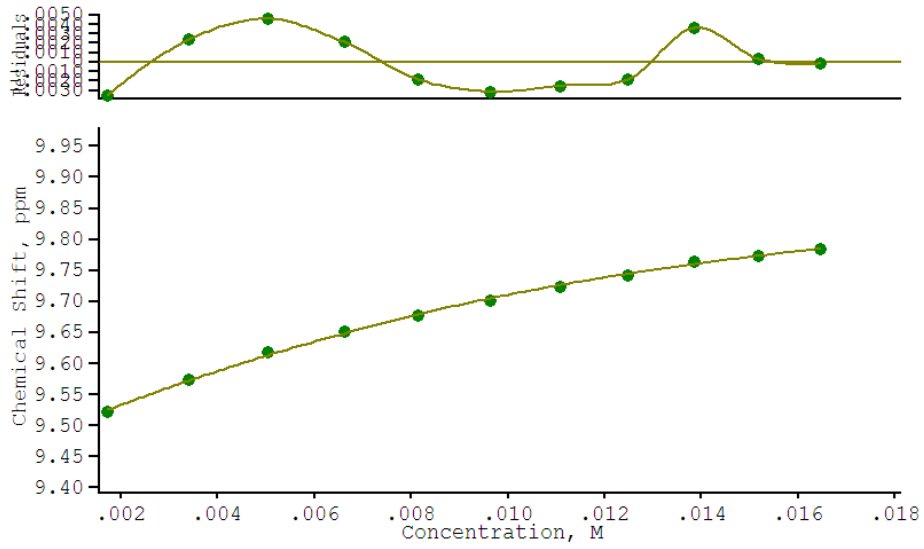

Figure A6.4 Fitplot for ^{1}HNMR titration experiment of $\mathbf{L_4}$ with $[n\text{-}Bu_4N^+]HSO_4^-$ (NH proton at δ = 9.34 ppm. Ka= 170M^{-1}).

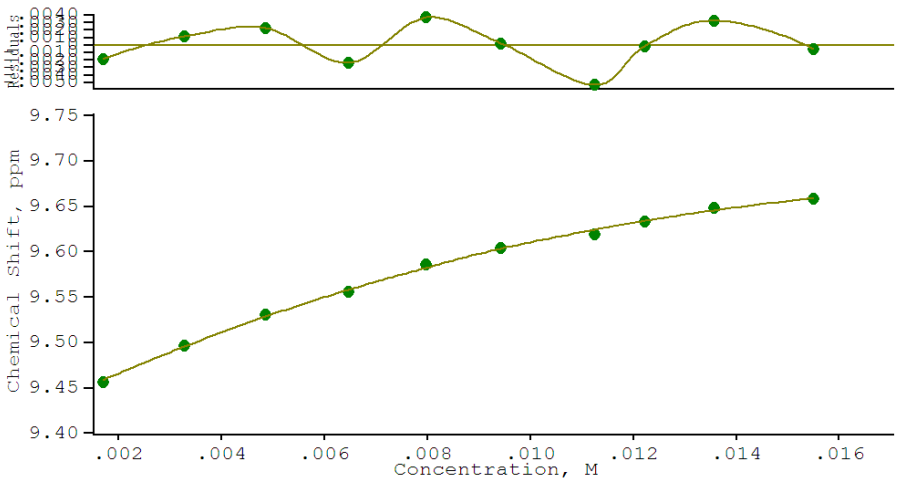

Figure A6.5 Fitplot for ^{1}HNMR titration experiment of Li^{+}·**L₄** with [*n*-Bu_4N^{+}]HSO_4^{-} (NH proton at δ = 9.34 ppm. Ka= 224M^{-1}).

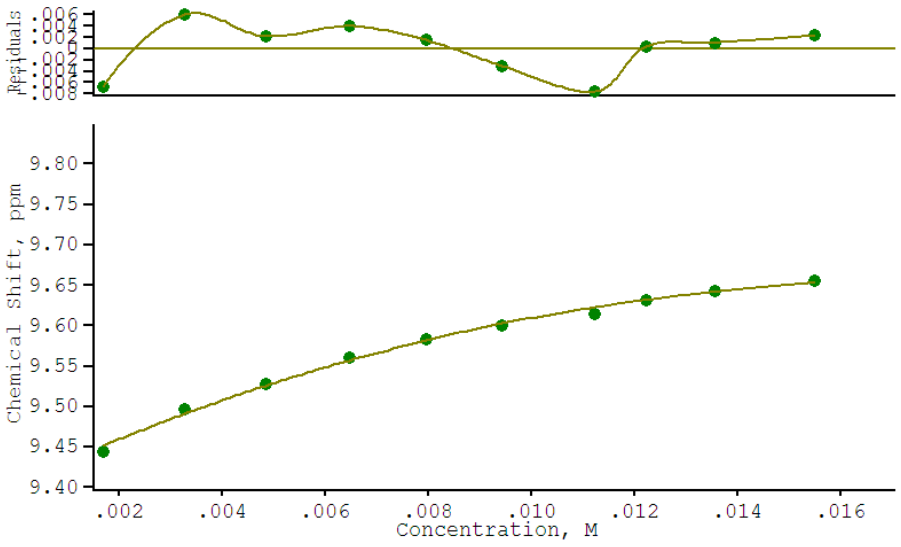

Figure A6.6 Fitplot for ^{1}HNMR titration experiment of Na^{+}· **L₄** with [*n*-Bu_4N^{+}]HSO_4^{-} (NH proton at δ = 9.34 ppm. Ka= 338M^{-1}).

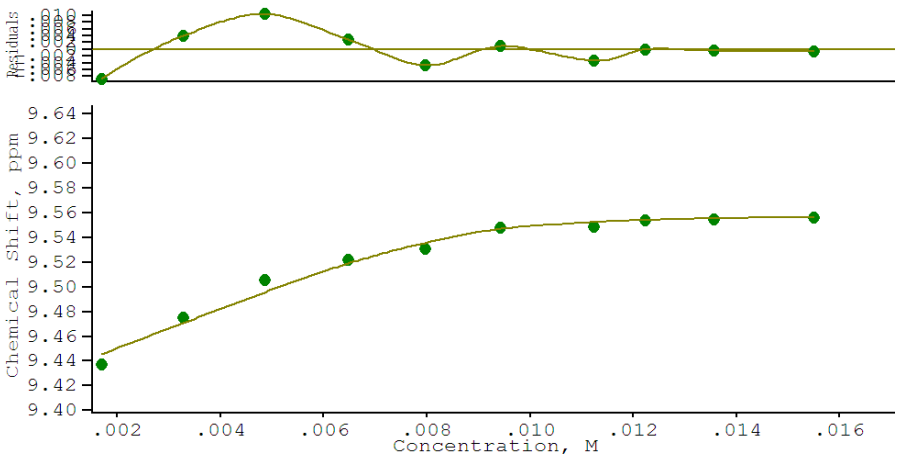

Figure A6.7 Fitplot for ^{1}HNMR titration experiment of 0.5K^+· **L_4** with [*n*-Bu_4N^+]HSO_4^- (NH proton at δ = 9.34 ppm. Ka= 4074M^{-1}).

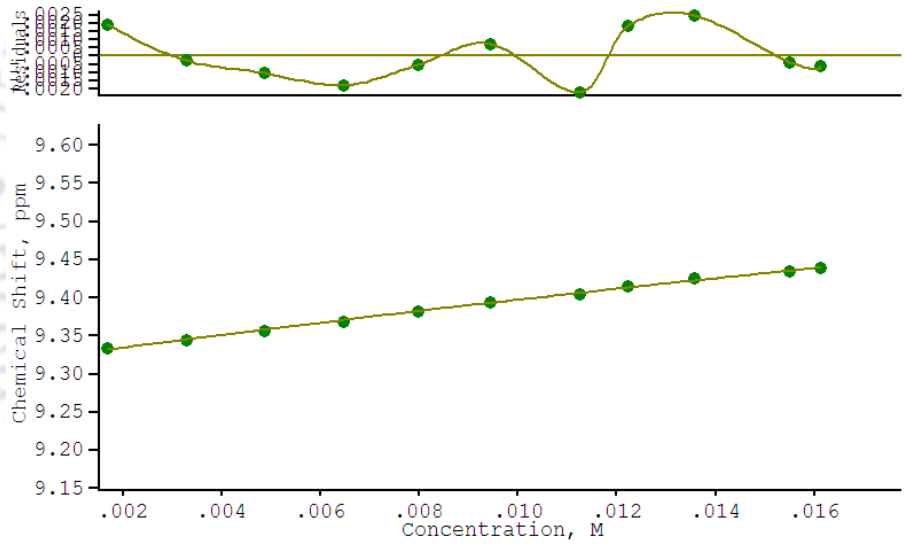

Figure A6.8 Fitplot for ^{1}HNMR titration experiment of K^+· **L_4** with [*n*-Bu_4N^+]HSO_4^- (NH proton at δ = 9.34 ppm. Ka= 11M^{-1}).

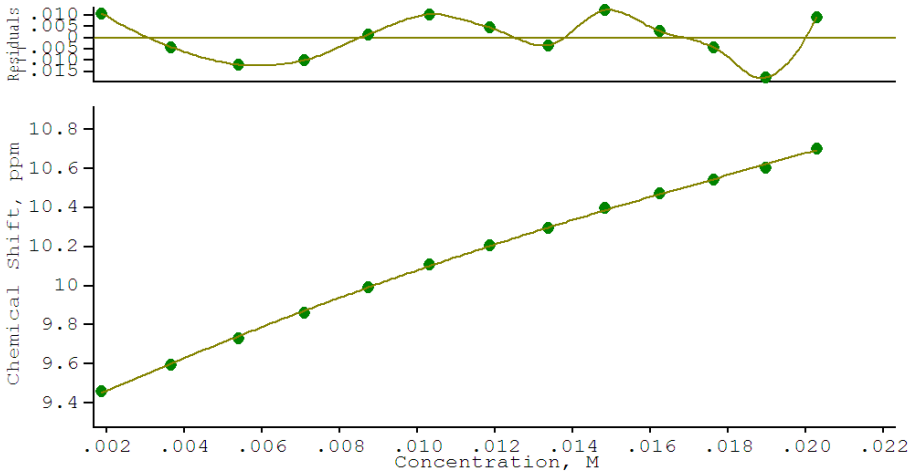

Figure A6.9 Fitplot for ^{1}HNMR titration experiment of **L$_4$** with [*n*-Bu$_4$N$^+$]H$_2$PO$_4^-$ (NH proton at δ = 9.34 ppm. Ka= 24M^{-1}).

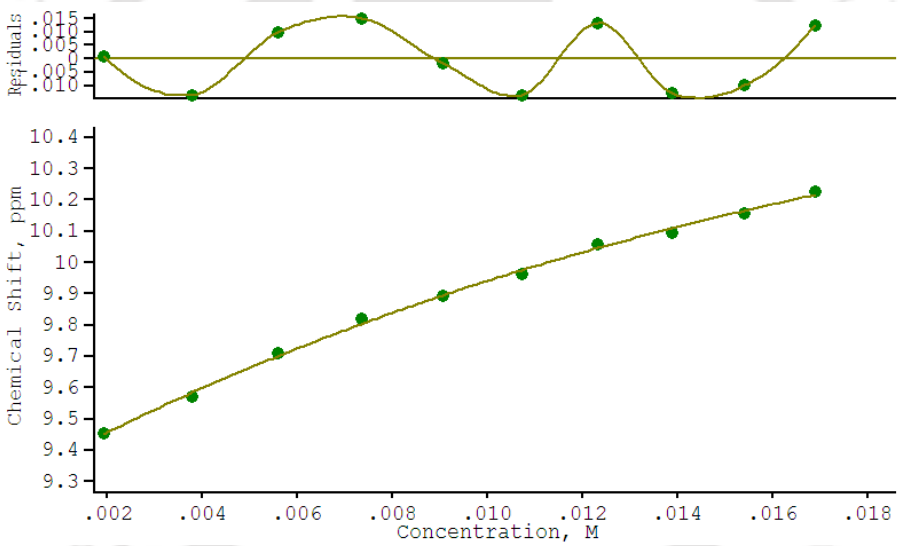

Figure A6.10 Fitplot for ^{1}HNMR titration experiment of Li$^+$· **L$_4$** with [*n*-Bu$_4$N$^+$]H$_2$PO$_4^-$ (NH proton at δ = 9.34 ppm. Ka= 66M^{-1}).

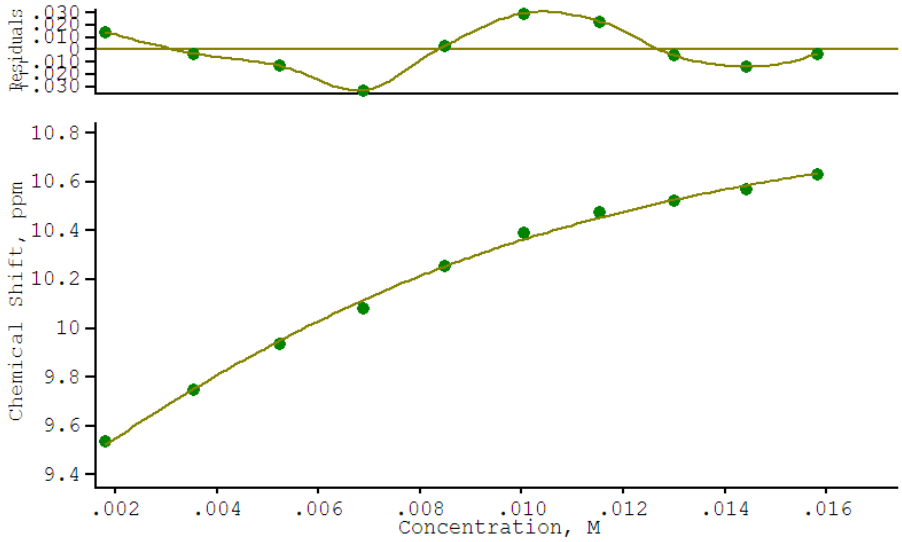

Figure A6.11 Fitplot for ^{1}HNMR titration experiment of $Na^{+}\cdot$ **L_4** with [*n*-Bu_4N^{+}]$H_2PO_4^{-}$ (NH proton at δ = 9.34 ppm. Ka= 269M^{-1}).

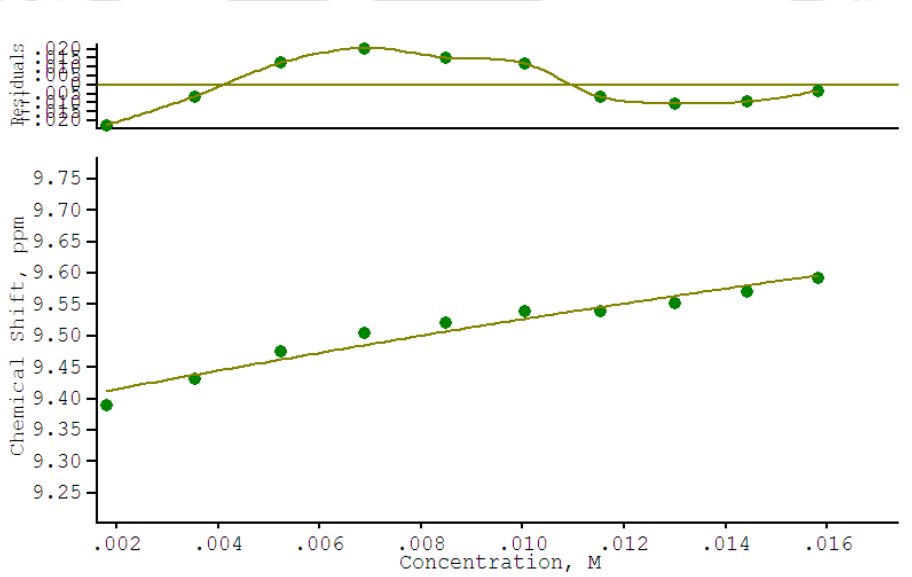

Figure A6.12 Fitplot for ^{1}HNMR titration experiment of $K^{+}\cdot$ **L_4** with [*n*-Bu_4N^{+}]$H_2PO_4^{-}$ (NH proton at δ = 9.34 ppm. Ka= 14M^{-1}).

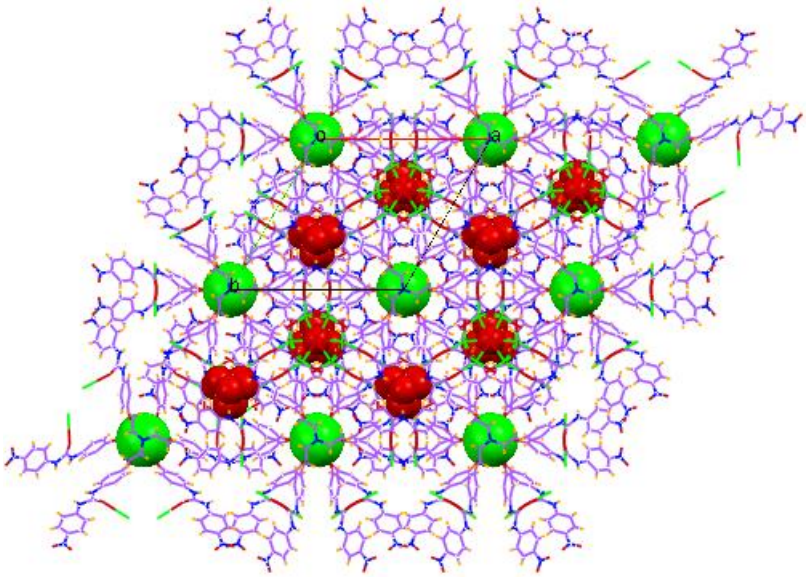

Figure A6.13 Showing packing diagram of complex **4c** along c axis.